Fall 12-2021

# Krüppel-like Factor 9 Is a Feed-forward Regulator of Glucocorticoid Signaling

Ian Gans
*University of Maine*, ian.gans@maine.edu

**KRÜPPEL-LIKE FACTOR 9 IS A FEED-FORWARD REGULATOR OF GLUCOCORTICOID SIGNALING**

By

Ian M. Gans

B.A. Arizona State University, 2006

B.S. University of Southern Maine, 2015

A DISSERTATION

Submitted in Partial Fulfillment of the

Requirements for the Degree of

Doctor of Philosophy

(in Biomedical Science)

The Graduate School

The University of Maine

December 2021

Advisory Committee:

James Coffman, Associate Professor, MDI Biological Laboratory, Advisor

Lucy Liaw, Professor, Maine Medical Center Research Institute

Steven Munger, Assistant Professor, The Jackson Laboratory

Alan Rosenwasser, Professor, University of Maine

Robert Wheeler, Associate Professor, University of Maine

**KRÜPPEL-LIKE FACTOR 9 IS A FEED-FORWARD REGULATOR OF GLUCOCORTICOID SIGNALING**

By Ian M. Gans

Dissertation Advisor: Dr. James A. Coffman, PhD

An Abstract of the Dissertation Presented
in Partial Fulfillment of the Requirements for the
Degree of Doctor of Philosophy
(in Biomedical Science)
December 2021

Epidemiological studies show that children of chronically stressed mothers are at higher risk for adverse health outcomes throughout life, but the pathological mechanisms underlying this increased risk remain poorly understood. Using zebrafish as a model system, the Coffman Lab at the MDI Biological Laboratory showed in 2016 that larvae exposed to chronically elevated levels of the glucocorticoid (GC) stress hormone cortisol exhibit elevated pro-inflammatory gene expression. Further, the Coffman Lab showed that immune gene response to injury or infection was blunted in adult fish raised from cortisol treated larvae, presenting a novel paradigm for the investigation of disease mechanisms involving chronic GC exposure during development. The two most consistently overexpressed GC targets in the 2016 study and follow-up experiments were *fkbp5*, a well-known regulator of the receptor for cortisol (the glucocorticoid receptor, or GR, a nuclear hormone receptor), and the transcription factor Krüppel-Like Factor 9 (Klf9). The Krüppel-Like family of transcription factors is known to include effectors of nuclear receptor signaling, but less is known about the role of Klf9 in GC signaling. Thus, I used CRISPR to generate a mutant zebrafish line lacking functional Klf9. Using this knockout line we discovered that *klf9* mediates aspects of the physiological response to GC

signaling by 1) facilitating immune gene response to cortisol, 2) repressing the expression of GR regulator *fkbp5*, and 3) regulating metabolism downstream of hormone signal. These results are described in detail in the following chapters.

## DEDICATION

This work is dedicated to Marina. Your support and sacrifices allowed me to get wrapped up in all of this while you did the heavy lifting of starting our family. Two kids, four moves, a global pandemic and a PhD later, I can't imagine going through it all with anyone else. Of course, I also dedicate this to Iris and Margot. Thank you for making me smile every day. You two are the greatest gifts. I love you all.

**ACKNOWLEDGEMENTS**

First and most importantly, I'd like to thank family who have been unwaveringly supportive with words and deeds. These have been incredibly busy years and you helped make everything more manageable.

I thank my committee for their patience, and my mentor Jim for his thoughtful guidance.

Last, I want to acknowledge the incredible community at MDI Biological Laboratory for the support I've received. I'll always think fondly of this place and my time here.

**TABLE OF CONTENTS**

## LIST OF TABLES

**LIST OF FIGURES**

# CHAPTER 1

# INTRODUCTION

## 1.1. Glucocorticoid hormones

Glucocorticoids (GC) are steroid hormones produced by the adrenal glands that dynamically regulate diverse physiological functions including metabolism and immunity in order to maintain organismal homeostasis within a constantly changing environment. The role of GC in human health was first glimpsed in the late 19$^{th}$ century when Thomas Addison found that adrenal extract had therapeutic properties for patients with a multi-symptom wasting disease (now known as Addison's Disease or adrenal insufficiency)[1]. Decades later in the early-mid 20$^{th}$ century, it was noted by Philip Hench that temporary remissions of rheumatoid arthritis were associated with conditions thought to stimulate the adrenal cortex, including pregnancy (a condition now known to increase maternal GC levels several-fold). In 1946 four adrenal products were purified by Edward Kendall and Compound E, now known as cortisol (CORT), was found by Hench to have remarkable benefits for patients with severe arthritis[2]. This led to the award of the Nobel Prize in Physiology and Medicine in 1950, and today synthetic GC are widely prescribed for their anti-inflammatory properties.

CORT, the active GC hormone in humans and zebrafish, is commonly referred to as a (or inaccurately as "*the*") stress hormone and is one of the key hormonal regulators of the physiological response to stress (along with adrenaline and noradrenaline). In response to stress, these hormones orchestrate the usage of energy stores and prime the body to respond to threat. In contrast to the physiological effects of adrenaline which occur almost instantaneously, the effects of GC largely involve changes in gene transcription and thus require

several minutes to occur. More rapid, non-genomic mechanisms of GC action also exist, however these are less well understood[3]. The focus of the work contained herein focuses primarily on the effects that GC exert through regulation of gene expression.

### 1.1.1. Glucocorticoid production by the hypothalamus-pituitary-adrenal axis

The release of endogenous GC (cortisol in humans and fish, corticosterone in rodents, referred to hereafter as CORT in either case) into the bloodstream is the end result of a hormone cascade that occurs upon activation of the Hypothalamus-Pituitary-Adrenal (HPA) neuroendocrine axis (Fig. 1.1). HPA activation occurs when cues integrated by the central nervous system cause corticotrophin releasing hormone (CRH) to be released by the hypothalamus into the pituitary portal circulation. CRH then acts on the anterior pituitary gland causing the release of adrenocorticotropic hormone (ACTH) which travels through the blood stream to the adrenal glands triggering the release of GC into the blood. Note that in zebrafish

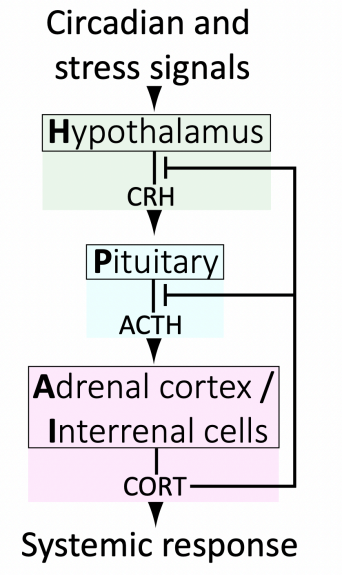


**Figure 1.1. Schematic of the hypothalamus-pituitary-adrenal/interrenal axis.** Cues integrated in the brain lead to a cascade of hormones culminating in release of CORT from adrenal glands in mammals or interrenal cells in zebrafish.

CORT is produced by interrenal cells within the head kidney rather than a distinct gland, and thus the zebrafish axis is referred to as the HPI (hypothalamus-pituitary-interrenal).

### 1.1.2. Regulation of gene expression through cognate receptors

As small lipophilic molecules, GC freely diffuse from the blood stream through cell membranes and into the cytoplasm of cells. Once inside cells GC bind and activate cognate receptors, the glucocorticoid receptor (GR, coded for by the *NR3C1* gene) and the closely related mineralocorticoid receptor (MR). These receptors are protein transcription factors which translocate to the nucleus once bound by ligand and regulate gene transcription (Fig. 1.2). Both corticosteroid receptors have a central DNA binding domain flanked by an N-terminal domain and a C-terminal ligand-binding domain (see Fig. 3.1). The high affinity of the MR for GC as well as other steroid hormones leads to its activation at even low physiological levels of GC hormone[4,5]. In comparison, the GR has a nearly 10-fold lower binding affinity for GC, and its activation is thus sensitive to fluctuations in GC levels that occur with circadian (roughly 24-hour) rhythmicity and on more rapid timescales (within minutes in response to acute stressors). Because the GR is expressed in nearly all cell types and binds thousands to tens-of-thousands of genomic sites in a given target tissue[6], changes in circulating GC levels produce broad changes in gene expression, physiology and behavior and are a primary means of coordinating an adaptive organism-level response to stress and/or a changing environment.

Within the nucleus, regulation of gene expression by the GR is accomplished in large part through its direct binding to glucocorticoid response elements (GRE) in regulatory DNA regions.

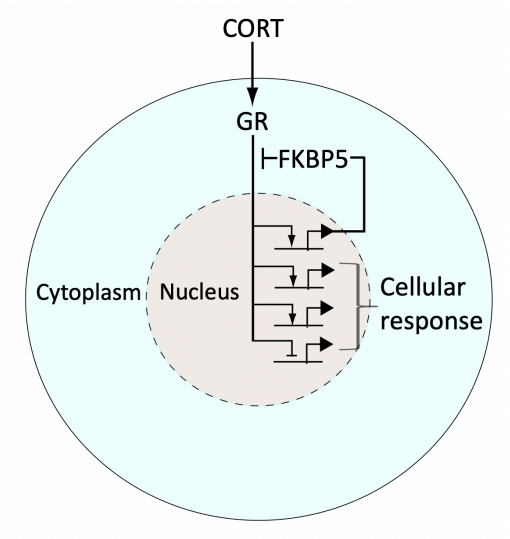


**Figure 1.2. Cortisol regulates gene expression via the glucocorticoid receptor.** Once bound by CORT, the GR translocates from the cytoplasm to the cell nucleus where it binds DNA to regulate transcription of target genes. One well-known target is *fkbp5*, which codes for a cytoplasmic chaperone of the GR and forms an intracellular negative feedback loop that regulates GR activity (shown above).

In the canonical pathway, nuclear GR dimers interact with palindromic GRE sites. However, binding of GR monomers to half sites, inverted GRE (half sites occurring on opposite strands) and indirect "tethered" interactions with DNA mediated by other transcription factors, also occur (reviewed thoroughly here[7]). The regulation of transcription by the GR involves recruitment of numerous cofactors, can be activating or repressive, and is highly context dependent. The GR is also subject to various post-translational modifications (e.g. acetylation, phosphorylation, sumoylation, ubiquitylation, nitrosylation) that further control its activity. Thus, although the GR is among the most well-studied transcription factors, the various modes and contextual determinants of its function continue to be fertile ground for research.

### 1.1.3. Glucocorticoid signaling dynamics

The HPA axis is a highly dynamic and responsive system. To understand how the HPA axis maintains both homeostasis and stress responsiveness, we must consider how its output is temporally regulated. It is generally accepted that systemic negative feedback exists between HPA tissues, wherein circulating GC act upon the hypothalamus and pituitary to downregulate further CRH, ACTH, and GC release. However, HPA regulation is much more complex and our understanding remains incomplete. At the top level, the hypothalamus receives inputs from complex neural circuits involving the hippocampus, amygdala and prefrontal cortex which regulate CRH release, and each of these brain regions exert different and context-dependent controls. For example, the hippocampus and amygdala have been shown respectively to exert primarily inhibitory and facilitative influences on hypothalamic CRH production[8]. In even more granular detail, different loci within a brain region may govern responses to different modes of stimuli. For example, the central and medial nuclei of the amygdala have been found to separately facilitate HPA responses to systemic (e.g. inflammation) or psychogenic (e.g. restraint) stress. It is also of interest to note that CRH is a neuropeptide produced throughout the brain, and that hypothalamic neurons are the only population which respond to GC by downregulating CRH[9,10]. In contrast, CRH production is strongly stimulated by GC in the amygdala in a manner inverse to the repression by GC on hypothalamic CRH. The amygdala has also been shown to mediate aspects of GC induced anxiety and fear, and it is thought that it may activate the hypothalamus through interruption of basal inhibition[11,12]. In all, the ability of HPA activity to be determined by integration of complex circuits almost certainly provides a survival advantage by conferring adaptive plasticity. However, this distributed regulatory

framework also appears to allow for basic negative feedback mechanisms and normal dynamics to be overridden. For instance chronic stress can remodel brain regions, shrinking dendrites in the hippocampus while expanding them in the amygdala[13,14], potentially altering the ratio of inhibitory/activating inputs on the hypothalamus and affecting HPA dynamics. Under normal conditions these dynamics involve regular fluctuations on circadian and ultradian timescales, but these dynamics can be altered in unhealthy scenarios, as will be discussed further in following sections.

#### 1.1.3.1. Circadian dynamics

Within the hypothalamus, the suprachiasmatic nucleus (SCN) is the well-established site of the central circadian clock, sitting above the optic chiasma and receiving input directly from light-sensitive neurons. Nearby, the paraventricular nucleus (PVN) is the source of hypothalamic CRH secretion and receives inputs from the SCN, generating light-dependent activation of the HPA axis and circadian oscillations in GC production[15]. GC thus relay information from the central or "master" circadian pacemaker to so-called "slave" clocks in additional tissues to coordinate organism-wide timing, with daily peaks in GC levels preceding the active behavioral phase (early morning in humans and zebrafish, evening in rodents). Various and layered mechanisms coordinate with circadian levels of GC to generate robust rhythmicity in GC-signaling. Examples include downregulation of GR protein activity through post-translational acetylation by the core circadian protein CLOCK (Circadian Locomoter Output Cycles Kaput, a transcription factor and acetyltransferase)[16], as well as diurnal rhythmicity in levels of GC transport proteins that regulate the availability of free CORT in the blood stream[17].

Most cells possess autonomous 24-hour clocks, but phase coherency at the tissue or whole-organism level requires synchronization by circadian signals, many of which (including GC rhythmicity) originate from the SCN[18]. Strikingly, a short pulse of the synthetic GC dexamethasone (DEX) is sufficient to synchronize circadian gene expression in cell cultures, while injections of DEX are able to shift or reset the phase of circadian gene expression in peripheral tissue of live mice based on the timing of the injection[19]. This ability of GC to alter the circadian phase does not apply to cells of the SCN, however, where the notable lack of GR expression likely protects the central clock from the influence of acute hormone spikes.

In zebrafish, tonic concentrations of DEX have been shown sufficient to rescue 24-hour cell-cycle rhythms in larvae lacking corticotrope cells, suggesting that the presence of GC above a threshold concentration is sufficient for synchronization of some peripheral clocks, and that rhythmicity of GC levels may be dispensable for some processes[20]. The cell cycle is not the only rhythmic biological process, however, and it's possible that while peak GC entrain cell-cycle, trough periods may provide rhythmic impetus for other processes (especially considering that the GR may act as either an activator or repressor of target gene transcription). Diurnal lulls in GC levels could also free up a cell's signaling bandwidth for response to additional or subsequent signals, including providing slack in the system necessary for HPA re-activation, such as in a "fight-or-flight" scenario. Dynamic flexibility allows for additional GC peaks to be superimposed on the 24-hour light-driven oscillations as may be warranted by altered feeding habits, perceived threats, or other conditions. For example, robust feeding-induced GC rhythms depend on an adrenal clock which normally reinforces SCN clock timing but can become uncoupled from it and generate independent hormone dynamics[21].

#### 1.1.3.2. Ultradian dynamics

The circadian profile of circulating GC is not achieved through smooth continuous release, but rather is driven by pulsatile release of hormone occurring on the order of hourly, or in other words with ultradian frequency[22–24]. While the frequency of these pulses remains relatively constant, varying amplitude drives circadian GC level, with the highest pulses occurring just prior to the waking phase. It was once thought that an ultradian pacemaker must reside in the brain, however studies in the last decade by the Lightman lab using automated hormone infusions and measurements in rats have demonstrated these pulsatile characteristics result from the combination of feedback and feedforward signals and delays among HPA tissues[25–27]. As predicted by initial computational modeling, pulsatile infusions of ACTH were found to induce pulsatile corticosterone release in rats whose endogenous ACTH production was suppressed by the synthetic GC methylprednisolone. This was followed by pulsatile transcription of genes involved in steroidogenesis, similar to gene pulsing effects previously seen *in vitro* with cycles of GR activation and association with chromatin leading to ultradian pulses of gene transcription[24]. Interestingly, constant infusion of ACTH caused no induction of GC (similar to saline control), indicating that the pulsatile nature of ACTH signal is key to normal adrenal function. On the contrary, constant infusion of CRH was found sufficient to drive pulsatile release of both ACTH and corticosterone, with the pulse of ACTH occurring in advance of CORT pulse. Increasing the constant dosage of CRH had the effect of pushing the trough levels of CORT toward a ceiling of maximal production, eventually attenuating the rhythmicity. It has been estimated that biosynthesis of CRH requires 60-90 minutes, thus making it likely that hormonal feedback regulation of CRH production is more involved in recuperation rate or

adaptation to chronic stress than initial response[10]. Together these findings support the concept of dynamic equilibrium of the HPA axis rather than a controlled steady state, with rapidly fluctuating dynamics maintaining plasticity and responsiveness of the system. It has been proposed that pulsatile dynamics also may serve to filter out random low-level stimuli to avoid unnecessary activation of the system[28]. In support of this idea that ultradian dynamics govern the degree of HPA activation, the magnitude of stress response has been shown to depend on whether a stressor occurs during a rising or falling ultradian phase of hormone release[29,30].

#### 1.1.3.3. Disruptions of dynamics are associated with disease

Timing of gene expression programs is one way in which organisms may maximize the efficient usage of nutrients, cofactors, and other macromolecules, thereby enhancing fitness[31–34]. Conversely, disruption of this timing comes at a cost to fitness, and scenarios where GC dynamics become disrupted—either due to chronic stress, interference with circadian cues (e.g. shift work, jet lag), or a disease condition—are associated with multi-systemic disorders, including immune, psychological and metabolic syndromes[35,36].

##### 1.1.3.3.1. Loss of circadian rhythmicity

Perhaps the best-known example of attenuated diurnal CORT levels is in Cushing's Syndrome, where a pituitary or adrenal tumor leads to CORT overproduction and loss of rhythmicity. Due to the important role of the GR in most tissues, Cushing's hypercortisolemia usually presents with multiple comorbidities including metabolic syndromes, hypertension, osteoporosis, cognitive decline, defects in wound healing and increased risk of infections. This collection of maladies is also associated with aging, and it also happens that changes in HPA axis

rhythmicity has been associated with aging. The most consistently reported change in CORT levels with age has been an elevation of the evening nadir level in aged individuals, although total increase, circadian phase advancement, and sex dependent differences have also been reported[37–39]. Interestingly, elevated trough level of CORT can also result from mild chronic stress and cause metabolic imbalance[40]. Higher CORT nadir and thus reduced diurnal slope have also been reported in Type 2 diabetics[41].

The technical challenges of getting truly basal hormone measurements in a stress-responsive system with ultradian rhythmicity should be acknowledged. These challenges along with variations among populations and experimental designs may be why studies suggest depressive adolescents exhibit a flatter diurnal profile but there is a lack of consensus on how diurnal CORT is effected in adults with depression[42]. However, patients with Cushing's Syndrome are at a high risk (50-80%) for depression, as are patients treated with oral synthetic GC widely prescribed for their anti-inflammatory properties[43]. Meta-analysis also strongly indicates that elevated CORT is associated with depression, with the effect being larger in older patients[44]. This age-dependent finding highlights the potential of interactions to exist among conditions associated with HPA hyperactivity, and the difficulties that can arise in untangling cause and effect.

#### 1.1.3.3.2. Altered ultradian pulsatility

With ultradian pulsatility underlying the circadian profile of CORT, it is perhaps not surprising to find that increased ultradian pulse amplitude has also been described in some cases of acute depression[36,45]. Adjuvant-induced arthritis has also been shown capable of inducing increased ultradian GC pulse amplitude in rats[46]. Windle et al. described this effect of

mycobacterium-induced inflammation as an increase in frequency of pulses (in terms of more corticosterone pulses counted *per 24 hours*). However, this increase in "frequency" was driven mainly by the occurrence of measurable pulses of GC throughout the day in treated animals, whereas in controls GC pulses were not detectable during the circadian trough period. When detected, pulses occurred with an ultradian period of ~33 minutes regardless of treatment, however amplitude remained high throughout the day in arthritic rats whereas pulse amplitude had a circadian profile in controls. In humans, ultradian CORT pulse frequency has been shown to remain relatively constant even at low hormone levels[47]. That pulsatile GC release is detectable even during circadian nadirs and may be induced to maintain a constant high amplitude by chronic stimuli suggest that the HPA axis is a system that oscillates even during circadian troughs rather than entering a static inactive state.

It has been suggested that oscillating biological systems may emerge from evolutionary tuning of discreet pulsatile responses which are well-suited for adapting to *changes* in environment rather than to the level of an environmental input itself[48]. Negative feedback regulation can be used to enhance responsiveness to stimulus but can also generate overshoot and oscillations. Additional feedback and feedforward regulatory elements can be combined to stabilize and tune such a system to achieve an optimal combination of responsivity and stability[49,50]. With this in mind, the HPA axis may be thought of as an oscillating system primed to generate adaptive, pulsed responses. These dynamic characteristics can confer benefits such as enhanced responsivity and adaptation, amenability to entrainment and/or filtering out of noisy/trivial activating stimuli[49]. However, as described above the HPA axis appears also to have some inherent vulnerability to repeated or chronic activation.

### 1.1.4. The allostatic model of pathogenesis

A useful concept for relating GC and HPA dynamics to disease states is that of 'allostasis', i.e. stability through adaptation[51,52]. Building from the principle of homeostasis and set points for physiology that are optimal for fitness, allostasis emphasizes the work required by a system (such as the HPA axis) to maintain homeostasis under changing conditions (which can include adaptive deviations from previous homeostatic parameters). Biological systems have a capacity to mount transient adaptive responses to many types of stress. As a simplified and generic example, consider a stress leading to a stepwise increase in hormone level, activation of a nuclear hormone receptor and transcription of a target Gene X. From a systems design perspective, this transcriptional response would be considered perfectly adaptive if transcription of Gene X increases transiently before returning to the pre-stimulus level upon either resolution of the stressful event or recalibration by the system to the new steady-state input level[49,53]. The pulsed response by Gene X might also occur but resolve with a new steady state of transcriptional output (e.g. higher than the pre-stress level), termed "imperfect adaptation" (Fig. 1.3). The allostatic model of disease posits that if adaptive responses are

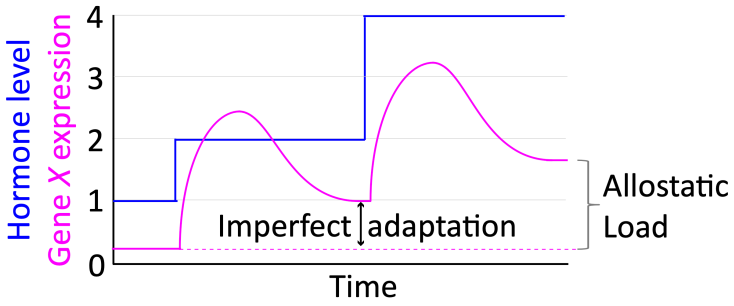


**Figure 1.3. Imperfect adaptation may contribute to allostatic load.** In this conceptual model, increasing hormone levels cause pulsatile increases in Gene X expression. These transient activations resolve to an elevated baseline that generates allostatic load.

repeatedly or chronically activated they may culminate in a state of systemic imbalance, generating a change in homeostatic set point (i.e. set-point drift) referred to as an "allostatic load" that is deleterious for health. The regulation of blood sugar by GC is an illustrative example. During the acute stress response GC cause release of glucose by the liver while simultaneously antagonizing insulin signaling and decreasing glucose uptake in skeletal muscle and adipose tissue[54]. The net result of this is increasing glucose availability to the brain, which relies almost exclusively on glucose for its high energy demands (~20% of glucose metabolized by an organ which accounts for ~2% of body mass)[55]. Chronic stress, however, can contribute to chronic hyperglycemia that can in turn cause inflammation, insulin resistance and eventual development of diabetes and related metabolic syndromes.

#### 1.1.4.1. The allostatic load index

The progression of disease due to allostatic load can be divided into three phases. First, a change in a primary mediator of allostasis (such as CORT) that results in a secondary effect on physiology (such as hyperglycemia) followed by a tertiary manifestation of a clinically recognized disorder (such as diabetes). To translate the concept of allostatic load into a clinical/biomedical tool, various permutations of an Allostatic Load Index have been tested using combinations of measurable primary and secondary biomarkers to predict clinical outcomes. As a primary mediator of adaptation to stress, CORT measurement was included among ten measurements in the original Allostatic Load Index, developed as part of a MacArthur study on successful aging[56]. In this study of a selected 'high-functioning' elderly population, scoring poorly on the Allostatic Load Index was associated with (and predictive of) poor physical health and cognitive decline, with CORT level contributing to the index's

predictive capacity[57]. Encouragingly, decreases in allostatic load were found to reduce risk of death in a follow up study[58]. Since the initial MacArthur study, CORT has remained frequently (but not always) included in subsequent studies using variations of the index, alongside other neuroendocrine, metabolic, and immune markers and physiological measurements (blood pressure and waist-to-hip ratio, for example)[59].

#### 1.1.4.2. Allostatic load in working populations

As work is considered a common source of stress, more than a dozen studies have looked at allostatic load in working populations, and high allostatic load has been shown to correlate with reported stress level, effort-reward imbalance, and low safety as well as low socio-economic standing[60]. However, considerable variations in design and lack of a standardized index among these studies—dozens of different biomarkers being used in at least one study—limits meta-analysis. In one such study low CORT was associated with symptoms of burnout but not depression[61], but broadly speaking variations in populations, study designs, timing and frequency of CORT collections and sample type (CORT can be measured in urine, saliva, plasma, or hair) have led to inconsistent results and lack of consensus on the specific contribution of CORT to Allostatic Load in working populations[62]. Nevertheless, it is worth considering that work-related stress may contribute to differential CORT levels as well as other markers/outcomes of allostatic load.

#### 1.1.4.3. Early-life allostatic load and long-term consequences

A number of studies have linked early-life stress (e.g. traumatic childhood experiences or development in adverse environments) with measurably increased Allostatic Load Index in

children[63], and adverse childhood events have been shown to cumulatively increase long-term risk of mental, physical, and behavioral disorders[64]. Quality of care has been shown to have an effect on the diurnal CORT profile in pre-school aged children, who display the expected diurnal decrease in CORT when at home but often experience an increase in CORT from morning to afternoon when at daycare, particularly if care quality is lower[65–67]. In one study, this elevated afternoon CORT in school children was found to correlate with lower antibody production[68]. School-age children from lower socio-economic backgrounds have been shown to have elevated CORT levels compared with children from more affluent families[69]. Enriched environments have been shown in some instances to decrease CORT, while the emotional stress of having depressed parents or being rejected by peers leads to CORT elevation[70].

Although the long-term effects of elevated CORT during childhood are not well understood, exposure to early-life stress has been shown to modulate the activity of the HPA axis later in life. But as with the effects of allostatic load in adult populations, the outcomes appear context dependent[71]. For example, while mild-to-moderate early life stress can lead to HPA axis hyperactivity as seen in depression, more severe trauma can lead to hypo-responsiveness, with developmental timing of stress exposure also factoring into outcomes. Nevertheless, low socio-economic standing in childhood has been linked to an increase in basal CORT in adulthood, independent of adult socio-economic standing and other lifestyle factors[72]. This was accompanied by a decrease in GR-target gene expression in immune cells and an increase in markers of inflammation, supportive of the authors' hypothesis that early-life stress promotes a "defensive" phenotype that could be beneficial during acute stress but more susceptible to chronic disease. Low childhood socioeconomic standing has also been linked to increased

infection susceptibility, risk for cardiovascular disease, and overall mortality[73–75]. Thus, stress experienced during childhood is linked to poor long-term health outcomes as well as altered CORT production during childhood and into adulthood, strongly indicating that early-life HPA programming contributes to disease risk.

### 1.1.5. Pre- and peri-natal stress and glucocorticoid exposure

Given the evidence that elevated stress levels in childhood can have long-term effects on HPA function and overall health, it may come as no surprise that abundant research indicates that mal-adaptive HPA programming can begin *in utero*. Due to the rapid growth and development occurring during the earliest stages of life, the pre- and peri-natal periods are generally considered to be times of high plasticity and vulnerability to intervention.

Endogenous GC are crucial for early mammalian development, aiding the maturation of fetal organs. In 1969, it was reported that synthetic GC induced inflation of lungs in premature lambs[76]. Mice lacking a GR die soon after birth due primarily to defects in lung surfactant production and respiratory distress[77]. In humans, respiratory distress is a leading cause of death in pre-term newborns, and so synthetic GC are regularly administered to hasten lung maturation when there is risk of a pre-term birth[78]. As will be discussed in the following sub-sections, development of the brain and the HPA axis itself are also finely regulated by GC and elevated exposure can be detrimental.

#### 1.1.5.1. Pre-natal exposure to synthetic glucocorticoids

The use of synthetic GC has been endorsed by the NIH to aid fetal maturation in pregnancies at risk for premature delivery[79–81]. Though there are definite benefits of

administered GC for survival of premature infants, these benefits may not extend to pregnancies carried to term, in which case there may instead be negative effects, and the use of multiple courses is also controversial[82,83]. How prenatal synthetic GC administration affects long-term health is not yet fully understood, as the practice only began in earnest in the 1990s. There are however multiple reports of adverse associations. Antenatal treatment with synthetic GC has been reported to cause higher blood pressure in adolescents and elevated insulin in 30-year-old adults[84,85]. Decreased head size, hyperactivity, and increased distractibility were reported in children treated with repeated antenatal courses of the synthetic betamethasone[86]. Pre-mature infants treated for respiratory distress with dexamethasone after birth have been reported to have less cerebral grey matter at term, and to have delayed growth, impaired cognitive, neuromotor function and IQ, and increased risk for disability at age 8[87,88]. In one study, multiple courses of synthetic GC were associated with increased risk of neurosensory disability at 5 years of age, relative to risk from a single course treatment[89]. Another study which found a benefits of multiple courses of antenatal GC in terms of decreased newborn respiratory distress reported no increased risk of neurosensory disability in follow-ups, but did find increased risk for hyperactivity at age 2 and borderline associations with behavioral regulation and ADHD in 6-8 year olds[90–92].

In rhesus monkeys, a dose-dependent degeneration of neurons was reported after antenatal DEX[93]. In sheep, repeated maternal doses of betamethasone increased lung function in pre-term lambs, but also led to lower birth-weight, a significant indicator of long-term health risk in human babies[94,95]. Contributing to the decrease in ovine birthweight due to prenatal GC was the significant decrease in weight of a number of organs including the thymus, kidney,

liver, and brain (where decreased myelination was reported as well[96]). Interestingly, lambs given one betamethasone dose during the third-trimester were found to have increased CORT production in response to CRH at 1 year of age, while those receiving the initial dose followed by three additional antenatal doses did not[97]. In a rat cell culture model of neuronal development, a subclinical dose of DEX was found to enhance cell viability at the expense of DNA synthesis and neuronal differentiation, as well as promoting adrenergic over cholinergic fate[98]. Another cell culture model using human hippocampal progenitor cells found that chronic DEX treatment during proliferation/differentiation led to long-lasting methylation changes in poised bi-valent promoters and an increased transcriptional response to subsequent acute challenge[99]. Intriguingly, the largest long-lasting effect (-20.1% methylation compared to control after 20-day) was found in the locus of the GR chaperone *FKBP5.*

#### 1.1.5.2. Fetal exposure to maternal cortisol

While synthetic GC administered to the mother are believed to freely cross the placental barrier, the exposure of fetal tissues to endogenous GC is limited by the expression of the enzyme 11ß-hydroxysteroid dehydrogenase type 2 (HSD2), which converts endogenous GC molecules to inactive ketone forms. This enzyme is expressed dynamically in fetal tissues throughout development as well as in the placenta where it inactivates the majority of maternal GC[100,101]. However, correlation has been shown between maternal and fetal GC levels, and even a small percentage of maternal CORT passing through the placental barrier can double the normal fetal blood concentration, which is much lower than that of the mother[102,103]. Chronic maternal stress may also decrease the efficacy of the GC barrier, as in animal models chronic stress has been shown to decrease HSD2 expression and increase fetal

exposure to maternal GC[104,105]. The placenta also produces CRH when stimulated by maternal CORT (and by fetal CORT once the fetal HPA axis comes online). This placental CRH leads to fetal ACTH and CORT production, in addition to that produced by the mother. Importantly, in contrast to the negative feedback between CORT and hypothalamic CRH production, CORT has a positive feed-forward effect on placental CRH which increases steadily throughout pregnancy and rapidly as birth nears, and may play a role in timing parturition[106].

#### 1.1.5.2.1. Long-term health effects of pre- and peri- natal stress

It is estimated that ~15% of pregnant women experience extended non-psychotic mental disorders such as depression and anxiety[107]. Although no broad consensus exists for how these complex emotional states relate to CORT levels their risk factors include low socio-economic standing and lack of supportive relationships, highlighting a similar etiology with chronic psychosocial stress and allostatic load. Thus, the prevalence of these states may offer a reasonable (and likely conservative) proxy for prevalence of chronic maternal stress. As noted above, maternal stress mediators including CORT can be vertically transferred to the developing fetus, and there is evidence that a maternal state of chronic stress programs long-term changes in function of the offspring's HPA axis and disease risk[71,81,108]. One theory is that maternal GC serve to tune the fetal HPA axis to respond appropriately to the environment outside the womb, but that this can be mal-adaptive if the environment later in life is incongruent with the developmental one. This has been called the "Match/Mismatch" theory, and is essentially an evolution of the "Thrifty Phenotype" or Barker Hypothesis regarding the Developmental Origins of Health and Disease, although Barker focused primarily on negative long-term effects of early-life malnutrition[109,110].

#### 1.5.2.1.1. Human studies of long-term health effects from maternal stress/cortisol

Both the Barker and Match/Mismatch theories place fetal programming at the origin of long-term health, and relate to the Allostatic Load model of disease as biomarkers of Allostatic Load in a mother (e.g. CORT) clearly influence fetal development. Maternal salivary CORT level during a stressful prenatal procedure (amniocentesis) has been shown to be predictive of birthweight[111]. As birthweight is a strong indicator of long-term health, this indicates that reactivity of the maternal HPA axis may predict future offspring health. This also demonstrates the overlapping domains of stress and metabolic programming. More direct evidence of an HPA axis programming effect exists. In one study, high amniotic CORT at mid-gestation was correlated with a higher basal CORT level at 17 months of age as well as an inverted CORT response to separation from the mother[112]. Correlation between mid-gestational maternal and neonatal ACTH and CORT levels was demonstrated in another study, although a prevalence of major depressive and bipolar disorders in that study population may limit generalization[113]. In a more broadly inclusive study of mother/infant dyads elevated CORT response and blunted recovery to heel prick procedure were found in infants of mothers with higher CORT levels measured at mid-gestation[114]. Higher maternal perceived stress during early/mid pregnancy also correlated with more aroused infant behavior during recovery from the heel prick. Pregnancy-specific prenatal anxiety (e.g. fear that the child will be born with disability) has also been linked to infant CORT reactivity[115].

The effects of prenatal stress on offspring HPA function may extend through childhood, as modest correlations with a child's CORT level on the first day of school and adolescent diurnal CORT levels have also been measured[116,117]. Neurobehavioral phenotypes in childhood have

also been linked to prenatal maternal stress and CORT levels. These include ADHD (as with synthetic GC administration) and autistic traits[118] as well as anxiety[119]. One retrospective study using plasma samples frozen between 1959 and 1966 has reported an association of higher maternal CORT during the third trimester with decreased IQ at age 7[120]. However, the reliance of this study on dated questionnaires and the lack of controls for important factors such as sampling time of day and food intake (participants had not fasted) calls for caution in interpreting these results. Decreased grey matter at 6 to 9 years of age has also been linked to mid-gestation maternal anxiety levels[121], but another recent study has shown that higher CORT (while within the normal range) during the third trimester leads to thicker brain cortex and improved performance on intelligence tests of children in the same age group[122]. This fits with the fetal maturation role of rising GC in late pregnancy. Yet another study found that multiple major stress events during pregnancy led to lower reading scores in 10-year-old girls but higher reading and math scores in boys[123]. It is intriguing to note that maternal CORT level during early (but not late) pregnancy has been linked to a significant increase in amygdala volume in 7-year-old girls but a trend toward increase in hippocampal volume in boys of the same age, effects with potentially opposite effects on HPA regulation[124]. Similarly, sex-specific differences were found in assessments of executive function in 6-to-9 year old children, where level of Pregnancy-Specific Anxiety during the first two trimesters (but not third) accounted for a decrease in inhibitory control in girls but not boys[125]. Studies indicate that Pregnancy-Specific Anxiety occurs most often early on and decreases over the course of gestation, while at the same time risk for depression increases[126], and these data highlight the potential for complex and dynamic interactions of sex, timing, and nature of maternal stress of early development.

Although many of the above-noted correlations between maternal stress/CORT and offspring outcomes could be attributable to prenatal exposure to maternal GC, they could also be driven by underlying genetics, inherited predisposition, or learned/acquired behavior. A few human studies have attempted to separate the contributions of prenatal environmental stress from genetics. A study of in-vitro fertilized offspring found significant effects of maternal stress level on birth weight (lower) and antisocial behavior (higher) in both related and cross-fostered mother-child pairs. Conversely, an effect of prenatal stress on ADHD was only found in biologically related pairs, indicating a genetic drive, while the effect on child anxiety level was found to be mediated by the mother's post-natal mood[127]. In another study, child cognitive development was found to suffer a deficit in mothers who had increased objective exposure to life-stress related to a severe ice storm during their first or second trimester[128]. A Finnish study using maternal fear of exposure to radiation from the Chernobyl disaster as the "natural" source of prenatal stress found that fetuses in the second trimester of development at the time were at a greater risk for depression and ADHD as adolescents[129]. However, the underlying population here was selectively enriched for those at higher risk of familial alcoholism and so may not be broadly representative. There were also potentially confounding differences in socioeconomic status and weight at birth among study populations. Although the authors pointed to higher birth weight in the prenatally stressed group as evidence of good health and no ill effects of actual radiation exposure, this may not necessarily be the case. A different study found that prenatal stress exposure due to maternal bereavement increased the risk of overweight/obesity in adolescents[130]. In all, human studies point convincingly to effects of prenatal stress on long-term health, however they also illustrate the difficulties of performing

human studies with enough experimental control to pinpoint cause and effect. Further, none of these mentioned studies which attempted to untangle developmental programming from hereditary factors measured CORT or affiliated biomarkers directly. Lastly, at this time few if any studies have looked at how/whether the effects of perinatal HPA programming extend into late adulthood.

**1.1.5.2.1.2. Evidence from animal studies for programming effects of maternal stress**

Studies using animals point more convincingly to mechanisms of fetal HPA programming by maternal stress. Chronic restraint stress in pregnant rats has been shown to decrease placental HSD2 expression, thus increasing fetal exposure to maternal GC[104,105]. Fetuses subjected to the prenatal restraint stress regime also had lower body weight, less pancreatic beta-cell mass, and lower ACTH and blood glucose. Higher methylation of CpG dinucleotides in the HSD2 promoter in stressed placentas was shown to coincide with the decrease in placental HSD2 expression. This was also correlated with lower HSD2 promoter methylation in the fetal hypothalamus, evidence of epigenetic programming. Chemical inhibition of HSD2 in pregnant rats also caused decreased birthweights, as well as increases in adult offspring blood glucose and insulin. Importantly, these effects were dependent on the mother having intact adrenal glands[131].

There is abundant evidence that developmental calibration of the HPA axis continues in the period directly following birth, during which mammalian young experience a period of stress hypo-responsiveness that may protect brain development from the detrimental effects of high GC. Though human infants are born with an intact CORT response to stressor (e.g. separation from mother for doctor's examination), this responsiveness decreases between 2-6 months of age and remains low until ~15-18 months. But this state of suppressed CORT is dependent on

parental caregiving and attentiveness[132–134]. In the rat, the stress hypo-responsive period occurs from roughly postnatal days 3-14, and is maintained by maternal care (i.e. licking, grooming, and nursing behavior) and disrupted by prolonged maternal separation, which increases pup HPA activity[135]. Rodent pups, like human newborns, are underdeveloped at birth and dependent on maternal care. Rat dams can be segregated by the level of care they show newborn pups under undisturbed circumstances into "high-licking" and "low-licking" subgroups. Adult offspring of "low-licking" dams (i.e. those receiving less maternal attention) show HPA hyperactivity in terms of both ACTH and GC levels, increased CRH mRNA, and decreased GR expression in the hippocampus likely indicating impaired negative HPA feedback[136]. This decreased expression of hippocampal GR was subsequently shown to be accompanied by increased CpG methylation in the GR promoter, suggesting epigenetic programming of the HPA axis by maternal care[137]. Intriguingly, both hippocampal GR expression and HPA hyperactivity could be rescued in the adult offspring by cerebral infusion with a histone deacetylation complex inhibitor.

In rat cross-fostering studies, maternal behavior and level of fearfulness were shown to be transferred to rat offspring through maternal care[138]. Behavioral defects were accompanied by decreased hippocampal GR expression and increased CRH expression. All of these outcomes, however, could be reversed by daily mild handling of pups of low-licking mothers, a protocol that has been long recognized to impart a level of stress resilience to pups[139]. Handling also rescued the reduced expression of anxiety-inhibiting benzodiazepine receptors in the amygdala of offspring of low-licking dams. In a study where *pre*-natal stress (repeated maternal restraint with bright illumination) was found to induce prolonged GC production in adults in response to

stress, as well as increased anxiety behavior, mild postnatal handling was found to have the opposite effect on behavior[140]. These data suggest that early-life stress exposure is 25avid25on (with an inverted U-shaped response similar to direct GC exposures[141–144]), conferring resilience or other benefits below a threshold, but harmful if too severe.

The susceptibility to effects of pre- and peri-natal stress show dependence on genetics. In mice for instance, C57BL/6J (B6) dams have been reported to display a measurably higher level of baseline maternal care than BALB/c, and this correlates with decreased anxious behavior and CORT response to stress in their offspring. Cross-fostering of BALB/c pups to B6 dams significantly decreased anxiety-like behavior in adult offspring. Cross-fostering in the opposite direction produced elevated basal GC in B6 mice fostered by BALB/c dams but not a significant increase in anxious behavior, likely indicating some inherent resilience[145]. Strain-specific effects of pre-natal stress on CORT and hippocampal gene expression response to stress have also been reported in rats[146]. In human studies, prenatal stress has been shown to interact with gene variants involved in GC and neuronal signaling pathways to modulate risk of psychiatric and behavioral disorders[147].

### 1.1.6. Zebrafish as a model for glucocorticoid research

Over the previous two decades the zebrafish, *Danio rerio*, has emerged as a powerful model organism for studying GC signaling, with the majority of such studies having taken place in just the last five years (via PubMed). However, several intrinsic characteristics had previously made zebrafish a favored organism among developmental biologists. These include the large number of offspring produced (up to 200-300 per mating pair), external fertilization and embryonic development, and optical transparency of the embryo. Zebrafish embryos also develop rapidly,

going from single cell to free-swimming larva in a few days. With the rise of genetic manipulation techniques such as morpholinos for gene knockdown, transposon-mediated transgenics, and eventually CRISPR for gene editing, the large one-cell stage of the embryo provides a relatively easy target for micro-injection protocols. These techniques can be used with great success in zebrafish. In the Coffman Lab, for example, we have at times achieved greater than 80% editing efficiency in F0 CRISPR knockouts.

#### 1.1.6.1. Conservation of glucocorticoid signaling mechanisms, and notable divergences

Despite evolutionary distance, the zebrafish and human genomes are similar, with roughly 70% of zebrafish genes having identifiable human orthologs and vice versa[148]. Due to multiple whole genome duplications in vertebrate ancestry, including one duplication since the divergence of teleost and tetrapod lineages, many human genes have two or more zebrafish orthologs. Approximately 2900 zebrafish genes have such duplicates but, in contrast to many teleosts that have been studied, zebrafish have retained only one copy of the *nr3c1* gene that codes for the GR, the DNA- and ligand- binding regions of which are highly conserved across vertebrata[149]. As in humans, alternative splicing results in a lowly expressed beta isoform of the GR protein in zebrafish; however, the function of this minor isoform remains unresolved in both species[150]. Also, in common with its human ortholog, the zebrafish *nr3c1* gene contains multiple potential translational start codons, and data from our lab has indicated these are functional (see results in Chapter 3). Upstream in the GC signaling pathway, zebrafish have only one copy of the *crh* gene, like mammals and unlike many fish. Zebrafish do retain a duplicate copy of the *pomc* gene that codes for the proopiomelanocortin protein that is cleaved to produce ACTH. However, the cleavage site of one paralog has been mutated so that only one gene generates

functional ACTH[151]. It is a bit of a curiosity that zebrafish have lost duplicate copies of genes involved in each level of the HPA axis, however it makes *D*. *rerio* a tractable model for studying the vertebrate GC signaling axis.

The tissues of the HPA axis and their functions are essentially conserved from humans to zebrafish, with the caveat that in *D. rerio* and other teleosts CORT is produced by interrenal cells dispersed throughout the head kidney rather than by a gland proper. Hence the HPA axis is referred to as HPI (Interrenal) axis in fish. However, more notable differences between zebrafish and mammalian corticosteroid signaling do exist. Teleosts lack the *cyp11b2* gene and thus do not produce the mineralocorticoid aldosterone[152]. The lack of this competing ligand may make the MR relatively more responsive to CORT levels in zebrafish (although the MR has affinity for other steroids as well) and work comparing the acute stress response in GR and MR mutant zebrafish has shown that the two receptors work together to regulate CORT dynamics and behavior[153]. CORT transport through the blood also may be significantly different in zebrafish than mammals. In mammals, albumin accounts for a large percentage of plasma protein and, along with the dedicated corticosteroid binding globulin (CBG), binds roughly 90% of GC creating a reservoir of inactive hormone in the plasma. Although the majority of protein types detected in zebrafish plasma are also found in human plasma, zebrafish lack albumin and CBG[154]. Zebrafish do have a Vitamin D binding protein (*dbp*) with some homology to albumin[155], but whether this or other zebrafish blood proteins play a role in transporting CORT is unknown.

#### 1.1.6.1.1. Glucocorticoid receptor mutants

Zebrafish mutants lacking functional GR have the advantage of being viable throughout adulthood, in contrast to mammalian systems wherein loss of the receptor results in neonatal death through mechanisms previously described. Several viable GR mutant zebrafish lines have been published, and locations of these mutations are shown in Figure 3.1. However, our lab and others have noted decreased survival rate in mutants at embryonic (unpublished data) and post-larval stages[156]. In 2012, a GR mutant, *s357*, was identified in a behavioral screen for depressive-like behavior[157]. A single nucleotide polymorphism was found to disrupt the DNA-binding domain (DBD) of the GR and abolish DNA binding and transcriptional regulation of target genes (though preserving the ability of the GR to bind CORT and translocate into the nucleus, as well as potential for protein-protein interactions). These mutants displayed HPI hyperactivity, with elevated basal and stressed levels of CORT and basal *crh* and *pomc* expression, as well as lack of suppression of CORT after treatment with DEX (i.e. the dexamethasone suppression test) indicating that negative feedback regulation of the HPI axis was not intact. Behavioral rescue in mutants with anti-depressant and anxiolytic drugs revealed a crosstalk between genomic GR signaling and GABA- and serotonergic circuitry, but not norepinephrine or dopamine pathways.

GR *s357* mutants have been found to suffer tissue defects in heart (reduced trabecular network) and intestine (shortened villi) that progress with age, and increased sub-cutaneous fat stores[156]. Lower heart rate and blunted inflammatory gene response were also measured in mutant larvae. This blunted inflammatory response is particularly intriguing as our lab has noted similar defects in inflammatory gene expression in adult WT fish exposed to elevated

CORT only during early development[158]. The latter inflammatory defects were measured in response to both tail-fin injury and response to lipopolysaccharide (LPS, mimicking bacterial infection). Subsequently, we have found broad similarities in the transcriptomes of vehicle-treated $GR^{-/-}$ larvae and WT larvae treated with chronic CORT, suggesting that chronic CORT treatment induces resistance to genomic GC signaling[159]. Mutation of GR and treatment with exogenous GC have also been shown to alter zebrafish leukocyte migration in response to injury, although the reported effects differ depending on timing and nature of treatment and injury[160].

With the advent of CRISPR, several labs including our own have generated GR mutant zebrafish lines to further exploit the usefulness of zebrafish to investigate vertebrate GC signaling[161]. Like the *s357* strain, mutants with a 7-bp deletion in exon 2 leading to a truncated protein display hyper-cortisolemia. These mutants were also found to have increased muscle mass and protein synthesis, along with decreased protein catabolism and abrogated blood glucose response to stress[162]. These findings beautifully illustrated the role of the GR in systemic energy balance, and that restriction of glucose uptake by muscle cells is key to elevating blood glucose in response to challenge, likely as fuel for the brain. The same mutant line was also used alongside a MR knockout to demonstrate the coordination of the two corticosteroid receptors in maintaining postnatal growth, insulin and triglyceride levels[163,164].

Like humans, zebrafish are diurnal, and display circadian behavior patterns that are entrained by rhythmic stimuli such as light cycles or feeding schedules. In this context, it has been shown that treatment with a high level of the synthetic GC prednisolone increases the amplitude of expression of a luciferase reporter for the circadian *per3* gene, and that this

increase of expression is dependent on a GR with functional DNA binding. In our lab we have similarly found that chronic treatment with CORT induces a modest increase in expression of the paralogous *per1a.* Elsewhere, a functional GR has been shown necessary to entrain circadian feeding behavior in zebrafish[165]. The GR has also been shown necessary for retinal light adaptation[166], and somewhat reciprocally, eyeless mutants for the retinal homeobox gene *rx3* are CORT deficient[167]. Comparison of transcriptomes of these *rx3* mutants with WT larvae indicated altered expression of roughly half of rhythmically expressed genes (nearly a quarter of all genes measured). These affected genes were enriched for involvement in metabolism and cell cycle regulation. Strikingly the rhythmic expression of more than half of the affected genes was rescued by treatment with a *constant* concentration of DEX, indicating that rhythmicity of GC levels may be more important for some downstream processes than others.

**1.1.6.2. Zebrafish prenatal stress models**

Given the high level of conservation in the GC signaling axis and the ease of manipulating externally developing embryos, several labs have begun to use zebrafish as a model to look at the effects of prenatal stress and CORT. This work has built on work done around the turn of the 21st century that established the basic timing of HPI development in *D. rerio.* Maternal GR mRNA and CORT are deposited in the embryo but are largely depleted by the time of hatching around ~48 hours post-fertilization (hpf), at which point embryonic transcription is well underway and tissues of the HPI axis are established and functional[149,168]. In our lab, the expression of GR targets *fkbp5* and *klf9* follows GR mRNA expression, being relatively high immediately after fertilization, then decreasing to a minimal level by 2-3 days post-fertilization (dpf) before rebounding again by day 4 (see Figure 4.1). Though embryos can produce a basal

level of CORT by 48 hpf, a measurable CORT response to stress is not mounted until roughly 4 dpf. The lapse between CORT productivity and stress responsiveness appears to be due to lack of neurodevelopment and thus sensitivity to stimuli, as CRH and ACTH are also produced by 1-2 dpf and thus not limiting factors. This stress hypo-responsive period is reminiscent of that found in mammals. Also reminiscent of mammalian development, maternally deposited GR may play a role in inflation of the zebrafish swim bladder (homologous to the mammalian lung) as defects in inflation were found alongside other developmental defects following blocking translation of maternally deposited GR transcript with morpholino[169]. Morpholinos have also been used to demonstrate that the GR-target matrix metalloprotease 13 (*mmp13*, a collagenase) is necessary for normal early development[170]. However, use of morpholinos has fallen out of favor due to concerns about potential off-target effects[171].

There is some limited evidence that elevated maternal CORT in zebrafish results in more CORT deposited in the embryo, and as in mammals there appears to be protection in place to limit this occurrence. Five days of fasting stress were shown to increase whole body CORT ~4-fold in female adults[172]. Embryo CORT content however was only significantly increased in embryos laid by stressed females toward the end of a 10-day breeding period following the fast. In another experiment, female fish were fed a diet spiked with CORT for 5 days and then spawned over the course of the following ten days. CORT-fed females produced embryos with significantly higher CORT levels only on the third day after the end of their feeding regime, but not the days before or after[173]. One possibility suggested by the authors was that CORT incorporation into the eggs would be maximal only in oocytes undergoing yolk body accumulation during the treatment window. Given the range and variability of embryonic CORT

measured, alternate explanations could include genetic variability among the females as well as unaccounted for confounding stressors. Repeated spawning—although limited in these studies to every other day for a given fish—is considered by some an unhealthy stress for fish. Unlike fasting stress, dietary CORT did not result in elevated whole-body CORT and was cleared quickly. Also, unlike fasting, dietary CORT did cause significantly higher CORT in ovaries, potentially indicating different routes of transport/clearance. Subsequently, dissected ovaries treated *ex vivo* with CORT showed a marked upregulation of *hsd11b2* expression, indicating a protective maternal barrier like that found in mammalian placenta. In a separate study, no effect of dominant/subordinate hierarchical status was found either on maternal whole-body or embryo-deposited CORT, although offspring of subordinate females produced elevated CORT and *crh* levels at 48 hpf[174]. It should be emphasized here that whole body CORT measurements represent something of a "black box" in relation to tissue specific rates of CORT production, utilization, and clearance. In our lab we have found evidence of long-term programming on rates of CORT production and tissue transport[175].

Given the known ability of maternal CORT to cross the placental barrier and affect development in mammals, it follows that our lab and others have taken advantage of the external fertilization and development of zebrafish embryos to circumvent some of the complex interactions inherent in mammalian maternal stress models. In zebrafish, direct manipulations of embryonic GC levels can be made fairly easily. While this approach does not model the numerous signaling pathways involved in maternal stress, it does allow for fine control of embryonic exposure to CORT. One method that has been used with some success by the Vijayan Lab is microinjection of embryos. CORT (32 picograms) delivered in this manner at the

one-cell stage was found to lead to an increased rate of heart deformities and under-expression of cardiac genes in the period leading up to hatching, as well as reduced heart-rate in response to a stressor in post-hatch (72 hpf) larvae that displayed mild or no apparent heart deformities[176]. This single injection of CORT was sufficient to increase the CORT level throughout the window of the study. For comparison, injection of antibodies to CORT were used to decrease the hormone's availability during development[177]. This led to increased *crh, pomc, hsd11b2, star* (Steroidogenic Acute Regulatory Protein) and *nr3c2* (Mineralocorticoid Receptor) transcript levels at 48hpf, as well as an accentuated CORT stress response at 72 hpf, effects all opposite of those seen in embryos injected with CORT. These results strongly support the theory that CORT levels during early development programs the HPI axis. Injection with CORT antibodies also led to an upregulation of GR mRNA and mesodermal defects. A subsequent study by the same group found that injection of 75 pg of CORT into one-cell embryos led to increased neurogenesis in certain brain regions (including the pre-optic region of the hypothalamus) as well as decreased thigmotactic behavior in 4 dpf larvae[178]. The authors interpreted the reduced thigmotaxis as evidence of increased boldness (or reduced fearfulness). In our experience, 4 dpf larvae swimming behavior is largely reactive to stimulus (and less free-swimming than at 5 dpf when feeding begins, for example), and another interpretation of the data is that the injected CORT increased sensory input or sensitivity. This idea is supported by the elevated swimming response to light that the authors reported as well as the enhanced neurogenesis in the pre-optic area, a region which receives sensory input.

A separate study by Higuchi has recently reported that 4 days of maternal fasting led to increased (though not statistically significant) maternal CORT measured in 10 hpf embryos, and

suppressed neurogenesis in the forebrain of larvae as measured at 5 dpf[179]. No morphological or volumetric differences were found in brains due to treatment. Given that there was a significant increase in the mitotic marker phosphorylated histone H3 reported at 3 dpf, one possibility is that elevated CORT in fact accelerated the course of neurogenesis. This would agree with, rather than contradict, the report from the Vijayan Lab of increased neurogenesis, which although measured in 5 dpf larvae was labeled by EdU pulse at 24 hpf. Higuchi also found that treating developing embryos with 5µM CORT in the media from 0-5 dpf also decreased staining for markers of proliferation in 5 dpf forebrain.

Adding treatments directly to the media of developing embryos/larvae is an approach several labs including our own have used. D'Agostino, et al., found that treatment with a high level of exogenous CORT (100µM) for the first 48 hours after fertilization increased the hatching rate of embryos. Expression level of *hsd11b2* (coding for the CORT metabolizing HSD2 enzyme) was significantly and dynamically affected by the treatment as well, being ~7-fold higher than controls at 48 hpf, then decreasing to 1/3 of control levels at 72 hpf before rebounding back to greater than 2-fold controls at 96 hpf. Basal expression levels of the stress-responsive neuronal gene *c-fos* were increased by the treatment, while levels in response to physical (swirling) and osmotic challenges were respectively blunted and enhanced after treatment. In another study, treatment with 100µM of the potent synthetic GC dexamethasone for the first 5 days of development was found to suppress endogenous CORT while also accelerating the hatch rate of embryos[180]. Conversely, knockdown of GR with morpholino was found to delay development and decrease larval activity and response to stimuli at 4 dpf. Larvae from both DEX and GR knockdown treatment groups were followed into adulthood, where fish treated with DEX

during development were found to be larger and have elevated blood glucose and hepatic expression of the gluconeogenic gene *pepck*. DEX treated adults also displayed more bold behavior and an increased CORT response to stress, indicating long-term effects on HPI function of the developmental exposure. Interestingly, the authors also looked at developmental hypoxia as an experimental condition and found that the effects on larval development were similar to those of GR knockdown. Intricate cross-regulation between hypoxia-inducible factor (HIF) and GC signaling pathways has recently been demonstrated using zebrafish larvae[181], and stressors including HIF signaling have also been shown to regulate embryonic hematopoiesis via the HPI axis[182].

Given the ease of adding treatments to water, zebrafish are increasingly used in screening for toxicant effects. In a screening of steroid hormones, modest decrease in activity level was found in larvae treated with GC, along with a significant increase in trough expression level of circadian genes including *per1a* and *nr1d2a*[183], two genes our lab has also found increased by chronic CORT exposure. Another group found that low concentrations of CORT and the synthetic prescription GC clobetasol propionate that are found in the environment impacted larval muscle and heart function, as well as expression of genes involved in immunity, glucose metabolism, development and the circadian clock[184]. Interestingly, while clobetasol had larger effects on immune and developmental genes, CORT had a greater effect on genes involved in glucose metabolism including *g6pca*, a gene our lab has found consistently elevated by chronic CORT treatment as well. Effects of treatments on some genes were inconsistent when measured at different timepoints (96 or 120 hpf), or not significant until the later timepoint, perhaps highlighting the rapidly changing dynamics of gene expression in developing zebrafish.

#### 1.1.6.2.1. Previous work by the Coffman Lab

In the studies discussed above, a range of dosage and variety of synthetic and endogenous GC have been utilized. In the Coffman Lab the primary focus has been on the effects of a chronic 1μM dose of CORT, to model a more physiologically relevant exposure. In 2016, Hartig et al. reported that this concentration was sufficient to significantly elevate GR receptor activity in larvae as measured *in vivo* by a fluorescent transgene reporter, and to elevate heart rate and staining for reactive oxygen species[158]. RNA-sequencing (RNA-seq) of whole larvae at 5dpf indicated that CORT treatment from 0-5 dpf led to increased expression in genes involved largely in innate immunity and inflammation, as well as lipid catabolism, while genes involved in membrane polarization, synaptic transmission and cell communication were under-expressed. Using an adult tail-fin injury model it was found that though CORT treatment ended at 5dpf, effects on immune gene regulation were carried into adulthood[158]. Whereas control fish responded to injury by upregulating a collection of immune genes in the injured tissue at 2 days post-injury (dpi) and then resolved this response by 4dpi, tail fins of fish raised from treated embryos displayed generally higher basal expression of the same immune genes and a blunted or inverted dynamic response, which correlated with a higher percentage of defective tail fin regeneration. Similarly, the immune gene response to interperitoneally injected lipo-polysaccharide (to mimic bacterial infection) resulted in a blunted immune gene response in adults treated with chronic CORT during early development.

Hartig also found that chronic CORT treatment during development caused increased whole-body CORT in adulthood, indicating long-term effects on HPI output[158]. In a follow-up experiment, evidence was found that CORT production was increased in the head kidney (the

site of interrenal cells) of fish treated with developmental CORT, and that in response to fasting stress more CORT was taken up in target tissues including that brain[175]. Correspondingly, blood CORT was higher than in controls in fed animals but lower than controls after fasting stress, seemingly indicating altered binding/transport kinetics. In unpublished preliminary data, I also found evidence of defective blood glucose homeostasis in these adult fish. Whereas in control fish blood glucose levels were similar whether fed or fasted, fish exposed to elevated CORT as embryos had depleted blood glucose after fasting, and elevated glucose after being re-fed. Together these data begin to illustrate a set of long-term multisystemic effects due to developmental CORT exposure, which involve changes in HPI axis dynamics and physiological processes governed by the axis including immunity, metabolism, and homeostasis.

To elucidate molecular mechanisms underlying these long-term physiological symptoms of developmental CORT exposure, our lab performed an Assay for Transposase-Accessible Chromatin using Sequencing (ATAC-seq) on blood cells of adult fish[175]. This technique was used to assay whether chronic CORT treatment from 0-5 dpf had long-term effects on chromatin accessibility. Among the loci where chromatin accessibility was most increased in treated animals were the promoters of several known GC targets including *sgk1, glcc1l,* and the GR chaperone *fkbp5.* The promoter of *klf9* was the third-most affected site in the genome as well as the top-ranked transcription factor, and a further analysis of the ATAC-seq dataset showed that the binding motif for Klf9 was highly enriched in sequences from the top 250 peaks displaying more accessible chromatin. These data suggested that *klf9* may be not only a target of the GR, but a feed-forward regulator of the transcriptional response to GC. Among the most significantly affected genes in the ATAC-seq data *klf9, fkbp5*, and *chac1* (involved in redox and

neurogenic pathways) were notable for also being among the most significantly upregulated genes in RNA-seq of treated 5dpf larvae. Chromatin immunoprecipitation (ChIP) using antibodies for histone 3 lysine 4 tri-methylation (H3K4me3) was also performed and it was found that this epigenetic mark of active transcription was increased in the promoters of both *klf9* and *fkbp5* in the blood of treated adults. Across several experiments using quantitative polymerase chain reactions (qPCR) to ascertain gene expression, levels of *klf9* and *fkbp5* were found to be highly correlated, and significantly increased by CORT treatment overall, although not in every instance. These data were sufficient to pique our lab's interest in further investigating a role for *klf9* in GC signaling. Further, literature that had previously been published and steadily accumulated during the period studies in this dissertation were performed reinforced our interest in *klf9*. That literature will be discussed in the remaining sections of this chapter.

### 1.2. Krüppel-Like Factor 9

Krüppel-Like Factor 9 (Klf9) is a member of the Krüppel-Like Factor (KLF) family of transcription factors, all of which share similarity to the transcriptional repressor Krüppel (German for "cripple") first discovered in *Drosophila* for involvement in patterning the segmented larval body plan[185]. In vertebrates KLFs play important roles in development as well, and are expressed dynamically throughout development in tissues derived from all three germ layers (endoderm, mesoderm and ectoderm)[186]. Eighteen KLFs have been identified in the human genome, and 24 in the genome of zebrafish, with six human KLF (but not Klf9) having duplicate paralogs in *Danio*[187]. All KLF members share a highly conserved DNA-binding domain (DBD) toward the C-terminus of the protein comprising three C2H2 zinc-finger domains. The

DBD binds to GC-rich sequence motifs common throughout the genome. The N-terminal ends of KLF proteins are more variable and contain domains for interacting with various transcriptional co-regulators. For an example, see Figure 3.2A. The N-terminus of Klf9 and its most closely related KLFs (sometimes referred to as "Group 3") contains a domain for interacting with the Sin3a histone de-acetylation complex, while other KLF subgroups contain N-terminal domains known to interact with alternate co-regulators including acetyl-transferases and the repressive C-terminal Binding Protein[188]. Thus, regulation by KLFs may either promote or repress target gene expression, depending on the particular KLF as well as the cellular context and cofactor milieu. Both activating and repressive activities have been reported for Klf9[189,190] though recent evidence also suggests that Klf9's functional role can be predominantly repressive in a given tissue such as hippocampus[191]. Given the variety of cofactors among different KLFs and their ability to bind similar genomic sequence motifs it is believed that KLF proteins provide a context-sensitive level of fine-tuned transcriptional regulation; the precise regulation of target gene expression will depend upon which KLFs are expressed in a given tissue, as well as what upstream signals they are responsive too. KLFs respond to numerous signals including insulin and circulating hormones, and are effectors of various nuclear hormone receptors, and it seems that they function as nodes to integrate and potentiate various inputs into a coordinated transcriptional response[192].

KLFs play important roles in basic cellular processes such as metabolism, where they contribute to matching the usage of macronutrients to energetic demands of the whole organism[193,194]. KLFs are also involved in determination of cell fate[186]. In fact, Klf4 was one of the four "Yamanaka Factors" first used to reprogram fibroblasts into pluripotent stem cells[195],

and a core group of KLFs including Klf2, Klf4, and Klf5 was found necessary to maintain pluripotency of embryonic stem cells[196]. These KLFs are all members of a KLF subgroup (sometimes referred to as "Group 1") defined by an N-terminal trans-activating domain. Loss of members of this group leads to embryonic or neonatal death in mice. Among these, *Klf2* and *Klf5* mutants exhibit defects in lung expansion[197] and surfactant production[198]. In mouse macrophages *Klf2* has been shown to respond to dexamethasone treatment[199]. It is possible that a molecular pathway involving GC and *Klf2* response could contribute to the enhanced fetal lung maturation caused by prenatal GC administration, but this possibility has not been tested to my knowledge. Interestingly, in mouse macrophages *Klf9* transcription was also induced by DEX, and the pulsatility of *Klf2* response to DEX was lost when *Klf9* was knocked out, suggesting dynamic regulation of *Klf2* by an incoherent feedforward loop between the GR and KLF9.

### 1.2.1. Identification of Klf9 as a direct glucocorticoid receptor target

A body of evidence revealing that Klf9 is a direct target of the GR has come from the Denver Lab at the University of Michigan. However, studies first identified Klf9 (originally known as basic transcription element binding protein, BTEB or BTEB1) as a target of *thyroid* hormone (T3) in developing *Xenopus* and rat neurons[200,201]. In rat neuronal cell culture, T3 induced expression of Klf9 only once cells became post-mitotic, and the regulation of Klf9 by T3 in brain was lost by postnatal day 30. This evidence suggests a limited window for regulation of Klf9 by T3. Notably this window overlaps with the stress hypo-responsive period in pups, during which inability to produce GC in response to stress is thought to protect neurodevelopment (see previous sections). In confluent neuronal cell culture forced overexpression of Klf9 caused an increase in

neurite outgrowth, and in a related study Klf9 knock-down inhibited outgrowth[202]. However, work by others has shown that Klf9 suppresses axon growth and regenerative capacity after nerve injury[203,204]. These seemingly disparate results are likely explained by differences in experimental designs/contexts, but they also exemplify our limited understanding of how complex regulatory networks can utilize the same basic transcription factor to generate nearly opposite physiological results.

Further experiments by the Denver lab revealed that acute stress also induces *Klf9* expression in *Xenopus* brain, mediated by CORT and the GR. This response was not affected by inhibiting protein synthesis, suggesting Klf9 as an immediate target of the GR[205]. Chromatin immunoprecipitation using myc-tagged MR identified two putative MR/GR response elements (MRE/GRE) upstream of the *Klf9* TSS in HEK cells. In mouse hippocampal cells these response elements were found to bind GR and promote transcription in reporter constructs upon treatment with CORT, solidifying *Klf9* as a bona fide GC target[206]. Both corticosteroid response elements were found conserved among Therian mammals, and one of the elements is more broadly conserved amongst all tetrapods including *Xenopus.* Intriguingly, the GRE conserved in tetrapods neighbors a thyroid hormone response element, and together these hormone response elements form a regulatory module capable of synergistically enhancing *Klf9* expression via combination of T3 and GC signals[207]. Although the authors failed to identify either of the upstream GREs found in mammals in the genomes of zebrafish or other ray-finned fish, the *Danio* genomic sequence does in fact contain multiple putative GRE upstream of the *Klf9* TSS, including two found in approximately the same region as in tetrapods (roughly 5500bp and 3500bp upstream of the TSS, respectively). Using ATAC-seq our lab has found that

chromatin around the *Danio klf9* -3500bp GRE was significantly more accessible in the blood of adult fish raised from CORT-treated embryos, as was chromatin around another predicted GRE located just 277bp upstream from the TSS[175]. Although we did not identify an ATAC-seq peak at the -5500bp GRE this location does contain a potential thyroid hormone response element, which could perhaps be evidence of an ancestral ortholog to the tetrapod GC/thyroid hormone synergy module. The lack of an ATAC-seq peak in our blood assay at -5500bp could be due to tissue specificity, developmental stage, or other important context. Our lab is currently working to use CRISPR to tag the *Danio* GR with a ChIP-grade epitope that will allow for validation and further investigation of these putative GREs and their interactions, as will be described in a subsequent chapter. A recent study has shown that GC activation of *Klf9* expression in lung cells involves both proximal and distal GR-binding enhancer elements, combining constitutive enhancer-RNA production at proximal elements and rapidly inducible looping with distal enhancers[208].

### 1.2.2. Evidence for involvement of Klf9 in glucocorticoid signaling

Additional labs have found evidence of Klf9 involvement in GC signaling. Very recently, it was shown that *Klf9* induction by synthetic GC in mouse liver leads to hyperglycemia, while deletion of *Klf9* caused hypoglycemia and was protective in a model of GC-induced diabetes[209]. In adenocarcinoma lung cell culture DEX was found to induce expression of several KLFs, including *Klf9*[210]. Interestingly, in this study timing of GR-target gene expression generally differed with the direction of regulation: induction of GR-target gene expression happened significantly faster and in advance of repression of other GR targets. These dynamics are consistent with repressive feedforward regulatory logic playing a broad role in GC-dependent

gene regulation, wherein increase of certain GR-targets could lead directly to subsequent repression of additional GC targets. An example of one such incoherent feed-forward loop (IFFL) circuit involving regulation of *Klf2* by the GR and KLF9 has been suggested by transcriptional dynamics and GR binding sites assayed in macrophages (a cell type known to be highly responsive to GC)[199]. Direct interaction between KLF9 and *Klf2* was not tested, however. In human keratinocytes, *Klf9* expression has been shown to be circadian, induced by GC, and have an antiproliferative effect[211]. Also in keratinocytes, *positive* feed-forward regulation of GR activity by KLF9 was suggested by decreased GRE-luciferase reporter activity after KLF9 knockdown[212].

A recent meta-analysis of 17 transcriptomic studies investigating effects of GC in brain or central nervous system-derived cell lines found that *Klf9* was the third-most consistently induced target of GC treatment, being significantly upregulated in seven of the studies[213]. Notably *Klf9* expression was more consistently affected by GC than some very well-known GC targets including *Fkbp5*. *Klf9* was also *the most* consistently affected transcription factor. Interestingly, though 9,605 genes were reported significantly affected by GC treatment in at least one of the studies analyzed, only 88 of these genes (0.9%) showed consistent up- or down-regulation in at least four of the studies, and only two genes in more than half of the studies. The heterogeneity of these datasets illustrates one of the challenges to advancing understanding of the complex and highly responsive gene regulatory networks involving the GR, and is something our lab has begun to deal with by performing meta-analyses of multiple transcriptomic datasets we have produced in *Danio* (see results in following chapter).

### 1.2.3. Elucidating the role of Klf9 in GC signaling

In this chapter I have attempted to summarize literature about the human health costs of chronic stress and associated allostatic load, and how those relate to HPA function and dynamics. Epidemiology shows that detrimental effects can begin during early development and have lifelong and perhaps intergenerational consequences. As principal stress hormones which are also intricately involved in early development, GC are prime candidates for mediating some of these health risks. However, epidemiological studies in general have struggled to generate a consensus, due primarily to lack of experimental control and/or resolution. Biomedical model systems have increased our understanding of the molecular mechanisms by which GC exert their effects, but have also illuminated complex dependencies of those effects on contextual factors such as tissue-type, dosage, and timing in terms of both exposure and life stage. Because of its disease and societal relevance, I chose to perform the research described hereafter within a chronic developmental exposure paradigm that had largely been established by the Coffman Lab at MDI Biological Laboratory, within which *klf9* was identified as a gene of potential importance. In the following chapters I will document the molecular, genetic, and bioinformatic methods I have used, results indicating that Klf9 is a key regulator of the transcriptomic response to GC, and studies I have undertaken to understand the mechanisms of that regulation. Lastly, I will close with a discussion of the results, their significance, and future directions which may stem from this work.

# CHAPTER 2

# MATERIALS AND METHODS

In this chapter I will describe the methods and materials used to obtain the results in Chapters 3 and 4.

## 2.1. Zebrafish husbandry

All animal procedures were approved by the Institutional Animal Care and Use Committee (IACUC) of the MDI Biological Laboratory, and all methods were performed in accordance with the relevant guidelines and regulations. Wild-type AB zebrafish were obtained from the Univeristy of Maine, Orono, and maintained in the animal facility of the MDI Biological Laboratory, in a recirculating system with a water temperature of 28.5°C, conductivity of 600-700 microsemens, pH of 7.2. Lights were timed on a 14 h light/10 h dark cycle. Matings and embryo/larvae culture were carried out using standard procedures[214]. Spawning tanks were set up overnight to allow fish to acclimate, with male and female fish separated by a divider. The following morning dividers were removed, and animals allowed to spawn. Embryos were collected in the late morning or early afternoon and disinfected for one minute with peroxy-acetic acid solution consisting of 60ul concentrated Peroxy-Serve (Axela Medical) per 40ml of E2 media, followed by two 2-minute rinses in fresh E2 media. Embryos were then transferred to petri dishes containing 40ml of fresh E2 media at a density of 100 embryos per plate or fewer. Larvae were then raised up to 5dpf in an incubator set to 28.5$^{o}$C with a full spectrum incandescent lamp on a timer synchronized to the light schedule in the main zebrafish facility.

## 2.2. Hormone and drug treatments

For CORT treatment, stock solutions of cortisol-21-hemisuccinate sodium salt (Sigma H4881) in DMSO were added to the medium to achieve 1uM concentration. For vehicle control treatment an equivalent concentration of DMSO alone was used. CORT or vehicle (VEH) treatments began ~4 hpf (just after disinfection). CORT and control media were refreshed daily. For experiments using FK506 an overnight exposure (17 hours) to either 1uM drug or vehicle control was started on the afternoon of day 4 post-fertilization.

## 2.3. Analyses of gene expression

Three methods were used to measure gene expression: Quantitative Polymerase Chain Reaction (qPCR), RNA sequencing (RNA-seq), and the Nanostring probe hybridization platform. These are described in detail in the following sections.

### 2.3.1. Quantitative polymerase chain reaction

RNA for quantitative polymerase chain reactions (qPCR) was extracted using TRIzol (ThermoFisher) according to the manufacturer's instructions. Yield and quality were assessed using a DeNovis DS-11 FX spectrophotometer. Purified RNA (200-500ng total) was treated with DNAse I (NEB) and reverse transcribed into complementary DNA (cDNA) using the PrimeScript kit (TaKaRa Bio) using a 50/50 mix of OligoDT and random hexamer primers according to kit instructions. cDNA was diluted 1:5 in nuclease-free water and 4µl of diluted cDNA used as template in 10µl qPCR reactions along with 5µl PerfeCTa SYBR Green FastMix (VWR) and 1ul of 3uM primers (300nM final concentration, see Table 2.1 for sequences) ordered from Integrated DNA Technologies (IDT), Coralville, Iowa. Efficiency of primers was validated beforehand by standard curve. qPCR reactions were run on a Roche LightCycler 480 instrument with technical

and biological replicates. Specificity of primers was verified by melt-curve analysis. Relative expression of genes of interest was calculated using the delta-delta CT (ddCT) method[215] and *eif5a* as reference gene. Examination of the results of multiple prior RNA-seq data sets indicated that *eif5a* activity was highly stable across treatments and genotypes. In many experiments *beta-actin* and/or *rpl13a* were also used as a reference gene, and this did not substantially change the results. For time-course experiments, expression of gene of interest across time was calculated relative to the median expression level of the gene of interest in all samples in that experiment.

**Table 2.1. Sequences of primers used for qPCR**

| **Gene** | **Forward Primer (5'-3')** | **Reverse Primer (5'-3')** |
|---|---|---|
| *actb2* | tgtccctgtatgcctctggt | aagtccagacggaggatg |
| *crhb* | accaattacgcacagattctcct | tggaaaggcaacgagcagag |
| *egr4* | tcggttgaagagccagagca | ctcaaacaaccaatcagcgttc |
| *eif5a* | gcttctgccacttaccccat | ggtgaacctttgcatgaccg |
| *fkbp5* | gagaatcagaggacgtgggtg | aggcgtacttgggctttaggt |
| *irf1a* | tctgctggactgatgaaggactca | gctcgtgttcgtctgttctgttga |
| *irg1l* | agaccctggttgggctaaaag | ggcgttgaactggaaagaatg |
| *klf9 exon 2* | agacgacactcttcaacatccacatc | caccaactcactagcagagactcct |
| *klf9 pre-mrna* | tgtcactggaagactagaggatg | ggccaggtacactgaaaggg |
| *marco* | agccaaggggtaaaaggagac | ttggtccaggtgagccttttc |
| *mpeg1.2* | ggaccatctttacaaaacccacag | cctgcctcatagtcattgctcag |
| *mxc* | agtacgttttgggctggagg | acgctcacaggcaatcgtta |
| *ncf1* | tcaggaaaggcgaggaaacc | atggtcgaccttcttggtgg |
| *nfkbia* | ttccctaactacagcggacac | caggttctgcaggtctacgg |
| *npas4a* | gtcccgtccacccttctga | cctcgaacagcgactcgtcat |
| *rpl13a* | tctggaggactgtaagaggtatgc | agacgcacaatcttgagagcag |

#### 2.3.1.1. Notes on sample collection for time courses

Samples for measuring baseline (i.e., unstressed) gene expression were collected as rapidly as possible to avoid changes in gene expression due to stress induced in larvae by sample collection. For each sample less than 2 minutes were taken to capture n = 3-6 larvae, remove excess water and snap freeze samples in liquid nitrogen for later processing. For time-course experiments, each sample of pooled larvae was transferred to a small petri dish during media change on the day prior to sample collection. Density of larvae per ml of media was maintained. Dishes were arranged in the incubator so that each could be removed with minimal disturbance to others. During sample collection in the early morning prior to ZT 0 (i.e., light still off in incubator), noise and room lighting were kept minimal (a single desk lamp in far corner of the room).

#### 2.3.1.2. Modeling of time-course data

Sinusoid models were fit to time-course expression data using the equation

$$y = m + a * \exp(b * x) * \sin(c * (x + d))$$

where m=MESOR, a=amplitude, b=decay rate, c=2*pi*frequency, and d=phase shift. Nonlinear least squares regression was performed using either the *nls* function in the R Stats package or in Microsoft Excel using the "Solver" function (Kemmer and Keller, 2010); both methods generated the same solutions. Initial values for constants were chosen to generate a reasonable qualitative fit before iterative fitting programs were run. When generating random data sets and model fits (see Results), initial constants were set to best fit combined data from both conditions (either VEH- and CORT-treated, or wildtype and klf9-/-, depending on the experiment).

### 2.3.2. RNA sequencing and analysis

Samples for RNA sequencing were collected at ZT 3. For sample collection, a dish of larvae corresponding to a single condition was removed from the incubator, and four replicates of n = 10 larvae were collected and immediately snap frozen in liquid nitrogen with minimal water. All replicates from one condition were collected sequentially before moving on to the next condition. Collection of 16 samples occurred over 22 min. Total RNA was extracted using the Qiagen RNA-Easy Plus mini kit (Qiagen) according to manufacturer's instructions. RNA was prepared in batches on two different days. On the first day (experimental replicates 1 and 2) lysis buffer (Qiagen) was added to all 8 frozen samples on ice before homogenization with a motorized pestle. On the second day lysis buffer was added to each sample which was then immediately homogenized. Different sample preparation likely contributes to variance between samples prepared on days 1 and 2. Thus a two-level categorical batch variable was included in downstream analysis.

RNA yield/quality were assessed by spectrophotometer (DeNovis DS-11 FX) and gel electrophoresis (Bioanalyzer Nano Kit, Agilent) before sequencing. RNA was sent to the Oklahoma State Genomics Facility for sequencing and data were processed by the MDI Biological Laboratory's Bioinformatics Core as previously described[159] (see Appendix A). EDASeq[216] carried out in R version 3.6.1 was used to further normalize data for systematic effects, using gene-level length and GC-content as downloaded from Ensembl version 98. "WithinLane" normalization with GC content was judged as superior to that based on length. Final normalized gene-level counts (which = "full") were generated using GC-based WithinLaneNormalization followed by BetweenLaneNormalization. Differential expression

analysis was carried out in R version 3.6.2 with DESeq2[217] version 1.26.0, using genotype or treatment as the comparison.

The Gorilla algorithm[218] (https://cbl-gorilla.cs.technion.ac.il/) was used for Gene Ontology term enrichment analysis, and the data were visualized using REVIGO[219] (https://revigo.irb.hr/). Venn diagrams were generated using Venny 2.1 (https://bioinfogp.cnb.csic.es/tools/venny/). HOMER motif enrichment analysis[220] was used to analyze incidence of known vertebrate motifs in promoters of genes of interest with incidence in a background list of all zebrafish promoters by running the findMotifs program (for more information see https://homer.ucsd.edu/homer/microarray/index.html) using default settings except that sequence from − 1500 to + 500 bp relative to the transcription start site was searched for motifs from 10 to 18 bp in length (results in Section in 3.5 and as published in Gans et al., 2020) or from -2000 to +2000 bp for motifs 10 to 14 bp in length (Section 4.5). KEGG pathway analysis was performed using the DAVID Bioinformatics Resources website[221,222] (https://david.ncifcrf.gov/), comparing the list of differentially expressed genes against species-specific background. For principal component analysis of metabolic genes of interest (Appendix I) Z scores were generated using log transformed RNA-seq counts. Z scores were calculated within batches (RNA preparation day 1 and day 2, see above) and scores were then compiled. PCA was then run using *PCAtools* version 1.2.0 in R version 3.6.2.

### 2.3.3. NanoString

NanoString probe sets with target- and tag-specific sequences at 5’ and 3’ tailing ends were designed by NanoString with direction and approval of myself and Dr. Coffman (see Table 2.2). Probe sets made by IDT were mixed and diluted into pools, then combined with one of 8 unique

barcoded PlexSets. NanoString assays were performed by Dartmouth College's Molecular Biology Core Facility according to manufacturer's instructions (NanoString Technologies, Seattle, WA). The probes and PlexSet pools were combined and hybridized at 67°C for 18 h with their RNA targets, with a distinct PlexSet in each 8 wells of a column in a 96-well plate. Each of the 12 columns from the 96-well plate was then pooled for processing on the NanoString nCounter Prep Station for purification of target/probe complexes and then deposited in a cartridge, immobilized, and aligned for data collection. Data Collection was carried out in the NanoString nCounter Digital Analyzer. Images were processed and an algorithm tabulated digital counts for each barcode class. An initial RNA titration test was performed for each probe set with 50 ng, 100 ng, and 200 ng RNA to optimize the RNA concentration, and 100 ng was selected for the full time-course assay. Normalized counts were exported from the NanoString nSolver program[223]. Heat maps were generated from Z-transformed log2 counts using the *heatmap.2* function in gplots 3.1.1 package[224] in R. Hierarchical clustering was determined by *hclust* function in the R stats package with the "complete" method, and distance between rows calculated by the *dist* function and Euclidean method.

**Table 2.2. Sequences of NanoString RNA hybridization probes**

| Gene | Probe Sequence |
|---|---|
| *actb2* | ccaaatgtctggcaccgccacgttccacacagcttttacaatatgcccacgcgatgacgttcgtcaagagtcgcataatct |
| *cbx7a* | ctgtgaactgtgtcgttcacttggtcctgactaactgtacatgtttctaacaaagacgcctatcttccagtttgatcgggaaact |
| *crhb* | aggtcagatctagggaaatcggcggctcctccgacctggtcaagacttgcatgaggacccgcaaattcct |
| *diabloa* | tttacattcttctaatcgatcactaacctccacccgctggccaatgatgacgaacctaactcctcgctacattcctattgttttc |
| *eif5a* | gaatccctcgctgatgtcaaccaactggtagtcatttcttttgatgttagctaggacgcaaatcacttgaagaagtgaaagcgag |
| *fkbp5* | agagctgaagcgtgcagcatagagcttttacaggtggtcacagaattgcctcaagacctaagcgacagcgtgaccttgtttca |
| *g6pca.2* | gcctgttgaaagcctcggcaacaatcatgcctgaaatgacaccagcgaaactgttgagattattgagcttcatcatgaccagaag |

**Table 2.2. continued**

| Gene | Probe Sequence |
|---|---|
| *hsp90aa1.2* | ggtctgtgagactttcatagcggattttgtccaaagcatcagaggagcaccgtgtggacggcaactcagagataacgcatat |
| *irf1b* | gccactgcgaactatcgcgctccaattgccgagtgagctgaggctgttaaagctgtagcaactcttccacga |
| *irg1l* | aaaggaggcgagcacaggcagcagcactacccagacgattgctgcattccgctcaacgcttgaggaagta |
| *klf9* | tgttgtgtcaggtaggagggacagtcaaaatgcttaaacaccagcagacacatcctcttcttttcttggtgttgagaagatgctc |
| *mpeg1.2* | gttgacggcaagtaaagtcaccagtgtctggatttctttgtgcaaattcacctgccaatgcactcgatcttgtcatttttttgcg |
| *ncf1* | ctctctgctgtaagaagcgacggctctgtttccggcaaactggagagagaagtgaagacgatttaaccca |
| *nfkbiaa* | atgaaggcacgtgtgtccgctgtagttagggaaggtaagaatggaacgcaccaatttggttttactcccctcgattatgcggagt |
| *nr1d2a* | ggaaaactcttcccagacttcatgaccgggtctggaggcgtcaacaaacgcaacagccacttttttttccaaattttgcaagagcc |
| *nr3c1* | gagcagcggtttaacactcccatctttgaattttggtaactggttgctgacttccttcctgtgttccagctacaaacttagaaac |
| *per1a* | acatggtcatgtagcttggaggaaaagatgtacccactggagcaccgttgctttcgttgggacgcttgaagcgcaagtagaaaac |
| *pomca* | cttcctcggttggtctttatgcattacgtttttgaagagtgtgagccataaaattggttttgcctttcagcaattcaactt |
| *psme2* | atatgctgcttcatccttctcatgcactagagagcgataatccatcacatcagataaggttgttattgtggaggatgttactaca |
| *psme4a* | atcgtgaaggcagtccaaaagatccgccactagcttctcgtacttcctggagtttatgtattgccaacgagtttgtcttt |
| *rhcga* | gtccagtttgggtcgataaagaatccatgatattgtgaggccgtaataggcacaattctgcgggttagcaggaaggttagggaac |
| *socs1a* | ctctcctctagcatcgaggtggtgttggaaatgatcttgaagtctctttcgggttatatctatcatttacttgacaccct |
| *tsc22d3* | tcaggcaggtcaaatttcccctgtgagagtcggagccagcagacctgcaatatcaaagttataagcgcgt |
| *rpl13a* | atctcaactttcttcttggaatagcgcagcttggccttttccatttggaatgatgtgtactgggaataagacgacg |

## 2.4. Generation of mutant lines

In order to investigate the role of *klf9* in GC signaling I used Clustered Regularly Interspaced Palindromic Repeats (CRISPR) Cas9 technology to generate two mutant lines on the widely used wild-type AB genetic background. The first mutant line is a functional knockout, *klf9*$^{-/-}$, and harbors a frameshift deletion in exon 1 upstream of the DNA binding domain (DBD) that also leads to a premature stop codon and truncated transcript predicted to abolish the DNA-binding ability of Klf9 (see Fig. 3.2) In the second mutant line, Klf9-AM, sequence for a flexible “AM Tag” epitope (engineered by Active Motif, Carlsbad, CA) has been inserted 5’ to the endogenous stop

codon to allow for immunoprecipitation with a commercially available and highly specific ChIP-validated antibody. Further details on the engineering of each line are provided below. CRISPR guide RNA sequences for both lines are listed in Table 2.3.

### 2.4.1. *Klf9*$^{-/-}$ zebrafish line

To generate the klf9$^{-/-}$ mutant line fertilized AB embryos were injected at the 1-cell stage with < 20% cell volume of an injection mix consisting of 200 ng/ul Cas9 mRNA (transcribed from linearized Addgene plasmid pT3TS-nCas9n), 100 ng/ul guide RNA, 0.05% phenol red dye, and 0.2 M KCl. Short guide RNA (sgRNA) were designed using the Benchling online platform (Benchling.com) and selected for best on/off-target scores[225,226] (see Table 2.3 for sgRNA sequences and Appendix C for potential off-target sites). DNA oligos to make templates for sgRNA synthesis were ordered from IDT and templates were synthesized using fusion PCR protocol (see Appendix D). sgRNA were transcribed from templates using MegaScript T7 Transcription Kit (ThermoFisher), and purified by phenol:chloroform extraction. Four RNA guides targeting exons 1 and 2 were designed with the intent to induce a large (~2kb) deletion between the targeted regions[227]. However, no evidence of large deletions was found in screening of injected larvae. After injections, 16 surviving 2dpf larvae were randomly selected, euthanized, and genomic DNA (gDNA) was extracted according to established protocol[228]. One microliter of gDNA was used per reaction as template for High Resolution Melt-curve Analysis (HRMA) PCR assays with SYBR Green FastMix (VWR) and 200nM primers (see Table 2.4), run on the Roche 480 LightCycler to assess CRISPR efficacy (Fig. 2.1). 9-of-16 screened larvae showed evidence of targeted exon 1 mutation. Remaining F0 larvae were raised by the animal core until large enough for genotyping by fin clip. HRMA of fin clip DNA from three surviving adult F0 fish

followed by Sanger sequencing (see Table 2.4 for primers) identified two males with targeted mutations in exon 1 upstream of the DNA-binding domain. The third surviving F0 fish was determined to be WT. The two mutant F0 males were outcrossed to wild-type AB female fish, and a random selection of 15 F1 larvae were screened with HRMA to confirm germline transmission of mutations. 6-of-15 screened larvae showed heterozygous melt-curves. The remaining F1 larvae were raised to adulthood in the animal facility.

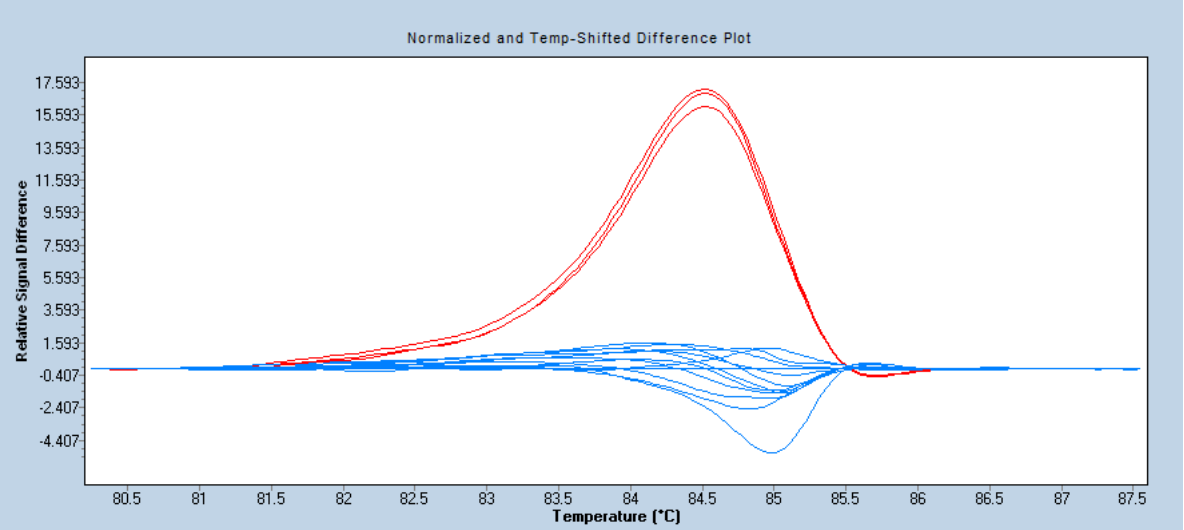


**Figure 2.1. High resolution melt-curve analysis distinguishes mutant DNA from wild-type.** A mutation in *klf9* results in a shift in the melt-curve of DNA amplified from an F0 larva injected with CRISPR/Cas9. Red lines represent technical replicates of melt-curve from a single mutant sample, shown as an example. Blue lines represent WT samples.

Once large enough, adult F1 mutants were identified by HRMA of genomic DNA from fin clips. Mutant DNA were sequenced, and three distinct mutant alleles identified (see Appendix M), each resulting from CRISPR editing events with sgRNA2 (see Table 2.3). Two of these mutations (3bp and 6bp deletions) maintained the reading frame. A 2bp mutation (see Fig. 3.2 and Appendix M) resulting in a reading frame shift and premature stop codon was identified in one F1 female, which was then outcrossed to wild-type AB. F2 progeny of this outcross were

screened with HRMA and two heterozygous male mutants were back-crossed to the F1 female. F3 offspring from the F1 x F2 (het x het) back-cross were screened by HRMA and fish determined to be homozygous by HRMA were Sanger sequenced (see Appendix M) to determine whether they were WT or homozygous mutants. A Mendelian ratio of WT/mutant F3 fish was observed. F3 homozygous mutants and wild-type siblings were used to spawn F4 embryos used in subsequent experiments.

### 2.4.2. Klf9 AM-Tag zebrafish line

DNA templates for sgRNA and homology directed repair (HDR) were synthesized using fusion PCR (see Appendix B: Klf9 AM-Tag Design) with Taq polymerase (NEB) and oligonucleotides ordered from IDT. Templates were run through agarose gel electrophoresis to confirm correct size. HDR template was extracted using EZNA Gel Extraction Kit (Omega Biotek) and confirmed by Sanger sequencing. HDR template sequence consisted of 99bp AM-Tag (Active Motif) sequence inserted in-frame prior to endogenous stop codon and flanked by ~60bp micro-homology arms. Silent and PAM mutations were designed into HDR template to prevent editing of template by CRISPR (see Appendix D). Two sgRNA (Table 2.3) were designed using online software at Benchling.com and selected for on/off-target efficiency scores[225,226] (see Appendix C for potential off-target editing sites). sgRNA were synthesized from DNA templates using MegaScript T7 Transcription Kit (ThermoFisher), and purified by phenol:chloroform extraction. Only a single sgRNA ("AMTag sgRNA 1") was used for injections due to a low yield obtained from the T7 reaction for the second sgRNA. Fertilized AB strain embryos were injected at the one-cell stage with a CRISPR mix containing the following: 200ng/µl Cas9 mRNA, 100ng/µl sgRNA, 200ng/µl HDR template, 0.1M KCl, and 0.05% Phenol

Red dye. F0 mutants were identified by fin-clip genotyping and outcrossed to WT AB strain fish. F1 heterozygous mutants were identified by fin-clip genotyping (see Table 2.4 for primers) and in-crossed to produce embryos for chromatin immunoprecipitation experiments.

**Table 2.3. CRISPR guide RNA sequences**

| Short guide RNA | Nucleotide sequence (5'-3') | Target | On/Off-Target Scores |
|---|---|---|---|
| Klf9KO sgRNA 1 | ttaaaccagtgcataccgag | Exon 1, coding, + strand | 77.8/48.4 |
| Klf9KO sgRNA 2 | gcgaatagtggacagtgatg | Exon1, coding, + strand | 70.3/87.3 |
| Klf9KO sgRNA 3 | gaccctggagcatactgggg | Exon 2, coding, - strand | 56.8/49.5 |
| Klf9KO sgRNA 4 | ggcgtgaccctggagcatac | Exon 2, coding, - strand | 33.6/49.5 |
| AMTag sgRNA 1 | tccagcgatcatatgtctgc | Exon 2, coding, + strand | 29.5/47.6 |
| AMTag guide 2 | aacgtgttgtgtcaggtagg | Exon 2, 3' UTR, - strand | 62.3/95.6 |

**Table 2.4. Primers used for genotyping Klf9 mutants**

| Primer | Nucleotide sequence (5'-3') |
|---|---|
| Klf9KO exon1 screen fwd | ggactctgttgatggtcgca |
| Klf9KO exon1 screen rvs | ttaccacagcctgcatacgg |
| Klf9KO exon2 screen fwd | aaagcgtttcatgtgcccac |
| Klf9KO exon2 screen rvs | tgtgtcaggtaggagggaca |
| AMTag screen fwd | agacgacactcttcaacatccacatc |
| AMTag screen rvs | caccaactcactagcagagactcct |

## 2.5. Cortisol measurements

Pooled larvae (n=15-20 per sample) were captured and snap frozen in liquid nitrogen in under one minute and stored at -80C prior to processing. For acute stress experiments, larvae were chased and captured with a transfer pipette and transferred to new media prior to freezing. Frozen samples were homogenized in PBS by motorized pestle. Two rounds of liquid-liquid extraction were performed with ethyl acetate and the organic phase collected. Solvent was evaporated and residue re-dissolved in extraction buffer (Neogen Corporation). CORT was measured using a PowerWave XS plate reader (Bio-Tek) and quantified with a standard curve according to the manufacturer's protocol (Neogen Corporation, detection range 0.04ng – 10ng/mL).

## 2.6. Chromatin Immunoprecipitation and qPCR (ChIP-qPCR)

ChIP was performed essentially as described previously[229] and as follows. DynaProtein A beads (Invitrogen) were blocked by washing 3X in blocking solution (0.5% BSA in PBS). Dyna beads were then incubated with antibody (anti-AM-Tag, 10µg/sample, Active Motif cat# 91111; anti-acetyl-H3K14, 5µg/sample, Active Motif cat# 39698; anti-Klf9, 3.5µg/sample, ABCam ab227920; non-specific IgG negative control, 3.5µg/sample, Invitrogen 02-6102; or anti-H3K4me3, 2.66µg/sample, ABCam ab8580, as positive control; all concentrations selected per manufacturers' guidelines) in blocking solution on a rotator at 4$^{o}$ C overnight.

### 2.6.1. DNA-protein crosslinking and chromatin preparation

Whole 5dpf larvae (60-80 per replicate) were euthanized with Tricaine (Sigma) and immediately incubated for 15 minutes on a room-temperature rotator in 1.85% formaldehyde in PBS to crosslink protein and DNA. Formaldehyde was then quenched with glycine added to a

concentration of 0.125M for 5 minutes. Larvae were then rinsed three times in cold PBS, pelleted by centrifuging briefly and either frozen at -80$^{o}$ C or immediately homogenized and lysed. Homogenization was performed with a motorized micro-pestle in cell lysis buffer (10mM Tris-HCl, pH 8; 10mM NaCl, 0.5% IGEPAL) with protease inhibitor (cOmplete, Roche, 1x final concentration prepared from 50x stock in PBS). Lysing suspension was kept on ice and homogenized periodically for at least 15 minutes and until lysate appeared homogenous. Nuclei were then pelleted in a cold centrifuge (12,000g for 5 minutes at 4$^{o}$C), supernatant removed, and pellet resuspended in nuclei lysis buffer (50mM Tris-HCl, pH8; 10mM EDTA, 1% SDS) with protease inhibitor. Nuclei lysis was incubated on ice for 10 minutes. Two volumes of IP dilution buffer were then added (16.7mM Tris-HCl pH 8, 167mM NaCl, 1.2mM EDTA, 0.01% SDS, protease inhibitor). Chromatin (<1ml in volume) was sheared into fragments using a Qsonica Q500 sonicator and microtip probe. Samples were sonicated on ice, with a series of 10-second pulses at 20% amplitude (lowest setting, to avoid foaming) separated by 20-second cooling intervals. During sonication, progress was monitored by running 5ul of sample on a 1% agarose gel with SybrSafe Dye (Invitrogen). Bands of sheared, crosslinked DNA at 800-1000bp were observed after 40-50 pulses, and subsequently determined to correspond to DNA fragments of <500bp (assayed again on 1% agarose gel after reversal of crosslinking, see below). 48ul of 10% Triton-X (Fisher) were added per 0.6ml of sonicated sample, and samples were then centrifuged at 4$^{o}$ C at 21,000g (top speed) for 15 minutes. A small volume of supernatant (e.g. 50ul) was saved as input control and the remaining supernatant was incubated with antibody-coated beads overnight at 4$^{o}$ C on a rotator.

### 2.6.2. Washing, elution, and reversal of crosslinks

Beads were spun down and collected with magnetic stand, and supernatant was removed. Beads were washed five times with RIPA buffer (50mM HEPES pH8, 1mM EDTA, 0.7% sodium-deoxycholate, 1% IGEPAL, 0.5M LiCl), spun down and collected by magnetic stand after each wash. Beads were washed with TBS, spun down and TBS was aspirated. DNA was eluted from beads in elution buffer (50mM NaHCO3, 1% SDS) at 65$^{o}$ C for 15 minutes with periodic vortexing. Beads were then spun down at max speed and supernatant transferred to a new tube. Four volumes of elution buffer were added to input control samples, and 5M NaCl was added to all samples to final concentration of 0.2M before incubation overnight at 65$^{o}$ C to reverse formaldehyde crosslinks.

### 2.6.3. Precipitation and DNA purification

RNAse A was added to a final concentration of 0.33ug/ul, and samples were incubated at 37$^{o}$ C for 2 hours. Samples were chilled briefly before proteinase K was added to 0.2ug/ul and incubated at 65$^{o}$C for 2 hours. After incubation, samples were chilled on ice and 1 volume of phenol/chloroform/isoamyl alcohol was added. Samples were mixed and spun at top speed (~21,000g) for 5 minutes in 4$^{o}$C centrifuge. Aqueous layer was transferred to a new tube and 20ug glycogen added. One tenth volume of 3M NaOAc and two volumes of 100% EtOH were added. Samples were mixed and then spun at 21,000g for 30 minutes in 4$^{o}$C centrifuge to pellet DNA. Supernatant was removed and pellets washed twice in 75% EtOH. Pellets were briefly air dried and then resuspended in 10mM Tris-HCl, pH 8. DNA concentration was assayed on a DeNovix spectrophotometer.

### 2.6.4. Analysis of ChIP by qPCR

Serial dilutions of input control DNA were used to generate standard curves covering the range of ChIP DNA samples. Input and immunoprecipitated samples were quantified in technical replicates of 10ul qPCR reactions consisting of 5ul SybrGreen FastMix (Quanta Bio), 1ul 3uM primers, and 4ul of diluted DNA template. Primers were designed to target a putative Klf9 binding site in the fkbp5 promoter (fwd: ccaaggcctgcccttaattt, rvs: cctctgcgagacatttggac). Concentration of ChIP DNA was calculated from standard curve and converted to percent recovery ([ChIP DNA] / [input control DNA])*100.

## 2.7. Oxygen consumption rate assay

Basal oxygen consumption rate (OCR) was analyzed using XF96e Extracellular Flux Analyzer (Agilent Technologies, CA), with guidance and assistance from the Jayasundara Lab at the University of Maine. Measurements were made per single 1dpf embryo transferred with 150 uL of either (a) egg water + vehicle (VEH group) or (b) egg water + CORT (CORT group), contained to an individual well in a spheroid microplate (Agilent Technologies, CA). Each embryo was centered in the spheroid chamber in the bottom of the well and air bubbles were removed. 7 minute basal measurement cycles, consisting of a 2:00 min mix, 2:00 min wait, and 3:00 min measure period, were collected over a course of at least 85 minutes (corresponding to 12 measurement cycles). A total of 60 individual embryos per treatment group was tested. Embryo specific OCR per treatment were normalized to background wells containing egg water + vehicle (VEH group) or (b) egg water + CORT (CORT group). The first data point is typically inconsistent in these runs, and therefore was excluded from the analysis. The remaining 11 data points were imported to GraphPad Prism 8.0 and plotted as a function of time. Time-series

data were analyzed using linear regression to determine the slope (rate of change in OCR over time) and Y-intercept, which serves as an indicator of basal metabolic rate. Statistical significance between treatment groups for the slopes and Y-intercepts were calculated based on two-factor ANOVA (treatment and genetic background as the two variables) followed by Šidák's multiple comparisons test (GraphPad Software, San Diego California USA). Significance was determined by a p value < 0.001). A possible confound that cannot be excluded is that CORT and VEH treatment solutions could have differences in oxygen solubility.

### 2.8. *In vitro* mRNA transcription and injection

Total RNA was extracted from 5dpf wild-type larvae using Trizol. RNA was treated with Dnase I (NEB), and full-length *nr3c1* cDNA was reverse transcribed using a specific primer (ggtcaaggttagtttaatgaattagtctgac) and Primescript RT kit (TaKara). Template DNA for transcripts was amplified from this cDNA using Q5 high fidelity polymerase (NEB), full-length (agtaatgcaaaatggatcaaggagg), truncated 310- (ctctttgggaacagctcgcc) or 369- (gggccagtttatgcttttcca) forward primers with upstream T7 promoters, and a common reverse primer (catcgtgtcctgctgttggg) downstream of the stop codon. Template DNA was run through an agarose gel to verify size, extracted and purified using E.Z.N.A. kit from Omega Biotek. Transcription reactions were run using mMessage mMachine Ultra T7 kit from Invitrogen, and yield quantified by spectrophotometry. Xenopus elongation factor 1a transcript from pTRI-Xef included in the mMessage mMachine kit was used as a control. Homozygous GR369- mutant embryos were injected at the one-cell stage with a mix containing 200 ng/ul mRNA and 0.05% phenol red dye, with an injection volume of ~ 20% cell volume. Injected embryos were snap-frozen at 6 h post fertilization for RNA extraction and qRT-PCR.

# CHAPTER 3

# RESULTS, PART ONE:

# Klf9 is a key feed-forward regulator of the transcriptomic response to glucocorticoids

## 3.1. Background and rationale

The Coffman lab has previously reported aberrant immune system function in zebrafish larvae treated for the first 5 days post-fertilization with a chronic dose of 1μM CORT, an endogenous stress hormone in both zebrafish and humans[158] (see Introduction). Among the changes seen in treated larvae was an increase in the expression of immune and inflammatory genes at 5 dpf. To further interrogate the role of the glucocorticoid receptor (GR) in this transcriptional response to chronic CORT, the lab used CRISPR-Cas9 targeted genetic engineering to introduce a frameshift deletion in the *nr3c1* gene, creating a mutant zebrafish line lacking a functional glucocorticoid receptor ($GR^{369-}$)[159]. The lab then performed RNA-seq comparing 1uM CORT treatment with vehicle-treated (VEH) controls in 5dpf larvae with and without functional GR (see Appendix A: Gans et al., 2020). In this analysis, the transcription factor Klf9 was identified as one of four genes the expression of which were significantly decreased in $GR^{369-}$ larvae and increased by CORT in animals with a functional GR. Among these four genes, two others (*per1a* and *hsp90aa1.2)* are known to be respectively involved in circadian aspects of GC signaling[210,230] and chaperoning GR protein[231]. This finding regarding *klf9* was consistent previous RNA-seq of wild-type (WT) larvae in which *klf9* was the most highly overexpressed transcription factor gene after CORT treatment. Given these data, we reasoned that *klf9* may play an important role in the transcriptional response to CORT, and I engineered a

mutant zebrafish line lacking functional Klf9 in order to test that hypothesis. In this chapter and the next, I will describe the creation of this mutant line and the experiments carried out with it. In the next chapter I will describe a second mutant line I created using CRISPR to place a ChIP-grade epitope at the C-terminus of the Klf9 protein, and evidence that Klf9 directly regulates the expression of *fkbp5*, a gene which codes for an important chaperone of the GR and is heavily implicated in the medical literature regarding HPA dysfunction. Altogether, the results demonstrate that *klf9* is a key feed-forward regulator of the transcriptional response to glucocorticoids.

### 3.2. Validation of the GR$^{369-}$ mutant line

Several labs have previously reported GR mutant zebrafish lines with frameshift mutations introduced up- and downstream of the DNA-binding domain (DBD)[153,232,233]. Another mutation, GR$^{s357}$, substitutes a cysteine for an arginine in the DBD, interfering with DNA binding[234]. The Coffman Lab's GR mutation (GR$^{369-}$)[159] was targeted to exon 3 and removed all possible alternate in-frame start codons, of which there are several in the human *nr3c1* ortholog that have been shown to generate functional protein isoforms with different N-termini[235] (Fig. 3.1A-C). The 20 bp deletion introduced by CRISPR resulted in a frame shift as well as a premature stop codon prior to the DBD. We experienced difficulty obtaining viable embryos from spawning of homozygous GR$^{369-}$ mutants, a phenomenon previously unreported in zebrafish GR mutants. We thus decided to test the efficacy of GR$^{369-}$ in comparison with previously published mutations targeting exon 2 and thus harboring potential alternate start codons. Messenger RNAs encoding full-length and N-terminally truncated (N369 and N310) GR were transcribed *in vitro* and micro-injected into 1-cell stage GRKO embryos (Fig. 3.1D). The GR-N310 transcript

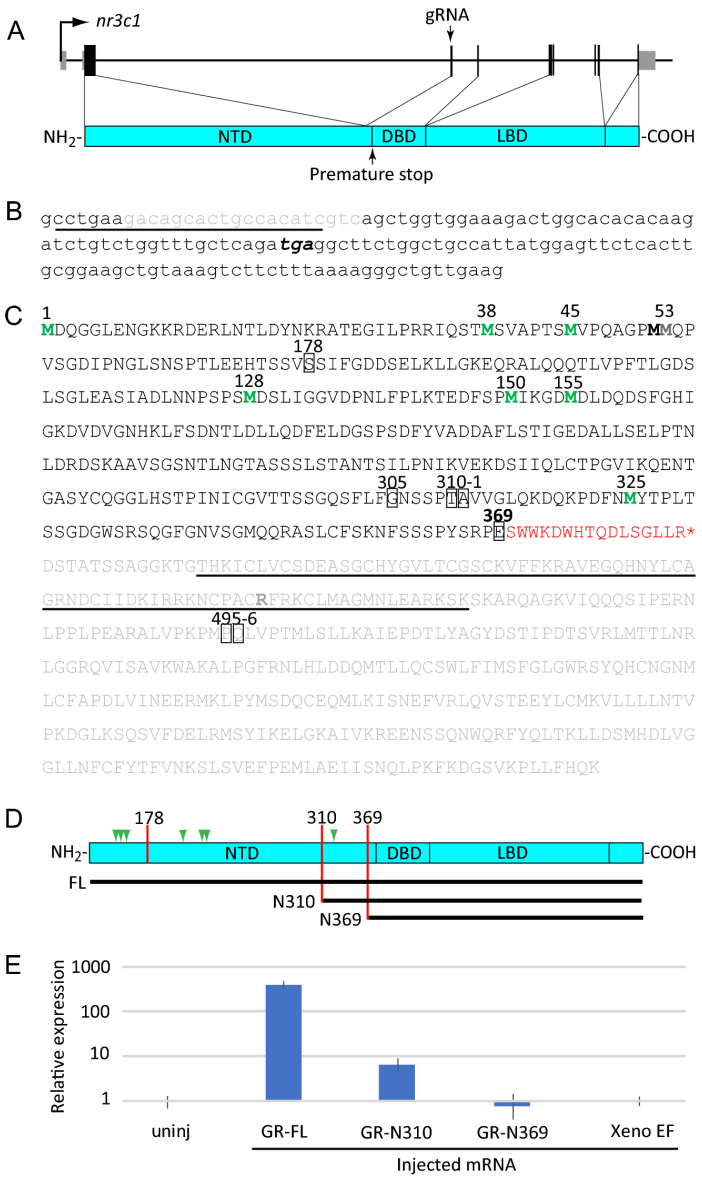


**Figure 3.1. The GR$^{369-}$ mutation eliminates DNA binding domain and decreases target transcript level.** (A) Schematic of the *nr3c1* gene and encoded GR protein (B) DNA sequence of *nr3c1* exon 3 with gRNA target underlined and deletion in grey. Resulting premature stop codon is bold italic. (C) Amino acid (aa) sequence of full-length GR protein plus sequence added by frameshift mutation (red). The DBD is underlined and aa lost are grey. Methionine coded by potential start codons are green. Reported frameshift mutations are boxed. The arginine mutated to cysteine in *gr$^{s357}$* mutants is bold grey. (D) Schematic of start codons, reported frameshift mutations, and microinjected transcripts. (E) Relative expression of *fkbp5* 6 hours after injection of one-cell embryos with GR transcripts or *Xenopus* elongation factor control (see Chapter 2.8 for more details)[159]. Data from three biological replicates of 10 pooled larvae, with 95% confidence bars. Figure from Gans et al., 2020[159]

provides for translation of an N-terminally truncated protein isoform that could be produced by the most 3' of all potential alternate start codons (Fig. 3.1D). Expression of the known GR target *fkbp5* was then measured at 6 hpf to assess functionality of the different length GR transcripts. Injection with the GR-N369 transcript induced no increase in *fkbp5* expression relative to either un-injected controls or controls injected with mRNA for *Xenopus* elongation factor 1a (Fig3.1E). Injection with the GR-N310 transcript led to a significant upregulation of *fkbp5* expression at 6hpf, although still ~50 times lower than injection with the full-length transcript. These results indicate that frameshift mutations introduced upstream of alternate start codons may allow some functional GR protein to be translated from shorter transcript isoforms, but that the new $GR^{369-}$ mutation eliminates this possibility.

### 3.3. Generation of a *klf9*$^{-/-}$ mutant line

RNA-seq carried out on 5 dpf offspring of a cross of $GR^{369-}$ heterozygotes identified *klf9* as both upregulated by CORT exposure in a GR-dependent way (consistent with the upregulation of *klf9* by CORT observed in a previous study using only WT larvae[158]), and under-expressed in $GR^{369-}$ homozygotes. This identified *klf9* a potential mediator of some transcriptomic effects of GR-mediated GC signaling[159]. Additionally, it was previously shown that in blood cells of adult WT fish, chromatin encompassing the *klf9* promoter region was one of the regions with the greatest increase in accessibility in response to developmental CORT exposure, as assessed by an assay for transposase-accessible chromatin with sequencing (ATAC-seq)[175]. To explore a potential role for *klf9* in GC signaling, I used CRISPR to induce a 2bp frameshift mutation in the first exon of *klf9* to induce a premature stop codon upstream of the DBD and abolish direct transcriptional regulation (Fig 3.2A-B). Klf9 mutation is viable in mice[236], and our zebrafish line

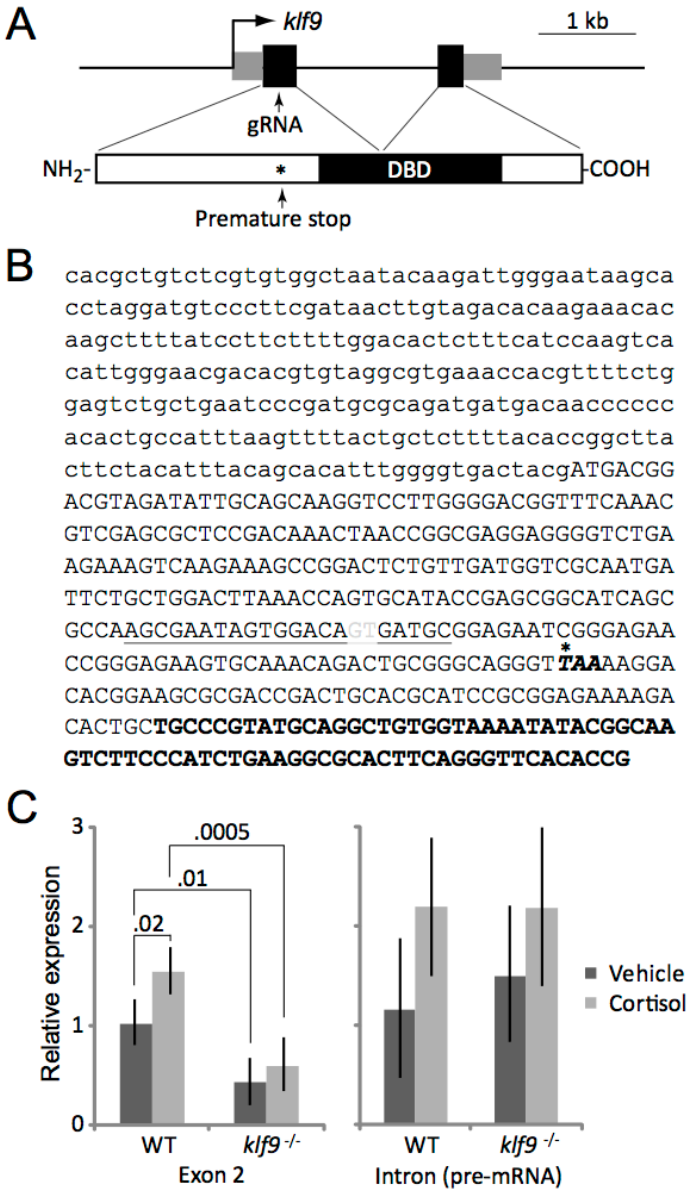


**Figure 3.2. A frameshift deletion in exon 1 of *klf9* eliminates the DNA binding domain and reduces mature transcript level.** (A) Schematic of the *klf9* gene, encoded protein, gRNA target site and induced premature stop codon. (B) Sequence of *klf9* exon 1, with 5' untranslated region (UTR) in lowercase and coding sequence in capitals. CRISPR guide target is underlined, and induced 2bp deletion is in light grey. The induced premature stop codon is in bold italic, and the beginning of the DBD is in bold. (C) Relative expression of *klf9* as measured with primers located in exon 2 (left) and the intron (pre-mRNA, right). Statistical significance was determined by ANOVA. Bars represent standard error of the mean of three biological replicates of 8 pooled larvae each. Figure from Gans et al., 2020[159].

Was bred to homozygosity, though female subfertility was noted. This subfertility was not completely unexpected, given that subfertility has been noted in *Klf9*-null mice, and that decreased *klf9* expression has been reported in uterine tissue of women with late-term pregnancy[237,238]. qPCR was carried out comparing expression of *klf9* pre- and total mRNA transcripts in VEH and CORT treatments (Fig. 3.2C). As expected, CORT treatment increased the expression of *klf9* in WT larvae, while *klf9*$^{-/-}$ larvae had significantly lower mature transcript levels than WT, presumably due to nonsense-mediated decay.

### 3.4. Klf9 mediates immune gene overexpression resulting from chronic cortisol exposure

To identify putative Klf9 targets and determine what role (if any) *klf9* plays in the response to chronic CORT, we treated WT and *klf9*$^{-/-}$ embryos/larvae from sibling parents with 1μM CORT or VEH and performed sequencing of RNA extracted from pooled samples frozen on 5 dpf. The samples were treated similarly and collected at the same time of day (mid-morning) as in the previous GR$^{369-}$ RNA-seq experiment[159], and the resulting data was processed through the same workflow by the MDI Biological Laboratory Bioinformatics Core (see Chapter 2 and Appendix A: Gans et al., 2020, for methods). However, principal component analysis (PCA) of the resulting gene-level expression data identified biological replicate (corresponding to sample collection and processing order) as the main source of variance within the data set, accounting for more than 60% of the total variance. Genes correlated with this first principal component (PC1) showed gene ontology enrichment (GOE) for increased neuronal processes and decreased translation in later samples (see Appendix C), suggestive of a physiological stress response developing over the course of being chased and captured during sequential sample collection. However, this interpretation was confounded by technical differences in RNA preparation on

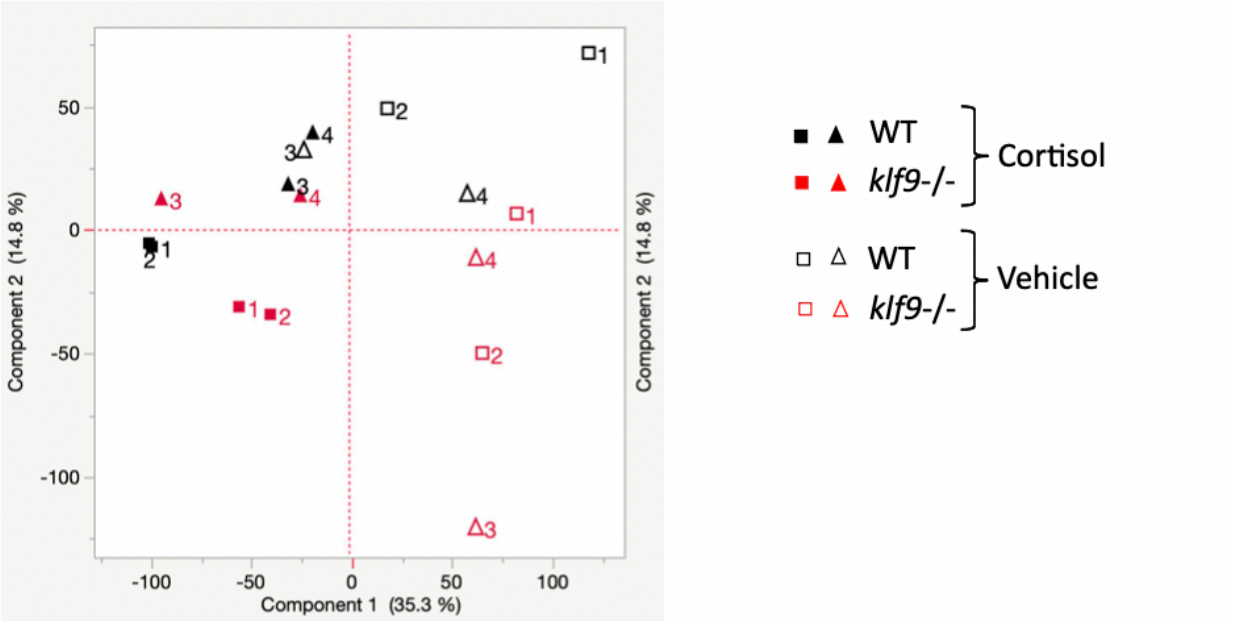


**Figure 3.3. Principal component analysis segregates RNA-seq samples by genotype and treatment.** WT or *klf9*$^{-/-}$ samples treated with either chronic CORT or vehicle control segregate by treatment (PC1, x-axis) and genotype (PC2, y-axis) after batch normalization.

Two separate days, with samples in replicates 1 and 2 processed separately from samples in replicates 3 and 4 (see Methods chapter for further detail). After normalizing for this potential batch effect, the samples segregated along two principal components reflecting treatment (35.3% of variance) and genotype (14.8%) (Fig. 3.3). Thus, a two-factor categorical covariate was included in subsequent analyses of differential gene expression (DGE) to account for any technical batch effect. One limitation of this approach is that it may also remove meaningful biological information about gene expression changes due to an acute stress response to sampling procedures in addition to the intended removal of technical artifacts.

A

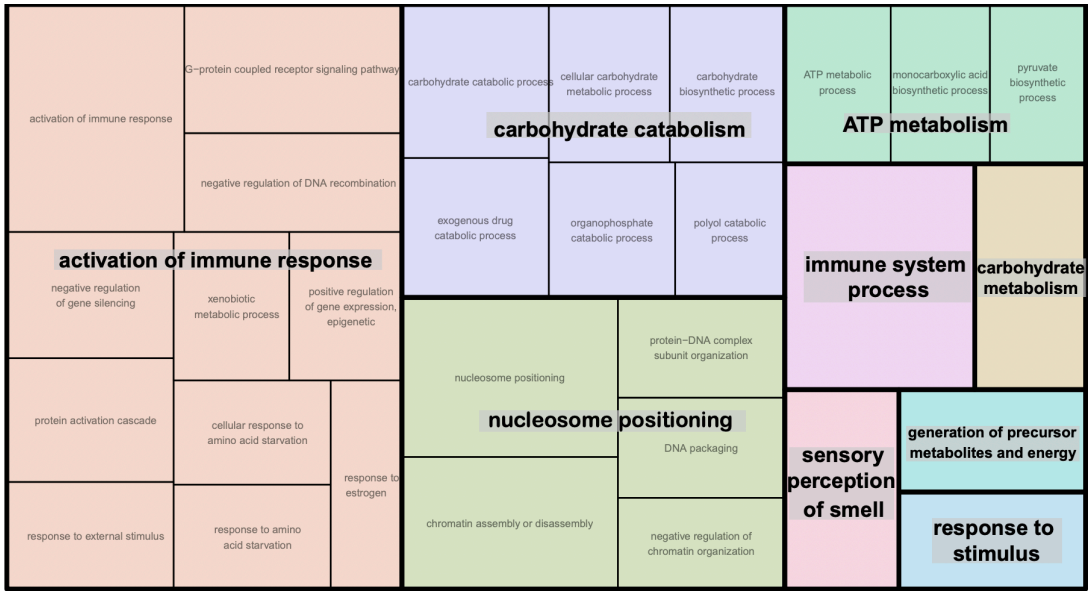


B

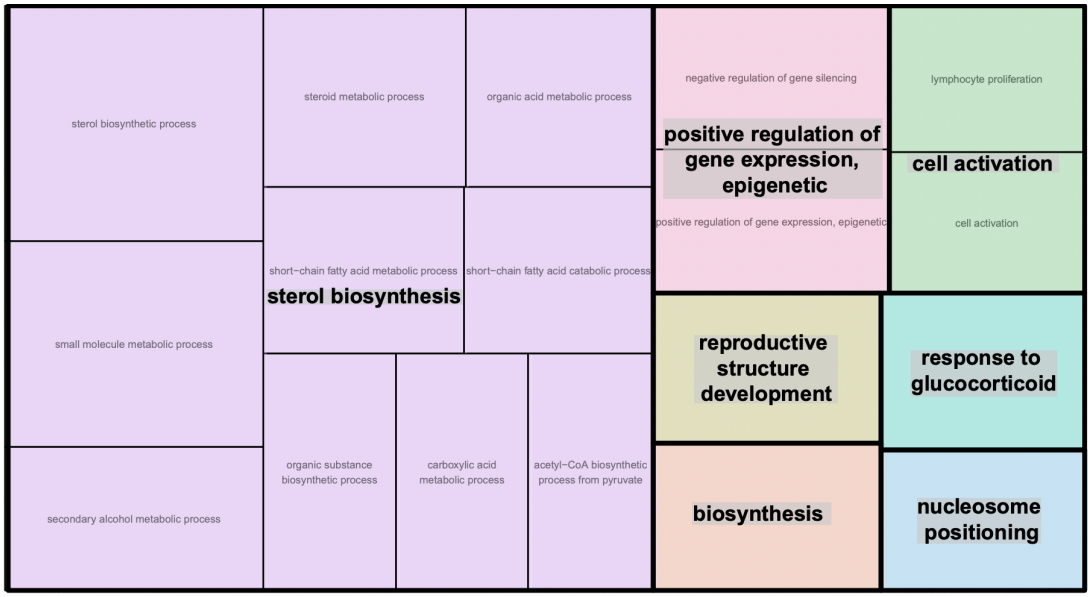


**Figure 3.4. Gene ontology term tree maps of processes effected by *klf9* mutation.** Processes upregulated (A) and downregulated (B) by loss of functional *klf9* gene in vehicle treated larvae. Enriched terms were found using differential gene expression data ranked by significance of genotype effect (adjusted p-value).

Using a false-discovery rate (FDR) of 0.05, 100 genes were found upregulated by loss of *klf9* in vehicle treated larvae, and GOE term analysis found this group of genes was enriched for involvement in processes including complement activation, glucose metabolism, and nucleosome positioning (Fig. 3.4A, Appendix D). Genes downregulated by loss of *klf9* in vehicle (139 genes) were largely involved in sterol metabolism (Fig. 3.4B, Appendix D). Notably, several carbohydrate metabolic processes upregulated in *klf9* mutants (e.g. glycolysis, pyruvate biosynthesis) had conversely found to be downregulated in $GR^{369-}$ mutants[159].

CORT treatment upregulated 584 genes in WT larvae, and 1079 genes in *klf9*$^{-/-}$ larvae, and downregulated 133 genes in WT and 1024 genes mutants (Appendix E). Although more genes were significantly dysregulated in mutants, they were so to a lesser degree and the most striking result was that most genes (70%) upregulated by CORT in WT larvae were not upregulated by CORT in *klf9*$^{-/-}$ (Fig. 3.5A, B). Genes that were upregulated by CORT in WT were enriched for involvement in defense and immunity (Fig. 3.5D), including a number of interferon regulatory factors and interleukin genes, similar to what was found in previous RNA-seq published by the Coffman Lab in 2016 looking at the effect of CORT in WT larvae[158]. On the contrary, no enrichment for immune processes was found among genes upregulated by CORT in *klf9*$^{-/-}$ larvae, which instead included a number of metabolic processes as well as genes annotated for involved in translation and aging (Appendix F). Roughly a quarter (91 of 408) of the individual genes whose upregulation by CORT was dependent on Klf9 in the current study were also found to be upregulated by CORT in the previous WT 2016 study. Examples include *marco* and *irg1l* (shown in Fig. 3.5C), as well as *irg1, irf1a, ifi35, mpeg1.1, mpeg1.2, mxc, socs1a,*

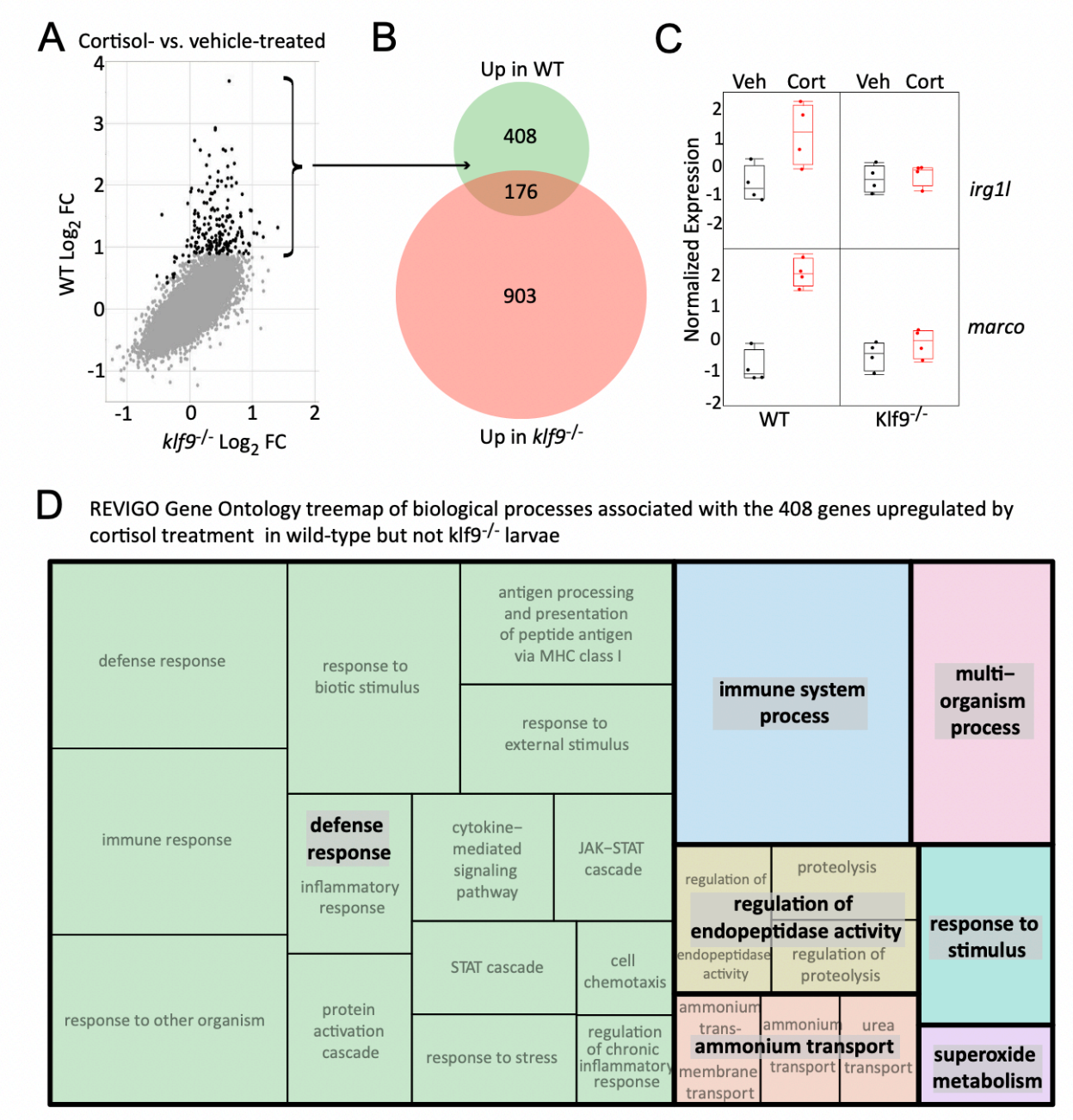


**Figure 3.5. Klf9 mediates the immune gene response to chronic cortisol in 5dpf larvae.**

**(4)** Scatterplot comparing differential gene expression from RNA-seq of WT and *klf9*$^{-/-}$ larvae treated with chronic CORT. (B) Venn diagram of genes upregulated by CORT in either WT and *klf9*$^{-/-}$ and overlap between the two groups. (C) Example of two genes whose CORT-induced overexpression is *klf9*-dependent. Both *irg1l* and *marco* were identified in previous studies as well. (D) Treemap of GO terms enriched among genes upregulated by CORT in WT but not *klf9* larvae. Figure from Gans et al., 2020[159].

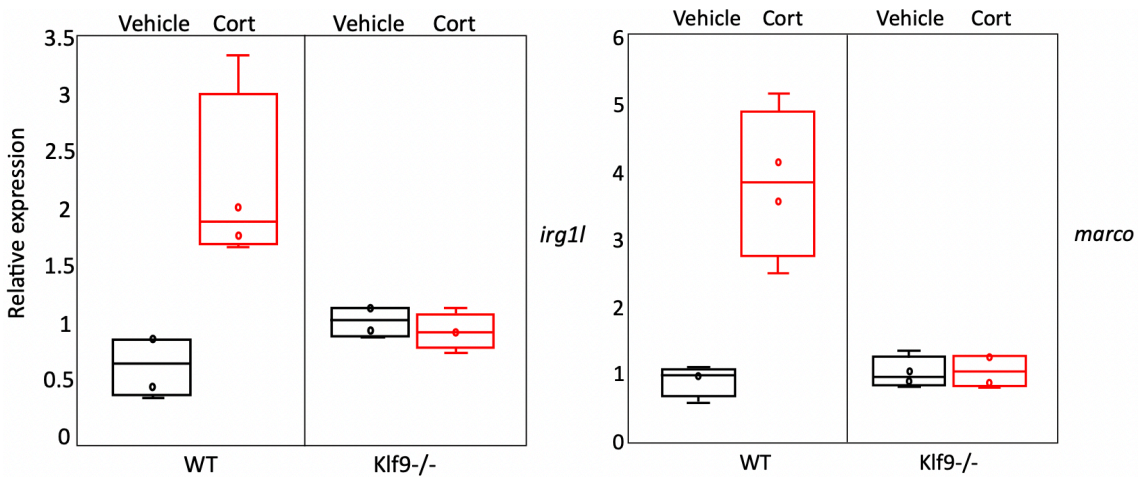


**Figure 3.6. Validation of RNA-seq data with qPCR.** Examples of two genes, *irg1l* and *marco*, which were identified by RNA-seq as being dependent on *klf9* for induction by CORT, and confirmed by qPCR. Data from four biological replicates of pooled larvae.

*Socs3b, stat1b*, and *stat4*. Relative expression levels for *marco* and *irg1l* were confirmed by qPCR (Fig. 3.6). These results indicate that *klf9* plays a significant role in mediating the immune gene response to chronic CORT.

### 3.5. Consensus Klf9 target motifs are enriched near transcription start sites of glucocorticoid responsive genes

To generate a high-confidence list of genes responsive to chronic CORT exposure, RNA-seq data from three experiments (*klf9*$^{-/-}$, GR$^{369-}$, [159] and 2016 WT[158]) were compared. Raw data from the 2016 experiment were re-processed by the MDIBL Bioinformatics Core through the WT same DGE pipeline as the two recent experiments. Gene expression data were used only from WT animals (in the *klf9*$^{-/-}$ and 2016 experiments) or animals with at least one functional GR allele from the GR$^{369-}$ experiment (2:1 ratio of pooled heterozygous:WT larvae from a heterozygous cross as identified by visual background adaptation assay[234]). The comparison

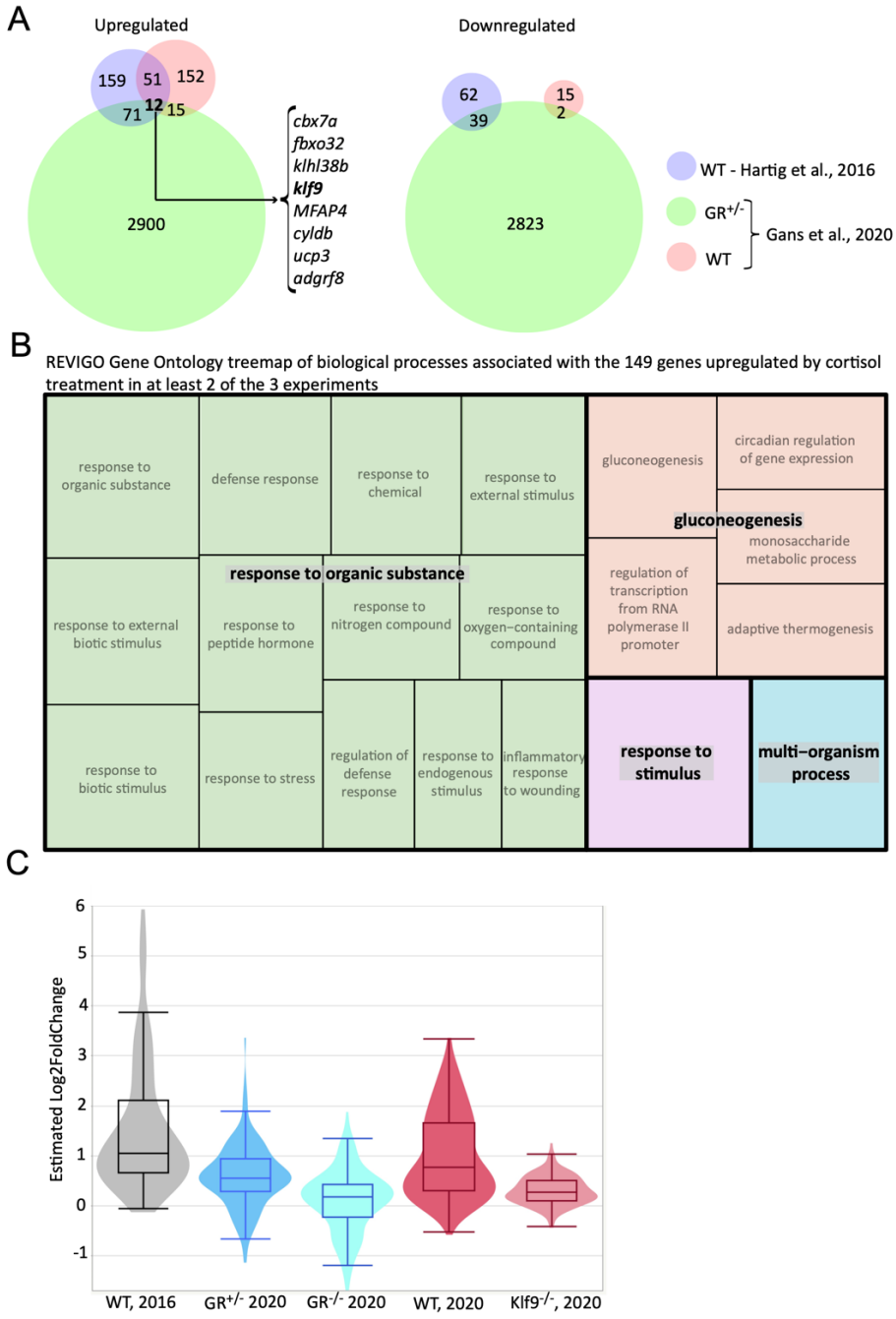


**Figure 3.7. Klf9 mediates responsiveness of genes upregulated by cortisol in multiple experiments.** (A) Venn diagram of genes significantly up- or down-regulated by CORT in three published RNA-seq experiments (each comprising at least 3 replicates of pooled larvae). Names of eight annotated genes up in all experiments shown. (B) GO tree map of processes enriched in 149 genes upregulated in 2-of-3 experiments. (C) Comparison by genotype of CORT-induced fold change of expression of 149 genes upregulated in two out of three RNA-seq experiments. $GR^{+/-}$ samples were pooled larvae (2:1 het/WT ratio) identified by visual background adaptation assay to have at least one functional GR allele. $GR^{-/-}$ were identified by the same assay.

Revealed 12 genes that were significantly upregulated (FDR < 0.05) by chronic CORT in all three experiments, and no genes that were significantly downregulated in all three (Fig. 3.7A). Notably, *klf9* was among the 12 overexpressed genes. Because many more genes are likely affected by chronic CORT exposure but statistical significance could be lost due to experimental variation (i.e. noise), an expanded list of 149 consistently upregulated targets was generated by including those genes significantly elevated in two out of three experiments (Appendix G). Reassuringly, GO analysis of the expanded 149 gene list showed enrichment primarily for defense response and gluconeogenesis (Fig. 3.7B), similar to terms found previously in WT larvae exposed to chronic CORT[158]. Interestingly, plotting the CORT-induced fold change of these 149 genes in all experiments showed a decreased response to CORT in both GR mutant and *klf9*$^{-/-}$ larvae, indicating a significant role for both the GR and *klf9* in the transcriptomic response to chronic GC (Fig. 3.7C). The data suggested an important role for Klf9 in mediating the effects of glucocorticoids on the transcriptome. Thus, I used the computer program HOMER (Hypergeometric Optimization of Motif EnRichment[220]) to search for predicted transcription factor binding sites in DNA flanking the transcription start sites (TSS) of 149 genes upregulated by CORT in at least two of the three RNA-seq experiments analyzed. The resulting list of significantly enriched motifs (adjusted P-value < 0.05) included several KLF proteins as well as the GR (Table 3.1). The most significantly enriched motif was the human Klf14 binding motif[239]. Klf14 is a member of the same KLF subfamily as Klf9 and its consensus motif, RGKGGGCGKGGC (Fig. 3.8), matches the Klf9 motif[240] and is thus predicted to bind Klf9 as well. On the contrary, similar HOMER analysis on the list of 408 genes upregulated by CORT in a Klf9-dependent manner did not reveal any enrichment for KLF motifs, but rather several interferon and other

immune-related motifs (Table 3.2). Together these findings suggest that although Klf9 may directly bind (and thus directly regulate) a significant number of GC-responsive genes, the Klf9-dependence of immune gene overexpression in response to CORT could be indirect. This would be consistent with previous findings of a primarily repressive role for Klf9[191]. However, differences in the generation of the lists of genes analyzed must also be considered. Whereas the list of 149 GC targets was generated by consensus among multiple experiments, the list of 408 Klf9-dependent immune genes comes from a single experiment and would reasonably be expected to contain more false positives (and false negatives by omission). The limitation of HOMER to analysis of +/- 2000bp from the TSS should also be born in mind when interpreting these results.

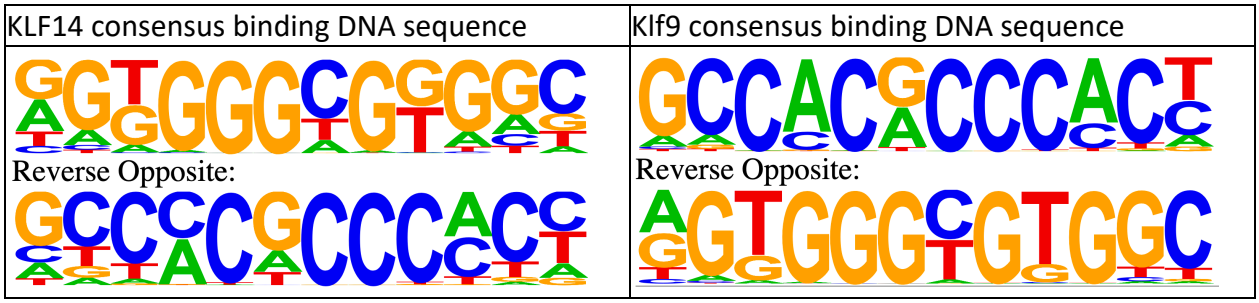


**Figure 3.8. Consensus binding motifs for Klf14 and Klf9.** The most significantly enriched transcription factor motif in TSS proximal regions of zebrafish genes upregulated by CORT matches empirically determined sites for human Klf14[239] (left panel) and Klf9[240] (right panel). Note the two motifs are nearly identical and predicted to bind various KLF proteins competitively[192].

**TABLE 3.1. Significantly enriched transcription factor binding motifs in TSS-proximal DNA of 149 genes consistently responsive to chronic cortisol exposure.**

| Motif Name | Consensus | P-value | P-adjusted (Benjamini) |
|---|---|---|---|
| KLF14(Zf)/HEK293-KLF14.GFP-ChIP-Seq(GSE58341)/Homer | RGKGGGCGKGGC | 1.00E-05 | 0.001 |
| Stat3+il21(Stat)/CD4-Stat3-ChIP-Seq(GSE19198)/Homer | SVYTTCCNGGAARB | 1.00E-04 | 0.0047 |
| GRE(NR),IR3/A549-GR-ChIP-Seq(GSE32465)/Homer | NRGVACABNVTGTYCY | 1.00E-04 | 0.0049 |
| GRE(NR),IR3/RAW264.7-GRE-ChIP-Seq(Unpublished)/Homer | VAGRACAKWCTGTYC | 1.00E-04 | 0.0066 |
| CarG(MADS)/PUER-Srf-ChIP-Seq(Sullivan_et_al.)/Homer | CCATATATGGNM | 1.00E-04 | 0.0068 |
| ARE(NR)/LNCAP-AR-ChIP-Seq(GSE27824)/Homer | RGRACASNSTGTYCYB | 1.00E-04 | 0.0068 |
| MITF(bHLH)/MastCells-MITF-ChIP-Seq(GSE48085)/Homer | RTCATGTGAC | 1.00E-03 | 0.0126 |
| KLF5(Zf)/LoVo-KLF5-ChIP-Seq(GSE49402)/Homer | DGGGYGKGGC | 1.00E-03 | 0.0126 |
| Sp2(Zf)/HEK293-Sp2.eGFP-ChIP-Seq(Encode)/Homer | YGGCCCCGCCCC | 1.00E-03 | 0.0127 |
| KLF1(Zf)/HUDEP2-KLF1-CutnRun(GSE136251)/Homer | VDGGGYGGGGCY | 1.00E-03 | 0.014 |
| NPAS(bHLH)/Liver-NPAS-ChIP-Seq(GSE39860)/Homer | NVCACGTG | 1.00E-03 | 0.014 |
| E2A(bHLH),near_PU.1/Bcell-PU.1-ChIP-Seq(GSE21512)/Homer | NVCACCTGBN | 1.00E-03 | 0.014 |
| Zic(Zf)/Cerebellum-ZIC1.2-ChIP-Seq(GSE60731)/Homer | CCTGCTGAGH | 1.00E-03 | 0.0163 |
| Klf4(Zf)/mES-Klf4-ChIP-Seq(GSE11431)/Homer | GCCACACCCA | 1.00E-03 | 0.0171 |
| Sp5(Zf)/mES-Sp5.Flag-ChIP-Seq(GSE72989)/Homer | RGKGGGCGGAGC | 1.00E-03 | 0.0229 |
| STAT1(Stat)/HelaS3-STAT1-ChIP-Seq(GSE12782)/Homer | NATTTCCNGGAAAT | 1.00E-03 | 0.0229 |
| BMAL1(bHLH)/Liver-Bmal1-ChIP-Seq(GSE39860)/Homer | GNCACGTG | 1.00E-03 | 0.0253 |
| NFkB-p65-Rel(RHD)/ThioMac-LPS-Expression(GSE23622)/Homer | GGAAATTCCC | 1.00E-02 | 0.0334 |
| KLF6(Zf)/PDAC-KLF6-ChIP-Seq(GSE64557)/Homer | MKGGGYGTGGCC | 1.00E-02 | 0.034 |
| NFkB-p65(RHD)/GM12787-p65-ChIP-Seq(GSE19485)/Homer | WGGGGATTTCCC | 1.00E-02 | 0.0447 |
| Usf2(bHLH)/C2C12-Usf2-ChIP-Seq(GSE36030)/Homer | GTCACGTGGT | 1.00E-02 | 0.0452 |

**Table 3.2. Significantly enriched (P-adjusted <0.05) transcription factor binding motifs in TSS-proximal DNA of 408 genes upregulated by chronic cortisol in a Klf9-dependent fashion.**

| Motif Name | Consensus | P-value | P-adjusted (Benjamini) |
|---|---|---|---|
| IRF2(IRF)/Erythroblas-IRF2-ChIP-Seq(GSE36985)/Homer | GAAASYGAAASY | 1.00E-12 | 0 |
| ISRE(IRF)/ThioMac-LPS-Expression(GSE23622)/Homer | AGTTTCASTTTC | 1.00E-11 | 0 |
| IRF1(IRF)/PBMC-IRF1-ChIP-Seq(GSE43036)/Homer | GAAAGTGAAAGT | 1.00E-09 | 0 |
| PU.1:IRF8(ETS:IRF)/pDC-Irf8-ChIP-Seq(GSE66899)/Homer | GGAAGTGAAAST | 1.00E-08 | 0 |
| IRF8(IRF)/BMDM-IRF8-ChIP-Seq(GSE77884)/Homer | GRAASTGAAAST | 1.00E-07 | 0 |
| IRF3(IRF)/BMDM-Irf3-ChIP-Seq(GSE67343)/Homer | AGTTTCAKTTTC | 1.00E-07 | 0 |
| ELF3(ETS)/PDAC-ELF3-ChIP-Seq(GSE64557)/Homer | ANCAGGAAGT | 1.00E-07 | 0 |
| ELF5(ETS)/T47D-ELF5-ChIP-Seq(GSE30407)/Homer | ACVAGGAAGT | 1.00E-05 | 0.0001 |
| STAT5(Stat)/mCD4+-Stat5-ChIP-Seq(GSE12346)/Homer | RTTTCTNAGAAA | 1.00E-05 | 0.0003 |
| STAT1(Stat)/HelaS3-STAT1-ChIP-Seq(GSE12782)/Homer | NATTTCCNGGAAAT | 1.00E-04 | 0.0043 |
| Stat3+il21(Stat)/CD4-Stat3-ChIP-Seq(GSE19198)/Homer | SVYTTCCNGGAARB | 1.00E-03 | 0.0058 |
| NFkB-p65-Rel(RHD)/ThioMac-LPS-Expression(GSE23622)/Homer | GGAAATTCCC | 1.00E-03 | 0.0058 |
| PU.1-IRF(ETS:IRF)/Bcell-PU.1-ChIP-Seq(GSE21512)/Homer | MGGAAGTGAAAC | 1.00E-03 | 0.0162 |
| STAT4(Stat)/CD4-Stat4-ChIP-Seq(GSE22104)/Homer | NYTTCCWGGAAR | 1.00E-02 | 0.0344 |
| CEBP(bZIP)/ThioMac-CEBPb-ChIP-Seq(GSE21512)/Homer | ATTGCGCAAC | 1.00E-02 | 0.0356 |
| IRF4(IRF)/GM12878-IRF4-ChIP-Seq(GSE32465)/Homer | ACTGAAACCA | 1.00E-02 | 0.0413 |
| Stat3(Stat)/mES-Stat3-ChIP-Seq(GSE11431)/Homer | CTTCCGGGAA | 1.00E-02 | 0.0436 |

# Chapter 4

# RESULTS, PART TWO:

# Klf9 regulates glucocorticoid receptor chaperone *fkbp5* and metabolism

## 4.1. Background and rationale

As noted in the previous chapter, the loss of functional Klf9 caused broad changes in the transcriptomic response of zebrafish larvae to chronic CORT exposure. The most striking difference was the lack of overexpression of immune genes in response to CORT in *klf9*$^{-/-}$ larvae in comparison with WT. However, the relative lack of Klf9 binding motifs near transcription start sites in the Klf9-dependent immune gene cluster raised the possibility of indirect mechanisms of regulation which would fit with previous evidence that direct regulation of transcription by Klf9 is predominantly repressive[191,241]. Preliminary data generated in the Coffman Lab suggested that morpholino knockdown of Klf9 in zebrafish embryos increased expression of *fkbp5,* an important target *and* cytoplasmic chaperone/negative-feedback regulator of GR activity[242,243]. In this intracellular negative feedback circuit Fkbp5 protein functions as a resistor to GC signaling, and mutations or epigenetic modifications altering expression levels of Fkbp5 have been linked with HPA dysfunction and associated diseases[244–247]. Knowledge of *fkbp5* transcriptional regulation is limited; however, repression of *fkbp5* by Klf9 would be consistent with a single report in the literature that forced overexpression of Klf9 in human skin cells decreased expression of *FKBP5*[211]. Elevated Fkbp5 is predicted to decrease nuclear localization of the GR, limiting its influence on transcription and presenting one mechanism by which loss of Klf9 could indirectly increase GC resistance. Notably, the Coffman

Lab has produced evidence for GC resistance in CORT-treated larvae: in an RNA-seq experiment, CORT treatment shifted WT transcriptomes toward those of $GR^{-/-}$ larvae[159]. The Coffman Lab has also found that CORT increases expression of *fkbp5* (e.g. it is among the list of 149 reliably GC-responsive genes described in Chapter 3, see also Appendix G). These data are consistent with GC resistance developing in animals with elevated *fkbp5* expression. Thus, I undertook experiments to test the hypothesis that Klf9 directly represses *fkbp5* expression, and in this chapter I will provide evidence that support this hypothesis. I will also present evidence of altered energy metabolism in *klf9*$^{-/-}$ larvae consistent with a previous study involving Fkbp5. Lastly, I will also provide data suggesting direct regulation by Klf9 of additional genes involved in glycolysis, gluconeogenesis and adjacent metabolic pathways known to respond to GC signals. Discussion of the data presented in this and the previous chapter will be reserved for the final chapter of this dissertation, along with discussion of future directions.

## 4.2. Expression dynamics of *klf9* and *fkbp5* are synchronous and similarly increased by chronic cortisol exposure

As mentioned above, a number of published[158,175] and unpublished experiments in the Coffman Lab have found elevated *fkbp5* expression in zebrafish treated with chronic 1µM CORT for the first five days of development. In an ATAC-seq experiment, the Coffman Lab also found that accessibility of chromatin in both the *fkbp5* and *klf9* promoter regions was significantly increased in blood cells of adults derived from embryos treated with chronic CORT[175]. In the same study, *fkbp5* and *klf9* transcripts were measured in the blood of adult fish treated with CORT or VEH control during early development. Across multiple experiments expression of both genes was significantly increased by developmental CORT, although not in every instance.

These data suggested that like *fkbp5*, *klf9* is a direct target of regulation by the GR. Given known circadian and ultradian HPA dynamics[22–24], I hypothesized that inconsistency in CORT-induced expression levels could be an artifact of measuring dynamic gene expression with insufficient temporal resolution, and therefore undertook high-density time-course sampling to measure *fkbp5* and *klf9* expression in 5 dpf larvae. I also reasoned that such time courses could provide valuable temporal context for data from other single timepoint experiments, including RNA-seq data sets that represent only a "snap-shot" of gene expression in time, despite their depth.

By 5 dpf, the zebrafish HPI axis is fully developed[149], and active as apparent by *fkbp5* and *klf9* transcript levels (Fig. 4.1), as well as the CORT response to stressor (see results below). Since both intracellular and systemic regulatory systems are functional, any changes measured due to chronic CORT would reflect not only cell-autonomous output but function of the HPI and any (mal)adaptation of larvae to treatment, and thus could provide insight about pathology stemming from chronic GC and associated allostatic load in other vertebrate systems. Although bulk analysis of larval gene expression lacks spatial resolution, I reasoned that such an analysis would be informative since both *fkbp5* and *klf9* are ubiquitously expressed[248,249] and transcription in peripheral zebrafish tissues is highly entrained to circadian rhythms via GC signaling[250,251]. For the time-courses, care was taken not to disturb larvae during sampling (see Chapter 2 for methods) and thus minimize stress-responsive expression.

The results revealed that at 5 dpf *klf9* and *fkbp5* are expressed with synchronous oscillations on both the circadian and ultradian time scales (Figs. 4.2A, 4.3). Transcript levels of

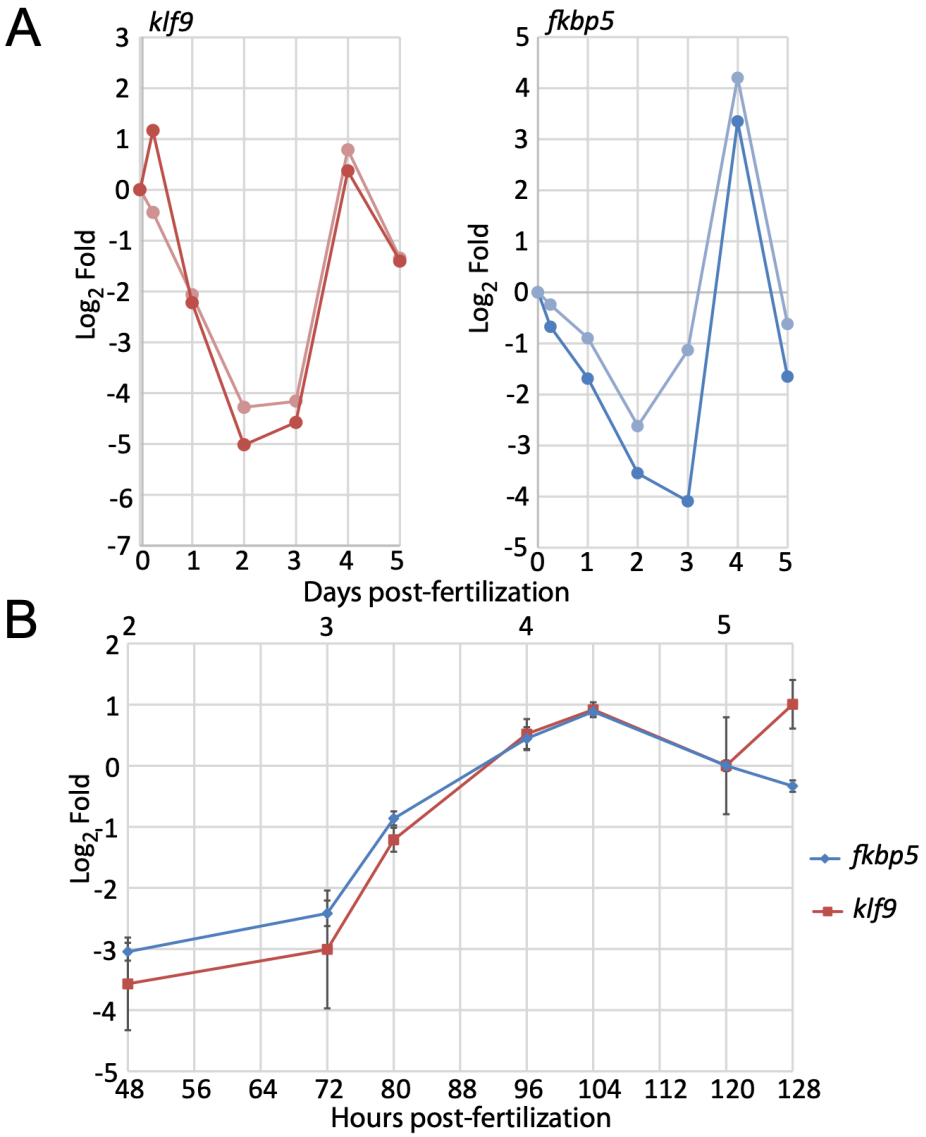


**Figure 4.1. Early developmental expression of *klf9* and well-known GR-target *fkbp5*.**
(A) Relative mRNA levels of *klf9* and *fkbp5* measured by qPCR over the first five days of development shows that both transcripts are maternally deposited and substantially depleted by 2dpf. Expression levels rise again after 3dpf following development of the larval HPI axis. Each line represents a biological replicate of pooled larvae. (B) Relative mRNA levels of each gene in a third biological replicate measured by qPCR on days 2-5 post-fertilization. Error bars represent 95% confidence interval of technical replicates.

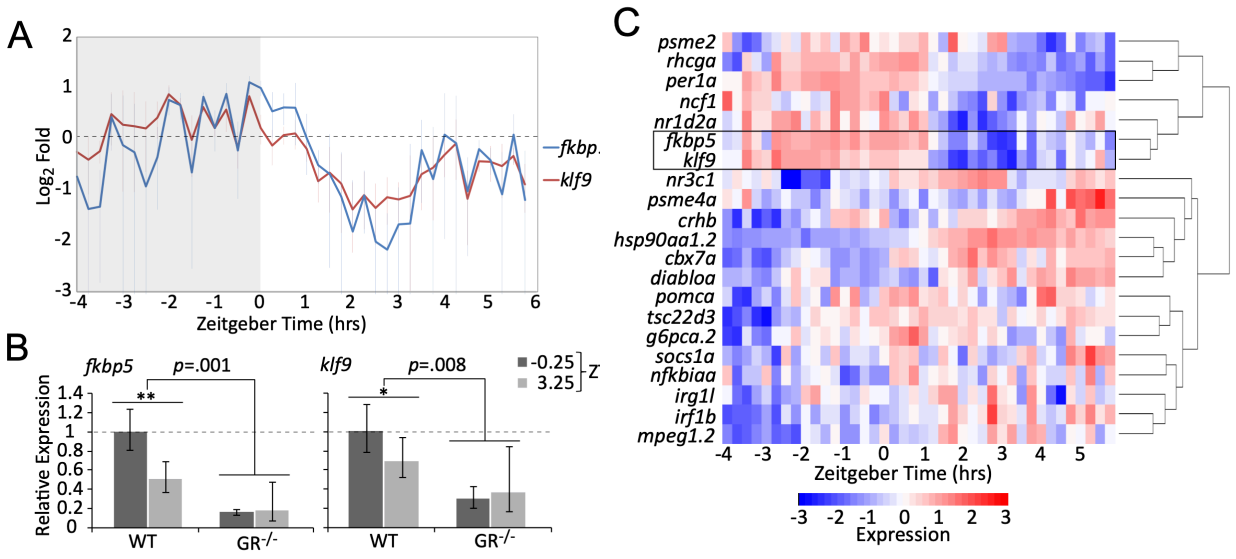


**Figure 4.2. The transcript levels of *klf9* and *fkbp5* are dynamic and synchronous.** (A) Average relative levels of *klf9* and *fkbp5* transcripts in three biological replicates of pooled (n = 3 to 6) 5dpf larvae snap-frozen every fifteen minutes from -4 to 6 hours ZT. Error bars are standard error of the mean. (B) Relative expression of *klf9* and *fkbp5* in WT and *nr3c1*-/- ($GR^{369-}$) mutant larvae at -0.25 and +3.25 ZT, time points that correspond to the activity peak and nadir of both genes in WT larvae. Error bars represent 95% confidence intervals of three biological replicates of pooled larvae (n=9 per sample). Significance calculated by two-factor (time and genotype) ANOVA, and one-tailed t-tests to assess the effect of time within each genotype; **p=.01; *p= .05. (C) Heat map of expression of *klf9*, *fkbp5*, and additional targets/regulators of GC signaling as measured on the NanoString platform. Counts data are normalized to reference genes (actb2, rpl13a, and eif5a) and scaled within each gene to normalize for different absolute levels of expression. RNA from a single time course replicate from (A) was used.

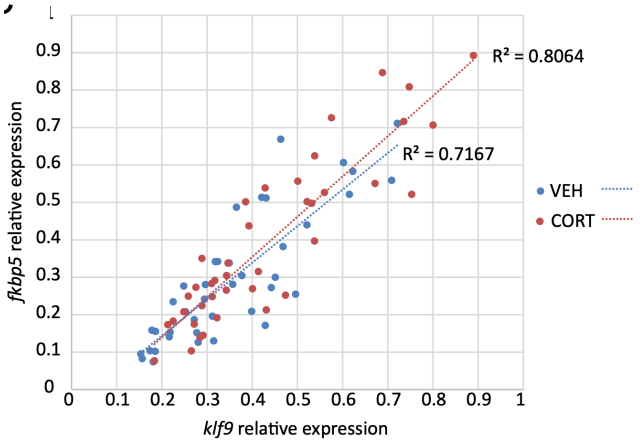


**Figure 4.3. Relative expression levels of *klf9* and *fkbp5* are correlated.** Data re-plotted from Fig. 4.2A.

A

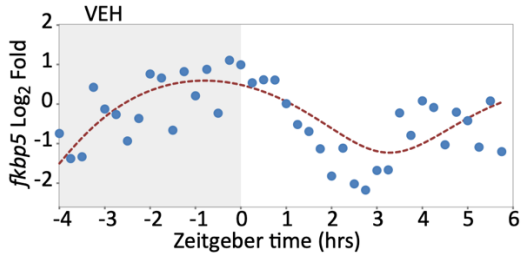


| Source | Degrees freedom | Sum of squares | Mean square | F | P value |
|---|---|---|---|---|---|
| Model | 4 | 5.56 | 1.39 | 9.03 | 4.03E-05 |
| Error | 35 | 5.38 | 0.15 | | |
| Total | 39 | 10.9 | | | |

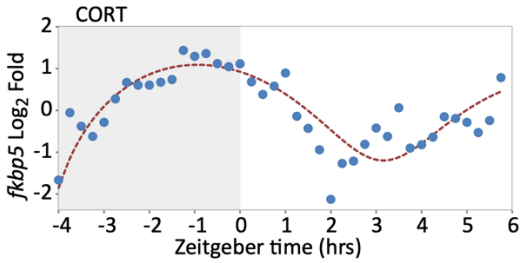


| Source | Degrees freedom | Sum of squares | Mean square | F | P value |
|---|---|---|---|---|---|
| Model | 4 | 1.46 | 0.364 | 30.5 | 5.73E-11 |
| Error | 35 | 0.418 | 0.012 | | |
| Total | 39 | 1.87 | | | |

B

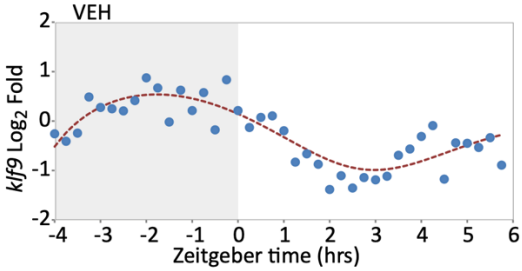


| Source | Degrees freedom | Sum of squares | Mean square | F | P value |
|---|---|---|---|---|---|
| Model | 4 | 4.34 | 1.09 | 22.7 | 2.54E-09 |
| Error | 35 | 1.67 | 0.05 | | |
| Total | 39 | 6.01 | | | |

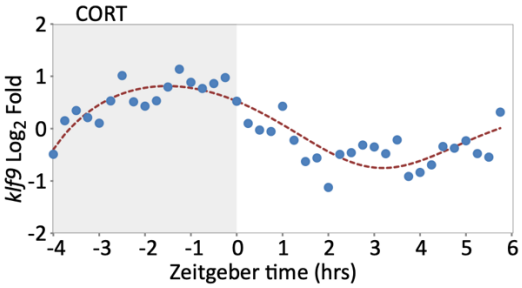


| Source | Degrees freedom | Sum of squares | Mean square | F | P value |
|---|---|---|---|---|---|
| Model | 4 | 6.57 | 1.64 | 30.5 | 5.60E-11 |
| Error | 35 | 1.88 | 0.05 | | |
| Total | 39 | 8.45 | | | |

**Figure 4.4. Gene expression time course data for *fkbp5* and *klf9* fit sinusoidal models.** Relative expression data for (A) *fkbp5* and (B) *klf9* from qPCR time courses fit sinusoidal wave models determined by nonlinear least squares regression (see Chapter 2 for detailed methods). Each data point represents the mean expression from three biological replicates of pooled (n= 3 to 6) larvae. Data are shown again with error bars in Fig. 4.6.

both genes peaked just prior to zeitgeber time 0 (ZT 0, corresponding to lights-on in the incubator), falling sharply thereafter. The data for both genes could be fit by nonlinear regression to sinusoidal models with calculated wavelength periods of 8.2 and 9.5 hours for *fkbp5* and *klf9* respectively (ANOVA $p<0.0001$, Fig. 4.4). However, it is important to note that the 10-hour sampling window was too narrow to draw conclusions about this periodicity. Thus, expression of *klf9*, *fkbp5* were measured alongside the known circadian gene *per1a*[230] over a 24-hour period. While *per1a* had a prototypical 24-hour oscillation, *klf9* and *fkbp5* did not, but were downregulated after lights on (Fig. 4.5). Transcript levels of all three genes peaked synchronously just before ZT 0 and dropped precipitously thereafter. I interpret these data as indicative of coordination of GR activity with the circadian clock, as whole-larva CORT levels show a similar diurnal drop (see Section 4.3 and Fig. 4.10) and GC have been demonstrated to drive circadian cell cycle and metabolic rhythms in zebrafish larvae[20,252].

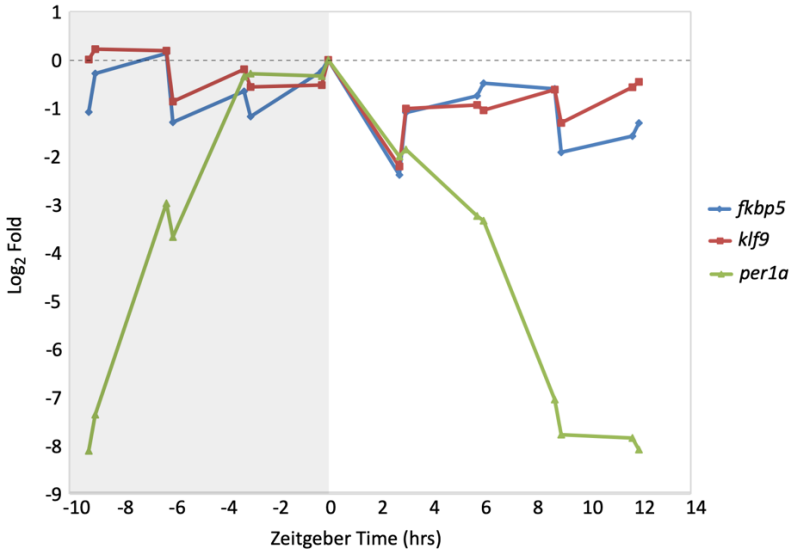


**Figure 4.5. *Klf9* and *fkbp5* expression are not prototypically circadian.** *Klf9* and *fkbp5* transcript levels measured in by qPCR over 24 hours alongside the known circadian gene *per1a*. Every three hours two samples were taken 15 minutes apart to account for ultradian variation. Data are from a single experiment using pooled WT larvae (n=10 per sample).

The GR-dependence of the diurnal activity dynamic of *klf9* and *fkbp5* was verified by comparing transcript levels in wild-type larvae and $GR^{-/-}$ ($GR^{369-}$) mutants. In the latter, both genes were lowly and flatly expressed, being significantly under-expressed at the wildtype (WT) expression peak of ZT -0.25 and remaining below WT at the 3.25 ZT expression nadir (Fig 4.2B).

To determine if the temporal dynamics shared by *klf9* and *fkbp5* are common to GC-responsive genes in general I re-measured one replicate (40 samples of pooled larvae) of qPCR time-course samples using the NanoString platform and a probe set (See Table 2.2) representing 21 genes known to be GR targets and/or that were identified by RNA-seq to consistently respond to CORT treatment, including *klf9* and *fkbp5*. Hierarchical clustering of these NanoString data distinguished two main time-dependent clusters of genes (Fig 4.2C). The tight correlation between *klf9* and *fkbp5* was underscored by these two genes clustering together on their own branch, which in turn clustered with other genes whose expression peaked in early morning hours, including circadian regulators *per1a* and *nr1d2a*, as well as the ammonium transporter and blood antigen *rhcga* and the neutrophil-specfic NADPH oxidase *ncf1*. Conversely for the second main cluster, which included the GR target *tsc22d3* (also known as GILZ) as well as several immune genes, expression was low in the early morning when endogenous CORT is high, then rose after ZT 0.

I next assessed the effect of chronic CORT exposure, shown by our previous studies to elevate *klf9* transcript levels at the 5 dpf mid-morning (~ZT 3) timepoint when samples were collected[158,159]. Overall, CORT treatment resulted in a significant elevation of both *klf9* and *fkbp5* transcripts across all timepoints ($p<0.005$, paired t-tests), albeit with instances of lower

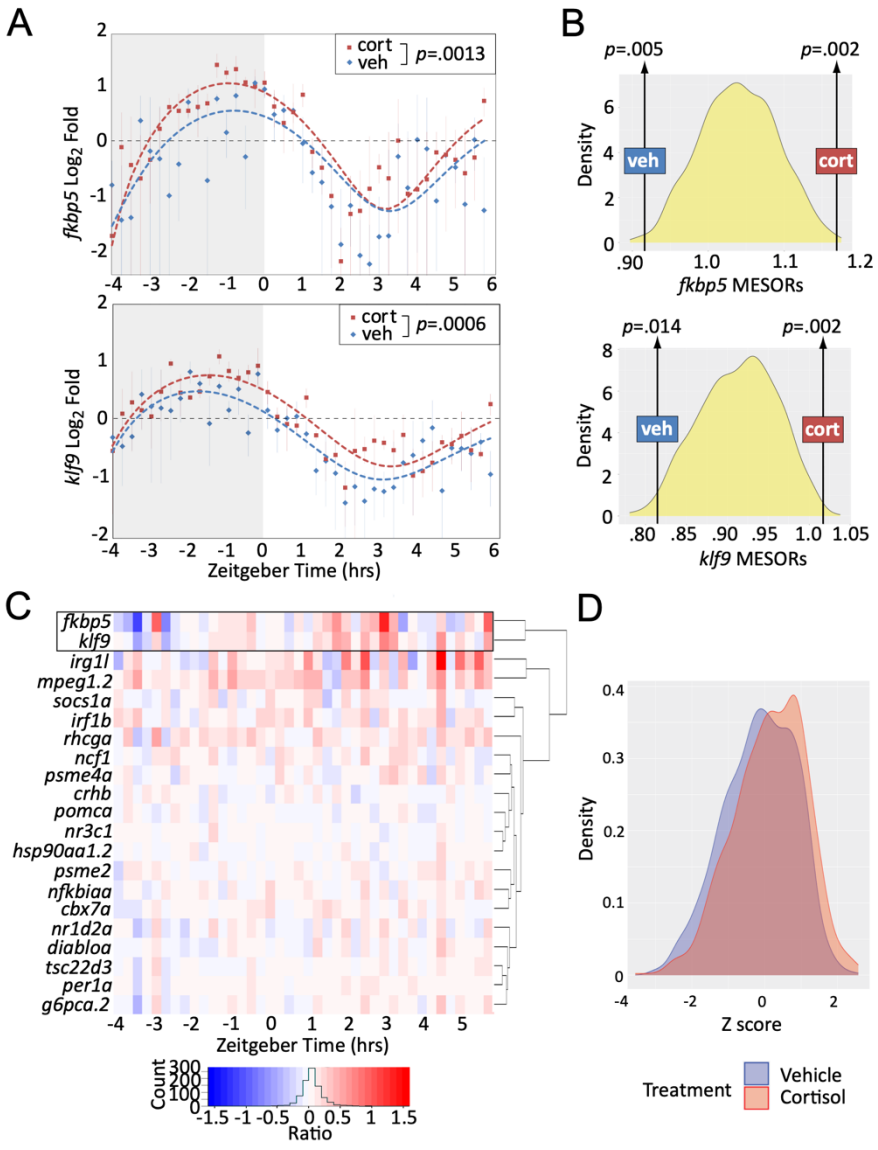


**Figure 4.6. Chronic cortisol similarly upregulates *klf9* and *fkbp5*.** (A) Sinusoid models fit to *fkbp5* (top) and *klf9* (bottom) qPCR relative expression data. Each data point represents the average of three biological replicates of pooled larvae (3 to 6 larvae per pooled sample; VEH-treated datapoints are the same as in Fig. 4.2A). P-values calculated using paired t-test (data paired at each timepoint). Fit of the model to the data was tested by ANOVA (P-value < 0.0001 in each case, see Fig. 4.4). (B) Distributions of Midline Estimated Statistics Of Rhythmicity (MESORs, a rhythm-adjusted mean) of datasets generated by randomly selecting expression data from VEH or CORT samples at each timepoint from experiments shown in (A). Experimentally determined MESORS of VEH and CORT datasets sit at either extreme. (C) Heat map of the expression ratio in CORT/VEH samples (log2 transformed) of *klf9*, *fkbp5*, and other targets of GC signaling in the NanoString data set. A single replicate of RNA from time course shown in (A) was used. (D) Density plot of Z-scored expression of all genes measured with NanoString indicates an overall increase in expression due to chronic CORT treatment.

Levels at ~20% of individual timepoints due to fluctuating dynamics (Fig. 4.6A). To rigorously test whether the CORT exposure significantly increased the average expression of these genes 1000 time series data sets were generated computationally in which either VEH or CORT measurements were randomly selected at each timepoint from the experimental data. Sinusoid models were then fit to each randomized time series. Each sinusoid equation includes five constants (see Chapter 2 for full methods), including the Midline Estimating Statistic Of Rhythm (MESOR, i.e. a rhythm-adjusted mean value). For both *fkbp5* and *klf9*, the MESORs of models fit to either VEH or CORT experimental data were located at opposite extremes of normal distributions (approximately) of MESORS compiled from all 1000 randomized models ($p<0.02$, Fig. 4.6B). This provided statistical confirmation that chronic CORT exposure produced a statistically significant increase in *klf9* and *fkbp5* transcript levels over the period data was collected.

To determine how the response of *klf9* and *fkbp5* to chronic CORT compares to that of the other GR targets in the NanoString probe panel, the expression ratio of CORT- to VEH-treated samples was calculated at each timepoint for each gene. The CORT response of *klf9* and *fkbp5* was correlated, clustering separately from that of all other genes and manifesting a stronger effect than most (Fig 4.6C). The immune genes *mpeg1*.2 and *irg1l* responded similarly in magnitude, but with different timing (rising rather than falling after ZT 0). The overall effect of the treatment across all genes was a subtle increase in transcript levels (Fig 4.6D).

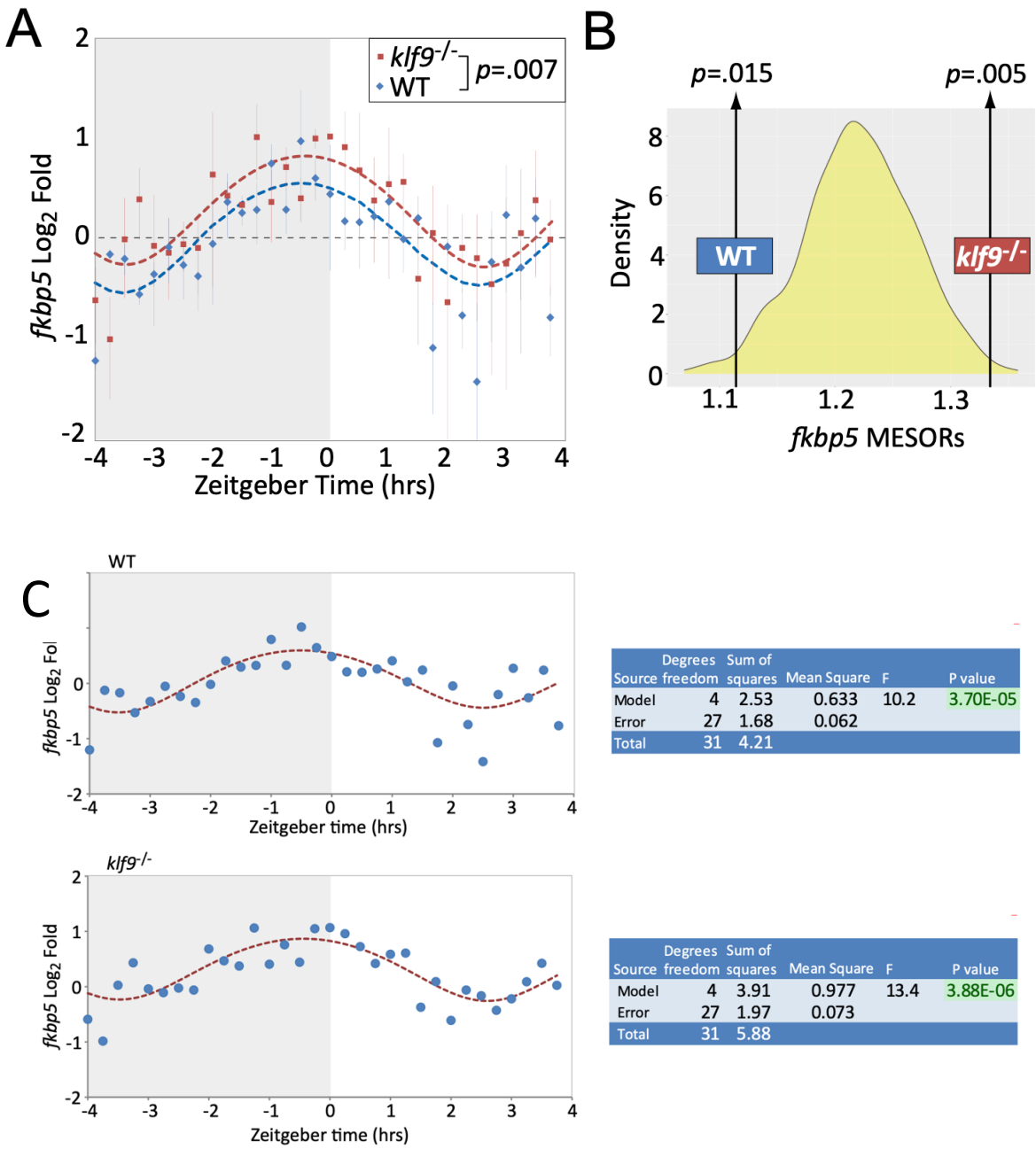


| Source | Degrees freedom | Sum of squares | Mean Square | F | P value |
|---|---|---|---|---|---|
| Model | 4 | 2.53 | 0.633 | 10.2 | 3.70E-05 |
| Error | 27 | 1.68 | 0.062 | | |
| Total | 31 | 4.21 | | | |

| Source | Degrees freedom | Sum of squares | Mean Square | F | P value |
|---|---|---|---|---|---|
| Model | 4 | 3.91 | 0.977 | 13.4 | 3.88E-06 |
| Error | 27 | 1.97 | 0.073 | | |
| Total | 31 | 5.88 | | | |

**Figure 4.7. *Fkbp5* expression is increased in *klf9* mutants.** (A) Sinusoid modeling of *fkbp5* time-course data obtained by qPCR of RNA extracted from WT and *klf9*$^{-/-}$ larvae. Each data point represents the average of three biological replicates of pooled larvae (4 to 5 larvae/sample). P-value calculated by paired t-test (data paired at each timepoint). Error bars represent standard error of the mean. Model fits tested by ANOVA (P-value <0.0001, see Fig. 3.16). (B) Distribution of MESORs of datasets generated by random sampling as described in Fig. 4.2 and methods. MESORs of measured WT and *klf9*$^{-/-}$ data sit at either extreme. (C) Statistical fit of sinusoid models to expression data.

### 4.3. Loss of Klf9 increases *fkbp5* expression

Preliminary data from the Coffman Lab (unpublished) using morpholino knockdown of Klf9 suggested regulation of *fkbp5* by Klf9 but were inconsistent. Given the dynamics of *fkbp5* expression I (again) reasoned that such inconsistencies could be due to insufficient temporal resolution. Thus, I again performed high-density time courses to test the hypothesis that *fkbp5* mRNA levels would be elevated in *klf9*$^{-/-}$ larvae compared to WT. Absent Klf9, *fkbp5* was elevated on average (Fig. 4.7A). The diurnal oscillation in *fkbp5* activity was conserved and sinusoid models fit to both WT and *klf9*$^{-/-}$ time-course data indicated a significant elevation of the *fkbp5* MESOR in the mutants (Fig. 4.7B & C). In addition, the circa-dawn peak of *fkbp5* activity was delayed by ~35 minutes in *klf9*$^{-/-}$ larvae, occurring ~30 minutes before lights-on in WT but several minutes after lights-on in mutants, and the time from peak to nadir was subsequently compressed from ~3 hours in WT to ~2 hours in mutants (Fig. 4.8). No significant horizontal phase shift was detected between models fit to WT and mutant data. However, there were significant differences in the model constants for amplitude ($p=0.001$) and decay rate of the wave ($p<0.0001$) suggestive of altered transcription and/or degradation rates in addition to increased mean expression (MESOR $p=0.02$); these possibilities require further testing.

Combining chronic CORT treatment with the *klf9*$^{-/-}$ mutation cumulatively increased *fkbp5* transcript levels in 5dpf larvae, consistent with direct regulation of *fkbp5* downstream of hormone signal (Fig. 4.9). Although I was unable to obtain an antibody suitable for measuring Fkbp5 protein level in zebrafish, similar transcript elevation was reported in mammalian cells

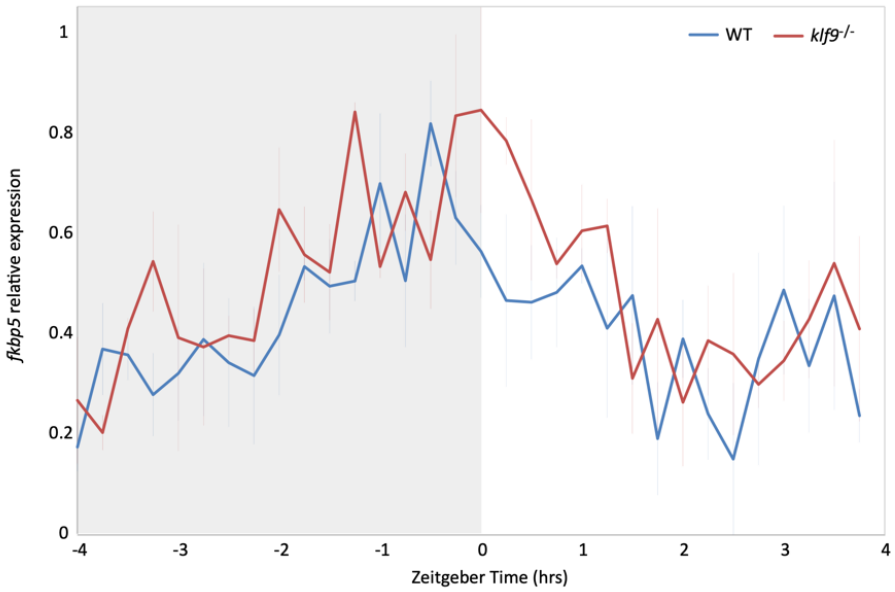


**Figure 4.8. Peak expression of *fkbp5* is delayed in *klf9*$^{-/-}$ larvae.** The expression data from Fig. 4.7A (average of three biological replicates) re-shown as line plot. Note the delayed peak expression in mutant larvae at 0 ZT.

After chronic GC treatment and was accompanied by increased protein expression[24]. Treating larvae with the Fkbp5 inhibitor FK506 (tacrolimus) increased *fkbp5* transcript levels, as predicted due to loss of Fkbp5-mediated inhibition of the GR (Fig. 4.9). FK506 treatment was less effective in *klf9*$^{-/-}$ larvae, however, increasing *fkbp5* transcripts ~3-fold compared with ~12-fold in WT. Although not conclusive, these findings are consistent with increased Fkbp5 protein in mutants.

Because gene ontology analysis of RNA-seq indicated that Klf9 may play a role in regulating steroid metabolism (see Fig 3.4B), it was possible that the increase in *fkbp5* transcripts seen in *klf9*$^{-/-}$ larvae could be due to mutants having higher endogenous CORT levels. However, measurement of whole-body CORT level in 5 dpf larvae did not detect any difference in either baseline CORT concentration or diurnal variation (Fig. 4.10A & B). In fact, the CORT response to the acute stress of chase with a pipette was slightly decreased in mutants (Fig.

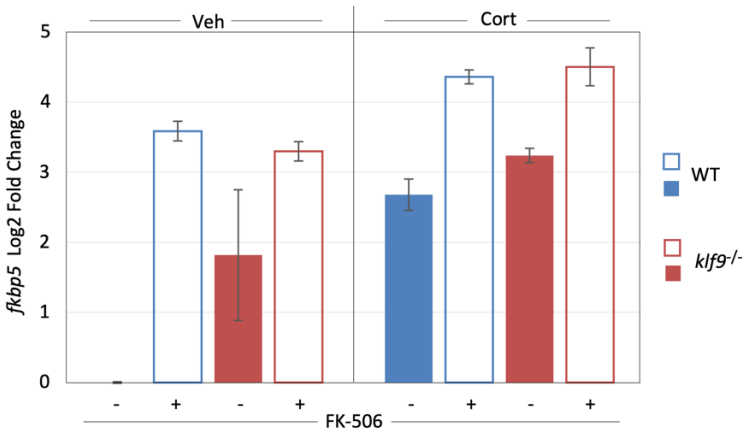


**Figure 4.9. *Klf9* mutation, chronic cortisol and Fkbp5 inhibitor cumulatively increase *fkbp5* expression**. Relative expression of *fkbp5* in WT and *klf9*$^{-/-}$ larvae treated with VEH or chronic 1µM CORT from 0-5dpf, and FK-506 or additional vehicle overnight from 4-5dpf. Error bars represent 95% confidence interval of two biological replicates of pooled larvae (n=8/sample).

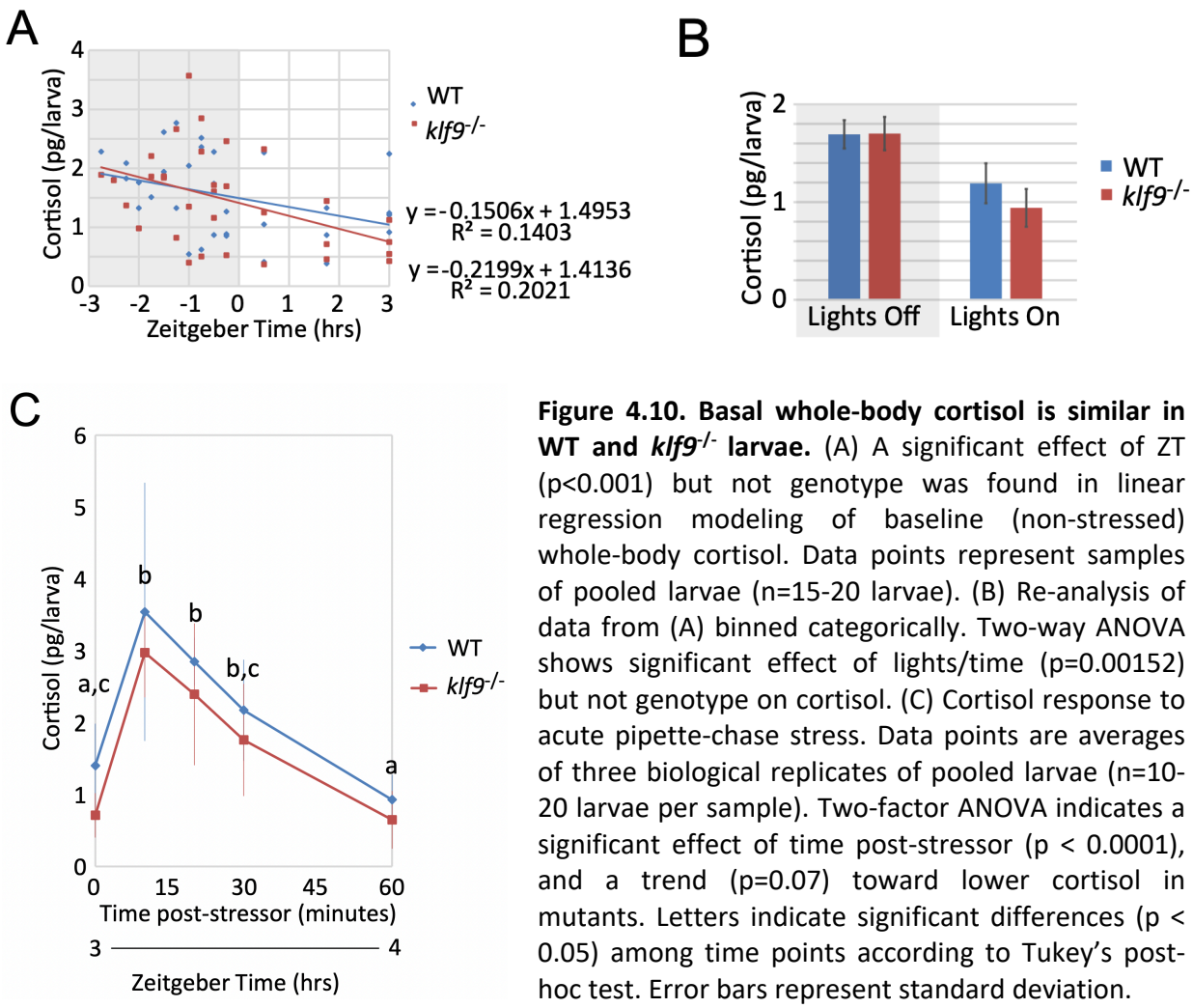


**Figure 4.10. Basal whole-body cortisol is similar in WT and *klf9*$^{-/-}$ larvae.** (A) A significant effect of ZT ($p<0.001$) but not genotype was found in linear regression modeling of baseline (non-stressed) whole-body cortisol. Data points represent samples of pooled larvae (n=15-20 larvae). (B) Re-analysis of data from (A) binned categorically. Two-way ANOVA shows significant effect of lights/time ($p=0.00152$) but not genotype on cortisol. (C) Cortisol response to acute pipette-chase stress. Data points are averages of three biological replicates of pooled larvae (n=10-20 larvae per sample). Two-factor ANOVA indicates a significant effect of time post-stressor ($p < 0.0001$), and a trend ($p=0.07$) toward lower cortisol in mutants. Letters indicate significant differences ($p < 0.05$) among time points according to Tukey's post-hoc test. Error bars represent standard deviation.

4.10C). Thus, the elevated *fkbp5* activity in *klf9*$^{-/-}$ larvae is unlikely to be due to systemically elevated CORT.

### 4.4. Klf9 binds *fkbp5* promoter-proximal chromatin

To determine if Klf9 physically interacts with *fkbp5*, ChIP-qPCR was performed using primers encompassing putative Klf9 target motifs identified via JASPAR in the *fkbp5* promoter region (Fig. 4.11). A commercial antibody for human Klf9 recovered significantly more *fkbp5* promoter region DNA than did a non-specific IgG, and this signal was reduced in *klf9*$^{-/-}$ mutants (Fig. 4.12). However, the commercial antibody recognizes an amino acid sequence highly conserved in zebrafish Klf13, and might be expected to interact with other KLF proteins as well. I therefore used CRISPR to engineer a new zebrafish line, in which a C-terminal "AM" epitope tag (developed by Active Motif, Carlsbad, CA) was incorporated by homology-directed repair into the endogenous *klf9* locus allowing Klf9-specific ChIP with the anti-AM antibody (Fig. 4.13 and Methods). Fish heterozygous for the tagged allele were crossed and ChIP was performed in pooled offspring (i.e. a mix of tagged and untagged larvae) and WT larvae from parental siblings were used as control. Recovery of *fkbp5* promoter DNA was enriched ~3-fold using chromatin from the AM-tagged line (Fig. 4.13C). While Klf9 has been implicated in both transcriptional activation and repression in different contexts[190], it functions predominantly as a repressor in mouse hippocampus, where it binds promoter-proximal DNA enriched for circadian E-Box motifs[191]. HOMER motif enrichment analysis of 149 genes consistently upregulated by chronic CORT revealed that 86% of those genes annotated had both promoter-proximal KLF and circadian E-Box motifs (while only 46% had glucocorticoid response elements, Fig. 4.14, and

GR: LASAGNA Transfac M00205; KLF9: JASPAR MA1107.1

**>*Dr_fkbp5*_upstream3000-exon1_refGene_NM_213149**

ctcttacacaaaacccatctgttatgtcactcacattatgttcctggattaactatccatctgaaattatttttaaa
aatcaggcttaaaaaagggaaatcaatcccttcaaacgcaggcaatcacgtatgccacctattgtgttcctgctgac
acctcttgttgctgtggtgaacgagccggaacattttgtaacagtttcagcctggagaggcttttgaggcaggtaa
catgttgccattactgatgtttattcaatgtttggcatggtaacttgatagactggatttgatcagaggatgatcacg
atgtacaatgctttcatgtagacattgtaaacatgaggttatttataattatttattgaaaatgttacttagcttta
aagattcattgtggattaaacttaacttttttaattaggcaatattcgcccccacttcagggacaatataaagtcaat
aaatcaaatactaattggatcaatgttgccttttaaggcaaatacctaaattgaatctattacttcagtcaaccaca
aataacaacaacatgttaaaagttgtacttcaattatccacttaaccaattaactcattactgggtaatgctgtggt
cacactaaagtttttagatgcaaaattgtgtccatattttaaaatttctgtacagagaggtcatgttttgattttcg
attagttttgcgaagtcaagtgatgcaatttcacaggtcagagttcaccaagcttgaaccttcaaatgcagtgaact
acgaaacttgtcgcacaagcttgcatttccagtttgttgctttcgcatgtgattgaatggaagtctaaggggcaaaa
tgagcagtgtgaccatggcttttgctggtaaatatattgattaattaacagttgctcatgatttatggatgttctcc
aattatacagttttaaattgcattatagaatcttaattattgctccaaccaattctgatatttaaaaaataactctg
caggttaaaaaactgactgaaataggccttttcaatagtttgaaataatttattgtataacatgtaatacatatata
acagaaaaagtactgaaagattaacaaatggtcttgattacctagacagtatatattgatggattgattgaacttca
catgataaagctgcaaaaatgtctatctatctatctatctatctatctatctatctatctatctatctatctatcta
tctatctatctatctatctatctatctatctatctatctatctatctatctatctatctatctatctatctatctatct
atctatctatctatatatctaactatccatccatccatccatccatccatccatccatccaccctatacaca
cacacacacacacacacacacatatttatatatatatatattatgcacatacatacatacatacatacatacatatc
agggctgtgtgatttggagaaaatatcaaattaaatttttttgacaaatattgttattgcgatttgaattacggttt
aattttgaagcagcagacgccataatcccacttgtcaatgctttccttttttttattgtaggcataattcagtagcgc
aattctgaaatggcagaatgaaagtgtgcccactcagttggctagttataaagccctggctggatcacacgatttcg
acatgatttccttcacgttgggtgtcgtggggagttgtaaatgactccaatagcatctggatgcagcctttatatgc
aagctgagattgcatcactcagcgatgcaatgtcagacaaaatgcactcaatggagtgagtgacgtcactgtacagc
gacaaatggatgtcatgacacaaaatttttttcttctcgtgtaatgtgccatagtttacgacagctgataccatgtct
catgacaccatcgcatgtttaattttcggactggttttgaagcacctcagatgctattcctcatcctggtttagata
aatacatattattaaatatatatagaggcctatatatatgtgtgtgtgtgtgtgtgtgtgtgtgtgtgtgtgtgtgt
gtatgtatgtatgtatatatatatatatatatatatatatatatatacacataatatatacataactaattgcaaca
tttcaagttgcgattgcgatttgactttgattaatcgcagagcttgttaattaatgatctctttatttttgtaacaa
gatctgcatcaaatatatggaagaaaaattattagcataatacttattgaaaaatctacaacaagcattaaacaaat
tagtgaacttatatttaaaaactatgctttatcgtatgaaaatacaggtttctttacaaactacagtaaaaaaaagc
ttctgcgcgttttataactttgaataataataataataataataataataataatcatgatgatgatgttgaattat
atcgctacaccggctctattcgattttatgctcaatatgctgctttagttctaggcttggtatagtgtcatcccgat
ggtgttgtgtgcagtctgttcttgctttctgtttcatcacctgcatcctcatcagaactgtaaaatataaacagcct
accatccaacacccacaatcgtcttcgtagtatgttttttctctacttatttttttacttccacatttttctcgac
gcaatctagtcgtgttgttctttccgcgtatcgctgtgctctgtgtggttgtacacgctgttcctaacttgagctgt
tcactcagcacacaacgggttacgggtcagggtgtctactaggacactgtgttctcatcagcgcgagctacagtaca
gccggaacattgtgttacttttgtggacagtttccaaggcctgcccttaatttatctccacaccgcccctccccagcg
tttactcctcctcctttagtctcatttcatttccccgtccaaatgtctcgcagaggcgtatcgtgttgatgatTAT
TGGTGTGGAGAAGTGTAAAATACTGCCGGTAGAACATCTAGTACTCTCGCGGTGCTGAGAGGGCGGGCTCATTCCCC
TTTAAGCCGCTACGCACAGGTTGTATTCGCCGGTGAGACTAAACAGAAGTTGTATACGGACGGATAAATGGTCAAAC
ACATGAGAGGAAACAACAACCAAAGGAATATTTTGGGAACAAGGGCATGTATGAGTGGTGAG

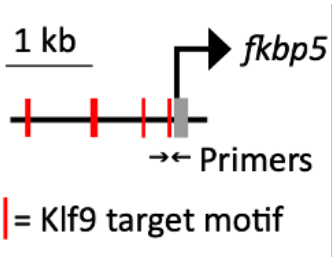


**Figure 4.11. *Fkbp5* proximal promoter region contains putative Klf9 binding sites.** (Top) Klf9 binding motifs (red) and GR binding motifs (green) identified respectively by JASPAR and LASAGNA using the indicated motif matrices. Upstream sequence (3 kb) is in lower case font; exon 1 sequence is in upper case. Primer target sequences are underlined. (Right) Schematic view of sequence shown above. (GR binding motifs omitted for clarity)

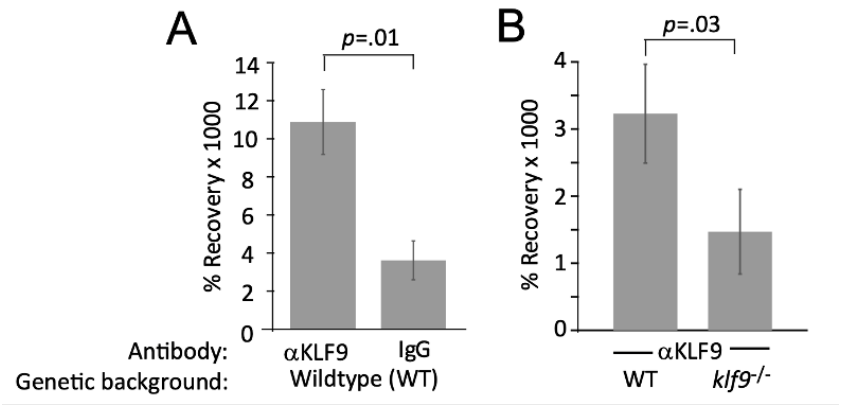


**Figure 4.12. Immunoprecipitation of *fkbp5* promoter DNA is enriched using an anti-Klf9 antibody.** (A) DNA immunoprecipitated with anti-Klf9 or non-specific IgG control antibody in WT larvae. Data are mean of four experimental replicates with standard error. (B) immunoprecipitation using anti-Klf9 antibody in WT or *klf9*$^{-/-}$ larvae. Data represent mean of two experiments with standard error. Significance calculated by paired Student's T-Test.

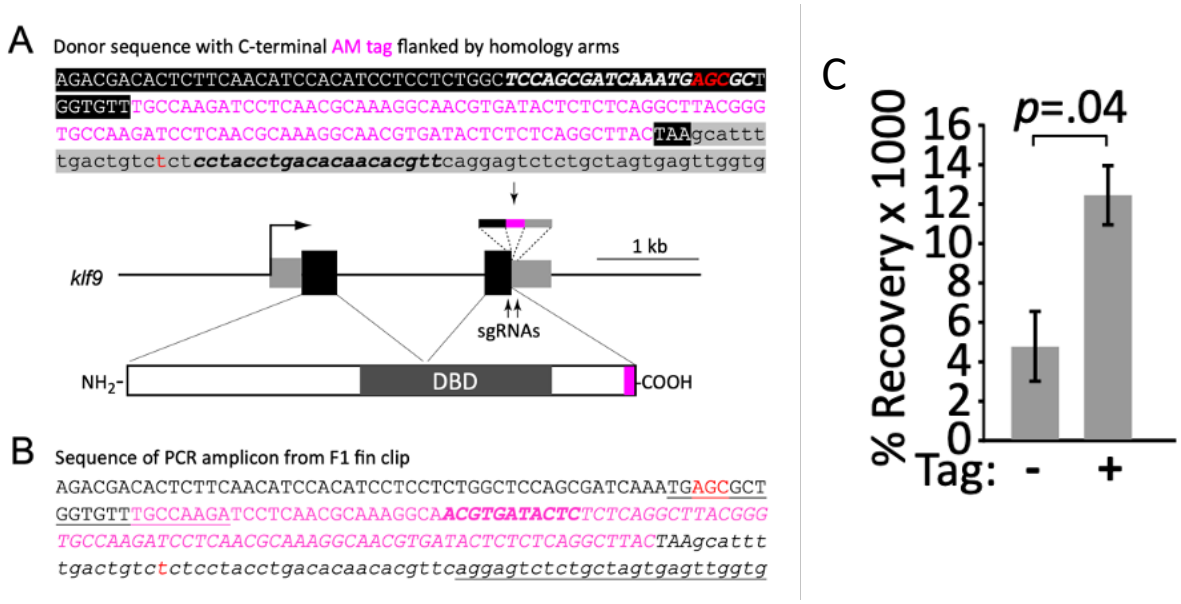


**Figure 4.13. Immunoprecipitation of *fkbp5* promoter with epitope-tagged Klf9.** (A) Schematic of donor template and strategy for CRISPR-mediated insertion of C-terminal AM tag into the *klf9* locus by homology directed repair. AM sequence in magenta is flanked by micro-homology arms of endogenous exonic (black) and intronic (grey) sequence. sgRNA target sites are italicized. Silent and PAM mutations (red) were included to prevent re-editing. A schematic of the resulting protein shows the location of resulting epitope tag. (B) Assembled sequence of PCR product amplified from mutants. Locations of primers are underlined. Sequence from forward primer is italic. Overlapping sequence is bold. (C) Recovery of *fkbp5* promoter DNA from WT (-) and Klf9-AM tagged (+) larvae by ChIP with anti-AM tag antibody. Data represent two biological replicates with standard error. Significance determined by T-Test.

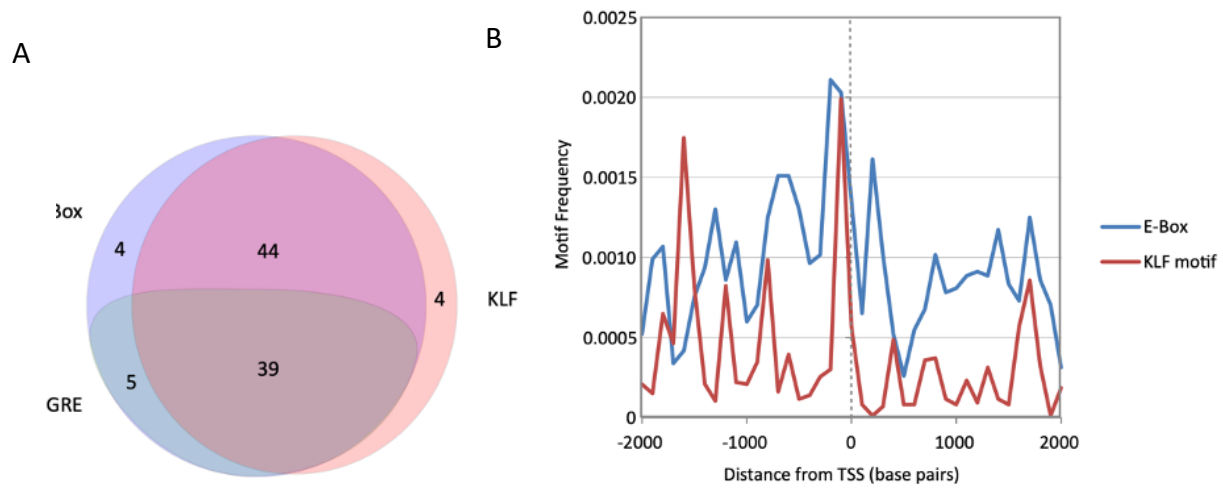


**Figure 4.14. KLF and E-Box motifs are enriched near transcription start sites of glucocorticoid responsive genes**. (A) Prevalence of KLF, GRE and E-Box motifs within 2000 bp of TSS in 96 genes consistently responsive to chronic GC. (B) Frequency distribution of KLF and E-Box motifs with respect to the TSS.

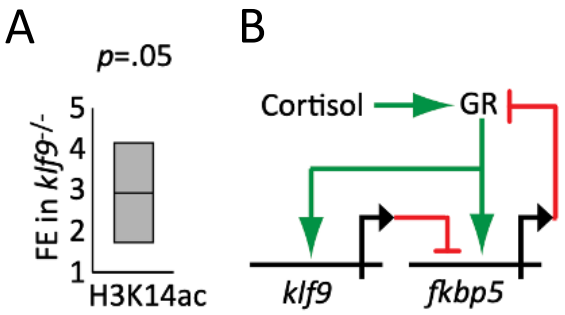


**Figure 4.15. Hyperacetylation of *fkbp5* promoter in *klf9* mutants and proposed regulatory circuit.** (A) A roughly 3-fold enrichment of *fkbp5* promoter DNA immunoprecipitated with anti-acetyl-H3K14 was found in *klf9*$^{-/-}$ larvae compared with WT, consistent with direct repression of *fkbp5* by Klf9. Data are from three experimental replicates using pooled larvae (between 75 and 90 larvae per sample, matched across conditions within each replicate) (B) Proposed gene regulatory circuit containing the GR, *fkbp5* and *klf9.* Activation is denoted by green arrows, repression by red lines.

Appendix H), with *fkbp5* having E-boxes at +154 and -1840bp. As the N-terminal domain of mammalian Klf9 interacts with the Sin3a histone de-acetylation complex[241], I hypothesized that Klf9 might repress *fkbp5* via de-acetylation of histone H3 at the *fkbp5* promoter. Using an antibody to H3K14ac and ChIP-qPCR, I found a ~3-fold increase in *fkbp5* promoter DNA recovery in *klf9*$^{-/-}$ larvae compared with WT ($p<0.05$, Fig. 4.15A). Taken together, the data described above indicate that Klf9 interacts physically with the *fkbp5* promoter region, forming a circuit predicted to regulate GR activity through a combination of Fkbp5-mediated negative feedback and Klf9-mediated incoherent feed-forward regulatory logic (Fig. 4.15B).

### 4.5. Loss of Klf9 decreases oxygen consumption rate and alters metabolic gene expression

Regulation of blood sugar and metabolic homeostasis by glucocorticoids is well known, and by regulating the GR through the circuit described above both *klf9* and *fkbp5* would be predicted to exert influence on metabolic homeostasis as well. Indeed, both *fkbp5* and *klf9* have previously been implicated in metabolic regulation (see next chapter for Discussion). Gene ontology analysis of RNA-seq data also indicated Klf9 is involved in intermediary metabolic processes in zebrafish larvae including sterol and carbohydrate metabolism (see Fig. 3.4). To determine how loss of Klf9 affects metabolism in developing zebrafish, basal oxygen consumption rate (OCR) of 1 dpf embryos was measured, revealing a ~10% decrease in *klf9*$^{-/-}$ mutants (Fig. 4.16). Interestingly, this effect was ameliorated somewhat by chronic CORT treatment, which on average decreased OCR in wild-type embryos while increasing it in *klf9*$^{-/-}$ mutants. Morpholino knockdown of *klf9* in zebrafish has been reported to disrupt erythropoiesis[249], so it is possible that decreased OCR in *klf9*$^{-/-}$ larvae could result from a deficit in red blood cells. However, the apparent lack of a non-specific control morpholino group in

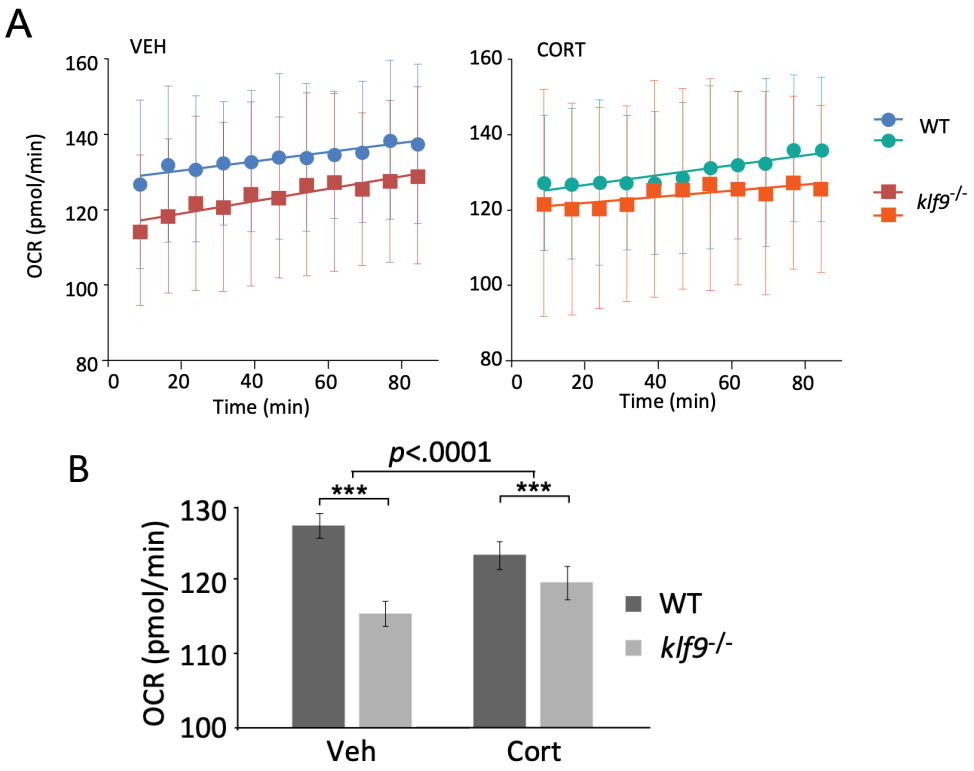


**Figure 4.16. Basal oxygen consumption rate is decreased in *klf9* mutants.** (A) Mean OCR and standard deviation of 60 embryos per genotype/treatment (three experimental replicates of 20 embryos each) measured over an 85-minute time period. Linear regression lines are also shown. (B) Bars representing the average Y-intercept of linear fits of time-course data in (A), +/- standard error. Two-way ANOVA indicated significant effects of genotype (WT vs. *klf9*$^{-/-}$, $p<0.0001$) and treatment (VEH vs. CORT, $p=0.04$), as well as a significant interaction ($p<0.0001$). ***Adjusted $p<0.0001$ by Šídák's multiple comparisons test.

That study renders the results difficult to interpret. It is also unclear to what extent larvae at that early stage would rely on red blood cells for oxygenation, as opposed to simple diffusion. Recently, it has been shown that *klf9* overexpression increases OCR in primary adipocyte cultures as well as in live transgenic mice[253]. This indicates that potential decreases in blood oxygen transport would likely be in addition to, or may result from, cell-autonomous metabolic effects.

For additional insight into the nature of metabolic regulation by *klf9*, I interrogated the *klf9*$^{-/-}$ RNA-seq dataset by performing a focused principal component analysis (PCA) on two gene lists curated by a research group independent of our own (Appendix I) and comprising targets of Hif1 and AMPK signaling, which respectively regulate glycolysis and oxidative metabolism. Because Hif1 and AMPK are regulated by protein degradation rate and phosphorylation, their transcript levels are not diagnostic. However mRNA expression of their downstream targets has been shown to accurately reflect changes in the metabolic phenotype in cancer cells, which rely more heavily on glycolysis as they become more malignant (i.e. the Warburg Effect)[254]. Given the decrease in OCR measured in *klf9*$^{-/-}$ mutants, as well as reports that Klf9 regulates stem cell metabolism[255] and acts as a tumor suppressor[256,257] I reasoned that this targeted PCA analysis might be informative here.

The first principal components (PC) of both datasets (respectively accounting for 28% and 27% of the variance) represented the effect of chronic CORT treatment, and plotting them against each other revealed a high degree of correlation between the two pathways (Fig. 4.17A). Top genes contributing to AMPK PC1 included insulin regulator *mafa* at the VEH pole

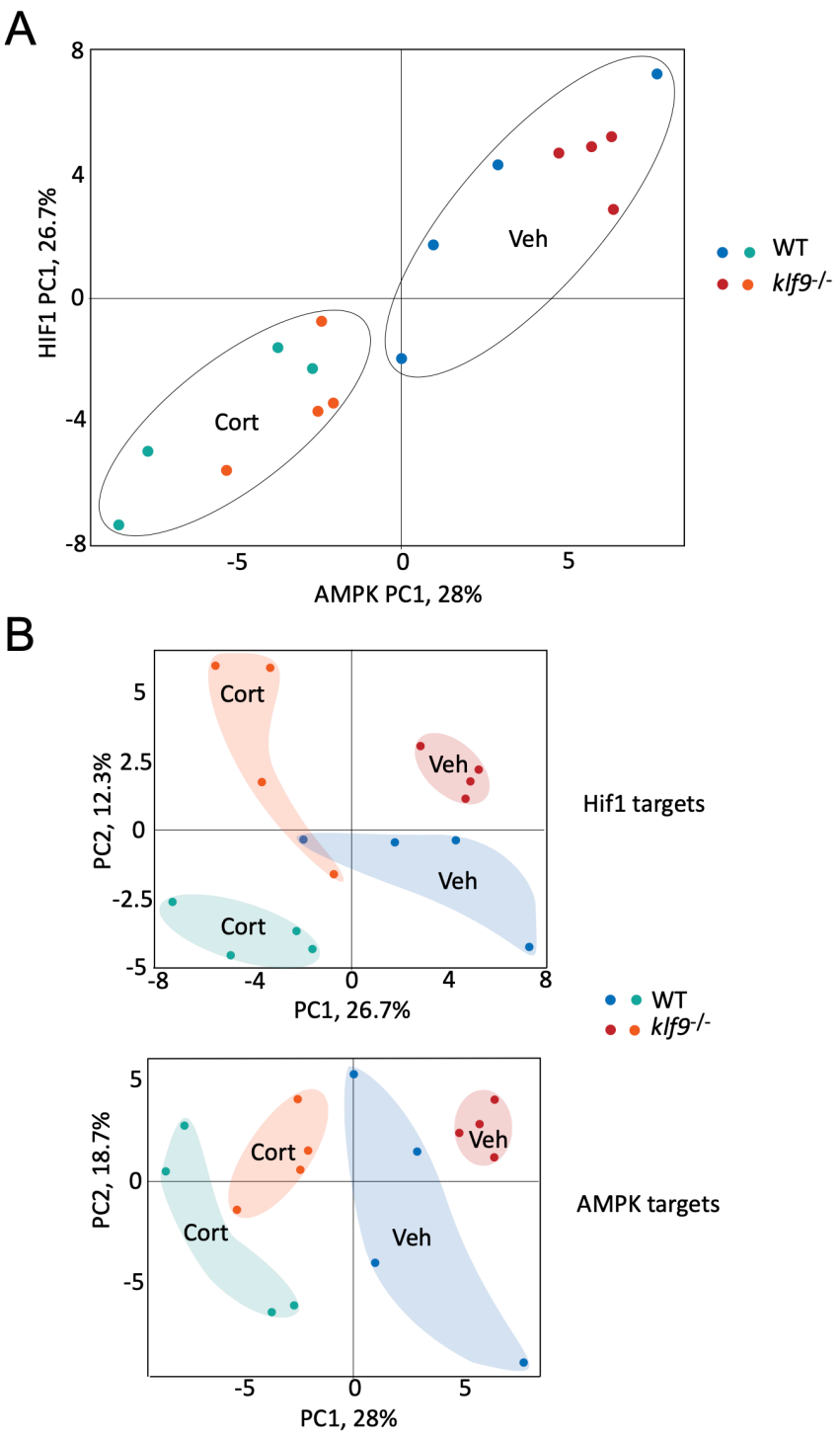


**Figure 4.17. PCA of Hif1 and AMPK pathway target genes** (A) Plotting PC1 of Hif1 target expression versus PC1 of AMPK target expression segregates samples by treatment and indicates strong co-regulation of the two pathways. (B) Plots of principal components 1 and 2 for genes in each pathway separately reveal broad effects of treatment and genotype.

While the CORT-treated pole was weighted by the GC target *g6pca*, two members of the stress-responsive *gadd45* family, and *acadm*, which encodes a catalyst of mitochondrial beta-oxidation. *Klf9*$^{-/-}$ mutant samples showed a shift away from the CORT pole of AMPK PC1, suggesting less influence of CORT (endogenous and treatment) on expression of these genes in mutants. Plotting PC1 vs PC2 within either the Hif1 or AMPK dataset segregated the samples by treatment and genotype (Fig. 4.17B). Hif1 PC2 (12% of variance) segregated WT from *klf9*$^{-/-}$ mutant samples, and examples of genes at either end of this axis included the Hif1a regulator *egln3*, upregulated in mutants (Fig. 4.18), and glutamyl-prolyl TRNA synthetase *eprs1*. Lactate dehydrogenase (*ldha*), responsible for conversion of pyruvate to lactate in the final step of glycolysis and a noted Hif1 target[258,259], was also upregulated in *klf9*$^{-/-}$ mutants (Fig. 4.18). Wild-type samples spanned AMPK PC2 (19% of variance), whereas *klf9*$^{-/-}$ samples were restricted to one pole (Fig. 4.17B), indicating less variation in expression of these genes in mutants, which included both the cytosolic and mitochondrial isozymes of gluconeogenic regulator phosphoenolpyruvate carboxykinase, *pck1* and *pck2*. As noted above, previous comparison of RNA-seq experiments found that genes involved in glycolysis and pyruvate metabolism were reciprocally regulated in *klf9*$^{-/-}$ and GR$^{369-}$ mutants under vehicle conditions, being upregulated in the former and downregulated in the latter[159]. Kyoto Encyclopedia of Genes and Genomes (KEGG) pathway analysis of the full set of genes significantly effected in *klf9*$^{-/-}$ larvae under all

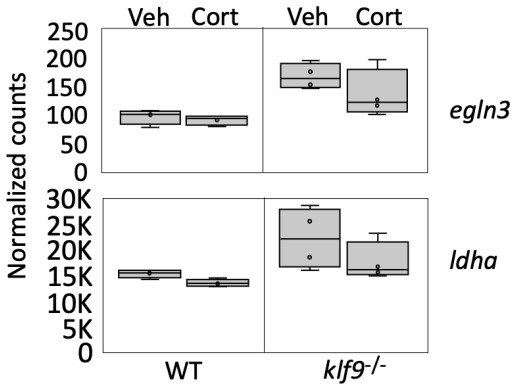


**Figure 4.18. Metabolic gene overexpression in mutant larvae.** Normalized RNA-seq counts of Hif1 target *egln3* and glycolytic gene *ldha.*

conditions (FDR q<0.05) also showed enrichment for genes involved in glycolysis/gluconeogenesis as well as the adjacent pentose phosphate pathway (PPP) (Table 4.2). Comparison of genes upregulated in CORT-treated *klf9*$^{-/-}$ larvae compared with CORT-treated WT larvae again included glycolysis, the PPP, and pyruvate metabolism (Tables 4.3 & 4.4). This indicates that genes involved in glycolysis and adjacent metabolic pathways are more dysregulated by chronic CORT in Klf9 mutants. Using HOMER to look for enriched transcription factor binding motifs within 2000 bp of the transcription start site (TSS) of genes upregulated in mutants treated with CORT revealed high enrichment of KLF motifs. Seven of the top ten results were KLF motifs, with Klf9 first on the list (adjusted p-value < 0.0001, Fig. 4.19). Notably, except for *fbp2*, all the glycolytic and PPP pathway genes that were overexpressed in *klf9*$^{-/-}$ mutants had potential KLF sites within 2000bp of the TSS (Fig. 4.20A). In contrast, genes downregulated in mutants showed no enrichment for KLF motifs, and were instead enriched for motifs for IRFs, HNF4a (hepatic nuclear factor), calcium responsive CREB5, and the retinoic acid receptor. These data suggest Klf9 functions predominantly as a repressor in *Danio* larvae (consistent with recent reports[191,240]) and regulates metabolism by repressing glycolytic genes. One predicted effect of this regulation would be the shunting of metabolic flux around glycolysis, through the PPP (Fig. 4.20B) and into the TCA.

**Table 4.1. KEGG pathway enrichment in genes upregulated in *klf9*$^{-/-}$ versus WT larvae.** Analysis of combined VEH + CORT samples.

| Term | Pvalue | Fold Enrichment | Bonferroni | Benjamini | FDR |
|---|---|---|---|---|---|
| dre00010:Glycolysis / Gluconeogenesis | 2.07E-05 | 5.57843 | 0.00221 | 0.00221 | 0.00209 |
| dre00030:Pentose phosphate pathway | 1.42E-04 | 8.35947 | 0.01509 | 0.00665 | 0.00627 |
| dre00591:Linoleic acid metabolism | 1.87E-04 | 10.5772 | 0.01976 | 0.00665 | 0.00627 |
| dre01130:Biosynthesis of antibiotics | 0.00366 | 2.38329 | 0.32462 | 0.08334 | 0.07866 |
| dre01100:Metabolic pathways | 0.00389 | 1.44427 | 0.34132 | 0.08334 | 0.07866 |
| dre00590:Arachidonic acid metabolism | 0.01130 | 4.35535 | 0.70363 | 0.19820 | 0.18709 |
| dre00982:Drug metabolism – cytochrome P450 | 0.01503 | 5.14174 | 0.80227 | 0.19820 | 0.18709 |
| dre00480:Glutathione metabolism | 0.01537 | 4.03860 | 0.80940 | 0.19820 | 0.18709 |
| dre04910:Insulin signaling pathway | 0.01667 | 2.36759 | 0.83452 | 0.19820 | 0.18709 |
| dre00980:Metabolism of xenobiotics by cytochrome P450 | 0.01973 | 4.74622 | 0.88153 | 0.21120 | 0.19936 |
| dre00565:Ether lipid metabolism | 0.02332 | 4.51470 | 0.91998 | 0.22691 | 0.21418 |
| dre00514:Other types of O-glycan biosynthesis | 0.04153 | 5.10628 | 0.98931 | 0.37033 | 0.34957 |
| dre01200:Carbon metabolism | 0.04999 | 2.36931 | 0.99586 | 0.41153 | 0.38845 |
| dre00520:Amino sugar and nucleotide sugar metabolism | 0.06237 | 3.30540 | 0.99898 | 0.47676 | 0.45002 |
| dre01230:Biosynthesis of amino acids | 0.07122 | 2.67618 | 0.99963 | 0.50803 | 0.47954 |
| dre00051:Fructose and mannose metabolism | 0.09636 | 3.61176 | 0.99998 | 0.62586 | 0.59076 |
| dre04912:GnRH signaling pathway | 0.09943 | 2.17767 | 0.99998 | 0.62586 | 0.59076 |

**Table 4.2. KEGG pathways enriched in genes upregulated in cortisol-treated *klf9*$^{-/-}$ larvae versus cortisol-treated WT**

| Term | Pvalue | Fold Enrichment | Bonferroni | Benjamini | FDR |
|---|---|---|---|---|---|
| dre00030:Pentose phosphate pathway | 1.38E-04 | 11.4959234 | 0.01154 | 0.01160 | 0.01133 |
| dre04512:ECM-receptor interaction | 3.59E-04 | 5.86623253 | 0.02970 | 0.01507 | 0.01471 |
| dre00010:Glycolysis / Gluconeogenesis | 0.00125 | 5.69546891 | 0.10001 | 0.03510 | 0.03426 |
| dre00591:Linoleic acid metabolism | 0.00477 | 11.3134485 | 0.33130 | 0.10036 | 0.09797 |
| dre04510:Focal adhesion | 0.02147 | 2.39498405 | 0.83853 | 0.36075 | 0.35216 |
| dre01130:Biosynthesis of antibiotics | 0.03924 | 2.29425081 | 0.96536 | 0.53459 | 0.52186 |
| dre01100:Metabolic pathways | 0.05198 | 1.37139532 | 0.98871 | 0.53459 | 0.52186 |
| dre00590:Arachidonic acid metabolism | 0.05241 | 4.65847878 | 0.98914 | 0.53459 | 0.52186 |
| dre00480:Glutathione metabolism | 0.06301 | 4.31968032 | 0.99577 | 0.53459 | 0.52186 |
| dre00520:Amino sugar/nucleotide sugar metabolism | 0.06580 | 4.24254317 | 0.99671 | 0.53459 | 0.52186 |
| dre04931:Insulin resistance | 0.07000 | 2.67950095 | 0.99774 | 0.53459 | 0.52186 |
| dre00500:Starch and sucrose metabolism | 0.09862 | 5.56833791 | 0.99983 | 0.69038 | 0.67394 |

**Table 4.3. Gorilla process enrichment in genes upregulated in cortisol-treated *klf9*$^{-/-}$ larvae versus cortisol-treated WT.** Top 12 processes, ranked by FDR.

| GO Term | Fold Enrichment | Description | P-value | FDR |
|---|---|---|---|---|
| GO:0016052 | 6.08 | carbohydrate catabolic process | 4.52E-08 | 3.85E-04 |
| GO:0042866 | 7.08 | pyruvate biosynthetic process | 8.50E-07 | 1.03E-03 |
| GO:0009168 | 5.3 | purine ribonucleoside monophosphate biosynthetic process | 7.44E-07 | 1.06E-03 |
| GO:0006754 | 7.05 | ATP biosynthetic process | 2.52E-07 | 1.07E-03 |
| GO:0009127 | 5.3 | purine nucleoside monophosphate biosynthetic process | 7.44E-07 | 1.27E-03 |
| GO:0006096 | 7.27 | glycolytic process | 6.48E-07 | 1.38E-03 |
| GO:0009135 | 6.41 | purine nucleoside diphosphate metabolic process | 2.31E-06 | 1.64E-03 |
| GO:0005975 | 2.71 | carbohydrate metabolic process | 2.54E-06 | 1.67E-03 |
| GO:0009145 | 5.59 | purine nucleoside triphosphate biosynthetic process | 3.10E-06 | 1.76E-03 |
| GO:0009179 | 6.41 | purine ribonucleoside diphosphate metabolic process | 2.31E-06 | 1.79E-03 |
| GO:0007155 | 2.4 | cell adhesion | 2.11E-06 | 1.80E-03 |
| GO:0006757 | 7.27 | ATP generation from ADP | 6.48E-07 | 1.84E-03 |

| Rank | Motif | Name | P-value | log P-pvalue | q-value (Benjamini) |
|---|---|---|---|---|---|
| 1 |  | Klf9(Zf)/GBM-Klf9-ChIP-Seq(GSE62211)/Homer | 1e-7 | -1.646e+01 | 0.0000 |
| 2 |  | KLF5(Zf)/LoVo-KLF5-ChIP-Seq(GSE49402)/Homer | 1e-5 | -1.305e+01 | 0.0005 |
| 3 |  | TR4(NR),DR1/Hela-TR4-ChIP-Seq(GSE24685)/Homer | 1e-5 | -1.299e+01 | 0.0005 |
| 4 |  | Pit1+1bp(Homeobox)/GCrat-Pit1-ChIP-Seq(GSE58009)/Homer | 1e-5 | -1.292e+01 | 0.0005 |
| 5 |  | KLF6(Zf)/PDAC-KLF6-ChIP-Seq(GSE64557)/Homer | 1e-5 | -1.264e+01 | 0.0005 |
| 6 |  | KLF14(Zf)/HEK293-KLF14.GFP-ChIP-Seq(GSE58341)/Homer | 1e-5 | -1.157e+01 | 0.0007 |
| 7 |  | Klf4(Zf)/mES-Klf4-ChIP-Seq(GSE11431)/Homer | 1e-4 | -1.084e+01 | 0.0012 |
| 8 |  | EKLF(Zf)/Erythrocyte-Klf1-ChIP-Seq(GSE20478)/Homer | 1e-4 | -9.962e+00 | 0.0026 |
| 9 |  | KLF1(Zf)/HUDEP2-KLF1-CutnRun(GSE136251)/Homer | 1e-3 | -8.150e+00 | 0.0141 |

**Figure 4.19. KLF binding motifs are enriched in genes upregulated in cortisol-treated *klf9*$^{-/-}$ larvae compared with cortisol-treated WT larvae.** The most significantly enriched motifs (determined by HOMER analysis) within +/-2000bp of TSS are shown.

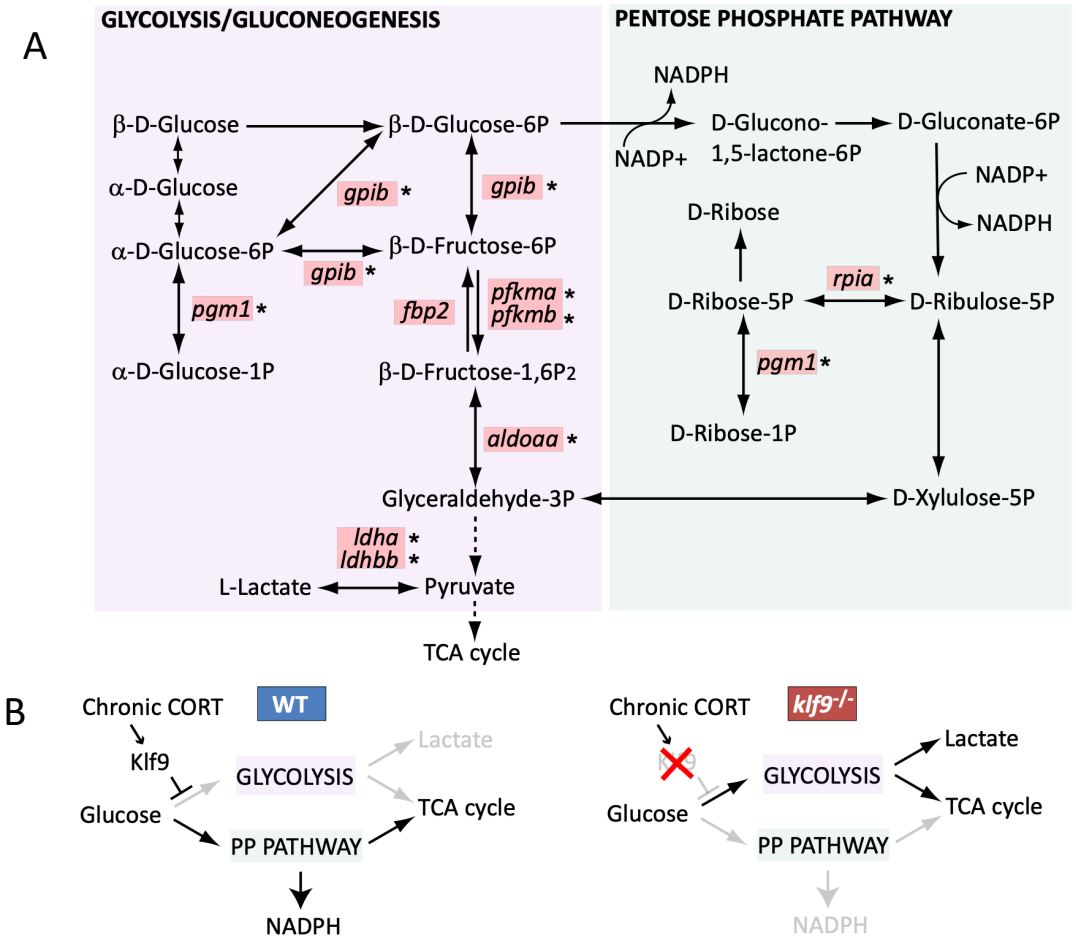


**Figure 4.20. Klf9 negatively regulates genes in the glycolysis/gluconeogenesis pathway.** Red boxes in (A) indicate genes significantly (FDR<0.05) over expressed in RNA-seq of *klf9*$^{-/-}$ larvae compared to WT. Asterisks denote genes with putative Klf9 binding sites identified by HOMER. (B) Model for Klf9-mediated regulation of metabolic flux. In response to stress, Klf9 is predicted to inhibit glycolysis, shunting flux through the Pentose Phosphate Pathway.

# CHAPTER 5

# DISCUSSION OF RESULTS

As detailed in Chapter 1 of this dissertation, chronic stress and associated allostatic load are risk factors contributing to morbidity. The stress hormone cortisol (CORT), acting primarily through its cognate glucocorticoid receptor (GR), is a potent modulator of gene expression in nearly every cell in the body. However, current knowledge is limited about how chronically elevated CORT alters gene expression and, ultimately, physiology. Because early development is a known window for susceptibility to elevated GC, I undertook studies building on the Coffman Lab's previous work describing the short- and long-term effects of exposing zebrafish to chronically elevated CORT during early development. Using this experimental paradigm designed to model chronic maternal/pre-natal stress, the gene *klf9* was identified by the lab as consistently elevated by chronic CORT, and as the most CORT-responsive gene encoding a transcription factor. Although Klf9 is largely unstudied in *Danio* this was consistent with evidence from *Xenopus* and mammals that *Klf9* is a GC target[205,206,208,213,260], and led to the hypothesis that Klf9 is a mediator of the transcriptomic response to CORT. In the two previous chapters, I have described experiments that tested this hypothesis, and results indicating that Klf9 is an important feed-forward regulator of CORT-induced changes in gene expression. In this chapter I will re-visit the main findings of my work, with added discussion about implications of the results, their relationship to existing knowledge, and promising avenues for future research that proceed from this study.

## 5.1. Klf9 is a key feedforward regulator of the transcriptomic response to GC

Using CRISPR to create a functional Klf9 knockout, I found that genetic ablation of Klf9's DNA-binding domain largely diminished immune gene upregulation caused by chronic CORT in 5dpf *Danio* larvae. At the same time, the mutation of Klf9 increased expression of genes largely involved in glucose metabolism. These data reveal that Klf9 regulates expression of genes involved in the immune response and metabolism downstream of CORT, two areas of physiology well known to be governed by GC.

Further evidence of an important role for Klf9 in GC signaling was found following a meta-analysis of new and existing RNA-seq datasets. The meta-analysis generated a high-confidence list of genes overexpressed in WT and $GR^{WT/369-}$ heterozygous larvae (i.e., larvae with at least one functional GR) exposed to chronic CORT, and revealed that fewer genes are reliably under-expressed in response to chronic CORT[159]. Among the consistently overexpressed GC targets, sequences predicted to bind Klf9 were the most highly enriched transcription factor motifs in TSS-proximal DNA (more so even than binding sites for the GR), heavily implicating Klf9 in the regulation of GC target gene expression[159].

Gene ontology (GO) analyses found that genes involved in a common subset of carbohydrate metabolic processes (e.g. glycolysis, pyruvate biosynthesis) were dysregulated in both *klf9*$^{-/-}$ and $GR^{369-}$ mutants[159]. However, GO processes down-regulated by loss of functional GR were up-regulated in Klf9 mutants, indicating opposite effects of the two transcription factors. This was corroborated by additional analysis which found that loss of Klf9 upregulates genes in similar glucose metabolic pathways in comparison with WT larvae. Further, genes involved in glycolysis and related pathways were even more highly expressed in Klf9 mutants

exposed to chronic CORT than similarly exposed WT, suggesting that the role of Klf9 in regulating genes involved in glucose metabolism is accentuated in chronic CORT. As with the set of genes consistently upregulated by CORT in WT, TSS-proximal DNA of genes overexpressed in CORT-treated Klf9 mutants compared with CORT-treated WT was highly enriched for putative Klf9 binding sites. Taken together, these data indicate that one role of Klf9 is to provide negative control to the transcriptional response stimulated by GC, including via putative direct repression of genes involved in glucose metabolism.

Because Klf9 is itself activated by the GR, this regulation of downstream targets constitutes feedforward logic. Oppositional regulation constitutes *incoherent* feedforward logic, a prevalent mode of control in biological systems[50,261]. Evidence of incoherent feedforward repression by Klf9 has previously been reported for a single GC-target gene, *Klf2*, in murine macrophages[199]. The transcriptomic data I present here suggest that incoherent feedforward repression by Klf9 may extend more broadly to genetic network modules and/or processes (e.g. glycolysis) stimulated by GC, with Klf9 acting generally as a brake or governor on activation by GC. The predominantly repressive role for Klf9 here is supported by the enrichment of Klf9-binding motifs near the TSS of genes upregulated, but not down-regulated, in *klf9*$^{-/-}$ larvae, and is consistent with reports from other systems[191,240]. These data also suggest that the Klf9-dependent upregulation of immune genes in response to CORT involves indirect mechanism(s) which will require further study to elucidate.

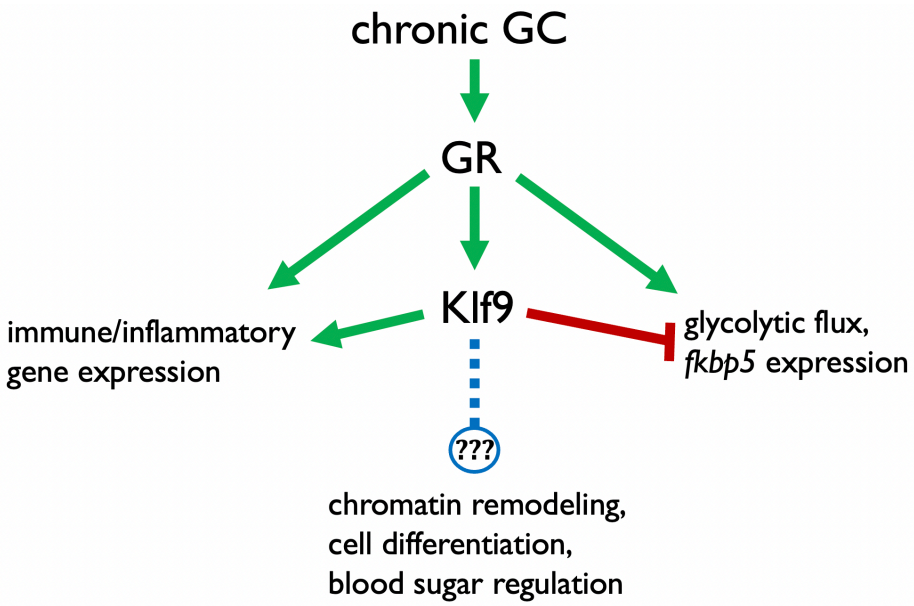


**Figure 5.1. Feedforward regulation of GC-responsive processes by Klf9.** Induced by GC via the GR, Klf9 regulates important aspects of the response to chronic GC. This feed-forward regulation by Klf9 may be positive (as in immune gene expression) or negative (as in expression of *fkbp5* and genes involved in glycolysis). Roles for Klf9 in other GC-associated processes such as chromatin remodeling, cell differentiation, and blood sugar regulation are suggested by gene expression data here and/or in existing literature but remain to be elucidated.

Incoherent feedforward repression can facilitate a number of complex dynamic responses—accelerated response time, fold-change detection, pulsatility, for examples—depending on context[261,262]. Investigating effects on expression of *bona fide* Klf9 targets will require a careful approach to measure changes in expression dynamics that may not be limited to simply up- or down- regulation. Using the novel, epitope-tagged Klf9 AM-Tag zebrafish strain that I generated using CRISPR, I have identified *fkbp5* as one such target (discussed in detail later in this chapter). The AM-Tag line will be a valuable tool for ChIP experiments to test suspected metabolic targets and identify additional targets.

### 5.1.1. Evidence for direct and indirect modes of regulation by Klf9 with respect to metabolism and immune genes

Given the lack of any significant enrichment for KLF binding sites in the group of largely immune genes upregulated by CORT in a Klf9-dependent manner, it seems likely that the role of Klf9 in that over-expression is not one of direct transcriptional activation. At least three modes of indirect regulation are possible, and I will touch briefly on two before delving into a third in more detail. First, Klf9 may increase expression of genes via protein-protein interactions with other transcription factors. ChIP-seq to identify peaks where Klf9 associates independent of KLF motifs can now be carried out using the AM-Tag line. Alternatively, co-immunoprecipitation assays for suspected factors can be done. Second, given evidence of Klf9's involvement in stem-cell differentiation and hematopoiesis (discussed more below), Klf9 might regulate development of immune cell populations, thereby affecting immune gene expression measured in whole larvae. Crossing the *klf9*$^{-/-}$ mutation into existing immune cell reporter lines is one approach currently underway to investigate effects on immune cells, to be used in conjunction with fluorescence microscopy and/or cell sorting assays. Third, because immunity and metabolism are intricately connected, dysregulation of immune gene expression may be a secondary effect of direct dysregulation of metabolic pathways.

Glucose metabolism specifically has been recognized as an important driver of immune cell function[263–265], and the data presented in the previous chapter suggest that Klf9 regulates glycolytic flux. Upregulated genes in mutants were enriched for involvement in glycolysis/gluconeogenesis and the adjacent PPP, and 8-out-of-9 upregulated genes in those pathways have predicted Klf9 binding sites (see Fig. 4.20A) within 2000bp of their TSS. These

data suggest a model (Fig. 4.20B) in which Klf9 represses genes involved in glycolysis/gluconeogenesis, which could direct flux through the adjacent PPP or other adjacent pathways and ultimately into oxidative mitochondrial pathways (e.g. the TCA cycle, beta-oxidation of fat). De-repression of glycolytic genes in Klf9 mutants may explain the ~10% decrease in oxygen consumption rate (OCR) observed in 1dpf *klf9*$^{-/-}$ embryos, as less oxygen is consumed when glucose proceeds through glycolysis to produce lactate rather than generating pyruvate to feed the TCA. This mode of metabolism predominates when oxygen is limited (such as in strenuous exertion) but also occurs in the presence of oxygen (i.e. aerobic glycolysis). Such aerobic glycolysis has long been associated with cancer cell proliferation, but is fast becoming recognized as an important driver of various processes in immune and other healthy cells[266]. Once considered a metabolic waste product, new evidence is emerging that lactate produced by glycolysis is an important signaling molecule and major pool of carbon fuel in the body[267–269]. High plasma lactate, however, is a sign of metabolic disorder associated with obesity and diabetes[270].

OCR is sometimes used as a proxy for overall metabolic rate, which makes sense in normally respiring cells primarily oxidizing sugar for maximal ATP production. But in rapidly proliferating cells the production of macromolecules for biosynthesis requires a significant increase in flux through anaerobic branches of glycolysis and the PPP. Such is the case, for example, in activated T Cells[271], and in cancer cells (i.e. the Warburg Effect[254]) that often outgrow their blood (and thus oxygen) supply. In these cases, OCR is clearly not a readout of the full metabolic activity of cells. This likely also applies during the rapid early stages of *Danio* development. Thus OCR here should be viewed strictly as a readout of the oxidative side of

metabolism, and additional assays will be necessary to gain a more complete understanding of the role of Klf9 in metabolic regulation. However, the decrease in OCR measured in 1dpf *klf9*$^{-/-}$ larvae fits a model in which Klf9 diverts flux from anaerobic glycolysis in favor of oxidative pathways. Given the diurnal timing of Klf9 expression, it's possible that Klf9 helps to adjust metabolism as part of the transition from resting to active behavior. This proposed role for Klf9 in partitioning metabolism is also supported by the results form targeted PCA of genes downstream of the metabolic master regulators Hif1a and AMPK, in which *klf9*$^{-/-}$ samples clearly segregated from wild-type. Hif1a and AMPK are thought of as respective "master regulators" of glycolysis and aerobic metabolism, and PCA of a curated list of their target genes was previously shown to reflect changes in the metabolic plasticity of cancer cells[254]. Thus the current results suggest differential metabolism in *Danio* larvae lacking Klf9 compared with WT, however the nature and extent of this remain to be studied further. As noted above, finding the direct targets of Klf9 will be a necessary step in testing the model. Changes in metabolite levels, such as increased lactate and decreased NADPH in Klf9 mutants, are predicted outcomes that can also be tested. As Klf9 is also responsive to acute stress[205], future studies should investigate a possible role for Klf9 in adjusting metabolism in response to acute stress. Given the interconnected and cyclical nature of metabolic pathways, metabolomics would be a worthwhile next step to distinguish the net effects of Klf9 loss, keeping in mind these may be exacerbated under GC stimulus.

Shunting of glucose metabolism around glycolysis and into oxidative metabolic pathways is consistent with (and may help explain) previous findings involving Klf9. For example, Klf9 has been shown to act as a tumor suppressor[256,257,272], and cancer cells rely heavily on glycolytic

metabolism for proliferation. Klf9 is also involved in regulating stem cell self-renewal, another process that requires fine balancing of glycolysis versus oxidative phosphorylation to produce daughter cells while maintaining potency. Generally, usage of the catabolic TCA and oxidative phosphorylation increase as cells proceed through differentiation (summarized well in a recent review[273]), and induction of Klf9 has been shown to correlate with transition of human embryonic and induced pluripotent stem cells through terminal differentiation[255]. Knockdown of Klf9 also impairs hematopoiesis[249]. In radial-glial neural stem cells, loss of Klf9 leads to supernumerary cell divisions and increases the ratio of symmetric-to-asymmetric divisions[274] (i.e. less differentiated daughter cells). In the same study, translational profiling of neural stem cells lacking Klf9 found upregulation of genes involved in fatty acid oxidation and lipogenesis. This could relate in some way (e.g. compensation) to decreased flux through the PPP, which is a source of NADPH for fatty-acid synthesis but can be compensated for if pharmaceutically blocked[275,276]. Given the involvement of the PPP in lipid metabolism, it is also interesting that in my study TSS-proximal DNA of Klf9-dependent immune genes was enriched with binding sites for interferon regulatory factors (see Table 3.2), which are known to regulate adipogenesis and lipid signaling[277–279]. Knock-down of Klf9 has also been shown to promote regeneration of injured retinal ganglia cells[203,204], and it's possible that knock-down allowed fully mature neurons to enter a metabolic state more conducive to regrowth.

Klf9 diverting glucose from glycolysis in favor of oxidative metabolism is also consistent with a reported role for Klf9 in amplifying oxidative stress. In a study using mouse fibroblasts, *Klf9* was induced by the transcription factor Nrf2 after cells were exposed to a high level of reactive oxygen species[280]. This in turn caused further ROS accumulation, intriguing given that Nrf2 is

normally associated with a protective, antioxidant response. In this case, however, ROS accumulation above a threshold led to apoptosis via activation of *Klf9* that amplified ROS accumulation through feedforward repression of genes involved in ROS metabolism. Among genes upregulated by CORT in a Klf9-dependent way in the present study, GO process enrichment was found for ROS metabolism and respiratory burst (Fig. 3.5D). Genes in this group included *ncf1, ncf2,* and *cyba* and *cybb,* which all code for NADPH oxidases key in generating ROS. Thus, following glucose mobilization instigated by GC, Klf9 might contribute to respiratory burst by increasing NADPH production via the PPP and promoting its subsequent enzymatic oxidation. Interestingly, a transient oxidative respiratory burst also accompanies nuclear reprogramming of induced pluripotent cells from the oxidative somatic metabolic phenotype to the more glycolytic stem phenotype[273]. This burst is thought to induce activation of Hif1a via Nrf2, stabilizing glycolytic metabolism. Respiratory burst is also key for certain immune cell functions where, as in stem cells, activation of Hif1a stabilizes flux through glycolysis and sustains pro-inflammatory macrophage polarization[281,282]. Production of ROS and disruption of glycolytic flux have also been shown to respectively promote inflammasome activation[283,284]. In the Coffman Lab, increased ROS has been measured in 5dpf larvae treated with chronic CORT[158], and it will be interesting to test in the future whether Klf9 contributes to inflammatory signaling by interrupting glycolysis, mediating GC-induced ROS production, and stimulating inflammasome activity.

## 5.2. GC and target gene dynamics provide context for RNA-seq data from cortisol-treated and mutant larvae

A large part of the work described in previous chapters was done within an experimental paradigm established by the Coffman Lab to model the effects of chronic CORT exposure during early development, an important topic given the associations between maternal stress during pregnancy and the long-term health of offspring (as detailed in Chapter 1). In this experimental paradigm, zebrafish embryos/larvae are exposed for the first five days of development to chronic 1μM CORT, an elevated but physiologically relevant concentration (healthy peak plasma CORT levels in humans are ~600-700nM[285]). As reviewed in Chapter 1 of this dissertation, circadian fluctuation driven by ultradian release of hormone release is a key aspect of GC signaling in mammals. Furthermore, ultradian pulses of GC have been shown to cause cycling of GR association with chromatin and pulsatile gene expression *in vitro*[24]. Ultradian GC pulses also drive cyclical nuclear localization and pulsatile gene expression in the hippocampus of intact rats[286], whereas a flattened GC profile decreases responsivity[287]. Given the import of circadian and ultradian oscillations for GC signaling, temporal context should be considered for datasets derived from perturbing the system, especially when using intact animals as done here. Despite being voluminous, RNA-seq data such as generated here nevertheless represents only a snapshot in time. Another important consideration when interpreting my data is the chronicity of the treatment paradigm. While exogenous CORT remained in constant excess in the media, differential effects of the treatment could manifest at different times, as steady exogenous supply interacts with the highly dynamic endogenous signaling axis. To put it simply, the effect of chronic treatment may depend on when the observation is made. Thus I will spend some

space here discussing the relationship between time course experiments I undertook to investigate the effects of chronic treatment on gene expression, RNA-seq data, and existing literature.

GC-dependent circadian rhythms in gene expression have previously been detected in whole *Danio* larvae at 5dpf[252]. Their detection in whole larvae composed of many different cell types is probably due in part to the high degree of synchronicity in *Danio* peripheral clocks, some of which stems from light sensitivity in peripheral tissues[288]. Circadian behavioral rhythms in *Danio* larvae[251] also display a degree of GR-dependence[*]. However no previous data existed on temporal dynamics of either *fkbp5* or *klf9* in *Danio* larvae, two genes of interest due to the significant effects of chronic CORT observed in previous Coffman Lab studies (albeit with inconsistencies when measured at single time points)[158,175]. Measurement of these transcripts across 0-5 dpf window revealed relatively high transcript levels at 6 hpf that decreased drastically by 2-3 dpf (Fig. 4.1). This drop is similar (but delayed by ~24h) to the depletion of maternally deposited *nr3c1* mRNA that has previously been reported around 1-2dpf[149]. Expression of *klf9* and *fkbp5* rebounded by 4 dpf, coinciding with the larval HPI becoming functional, and a sinusoidal dynamic in their expression was detectable by the morning of day 4 post-fertilization (Appendix J). A similar sinusoidal expression pattern occurred on the morning of day 5 post-fertilization, and this 5 dpf window was chosen for subsequent focus. This window was chosen due to 5dpf being the end of the lab's chronic treatment protocol and a time when

[*] As an interesting aside, the circadian behavior pattern in that study did not emerge until 6dpf, and its dependence on a functional GR decreased significantly by 7dpf, indicating additional mechanisms compensating and contributing to the development of rhythmic behavior. The development of biorhythms is poorly understood and a ripe area for future study.

many of the lab's experimental measurements (including prior RNA-seq) have been carried out. Larval development is also more complete at this time, as evident by full inflation of the swim bladder and active behavior. In individual experiments, data consistent with ultradian pulses of expression were observed. Some of this putative ultradian dynamic is recognizable in plotted averages of experimental replicates (e.g. Fig. 4.2A), but it is somewhat negated by averaging between experiments, likely due to horizontal phase shifts (showing up instead as high standard deviation). Nonetheless, observed ultradian pulses of gene expression with period of ~30-60 minutes are similar to ultradian observations in other systems occurring on the order of hourly, as well as recent work demonstrating that most mRNA have half-lives of only several minutes, and are degraded rapidly[289,290] . Diurnal drop in whole-larvae CORT correlated with overall *fkbp5* and *klf9* activity. Expression of both genes was found to be dependent on the GR, as both transcript levels were significantly lower in GR$^{369-}$ mutants and showed no variation between timepoints where reliable peak and trough expression occur in WT. Though not unexpected, the GR dependence of *klf9* (and *fkbp5*) was important to confirm in *Danio*, given more than 400 million years of divergence between zebrafish and tetrapod lineages in which *Klf9* has previously been identified as a GC target (see Section 1.2.1).

Measured alongside a panel of other known GC-responsive genes, *klf9* and *fkbp5* stood apart for their high responsiveness to chronic CORT treatment as well as their early morning peaks of expression (Figs. 4.2 & 4.6). The clustering of GC-targets into two groups with distinct overall temporal dynamics (i.e. peaking either before or after 0 ZT) could indicate different modes of regulation by the GR. As the later cluster contains immune genes such as *irg1l*, *irf1b*, and *mpeg1*.2, one possibility is that an early wave of GC responders may prime certain targets

for a subsequent response. Such a priming effect of GC has been documented for neuroinflammation, for example[291]. Given the early responsiveness of *klf9* and the dysregulation of genes involved in epigenetic modification in mutants (Fig. 3.4), it will be interesting to investigate whether Klf9 plays a role in such epigenetic priming of GC-targets, which could be yet another indirect mechanism of GC-induced immune gene regulation. Altogether, the diurnal profiles of CORT and GR-target gene expression in 5dpf larvae indicate *Danio* is a suitable model for studying vertebrate GC signaling dynamics.

Exposure of embryos/larvae to chronic CORT caused significant increase in the mean baseline expression of both *klf9* and *fkbp5* on 5dpf. However, large ultradian fluctuations in expression led to under-expression of either gene in CORT at nearly 20% of time points, consistent with previously reported data[175]. The diurnal expression pattern of either transcript was left largely intact, although elevation of *klf9* and *fkbp5* due to CORT was pronounced at certain timepoints corresponding to the pre-dawn peak (~ -1 ZT) and the mid-morning trough ( ~ 3 ZT). The elevated peak at -1 ZT could indicate a cumulative effect of chronic treatment and peak endogenous CORT production, but current data at this timepoint is limited and additional RNA-seq experiments are underway by the Coffman Lab to ascertain effects of CORT and Klf9 mutation at this timepoint. The raised floor of *klf9/fkbp5* expression at ~3 ZT is of greater interest currently. This is the same time current and previous Coffman Lab RNA-seq samples were collected, and because the GR is believed to be inactive during GC troughs increased GC availability during this time has the potential to aberrantly activate the GR. A good example is the core circadian gene and GR target *PER1,* which has been shown in human lung and epithelial cells to be hypersensitive to very low levels of GC (e.g. induction at 21nM CORT, and a

2-fold increase in 0.5nM DEX)[230]. Overexpression of *PER1* after a transient low-dose of DEX was followed by misexpression of additional circadian clock genes up to 12 hours after withdrawal of treatment. This indicates the potential for elevated trough GC to cause a coordinated shift in circadian gene expression and biological timing. In the same study, *PER1* was identified as the single most GC sensitive gene, and the hypersensitivity was attributed not to GR occupancy of an upstream enhancer alone, but also to high chromatin accessibility surrounding the GR binding site that allowed occupancy by additional transcription factors. Intriguingly, Klf9 has more recently been reported necessary for stress-induced *Per1* expression in mouse liver[292], a finding reminiscent of the Klf9-dependence I report here for immune gene expression. Interestingly, I found genes dysregulated (both up and down) in Klf9 mutants to be enriched for involvement in nucleosome positioning and chromatin remodeling (Fig. 3.4). It's possible that Klf9 plays a role in modulating the accessibility of some GC-responsive genetic loci, thus regulating their sensitivity. Klf9 has been shown to regulate activity of the progesterone receptor (a nuclear receptor closely related to the GR) via protein-protein interaction[293,294] and so one possibility is that Klf9 may also coordinate directly with the GR, which sometimes acts as a pioneering transcription factor capable of remodeling nucleosomes[295]. Alternately, Klf9 may function as a feed-forward transcriptional regulator of other factors involved in remodeling GC sensitive loci. In one study, nucleosome depletion by the GR was accompanied by flanking of the GR binding site with unstable replication-independent histone H2A.Z[295]. In the current RNA-seq dataset, Klf9 mutants over-express linker histone H1 variants *h1f0* and *h1fx*, both of which are also replication-independent (i.e. involved in remodeling not restricted to S phase of the

cell-cycle). Preliminary experiments using the NanoString platform have confirmed these transcripts are overexpressed in mutants, but functional significance remains to be explored.

Increased GC signaling during the circadian trough has also been linked to diabetes and development of metabolic syndrome in mammals[40]. Increases in steady-state GC sufficient to aberrantly activate the GR during this nadir can induce insulin overproduction, accrual of adipose tissue, and other metabolic effects. Keeping in mind that samples for the RNA-seq in this and previous Coffman Lab studies were collected around 3 ZT, (a low point for CORT, *klf9* and *fkbp5* levels) the affected genes and pathways indicated in these data may be relevant to GC-induced diabetes and metabolic syndrome. Indeed, knockdown of Klf9 was recently shown to decrease blood sugar in mouse diabetic models and alleviated GC-induced hyperglycemia, while DEX induced over-expression in mouse liver caused hyperglycemia[209]. In that study, however, increased hepatic gluconeogenesis was attributed to activation by Klf9 of the master regulator PGC1a, a different mechanism than suggested by the data presented here. But these mechanisms need not be mutually exclusive. Differing treatment paradigms (fasting or acute dexamethasone in adult animals versus chronic developmental CORT exposure) may activate different molecular mechanisms involving Klf9. Sample source (mouse hepatocytes versus whole *Danio* larvae) is another important factor that could contribute to the identification of different mechanisms. While the liver is a net contributor to blood glucose during stress, other tissues such as brain and muscle (all of which express GR, Klf9, and Fkbp5) respond to GC differently—by modulating glucose uptake or activating catabolic pathways for example. In any case, regulation of glycolysis and gluconeogenesis (largely inverse pathways involving reversible enzymatic steps) by Klf9 merits further attention. A significant limitation when interpreting the

data produced here is its derivation from whole larvae, and the *klf9*$^{-/-}$ and AM-Tag lines should be used in the future to explore the role of Klf9 in specific tissues. Future experiments should also determine whether Klf9 regulates these pathways similarly in *Danio* and mammalian systems, or whether there has been significant divergence of function. The recent report of decreased OCR in mice lacking Klf9[253] is similar to that noted here in *Danio* larvae and provides evidence of conserved function.

### 5.2.1. Increased *fkbp5* expression in whole larvae treated with chronic cortisol supports models of HPA hyperactivity and allostatic load

This is the first study to my knowledge to demonstrate dynamic expression *fkbp5* in an animal model with intact HPA/I, and basal elevation of *fkbp5* expression in response to chronic CORT independent of any additional stressor that might activate stress response mechanisms. This is significant, since human studies linking early-life stress to lasting health risks have limited ability to completely disentangle the effects of GC from other stress mediators and "knock-on" effects of early life stress. In well controlled biomedical studies where GC has been administered (in drinking water of mice for example), practical limits of sampling protocols or number of animals provide an incomplete picture of dynamic gene expression. The ability to directly treat a large number of externally developing zebrafish embryos with hormone allowed this study to focus on effects specifically of chronic CORT with high temporal resolution. While elevated *fkbp5* in response to chronic CORT was expected, the overall maintenance of diurnal expression illustrates a robustness of HPA/I dynamics. Because Fkbp5 is itself crucial to regulating HPA responsiveness via negative feedback, *fkbp5* overexpression in chronic 1µM CORT suggests that an elevated, but physiologically relevant, level of hormone may be

sufficient to alter HPA/I set point. This is consistent with an allostatic model of disease, in which altered HPA set point can lead to dysregulation and "wear and tear" throughout the body due to the ubiquitous expression of the GR and its many downstream targets. The long-term consequences of altering this set point are demonstrated in other work by the Coffman Lab linking chronic CORT during development with long-term elevation in whole-body CORT, elevated expression of *fkbp5* and *klf9* in blood (accompanied by epigenetic promoter modifications), and blunted immune gene response to injury/infection[158,175]. It is also in line with studies in mice in which blood and brain *Fkbp5* mRNA expression are significantly correlated with each other and mean plasma GC[296]. The expression fluctuations I have observed also support a previously proposed use of *Fkbp5* methylation in blood as a more stable readout than gene expression and valuable biomarker for chronic glucocorticoid and allostatic loads[296,297].

One limitation of the data I have produced here is that gene expression does not necessarily reflect Fkbp5 protein, however, similar increases in mRNA level were coupled to protein expression *in vitro*[24], and increasing brain *Fkbp5* mRNA expression affects physiological readouts including HPA response[298]. Nonetheless, validating an antibody or epitope tag to accurately measure Fkbp5 protein in *Danio* would allow for improved readout of GC, stress, and Klf9 perturbations in the future. Future work should also focus on perturbing *fkbp5* in specific tissues, including those of the HPA/I, to increase our understanding of pathophysiology stemming from chronic GC and HPA hyperactivity. Recent studies have just begun such work, and for example point to *Fkbp5* expression in the para-ventricular nucleus of the hypothalamus as a crucial regulator of HPA function and stress responsiveness[298,299].

### 5.3. Klf9 regulates expression of *fkbp5*

In addition to the novel *klf9*$^{-/-}$ zebrafish line, I used CRISPR with homology directed repair to create another *Danio* strain in which a flexible, ChIP-validated "AM"-Tag (sequence designed by Active Motif, Carlsbad, CA) was added to the endogenous Klf9 C-terminus. This AM-Tag line will be useful in future experiments to determine targets (both DNA and protein) that interact directly with Klf9. Using this line, I immunoprecipitated DNA with a ChIP-validated, anti-AM antibody and found that Klf9 associates with the promoter of *fkbp5,* which contains predicted Klf9 binding sites. Prior to this work, Klf9 had been suggested to regulate expression of *FKBP5* in a study of human keratinocytes[211]. The ChIP-qPCR results here corroborate gene expression time courses showing that loss of Klf9 elevates baseline *fkbp5* expression and delays the circa-dawn expression peak (Figs. 4.7 and 4.8). Further, hyper-acetylation of histone 3 lysine 14 (H3K14, a mark of active promoters) was also found in the *fkbp5* promoter of *klf9*$^{-/-}$ mutants(Fig. 4.15). The histone de-acetylase Sin3a is known to be recruited by mammalian Klf9[241] and hyperacetylation in mutants could result from a lack of Sin3a recruitment, although this activity is unknown in *Danio*. Klf9 target motifs have been found to co-occur at high frequency with circadian E-box motifs, in both mouse[191] and the present study where ~86% of consistent GC responsive genes having both motifs near the TSS (Fig. 4.14). Klf9 could play a role in tuning target promoter acetylation by the core circadian protein CLOCK, which binds E-Boxes and is itself a histone acetyltransferase known to acetylate H3K14[300,301]. De-acetylation by recruited Sin3a, or steric hindrance of acetylation by CLOCK are two possible mechanisms to be explored. But rather than exploring whether mammalian mechanisms are conserved in

*Danio*, it would be more biomedically relevant to investigate whether KLF9 directly regulates *Fkbp5* in human cells.

### 5.3.1. Potential significance of a GR-Klf9-Fkbp5 circuit

The results above imply a GR-Klf9-Fkbp5 regulatory circuit (Fig. 4.15B) which combines a well-known ultra-short GR-Fkbp5 negative feedback loop with incoherent feedforward regulation (i.e. feedforward repression) of *fkbp5* by Klf9 (see Fig. 4.15B). The combination of these two regulatory motifs is prevalent in biological networks capable of adaptation[50,53,261,262], and can provide robustness and superior dynamic control of that adaptation[49]. This is notable given that adaptation to environmental and internal cues is precisely the function of GC signaling. Transient, pulsatile responses such as exhibited by *klf9* and *fkbp5* are also a hallmark output of adaptive networks[53]. However, chronic or repeated activation may contribute to maladaptation, allostatic load and ultimately disease. Klf9-dependent maladaptive fear conditioning has recently been shown to occur in the brains of mice submitted to chronic repeated restraint stress, for example[302].

A key output of the proposed GR-Klf9-Fkbp5 circuit would be tuning the level of Fkbp5 in response to GC stimulus, which in turn generates resistance to the nuclear localization of GR and subsequent GC responsiveness. This resistance has been demonstrated elegantly in mouse brain, where regions with lower basal *Fkbp5* more readily increase *Fkbp5* transcription in response to stress than do regions with high basal expression[303]. Thus, *Fkbp5* is in a way autoregulatory. This, combined with the negative and incoherent feedforward branches of the proposed GR-Klf9-Fkbp5 circuit, make predictions about outcomes of perturbing the circuit difficult. Based on known properties of incoherent feed forward loops the role of Klf9 could, for

example, include protection against target overshoot, maintenance of pulsatility, and/or fold-change detection. Future experiments should investigate the function of this circuit with better resolution than whole larvae provide—in more homogenous cells or tissues of interest—and with tools to measure how transcript dynamics relate to the corresponding proteins of interest. Nonetheless, the data in hand indicating diurnal expression, co-regulatory embrace, and exceptional responsiveness of *klf9* and *fkpb5* to GC (see Figs. 4.2, 4.6) position them to govern periodic adjustments to homeostatic set points in response to GC—mobilizing energetic resources for daily transition from resting to active behavioral phase, for example, or in response to threat. Existing data on protein half-lives are limited but suggest that Fkbp5 may be stable for a day or more, while KLF proteins may be degraded within hours[304–306]. These figures allow for a tentative model in which the level of Fkbp5 (and GC resistance) can be incrementally increased over time via repeated or chronic GC exposure, with feedforward tuning by Klf9, altering HPA/I setpoint and associated allostatic load (Fig. 5.2).

Though the GR, Fkbp5 and Klf9 are ubiquitous[249,308], it shouldn't be assumed that a circuit involving them would function identically in all cells. For one, Fkbp5 does not chaperone the GR alone, but in a dynamic co-chaperone complex that varies with cell type. In the broadly accepted model of GR activation, Fkbp5 is displaced by the highly homologous Fkbp4 which then potentiates GR activity by increasing ligand affinity and associating with motor proteins for GR nuclear translocation[309]. Reality is certain to be more nuanced. For example, a selective effect of FKBP5 inhibition in mouse muscle compared with adipose tissue has been ascribed to

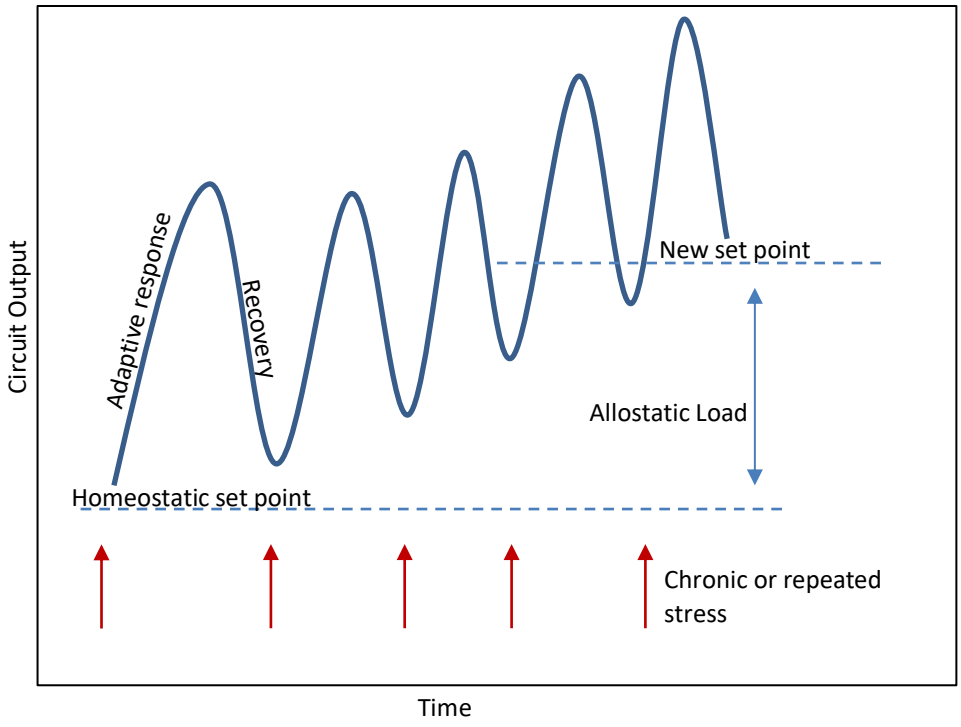


**Figure 5.2. Chronic activation of the GR-Klf9-Fkbp5 circuit leads to allostatic load.** A schematic of proposed effect of chronic/repeated activation of the GR-Klf9-Fkbp5 circuit. Repeated stimulus without full recovery leads over time to set point drift and allostatic load. Adapted from Lee, et al.[307]

inverted expression ratios of FKBP5 and FKBP4 in those tissues (FKBP5 being relatively high in muscle, low in fat; vice versa for FKBP4)[310]. The abundance of other chaperones also has important effects, such as the regulation by Hsp70 and Hsp90 of GR folding, ligand binding, and activity[311].

In experiments to further define the role of Klf9 in regulating Fkbp5 (and otherwise), the expression of various homologous KLF should also be considered. Functional redundancy of the closely related Klf13 has been described, for example, in mouse hippocampal cells. There, double knockout of Klf9 and Klf13 (but not either alone) abolished expression of the circadian *Dbp* gene[312]. Given that various KLF may bind the same DNA sequence with either activating or

repressive effects (see Chapter 1), the loss of Klf9 could be alternately compensated or exacerbated in a target cell type depending on what other KLF are present. In future studies, single-cell RNA sequencing could be used to determine which larval cells/tissues are most affected by loss of Klf9, and concomitant expression of co-regulatory factors.

In addition to its role as GR chaperone, Fkbp5 interacts with various other pathways governing cellular reactivity[313]. Given that the GR is crucial for its expression, Fkbp5 can be considered a hub connecting GC signaling with these other pathways to coordinate cell behavior. Thus changes in Fkbp5 expression may have multifaceted effects—Fkbp5 has been shown by different groups to regulate the epigenetic programmer DNMT1[314], to enhance autophagy through binding Beclin1[315], and to modulate metabolism via AKT2[310], for examples. In those cases, Fkbp5 seems to function mainly as a scaffold facilitating additional protein-protein interactions. But Fkbp5 is also a functional peptidyl-prolyl isomerase (PPI), capable of catalyzing *cis-trans* conversion of proline residues in target proteins[316]. This isomerase activity provides a molecular toggle switch for target protein conformation and interactions, and PPI are involved in regulating fundamental cellular processes such as RNA turnover rate, protein folding and turnover, cell cycle progression, cell signaling, and gating of ion channels[317,318]. Through association with the ubiquitous and prevalent heat shock protein Hsp90 (part of the cytoplasmic GR chaperone complex) Fkbp5 may come into proximity with many potential targets[319], but specific targets of Fkbp5's PPI activity are largely unknown.

Interestingly, *hsp90aa (*coding for a subunit of Hsp90) is consistently upregulated by chronic CORT in Coffman Lab experiments, which could implicate chronic CORT in remodeling the proteome, given the pervasive role of Hsp90 in protein folding and maturation. GO process

enrichment for regulation of proteolysis was also found among Klf9-dependent CORT-induced genes (see Fig. 3.5D). Due to high energy costs, translation is tightly regulated during stress, necessitating mechanisms for selectively either preserving or catabolizing existing proteins. Experiments to determine effects on the proteome due to chronic CORT and/or loss of Klf9, as well as potential involvement of Fkbp5's PPI activity are intriguing future avenues.

The results that loss of Klf9 increases *fkbp5* expression while decreasing OCR in *Danio* are consistent with a recent study in mice where global knockout of *Fkbp5* elevated the resting metabolic rate[310]. In the same study, *Fkbp5* knockout protected against obesity and increased glucose tolerance and uptake by muscle [†]. In humans, *FKBP5* expression has also been positively correlated with blood glucose and insulin resistance, along with a trend toward increased *FKBP5* in adipose tissue of Type 2 Diabetics[320]. A mutation causing elevated *FKBP5* has also been associated with reduced weight loss following bariatric surgery[321]. In zebrafish, loss of the GR (which is accompanied by loss of *fkbp5* expression, Fig. 4.2B) has been reported to increase growth and muscle mass[162]. Thus, modulation of *FKBP5* appears an important means for control of blood sugar, with lower *FKBP5* increasing the capacity of muscle to absorb glucose. Such associations, along with the increased stress resilience in mice lacking *Fkbp5*[322] and known involvement of *FKBP5* in mental disorders have prompted the suggestion that *fkbp5* may be vestigial "genetic baggage"[323]. But while stress resilience and protection from obesity are desirable traits, unnecessary energy expenditure at rest would be detrimental in scenarios where nutrients are scarce. In *Fkbp5* knockout mice, for instance, the enhanced glucose uptake

[†] Taken together with another recent finding that liver-specific *Klf9* overexpression drives hyperglycemia[209], a larger picture emerges in which regulation of organismal metabolic homeostasis relies on differential tissue-specific responses to GC, as well as cross-signaling between organs.

by muscle increased glucose tolerance, but also resulted in significantly lower blood sugar by the end of 24 hours of fasting[310]. Because the brain relies heavily on glucose for its high metabolic demand, a key outcome of the HPA response to stress is prioritizing blood sugar supply to the brain through various mechanisms. This includes limiting glucose uptake in muscle which can function for limited time on alternate energy sources (e.g. lactate, glycogen stores, proteolysis). Thus, while elevated Fkbp5 is associated with adverse health outcomes, this may reflect that high *FKBP5* expression is a function of increased GC signaling (and potential readout of allostatic load), not that organismal fitness would be improved by loss of *FKBP5*.

The involvement of the GC, Klf9 and Fkbp5 in regulation of metabolism, along with their temporal dynamics raise the possibility of their involvement in regulation of metabolic rhythms. Fascinating work done in yeast suggests that the cell-autonomous stress response is largely a commandeering of a fundamental ultradian metabolic oscillation. In nutrient-limited conditions (as would be found in the wild), yeast exhibit robust ultradian rhythms where genome-wide transcriptional oscillations are coupled with cycling metabolite levels, oxygen consumption rate, and cell growth/replication[31,34,324]. This rhythmicity efficiently segregates oxidative and reductive phases of metabolism, and certain accompanying processes. For example, expression of genes involved in energy intensive protein translation is largely gated to the high oxygen consumption phase when ATP is most abundant, while DNA replication occurs during the reductive phase to avoid damage from reactive oxygen[31,325]. Phases of this metabolic cycle have been shown to strongly correlate with stress-induced gene expression[326]—under environmental stress, yeast gene expression is similar to the reductive metabolic phase, while genes expressed during oxidative metabolism (e.g. involved in translation) are largely suppressed. The switch by

yeast to a low-oxygen consumption state is through to be protective. Various stressors such as heat shock or toxic metal exposure can induce oxidative damage, and in fact the survival rate of yeast in response to various stressors oscillates in sync with ultradian oxygen consumption rate (with survival being more likely when stress occurs during low oxygen consumption)[327].

A similar reciprocal coordination of two primary gene clusters comprising biosynthetic or stress-response genes was uncovered in human epithelial cells using stochastic single-cell profiling[326,328] and in fibroblast cultures responding to various stressors[326,329]. Interestingly the same reciprocal expression was not found in HeLa cells, which are metabolically dysregulated[326,329]. The transcriptional stress response in human cells also varied with the mode of stress, and it was generally enriched for additional processes important to higher eukaryotes, such as cell-cell signaling and apoptosis. Spaciotemporal partitioning of gene expression reminiscent of the yeast metabolic cycle has also been noted in *Danio* during somitogenesis[330], where oxidative metabolism and translation increase as cells proceed through differentiation. In all, there is evidence of a conserved temporal segregation in eukaryotic cells between oxidative and reductive metabolic programs, which may be often obscured in unsynchronized or heterogeneous cell populations. Preliminary data in the Coffman Lab suggest detectable ultradian transcriptome oscillations in 5dpf *Danio* between stress/signaling and growth/development programs. As neuroendocrine systems have evolved in higher eukaryotes to coordinate functions governed cell-autonomously in single ancestral cells, it will be interesting to investigate whether the response to GC involves appropriation of metabolic rhythms, and if so what role Klf9 may play.

### 5.4. Summary, significance and limitations of study

In conclusion, the work described in this dissertation show that Klf9 is an important feed-forward regulator of the transcriptional response to GC, regulating metabolic and immune gene expression downstream of the GR. In the disease-relevant context of chronic developmental CORT exposure, the data show that Klf9 works in dynamic opposition to the GR to regulate the metabolic response to GC. The RNA-seq data generated contain a trove of processes and novel individual gene targets regulated by GC, Klf9, or a combination thereof. Stemming from this data, as well as the finding that loss of Klf9 decreases aerobic respiration, I present a model of direct feed-forward repression of glycolytic genes to be tested by future studies. The *klf9*$^{-/-}$ and Klf9 AM-Tag zebrafish lines I have created using CRISPR will be instrumental in those future studies, as well as in experiments to explore the mechanisms of immune gene regulation by Klf9, which current data suggest are indirect. Using the AM-Tag line, I have also presented data showing that one target of feed-forward repression by Klf9 is the important GR target *fkbp5* that codes for Fkbp5 protein, a negative feedback regulator of GR activity implicated strongly in biomedical literature on GC signaling and HPA dysfunction. This expands the current knowledge about the regulatory circuit governing GR responsiveness to GC signals. Data presented here on dynamic expression and response to chronic CORT of *klf9, fkbp5,* and other GR-target genes (some well-known, some identified here for the first time) set the stage for future work to further determine mechanisms underlying the pathogenic effects of chronic CORT in specific cells and tissues of interest.

A major limitation of the data presented above is their derivation from samples of pooled whole larvae. High temporal resolution has been provided for expression of a small selection of

target genes and may help inform the design of future studies, however these data lack spatial, tissue-specific resolution. Some inference can be made as to what cells or tissue types might be involved or affected by bulk changes in immune or metabolic gene expression, however future studies directly examining target cells/tissues are called for. Another limitation of the current studies is the heavy reliance on mRNA expression as a readout. The relationships between transcript expression, abundance of encoded proteins, and physiological outcomes are frequently complex and non-linear. In the proposed GR-Klf9-Fkbp5 circuit, for example, multiple autoregulatory motifs function downstream of a dynamic CORT input, making predictions of output difficult. Validated antibodies for zebrafish proteins of interest and development of other protein-level tools (e.g. strains with epitope-tagged GR/Fkbp5 and/or reporter lines) will aid future studies of GC signaling in *Danio.*

## REFERENCES


1. Timmermans S, Souffriau J, Libert C. A general introduction to glucocorticoid biology. *Front Immunol*. 2019;10(JULY):1545. doi:10.3389/fimmu.2019.01545

2. Hench PS, Kendall EC, Slocumb CH, Polley HF. Adrenocortical Hormone in Arthritis : Preliminary Report. *Ann Rheum Dis*. 1949;8(2):97-104. doi:10.1136/ard.8.2.97

3. Panettieri RA, Schaafsma D, Amrani Y, Koziol-White C, Ostrom R, Tliba O. Non-genomic Effects of Glucocorticoids: An Updated View. *Trends Pharmacol Sci*. 2019;40(1):38-49. doi:10.1016/j.tips.2018.11.002

4. Reul JMHM, De Kloet ER. Two receptor systems for corticosterone in rat brain: Microdistribution and differential occupation. *Endocrinology*. 1985;117(6):2505-2511. doi:10.1210/endo-117-6-2505

5. Gomez-Sanchez E, Gomez-Sanchez CE. The Multifaceted Mineralocorticoid Receptor. In: *Comprehensive Physiology*. Vol 4. Hoboken, NJ, USA: John Wiley & Sons, Inc.; 2014:965-994. doi:10.1002/cphy.c130044

6. Sacta MA, Chinenov Y, Rogatsky I. Glucocorticoid Signaling: An Update from a Genomic Perspective. *Annu Rev Physiol*. 2016;78:155-180. doi:10.1146/annurev-physiol-021115-105323

7. Weikum ER, Knuesel MT, Ortlund EA, Yamamoto KR. Glucocorticoid receptor control of transcription: Precision and plasticity via allostery. *Nat Rev Mol Cell Biol*. 2017;18(3):159-174. doi:10.1038/nrm.2016.152

8. Jankord R, Herman JP. Limbic regulation of hypothalamo-pituitary-adrenocortical function during acute and chronic stress. In: *Annals of the New York Academy of Sciences*. Vol 1148. Blackwell Publishing Inc.; 2008:64-73. doi:10.1196/annals.1410.012

9. Watts AG, Sanchez-Watts G. Region-specific regulation of neuropeptide mRNAs in rat limbic forebrain neurones by aldosterone and corticosterone. *J Physiol*. 1995;484(3):721-736. doi:10.1113/jphysiol.1995.sp020698

10. Watts AG. Glucocorticoid regulation of peptide genes in neuroendocrine CRH neurons: A complexity beyond negative feedback. *Front Neuroendocrinol*. 2005;26:109-130. doi:10.1016/j.yfrne.2005.09.001

11. Hakamata Y, Komi S, Moriguchi Y, et al. Amygdala-centred functional connectivity affects daily cortisol concentrations: A putative link with anxiety. *Sci Rep*. 2017;7(1). doi:10.1038/s41598-017-08918-7

12. Kinner VL, Wolf OT, Merz CJ. Cortisol increases the return of fear by strengthening amygdala signaling in men. 2018. doi:10.1016/j.psyneuen.2018.02.020

13. McEwen BS, Nasca C, Gray JD. Stress Effects on Neuronal Structure: Hippocampus, Amygdala, and Prefrontal Cortex. *Neuropsychopharmacology*. 2016;41(1):3-23. doi:10.1038/npp.2015.171

14. Lakshminarasimhan H, Chattarji S. Stress Leads to Contrasting Effects on the Levels of Brain Derived Neurotrophic Factor in the Hippocampus and Amygdala. Hashimoto K, ed. *PLoS One*. 2012;7(1):e30481. doi:10.1371/journal.pone.0030481

15. Kalsbeek A, van der Spek R, Lei J, Endert E, Buijs RM, Fliers E. Circadian rhythms in the hypothalamo-pituitary-adrenal (HPA) axis. *Mol Cell Endocrinol*. 2012;349(1):20-29. doi:10.1016/j.mce.2011.06.042

16. Nader N, Chrousos GP, Kino T. Circadian rhythm transcription factor CLOCK regulates the transcriptional activity of the glucocorticoid receptor by acetylating its hinge region lysine cluster: potential physiological implications. *FASEB J*. 2009;23(5):1572-1583. doi:10.1096/fj.08-117697

17. Debono M, Harrison RF, Whitaker MJ, et al. Salivary Cortisone Reflects Cortisol Exposure Under Physiological Conditions and After Hydrocortisone. *J Clin Endocrinol Metab*. 2016;101(4):1469-1477. doi:10.1210/jc.2015-3694

18. Schibler U, Gotic I, Saini C, et al. Clock-Talk: Interactions between Central and Peripheral Circadian Oscillators in Mammals. *Cold Spring Harb Symp Quant Biol*. 2015;80:223-232. doi:10.1101/sqb.2015.80.027490

19. Balsalobre A, Brown SA, Marcacci L, et al. Resetting of circadian time in peripheral tissues by glucocorticoid signaling. *Science (80- )*. 2000;289(5488):2344-2347. doi:10.1126/science.289.5488.2344

20. Dickmeis T, Lahiri K, Nica G, et al. Glucocorticoids Play a Key Role in Circadian Cell Cycle Rhythms. Schibler U, ed. *PLoS Biol*. 2007;5(4):e78. doi:10.1371/journal.pbio.0050078

21. Chung S, Lee EJ, Cha HK, et al. Cooperative roles of the suprachiasmatic nucleus central clock and the adrenal clock in controlling circadian glucocorticoid rhythm. *Sci Rep*. 2017;7(1):1-10. doi:10.1038/srep46404

22. Veldhuis JD, Iranmanesh A, Lizarralde G, Johnson ML. Amplitude modulation of a burstlike mode of cortisol secretion subserves the circadian glucocorticoid rhythm. *Am J Physiol - Endocrinol Metab*. 1989;257(1). doi:10.1152/ajpendo.1989.257.1.e6

23. Jasper MS, Engeland WC. Synchronous ultradian rhythms in adrenocortical secretion detected by microdialysis in awake rats. *Am J Physiol - Regul Integr Comp Physiol*. 1991;261(5 30-5). doi:10.1152/ajpregu.1991.261.5.r1257

24. Stavreva DA, Wiench M, John S, et al. Ultradian hormone stimulation induces glucocorticoid receptor-mediated pulses of gene transcription. *Nat Cell Biol*. 2009;11(9):1093-1102. doi:10.1038/ncb1922

25. Walker JJ, Terry JR, Lightman SL. Origin of ultradian pulsatility in the hypothalamic-pituitary-adrenal axis. In: *Proceedings of the Royal Society B: Biological Sciences*. Vol 277. ; 2010:1627-1633. doi:10.1098/rspb.2009.2148

26. Spiga F, Waite EJ, Liu Y, Kershaw YM, Aguilera G, Lightman SL. ACTH-Dependent Ultradian Rhythm of Corticosterone Secretion. *Endocrinology*. 2011;152(4):1448-1457. doi:10.1210/en.2010-1209

27. Walker JJ, Spiga F, Waite E, et al. The Origin of Glucocorticoid Hormone Oscillations. Vidal-Puig AJ, ed. *PLoS Biol*. 2012;10(6):e1001341. doi:10.1371/journal.pbio.1001341

28. Rankin J, Walker JJ, Windle R, Lightman SL, Terry JR. Characterizing dynamic interactions between ultradian glucocorticoid rhythmicity and acute stress using the phase response curve. *PLoS One*. 2012;7(2):e30978. doi:10.1371/journal.pone.0030978

29. Windle RJ, Wood SA, Lightman SL, Ingram CD. The Pulsatile Characteristics of Hypothalamo-Pituitary-Adrenal Activity in Female Lewis and Fischer 344 Rats and Its Relationship to Differential Stress Responses [1]. *Endocrinology*. 1998;139(10):4044-4052. doi:10.1210/endo.139.10.6238

30. Sarabdjitsingh RA, Conway-Campbell BL, Leggett JD, et al. Stress responsiveness varies over the ultradian glucocorticoid cycle in a brain-region-specific manner. *Endocrinology*. 2010;151(11):5369-5379. doi:10.1210/en.2010-0832

31. Tu BP, Kudlicki A, Rowicka M, McKnight SL. Cell biology: Logic of the yeast metabolic cycle: Temporal compartmentalization of cellular processes. *Science (80- )*. 2005;310(5751):1152-1158. doi:10.1126/science.1120499

32. Lloyd D, Murray DB. Ultradian metronome: Timekeeper for orchestration of cellular coherence. *Trends Biochem Sci*. 2005;30(7):373-377. doi:10.1016/j.tibs.2005.05.005

33. Liu Y, Tsinoremas NF, Johnson CH, et al. Circadian orchestration of gene expression in cyanobacteria. *Genes Dev*. 1995;9(12):1469-1478. doi:10.1101/gad.9.12.1469

34. Klevecz RR, Bolen J, Forrest G, Murray DB. A genomewide oscillation in transcription gates DNA replication and cell cycle. *Proc Natl Acad Sci U S A*. 2004;101(5):1200-1205. doi:10.1073/pnas.0306490101

35. Silverman MN, Sternberg EM. Glucocorticoid regulation of inflammation and its functional correlates: From HPA axis to glucocorticoid receptor dysfunction. *Ann N Y Acad Sci*. 2012;1261(1):55-63. doi:10.1111/j.1749-6632.2012.06633.x

36. Oster H, Challet E, Ott V, et al. The functional and clinical significance of the 24-h rhythm of circulating glucocorticoids. *Endocr Rev*. 2016;38(1):er.2015-1080. doi:10.1210/er.2015-1080

37. Van Cauter E, Leproult R, Kupfer DJ. Effects of gender and age on the levels and circadian rhythmicity of plasma cortisol. *J Clin Endocrinol Metab*. 1996;81(7):2468-2473. doi:10.1210/jcem.81.7.8675562

38. Van Cauter E, Leproult R, Plat L. Age-related changes in slow wave sleep and REM sleep and relationship with growth hormone and cortisol levels in healthy men. *J Am Med Assoc*. 2000;284(7):861-868. doi:10.1001/jama.284.7.861

39. Gust DA, Wilson ME, Stocker T, Conrad S, Plotsky PM, Gordon TP. Activity of the Hypothalamic-Pituitary-Adrenal Axis Is Altered by Aging and Exposure to Social Stress in Female Rhesus Monkeys [1]. *J Clin Endocrinol Metab*. 2000;85(7):2556-2563. doi:10.1210/jcem.85.7.6696

40. Dallman MF, Akana SF, Bhatnagar S, Bell ME, Strack AM. Bottomed out: Metabolic significance of the circadian trough in glucocorticoid concentrations. *Int J Obes*. 2000;24:S40-S46. doi:10.1038/sj.ijo.0801276

41. Hackett RA, Steptoe A, Kumari M. Association of diurnal patterns in salivary cortisol with type 2 diabetes in the Whitehall II study. *J Clin Endocrinol Metab*. 2014;99(12):4625-4631. doi:10.1210/jc.2014-2459

42. Joseph JJ, Golden SH. Cortisol dysregulation: the bidirectional link between stress, depression, and type 2 diabetes mellitus. *Ann N Y Acad Sci*. 2017;1391(1):20-34. doi:10.1111/nyas.13217

43. Fardet L, Petersen I, Nazareth I. Suicidal behavior and severe neuropsychiatric disorders following glucocorticoid therapy in primary care. *Am J Psychiatry*. 2012;169(5):491-497. doi:10.1176/appi.ajp.2011.11071009

44. Stetler C, Miller GE. Depression and Hypothalamic-Pituitary-Adrenal Activation: A Quantitative Summary of Four Decades of Research. *Psychosom Med*. 2011;73(2):114-126. doi:10.1097/PSY.0b013e31820ad12b

45. Linkowski P, Mendlewicz J, Kerkhofs M, et al. 24-Hour Profiles of Adrenocorticotropin, Cortisol, and Growth Hormone in Major Depressive Illness: Effect of Antidepressant Treatment*. *J Clin Endocrinol Metab*. 1987;65(1):141-152. doi:10.1210/jcem-65-1-141

46. Windle RJ, Wood SA, Kershaw YM, Lightman SL, Ingram CD, Harbuz MS. Increased corticosterone pulse frequency during adjuvant-induced arthritis and its relationship to alterations in stress responsiveness. *J Neuroendocrinol*. 2001;13(10):905-911. doi:10.1046/j.1365-2826.2001.00715.x

47. Young EA, Carlson NE, Brown MB. Twenty-four-hour ACTH and cortisol pulsatility in depressed women. *Neuropsychopharmacology*. 2001;25(2):267-276. doi:10.1016/S0893-133X(00)00236-0

48. Cheong R, Levchenko A. Oscillatory signaling processes: The how, the why and the where. *Curr Opin Genet Dev*. 2010;20(6):665-669. doi:10.1016/j.gde.2010.08.007

49. Reeves GT. The engineering principles of combining a transcriptional incoherent feedforward loop with negative feedback. *J Biol Eng*. 2019;13(1):62. doi:10.1186/s13036-019-0190-3

50. Ma W, Trusina A, El-Samad H, Lim WA, Tang C. Defining Network Topologies that Can Achieve Biochemical Adaptation. *Cell*. 2009;138(4):760-773. doi:10.1016/j.cell.2009.06.013

51. McEwen B. PROTECTIVE AND DAMAGING EFFECTS OF STRESS MEDIATORS. *N Engl J Med*. 1998;338(3):171-179. https://www-nejm-org.prxy4.ursus.maine.edu/doi/pdf/10.1056/NEJM199801153380307. Accessed April 30, 2018.

52. Picard M, Juster R-P, McEwen BS. Mitochondrial allostatic load puts the “gluc” back in glucocorticoids. *Nat Publ Gr*. 2014. doi:10.1038/nrendo.2014.22

53. Shi W, Ma W, Xiong L, Zhang M, Tang C. Adaptation with transcriptional regulation OPEN. *Nat Publ Gr*. 2017. doi:10.1038/srep42648

54. Kuo T, McQueen A, Chen TC, Wang JC. Regulation of glucose homeostasis by glucocorticoids. *Adv Exp Med Biol*. 2015;872:99-126. doi:10.1007/978-1-4939-2895-8_5

55. Mergenthaler P, Lindauer U, Dienel GA, Meisel A. Sugar for the brain: The role of glucose in physiological and pathological brain function. *Trends Neurosci*. 2013;36(10):587-597. doi:10.1016/j.tins.2013.07.001

56. Seeman TE. Price of Adaptation—Allostatic Load and Its Health Consequences. *Arch Intern Med*. 1997;157(19):2259. doi:10.1001/archinte.1997.00440400111013

57. Karlamangla AS, Singer BH, McEwen BS, Rowe JW, Seeman TE. Allostatic load as a predictor of functional decline: MacArthur studies of successful aging. *J Clin Epidemiol*. 2002;55(7):696-710. doi:10.1016/S0895-4356(02)00399-2

58. Karlamangla AS, Singer BH, Seeman TE. Reduction in allostatic load in older adults is associated with lower all-cause mortality risk: MacArthur studies of successful aging. *Psychosom Med*. 2006;68(3):500-507. doi:10.1097/01.psy.0000221270.93985.82

59. Juster RP, McEwen BS, Lupien SJ. Allostatic load biomarkers of chronic stress and impact on health and cognition. *Neurosci Biobehav Rev*. 2010;35(1):2-16. doi:10.1016/j.neubiorev.2009.10.002

60. Mauss D, Li J, Schmidt B, Angerer P, Jarczok MN. Measuring allostatic load in the workforce: A systematic review. *Ind Health*. 2015;53(1):5-20. doi:10.2486/indhealth.2014-0122

61. Juster RP, Sindi S, Marin MF, et al. A clinical allostatic load index is associated with burnout symptoms and hypocortisolemic profiles in healthy workers. *Psychoneuroendocrinology*. 2011;36(6):797-805. doi:10.1016/j.psyneuen.2010.11.001

62. Dowd JB, Simanek AM, Aiello AE. Socio-economic status, cortisol and allostatic load: A review of the literature. *Int J Epidemiol*. 2009;38(5):1297-1309. doi:10.1093/ije/dyp277

63. Katz DA, Sprang G, Cooke C. The cost of chronic stress in childhood: Understanding and applying the concept of allostatic load. *Psychodyn Psychiatry*. 2012;40(3):469-480. doi:10.1521/pdps.2012.40.3.469

64. Anda RF, Felitti VJ, Bremner JD, et al. The enduring effects of abuse and related adverse experiences in childhood: A convergence of evidence from neurobiology and epidemiology. *Eur Arch Psychiatry Clin Neurosci*. 2006;256(3):174-186. doi:10.1007/s00406-005-0624-4

65. Tout K, De Haan M, Campbell EK, Gunnar MR. Social Behavior Correlates of Cortisol Activity in Child Care: Gender Differences and Time-of-Day Effects. *Child Dev*. 1998;69(5):1247-1262. doi:10.1111/j.1467-8624.1998.tb06209.x

66. Dettling AC, Gunnar MR, Donzella B. *Cortisol Levels of Young Children in Full-Day Childcare Centers: Relations with Age and Temperament*. Vol 24Psychone.; 1999.

67. Watamura SE, Kryzer EM, Robertson SS. Cortisol patterns at home and child care: Afternoon differences and evening recovery in children attending very high quality full-day center-based child care. *J Appl Dev Psychol*. 2009;30(4):475-485. doi:10.1016/j.appdev.2008.12.027

68. Watamura SE, Coe CL, Laudenslager ML, Robertson SS. Child care setting affects salivary cortisol and antibody secretion in young children. *Psychoneuroendocrinology*. 2010;35(8):1156-1166. doi:10.1016/j.psyneuen.2010.02.001

69. Lupien SJ, King S, Meaney MJ, McEwen BS. Child's stress hormone levels correlate with mother's socioeconomic status and depressive state. *Biol Psychiatry*. 2000;48(10):976-980. doi:10.1016/S0006-3223(00)00965-3

70. Gunnar MR, Donzella B. Social regulation of the cortisol levels in early human development. *Psychoneuroendocrinology*. 2002;27(1-2):199-220. doi:10.1016/S0306-4530(01)00045-2

71. Van Bodegom M, Homberg JR, Henckens MJAG. Modulation of the hypothalamic-pituitary-adrenal axis by early life stress exposure. *Front Cell Neurosci*. 2017;11:87. doi:10.3389/fncel.2017.00087

72. Miller GE, Chen E, Fok AK, et al. Low early-life social class leaves a biological residue manifested by decreased glucocorticoid and increased proinflammatory signaling. *Proc Natl Acad Sci U S A*. 2009;106(34):14716-14721. doi:10.1073/pnas.0902971106

73. Cohen S, Doyle WJ, Turner RB, Alper CM, Skoner DP. Childhood Socioeconomic Status and Host Resistance to Infectious Illness in Adulthood. *Psychosom Med*. 2004;66(4):553-558. doi:10.1097/01.psy.0000126200.05189.d3

74. Galobardes B, Smith GD, Lynch JW. Systematic review of the influence of childhood socioeconomic circumstances on risk for cardiovascular disease in adulthood. *Ann Epidemiol*. 2006;16(2):91-104. doi:10.1016/j.annepidem.2005.06.053

75. Galobardes B. Childhood Socioeconomic Circumstances and Cause-specific Mortality in Adulthood: Systematic Review and Interpretation. *Epidemiol Rev*. 2004;26(1):7-21. doi:10.1093/epirev/mxh008

76. Liggins GC. Premature delivery of foetal lambs infused with glucocorticoids. *J Endocrinol*. 1969;45(4):515-523. doi:10.1677/joe.0.0450515

77. Cole TJ, Blendy JA, Monaghan AP, et al. Targeted disruption of the glucocorticoid receptor gene blocks adrenergic chromaffin cell development and severely retards lung maturation. *Genes Dev*. 1995;9(13):1608-1621. doi:10.1101/gad.9.13.1608

78. Murphy VE, Smith R, Giles WB, Clifton VL. Endocrine regulation of human fetal growth: The role of the mother, placenta, and fetus. *Endocr Rev*. 2006;27(2):141-169. doi:10.1210/er.2005-0011

79. Gilstrap LC, Christensen R, Clewell WH, et al. Effect of Corticosteroids for Fetal Maturation on Perinatal Outcomes: NIH Consensus Development Panel on the Effect of Corticosteroids for Fetal Maturation on Perinatal Outcomes. *JAMA J Am Med Assoc*. 1995;273(5):413-418. doi:10.1001/jama.1995.03520290065031

80. Gilstrap LC. Antenatal corticosteroids revisited: Repeat courses - National Institutes of Health Consensus Development Conference Statement, August 17-18, 2000. In: *Obstetrics and Gynecology*. Vol 98. Obstet Gynecol; 2001:144-150. doi:10.1016/S0029-7844(01)01410-7

81. Harris A, Seckl J. Glucocorticoids, prenatal stress and the programming of disease. *Horm Behav*. 2011;59(3):279-289. doi:10.1016/j.yhbeh.2010.06.007

82. Roberts D, Brown J, Medley N, Dalziel SR. Antenatal corticosteroids for accelerating fetal lung maturation for women at risk of preterm birth. *Cochrane Database Syst Rev*. 2017;2017(3). doi:10.1002/14651858.CD004454.pub3

83. Räikkönen K, Gissler M, Kajantie E. Associations between Maternal Antenatal Corticosteroid Treatment and Mental and Behavioral Disorders in Children. *JAMA - J Am Med Assoc*. 2020;323(19):1924-1933. doi:10.1001/jama.2020.3937

84. Doyle LW, Ford GW, Rickards AL, et al. Antenatal corticosteroids and outcome at 14 years of age in children with birth weight less than 1501 grams. *Pediatrics*. 2000;106(1). doi:10.1542/peds.106.1.e2

85. Dalziel SR, Walker NK, Parag V, et al. Cardiovascular risk factors after antenatal exposure to betamethasone: 30-Year follow-up of a randomised controlled trial. *Lancet*. 2005;365(9474):1856-1862. doi:10.1016/S0140-6736(05)66617-2

86. French NP, Hagan R, Evans SF, Mullan A, Newnham JP. Repeated antenatal corticosteroids: Effects on cerebral palsy and childhood behavior. *Am J Obstet Gynecol*. 2004;190(3):588-595. doi:10.1016/j.ajog.2003.12.016

87. Yeh TF, Lin YJ, Lin HC, et al. Outcomes at School Age after Postnatal Dexamethasone Therapy for Lung Disease of Prematurity. *N Engl J Med*. 2004;350(13):1304-1313. doi:10.1056/NEJMoa032089

88. Murphy BP, Inder TE, Huppi PS, et al. Impaired cerebral cortical gray matter growth after treatment with dexamethasone for neonatal chronic lung disease. *Pediatrics*. 2001;107(2):217-221. doi:10.1542/peds.107.2.217

89. Asztalos E V., Murphy KE, Willan AR, et al. Multiple courses of antenatal corticosteroids for preterm Birth study outcomes in children at 5 years of age (MACS-5). *JAMA Pediatr*. 2013;167(12):1102-1110. doi:10.1001/jamapediatrics.2013.2764

90. Crowther CA, Haslam RR, Hiller JE, Doyle LW, Robinson JS. Neonatal respiratory distress syndrome after repeat exposure to antenatal corticosteroids: a randomised controlled trial. *Lancet*. 2006;367(9526):1913-1919. doi:10.1016/S0140-6736(06)68846-6

91. Crowther CA, Doyle LW, Haslam RR, Hiller JE, Harding JE, Robinson JS. Outcomes at 2 Years of Age after Repeat Doses of Antenatal Corticosteroids. *N Engl J Med*. 2007;357(12):1179-1189. doi:10.1056/NEJMoa071152

92. Crowther CA, Anderson PJ, McKinlay CJ, Harding JE, Ashwood PJ, Haslam RR, Robinson JS, Doyle LW; ACTORDS Follow-up Group. Mid-Childhood Outcomes of Repeat Antenatal Corticosteroids: A Randomized Controlled Trial. Pediatrics. 2016 Oct;138(4):e20160947. doi: 10.1542/peds.2016-0947. Epub 2016 Sep 20.

93. Uno H, Lohmiller L, Thieme C, et al. Brain damage induced by prenatal exposure to dexamethasone in fetal rhesus macaques. I. Hippocampus. *Dev Brain Res*. 1990;53(2):157-167. doi:10.1016/0165-3806(90)90002-G

94. Ikegami M, Jobe AH, Newnham J, Polk DH, Willet KE, Sly P. Repetitive prenatal glucocorticoids improve lung function and decrease growth in preterm lambs. *Am J Respir Crit Care Med*. 1997;156(1):178-184. doi:10.1164/ajrccm.156.1.9612036

95. Newnham JP, Evans SF, Godfrey M, Huang W, Ikegami M, Jobe A. Maternal, but not fetal, administration of corticosteroids restricts fetal growth. *J Matern Fetal Med*. 1999;8(3):81-87. doi:10.1002/(sici)1520-6661(199905/06)8:3<81::aid-mfm3>3.0.co;2-n

96. Huang WL, Harper CG, Evans SF, Newnham JP, Dunlop SA. Repeated prenatal corticosteroid administration delays myelination of the corpus callosum in fetal sheep. *Int J Dev Neurosci*. 2001;19(4):415-425. doi:10.1016/S0736-5748(01)00026-0

97. Sloboda DM, Moss TJ, Gurrin LC, Newnham JP, Challis JRG. *The Effect of Prenatal Betamethasone Administration on Postnatal Ovine Hypothalamic-Pituitary-Adrenal Function*. Vol 172.; 2002. http://www.endocrinology.org. Accessed February 22, 2021.

98. Jameson RR, Seidler FJ, Qiao D, Slotkin TA. Adverse neurodevelopmental effects of dexamethasone modeled in PC12 cells: Identifying the critical stages and concentration thresholds for the targeting of cell acquisition, differentiation and viability. *Neuropsychopharmacology*. 2006;31(8):1647-1658. doi:10.1038/sj.npp.1300967

99. Provençal N, Arloth J, Cattaneo A, et al. Glucocorticoid exposure during hippocampal neurogenesis primes future stress response by inducing changes in DNA methylation. *Proc Natl Acad Sci U S A*. 2020;117(38):23280-23285. doi:10.1073/pnas.1820842116

100. Brown RW, Diaz R, Robson AC, et al. The ontogeny of 11β-hydroxysteroid dehydrogenase type 2 and mineralocorticoid receptor gene expression reveal intricate control of glucocorticoid action in development. *Endocrinology*. 1996;137(2):794-797. doi:10.1210/endo.137.2.8593833

101. Shams M, Kilby MD, Somerset DA, et al. 11β-hydroxysteroid dehydrogenase type 2 in human pregnancy and reduced expression in intrauterine growth restriction. *Hum Reprod*. 1998;13(4):799-804. doi:10.1093/humrep/13.4.799

102. Takahashi LK, Turner JG, Kalin NH. *PROLONGED STRESS-INDUCED ELEVATION IN PLASMA CORTICOSTERONE DURING PREGNANCY IN THE RAT: IMPLICATIONS FOR PRENATAL STRESS STUDIES*. Vol 23.; 1998.

103. Zijlmans MAC, Riksen-Walraven JM, de Weerth C. Associations between maternal prenatal cortisol concentrations and child outcomes: A systematic review. *Neurosci Biobehav Rev*. 2015;53:1-24. doi:10.1016/j.neubiorev.2015.02.015

104. Mairesse J, Lesage J, Breton C, et al. Maternal stress alters endocrine function of the feto-placental unit in rats. *Am J Physiol - Endocrinol Metab*. 2007;292(6). doi:10.1152/ajpendo.00574.2006

105. Jensen Peña C, Monk C, Champagne FA. Epigenetic Effects of Prenatal Stress on 11β-Hydroxysteroid Dehydrogenase-2 in the Placenta and Fetal Brain. Sun K, ed. *PLoS One*. 2012;7(6):e39791. doi:10.1371/journal.pone.0039791

106. Majzoub JA, Karalis KP. Placental corticotropin-releasing hormone: Function and regulation. In: *American Journal of Obstetrics and Gynecology*. Vol 180. Mosby Inc.; 1999:S242-S246. doi:10.1016/s0002-9378(99)70708-8

107. Fisher J, de Mello MC, Patel V, et al. Prevalence and determinants of common perinatal mental disorders in women in low-and lower-middle-income countries: A systematic review. *Bull World Health Organ*. 2012;90(2):139-149. doi:10.2471/BLT.11.091850

108. Van Den Bergh BRH, Van Den Heuvel MI, Lahti M, et al. Prenatal developmental origins of behavior and mental health: The influence of maternal stress in pregnancy. 2017. doi:10.1016/j.neubiorev.2017.07.003

109. Gluckman PD, Hanson MA, Beedle AS. Early life events and their consequences for later disease: A life history and evolutionary perspective. *Am J Hum Biol*. 2007;19(1):1-19. doi:10.1002/ajhb.20590

110. Hales CN, Barker DJP. The thrifty phenotype hypothesis. *Br Med Bull*. 2001;60:5-20. doi:10.1093/bmb/60.1.5

111. Ghaemmaghami P, Dainese SM, La Marca R, Zimmermann R, Ehlert U. The association between the acute psychobiological stress response in second trimester pregnant women, amniotic fluid glucocorticoids, and neonatal birth outcome. *Dev Psychobiol*. 2014;56(4):734-747. doi:10.1002/dev.21142

112. O'Connor TG, Bergman K, Sarkar P, Glover V. Prenatal cortisol exposure predicts infant cortisol response to acute stress. *Dev Psychobiol*. 2013;55(2):145-155. doi:10.1002/dev.21007

113. Smith AK, Newport DJ, Ashe MP, et al. Predictors of neonatal hypothalamic-pituitary-adrenal axis activity at delivery. *Clin Endocrinol (Oxf)*. 2011;75(1):90-95. doi:10.1111/j.1365-2265.2011.03998.x

114. Davis EP, Glynn LM, Waffarn F, Sandman CA. Prenatal maternal stress programs infant stress regulation. *J Child Psychol Psychiatry Allied Discip*. 2011;52(2):119-129. doi:10.1111/j.1469-7610.2010.02314.x

115. Tollenaar MS, Beijers R, Jansen J, Riksen-Walraven JMA, De Weerth C. Maternal prenatal stress and cortisol reactivity to stressors in human infants. *Stress*. 2011;14(1):53-65. doi:10.3109/10253890.2010.499485

116. Gutteling BM, De Weerth C, Buitelaar JK. Prenatal stress and children's cortisol reaction to the first day of school. *Psychoneuroendocrinology*. 2005;30(6):541-549. doi:10.1016/j.psyneuen.2005.01.002

117. O'Donnell KJ, Glover V, Jenkins J, et al. Prenatal maternal mood is associated with altered diurnal cortisol in adolescence. *Psychoneuroendocrinology*. 2013;38(9):1630-1638. doi:10.1016/j.psyneuen.2013.01.008

118. Ronald A, Pennell CE, Whitehouse AJO. Prenatal Maternal Stress Associated with ADHD and Autistic Traits in early Childhood. *Front Psychol*. 2011;1(JAN):223. doi:10.3389/fpsyg.2010.00223

119. Davis EP, Sandman CA. Prenatal psychobiological predictors of anxiety risk in preadolescent children. *Psychoneuroendocrinology*. 2012;37(8):1224-1233. doi:10.1016/j.psyneuen.2011.12.016

120. Lewinn KZ, Stroud LR, Molnar BE, Ware JH, Koenen KC, Buka SL. Elevated maternal cortisol levels during pregnancy are associated with reduced childhood IQ. *Int J Epidemiol*. 2009;38(6):1700-1710. doi:10.1093/ije/dyp200

121. Buss C, Davis EP, Muftuler LT, Head K, Sandman CA. High pregnancy anxiety during mid-gestation is associated with decreased gray matter density in 6-9-year-old children. *Psychoneuroendocrinology*. 2010;35(1):141-153. doi:10.1016/j.psyneuen.2009.07.010

122. Davis EP, Head K, Buss C, Sandman CA. Prenatal maternal cortisol concentrations predict neurodevelopment in middle childhood. *Psychoneuroendocrinology*. 2017;75:56-63. doi:10.1016/j.psyneuen.2016.10.005

123. Li J, Robinson M, Malacova E, Jacoby P, Foster J, Van Eekelen A. Maternal life stress events in pregnancy link to children's school achievement at age 10 years. *J Pediatr*. 2013;162(3):483-489. doi:10.1016/j.jpeds.2012.09.007

124. Buss C, Davis EP, Shahbaba B, Pruessner JC, Head K, Sandman CA. Maternal cortisol over the course of pregnancy and subsequent child amygdala and hippocampus volumes and affective problems. *Proc Natl Acad Sci U S A*. 2012;109(20):E1312-E1319. doi:10.1073/pnas.1201295109

125. Buss C, Davis EP, Hobel CJ, Sandman CA. Maternal pregnancy-specific anxiety is associated with child executive function at 69 years age. *Stress*. 2011;14(6):665-676. doi:10.3109/10253890.2011.623250

126. Sandman CA, Glynn LM, Davis EP, Sandman CA, Glynn LM, Davis EP. Neurobehavioral Consequences of Fetal Exposure to Gestational Stress. 2016. doi:10.1007/978-3-319-22023-9_13

127. Rice F, Harold GT, Boivin J, Van Den Bree M, Hay DF, Thapar A. The links between prenatal stress and offspring development and psychopathology: Disentangling environmental and inherited influences. *Psychol Med*. 2010;40(2):335-342. doi:10.1017/S0033291709005911

128. King S, Laplante DP. The effects of prenatal maternal stress on children's cognitive development: Project Ice Storm. *Stress*. 2005;8(1):35-45. doi:10.1080/10253890500108391

129. Huizink AC, Dick DM, Sihvola E, Pulkkinen L, Rose RJ, Kaprio J. Chernobyl exposure as stressor during pregnancy and behaviour in adolescent offspring. *Acta Psychiatr Scand*. 2007;116(6):438-446. doi:10.1111/j.1600-0447.2007.01050.x

130. Li J, Olsen J, Vestergaard M, Obel C, Baker JL, Sørensen TIA. Prenatal Stress Exposure Related to Maternal Bereavement and Risk of Childhood Overweight. Calbet JAL, ed. *PLoS One*. 2010;5(7):e11896. doi:10.1371/journal.pone.0011896

131. Lindsay RS, Lindsay RM, Waddell BJ, Seckl JR. *Prenatal Glucocorticoid Exposure Leads to Offspring Hyperglycaemia in the Rat: Studies with the 11 b-Hydroxysteroid Dehydrogenase Inhibitor Carbenoxolone*. Vol 39.; 1996.

132. Gunnar MR, Cheatham CL. Brain and behavior interface: Stress and the developing brain. In: *Infant Mental Health Journal*. Vol 24. ; 2003:195-211. doi:10.1002/imhj.10052

133. Gunnar MR, Brodersen L, Krueger K, Rigatuso J. Dampening of Adrenocortical Responses during Infancy: Normative Changes and Individual Differences. *Child Dev*. 1996;67(3):877-889. doi:10.1111/j.1467-8624.1996.tb01770.x

134. Gunnar MR, Brodersen L, Nachmias M, Buss K, Rigatuso J. Stress reactivity and attachment security. *Dev Psychobiol*. 1996;29(3):191-204. doi:10.1002/(SICI)1098-2302(199604)29:3<191::AID-DEV1>3.0.CO;2-M

135. Rosenfeld P, Suchecki D, Levine S, Suchecki D, LEVINE Multifactorial S. *Multifactorial Regulation of the Hypothalamic-Pituitary-Adrenal Axis During Development*. Vol 16.; 1992.

136. Liu D, Diorio J, Tannenbaum B, et al. Maternal care, hippocampal glucocorticoid receptors, and hypothalamic- pituitary-adrenal responses to stress. *Science (80- )*. 1997;277(5332):1659-1662. doi:10.1126/science.277.5332.1659

137. Weaver ICG, Cervoni N, Champagne FA, et al. Epigenetic programming by maternal behavior. *Nat Neurosci*. 2004;7(8):847-854. doi:10.1038/nn1276

138. Francis D, Diorio J, Liu D, Meaney MJ. Nongenomic transmission across generations of maternal behavior and stress responses in the rat. *Science (80- )*. 1999;286(5442):1155-1158. doi:10.1126/science.286.5442.1155

139. Levine S, Lewis GW. *Critical Period for Effects of Infantile Experience on Maturation of Stress Response*. Vol 129.; 1959.

140. Vallée M, Mayo W, Dellu F, Moal M Le, Simon H, Maccari S. Prenatal stress induces high anxiety and postnatal handling induces low anxiety in adult offspring: Correlation with stress-induced corticosterone secretion. *J Neurosci*. 1997;17(7):2626-2636. doi:10.1523/jneurosci.17-07-02626.1997

141. Lupien SJ, Buss C, Schramek TE, Maheu F, Pruessner J. Hormetic Influence of Glucocorticoids on Human Memory. *Nonlinearity Biol Toxicol Med*. 2005;3(1):nonlin.003.01.0. doi:10.2201/nonlin.003.01.003

142. Pratsinis H, Tsagarakis S, Zervolea I, Stathakos D, Thalassinos N, Kletsas D. The Unexpected Anabolic Phenotype and Extended Longevity of Skin Fibroblasts after Chronic Glucocorticoid Excess. *Dose-Response*. 2006;4(2):dose-response.0. doi:10.2203/dose-response.05-007.pratsinis

143. Monaghan P, Haussmann MF. The positive and negative consequences of stressors during early life. *Early Hum Dev*. 2015;91(11):643-647. doi:10.1016/j.earlhumdev.2015.08.008

144. Gopi IK, Rattan SIS. Biphasic Dose–Response and Hormetic Effects of Stress Hormone Hydrocortisone on Telomerase-Immortalized Human Bone Marrow Stem Cells In Vitro. *Dose-Response*. 2019;17(4). doi:10.1177/1559325819889819

145. Priebe K, Brake WG, Romeo RD, et al. Maternal influences on adult stress and anxiety-like behavior in C57BL/6J and BALB/CJ mice: A cross-fostering study. *Dev Psychobiol*. 2005;47(4):398-407. doi:10.1002/dev.20098

146. Neeley EW, Berger R, Koenig JI, Leonard S. Strain dependent effects of prenatal stress on gene expression in the rat hippocampus. *Physiol Behav*. 2011;104(2):334-339. doi:10.1016/j.physbeh.2011.02.032

147. Abbott PW, Gumusoglu SB, Bittle J, Beversdorf DQ, Stevens HE. Prenatal stress and genetic risk: How prenatal stress interacts with genetics to alter risk for psychiatric illness. *Psychoneuroendocrinology*. 2018;90:9-21. doi:10.1016/j.psyneuen.2018.01.019

148. Howe K, Clark MD, Torroja CF, et al. The zebrafish reference genome sequence and its relationship to the human genome. *Nature*. 2013;496(7446):498-503. doi:10.1038/nature12111

149. Alsop D, Vijayan MM. Development of the corticosteroid stress axis and receptor expression in zebrafish. *AJP Regul Integr Comp Physiol*. 2008;294(3):R711-R719. doi:10.1152/ajpregu.00671.2007

150. Chatzopoulou A, Schoonheim PJ, Torraca V, Meijer AH, Spaink HP, Schaaf MJM. Functional analysis reveals no transcriptional role for the glucocorticoid receptor β-isoform in zebrafish. *Mol Cell Endocrinol*. 2017;447:61-70. doi:10.1016/j.mce.2017.02.036

151. Alsop D, Vijayan M. The zebrafish stress axis: Molecular fallout from the teleost-specific genome duplication event. *Gen Comp Endocrinol*. 2009;161(1):62-66. doi:10.1016/j.ygcen.2008.09.011

152. Bridgham JT, Carroll SM, Thornton JW. Evolution of hormone-receptor complexity by molecular exploitation. *Science (80- )*. 2006;312(5770):97-101. doi:10.1126/science.1123348

153. Faught E, Vijayan MM. The mineralocorticoid receptor is essential for stress axis regulation in zebrafish larvae. *Sci Rep*. 2018;8(1):18081. doi:10.1038/s41598-018-36681-w

154. Li C, Tan XF, Lim TK, Lin Q, Gong Z. Comprehensive and quantitative proteomic analyses of zebrafish plasma reveals conserved protein profiles between genders and between zebrafish and human. *Sci Rep*. 2016;6(1):1-15. doi:10.1038/srep24329

155. Noël ES, Dos Reis M, Arain Z, Ober EA. Analysis of the Albumin/α-Fetoprotein/Afamin/Group specific component gene family in the context of zebrafish liver differentiation. *Gene Expr Patterns*. 2010;10(6):237-243. doi:10.1016/j.gep.2010.05.002

156. Facchinello N, Skobo T, Meneghetti G, et al. nr3c1 null mutant zebrafish are viable and reveal DNA-binding-independent activities of the glucocorticoid receptor. *Sci Rep*. 2017;7(1):4371. doi:10.1038/s41598-017-04535-6

157. Ziv L, Muto A, Schoonheim PJ, et al. An affective disorder in zebrafish with mutation of the glucocorticoid receptor. *Mol Psychiatry*. 2013;18(6):681-691. doi:10.1038/mp.2012.64

158. Hartig EI, Zhu S, King BL, et al. Cortisol-treated zebrafish embryos develop into pro-inflammatory adults with aberrant immune gene regulation. *Biol Open*. 2016;5(8):1134-1141. doi:10.1242/bio.020065

159. Gans I, Hartig EI, Zhu S, et al. Klf9 is a key feedforward regulator of the transcriptomic response to glucocorticoid receptor activity. *Sci Rep*. 2020;10(1):11415. doi:10.1038/s41598-020-68040-z

160. Chatzopoulou A, Heijmans JPM, Burgerhout E, et al. Glucocorticoid-Induced Attenuation of the Inflammatory Response in Zebrafish. doi:10.1210/en.2015-2050

161. Dinarello A, Licciardello G, Fontana CM, Tiso N, Argenton F, Valle LD. Glucocorticoid receptor activities in the zebrafish model: A review. *J Endocrinol*. 2020;247(3):R63-R82. doi:10.1530/JOE-20-0173

162. Faught E, Vijayan MM. Loss of the glucocorticoid receptor in zebrafish improves muscle glucose availability and increases growth. *Am J Physiol Metab*. 2019;316(6):E1093-E1104. doi:10.1152/ajpendo.00045.2019

163. Faught E, Vijayan MM. Glucocorticoid and mineralocorticoid receptor activation modulates postnatal growth. *J Endocrinol*. 2020;244(2):261-271. doi:10.1530/JOE-19-0358

164. Faught E, Vijayan MM. Postnatal triglyceride accumulation is regulated by mineralocorticoid receptor activation under basal and stress conditions. *J Physiol*. 2019;597(19):4927-4941. doi:10.1113/JP278088

165. Morbiato E, Frigato E, Dinarello A, et al. Feeding Entrainment of the Zebrafish Circadian Clock Is Regulated by the Glucocorticoid Receptor. *Cells*. 2019;8(11). doi:10.3390/cells8111342

166. Muto A, Taylor MR, Suzawa M, Korenbrot JI, Baier H. Glucocorticoid receptor activity regulates light adaptation in the zebrafish retina. *Front Neural Circuits*. 2013;7(SEP). doi:10.3389/fncir.2013.00145

167. Weger BD, Weger M, Görling B, et al. Extensive Regulation of Diurnal Transcription and Metabolism by Glucocorticoids. *PLoS Genet*. 2016;12(12):1-24. doi:10.1371/journal.pgen.1006512

168. Alsop D, Vijayan MM. Molecular programming of the corticosteroid stress axis during zebrafish development ☆. *Comp Biochem Physiol Part A*. 2008;153:49-54. doi:10.1016/j.cbpa.2008.12.008

169. Pikulkaew S, Benato F, Celeghin A, et al. The knockdown of maternal glucocorticoid receptor mRNA alters embryo development in zebrafish. *Dev Dyn*. 2011;240(4):874-889. doi:10.1002/dvdy.22586

170. Hillegass JM, Villano CM, Cooper KR, White LA. Matrix Metalloproteinase-13 Is Required for Zebra fish (Danio rerio) Development and Is a Target for Glucocorticoids. *Toxicol Sci*. 2007;100(1):168-179. doi:10.1093/toxsci/kfm192

171. Kok FO, Shin M, Ni CW, et al. Reverse genetic screening reveals poor correlation between morpholino-induced and mutant phenotypes in zebrafish. *Dev Cell*. 2015;32(1):97-108. doi:10.1016/j.devcel.2014.11.018

172. Best, C. (2015). Developmental Effects of Cortisol on the Stress Response and Behaviour in Zebrafish (Unpublished master's thesis). University of Calgary, Calgary, AB. doi:10.11575/PRISM/25631

173. Faught E, Best C, Vijayan MM. Maternal stress-associated cortisol stimulation may protect embryos from cortisol excess in zebrafish. *R Soc Open Sci*. 2016;3(2). doi:10.1098/rsos.160032

174. Jeffrey JD, Gilmour KM. Programming of the hypothalamic-pituitary-interrenal axis by maternal social status in zebrafish (Danio rerio). *J Exp Biol*. 2016;219(11):1734-1743. doi:10.1242/jeb.138826

175. Hartig EI, Zhu S, King BL, Coffman JA. Chronic cortisol exposure in early development leads to neuroendocrine dysregulation in adulthood. *BMC Res Notes*. 2020;13(1):366. doi:10.1186/s13104-020-05208-w

176. Nesan D, Vijayan MM. Embryo exposure to elevated cortisol level leads to cardiac performance dysfunction in zebrafish. 2012. doi:10.1016/j.mce.2012.07.010

177. Nesan D, Vijayan MM. Maternal cortisol mediates hypothalamus-pituitary-interrenal axis development in Zebrafish. *Sci Rep*. 2016;6:1-11. doi:10.1038/srep22582

178. Best C, Kurrasch DM, Vijayan MM. Maternal cortisol stimulates neurogenesis and affects larval behaviour in zebrafish. *Sci Rep*. 2017;7(1):40905. doi:10.1038/srep40905

179. Higuchi M. Maternal stress suppresses cell proliferation in the forebrain of zebrafish larvae. *Genes to Cells*. 2020;25(5):350-357. doi:10.1111/gtc.12761

180. Wilson KS, Tucker CS, Al-Dujaili AS, et al. Early-life glucocorticoids programme behaviour and metabolism in adulthood in zebrafish. *J Endocrinol*. 2016;230:125-142. doi:10.1530/JOE-15-0376

181. Marchi D, Santhakumar K, Markham E, et al. Bidirectional crosstalk between hypoxia-inducible factor and glucocorticoid signalling in zebrafish larvae. *PLoS Genet*. 2020;16(5):e1008757. doi:10.1371/journal.pgen.1008757

182. Kwan W, Cortes M, Frost I, et al. The Central Nervous System Regulates Embryonic HSPC Production via Stress-Responsive Glucocorticoid Receptor Signaling. *Cell Stem Cell*. 2016;19(3):370-382. doi:10.1016/j.stem.2016.06.004

183. Zhao Y, Zhang K, Fent K. Regulation of zebrafish (Danio rerio) locomotor behavior and circadian rhythm network by environmental steroid hormones. *Environ Pollut*. 2018;232:422-429. doi:10.1016/j.envpol.2017.09.057

184. Willi RA, Faltermann S, Hettich T, Fent K. Active Glucocorticoids Have a Range of Important Adverse Developmental and Physiological Effects on Developing Zebrafish Embryos. *Environ Sci Technol*. 2018;52(2):877-885. doi:10.1021/acs.est.7b06057

185. Licht JD, Grossel MJ, Figge J, Hansen UM. Drosophila Krüppel protein is a transcriptional represser. *Nature*. 1990;346(6279):76-79. doi:10.1038/346076a0

186. Bialkowska AB, Yang VW, Mallipattu SK. Krü ppel-like factors in mammalian stem cells and development. 2017. doi:10.1242/dev.145441

187. Xue Y, Gao S, Liu F. Genome-wide analysis of the zebrafish Klf family identifies two genes important for erythroid maturation. *Dev Biol*. 2015;403(2):115-127. doi:10.1016/j.ydbio.2015.05.015

188. McConnell BB, Yang VW. Mammalian Krüppel-Like factors in health and diseases. *Physiol Rev*. 2010;90(4):1337-1381. doi:10.1152/physrev.00058.2009

189. Imataka H, Sogawa K, Yasumoto K, et al. Two regulatory proteins that bind to the basic transcription element (BTE), a GC box sequence in the promoter region of the rat P-4501A1 gene. *EMBO J*. 1992;11(10):3663-3671. doi:10.1002/j.1460-2075.1992.tb05451.x

190. Mitchell DL, DiMario JX. Bimodal, reciprocal regulation of fibroblast growth factor receptor 1 promoter activity by BTEB1/KLF9 during myogenesis. *Mol Biol Cell*. 2010;21(15):2780-2787. doi:10.1091/mbc.E10-04-0290

191. Knoedler JR, Subramani A, Denver RJ. The Krüppel-like factor 9 cistrome in mouse hippocampal neurons reveals predominant transcriptional repression via proximal promoter binding. *BMC Genomics*. 2017;18(1):299. doi:10.1186/s12864-017-3640-7

192. Knoedler JR, Denver RJ. Krüppel-like factors are effectors of nuclear receptor signaling. doi:10.1016/j.ygcen.2014.03.003

193. Pollak NM, Hoffman M, Goldberg IJ, Drosatos K. Krüppel-Like Factors: Crippling and Uncrippling Metabolic Pathways. *JACC Basic to Transl Sci*. 2018;3(1):132-156. doi:10.1016/j.jacbts.2017.09.001

194. Hsieh PN, Fan L, Sweet DR, Jain MK. The Krüppel-like factors and control of energy homeostasis. *Endocr Rev*. 2018;40(1):137-152. doi:10.1210/er.2018-00151

195. Takahashi K, Tanabe K, Ohnuki M, et al. Induction of Pluripotent Stem Cells from Adult Human Fibroblasts by Defined Factors. *Cell*. 2007;131(5):861-872. doi:10.1016/j.cell.2007.11.019

196. Jiang J, Chan YS, Loh YH, et al. A core Klf circuitry regulates self-renewal of embryonic stem cells. *Nat Cell Biol*. 2008;10(3):353-360. doi:10.1038/ncb1698

197. Wani MA, Wert SE, Lingrel JB. Lung Kruppel-like factor, a zinc finger transcription factor, is essential for normal lung development. *J Biol Chem*. 1999;274(30):21180-21185. doi:10.1074/jbc.274.30.21180

198. Wan H, Luo F, Wert SE, et al. Kruppel-like factor 5 is required for perinatal lung morphogenesis and function. *Development*. 2008;135(15):2563-2572. doi:10.1242/dev.021964

199. Chinenov Y, Coppo M, Gupte R, Sacta MA, Rogatsky I. Glucocorticoid receptor coordinates transcription factor-dominated regulatory network in macrophages. *BMC Genomics*. 2014;15(1). doi:10.1186/1471-2164-15-656

200. Denver RJ, Pavgi S, Shi YB. Thyroid hormone-dependent gene expression program for Xenopus neural development. *J Biol Chem*. 1997;272(13):8179-8188. doi:10.1074/jbc.272.13.8179

201. Denver RJ, Ouellet L, Furling D, Kobayashil A, Fujii-Kuriyama Y, Puymirat J. Basic transcription element-binding protein (BTEB) is a thyroid hormone- regulated gene in the developing central nervous system: Evidence for a role in neurite outgrowth. *J Biol Chem*. 1999;274(33):23128-23134. doi:10.1074/jbc.274.33.23128

202. Cayrou C, Denver RJ. *Suppression of the Basic Transcription Element-Binding Protein in Brain Neuronal Cultures Inhibits Thyroid Hormone-Induced Neurite Branching*.; 2002. https://academic.oup.com/endo/article/143/6/2242/2989664. Accessed May 2, 2021.

203. Apara A, Galvao J, Wang Y, et al. KLF9 and JNK3 interact to suppress axon regeneration in the adult CNS. *J Neurosci*. 2017;37(40):9632-9644. doi:10.1523/JNEUROSCI.0643-16.2017

204. Galvao J, Iwao K, Apara A, et al. The Krüppel-like factor gene target dusp14 regulates axon growth and regeneration. *Investig Ophthalmol Vis Sci*. 2018;59(7):2736-2747. doi:10.1167/iovs.17-23319

205. Bonett RM, Hu F, Bagamasbad P, Denver RJ. Stressor and glucocorticoid-dependent induction of the immediate early gene kr??ppel-like factor 9: implications for neural development and plasticity. *Endocrinology*. 2009;150(4):1757-1765. doi:10.1210/en.2008-1441

206. Bagamasbad P, Ziera T, Borden SA, et al. Molecular Basis for Glucocorticoid Induction of the Krüppel-Like Factor 9 Gene in Hippocampal Neurons. 2012. doi:10.1210/en.2012-1303

207. Bagamasbad PD, Bonett RM, Sachs L, et al. Deciphering the Regulatory Logic of an Ancient, Ultraconserved Nuclear Receptor Enhancer Module. *Mol Endocrinol*. 2015;29(6):856-872. doi:10.1210/me.2014-1349

208. Mostafa MM, Bansal A, Michi AN, et al. Genomic determinants implicated in the glucocorticoid-mediated induction of KLF9 in pulmonary epithelial cells. 2021. doi:10.1074/jbc.RA120.015755

209. Cui A, Fan H, Zhang Y, et al. Dexamethasone-induced Krüppel-like factor 9 expression promotes hepatic gluconeogenesis and hyperglycemia. *J Clin Invest*. 2019;129(6). doi:10.1172/JCI66062

210. Reddy TE, Pauli F, Sprouse RO, et al. Genomic determination of the glucocorticoid response reveals unexpected mechanisms of gene regulation. *Genome Res*. 2009;19(12):2163-2171. doi:10.1101/gr.097022.109

211. Spörl F, Korge S, Jürchott K, et al. Krüppel-like factor 9 is a circadian transcription factor in human epidermis that controls proliferation of keratinocytes. *Proc Natl Acad Sci U S A*. 2012;109(27):10903-10908. doi:10.1073/pnas.1118641109

212. Lili LN, Klopot A, Readhead B, Baida G, Dudley JT, Budunova I. Transcriptomic Network Interactions in Human Skin Treated with Topical Glucocorticoid Clobetasol Propionate. *J Invest Dermatol*. 2019;139(11):2281-2291. doi:10.1016/j.jid.2019.04.021

213. Juszczak GR, Stankiewicz AM. Glucocorticoids, genes and brain function. *Prog Neuro-Psychopharmacology Biol Psychiatry*. 2017;82(November 2017):136-168. doi:10.1016/j.pnpbp.2017.11.020

214. Nasiadka A, Clark MD. Zebrafish breeding in the laboratory environment. *ILAR J*. 2012;53(2). doi:10.1093/ilar.53.2.161

215. Schmittgen TD, Livak KJ. Analyzing real-time PCR data by the comparative CT method. *Nat Protoc*. 2008;3(6):1101-1108. doi:10.1038/nprot.2008.73

216. Risso D, Schwartz K, Sherlock G, Dudoit S. GC-Content Normalization for RNA-Seq Data. *BMC Bioinformatics*. 2011;12(1):480. doi:10.1186/1471-2105-12-480

217. Love MI, Huber W, Anders S. Moderated estimation of fold change and dispersion for RNA-seq data with DESeq2. *Genome Biol*. 2014;15(12):550. doi:10.1186/s13059-014-0550-8

218. Eden E, Navon R, Steinfeld I, Lipson D, Yakhini Z. GOrilla: a tool for discovery and visualization of enriched GO terms in ranked gene lists. *BMC Bioinformatics*. 2009;10(1):48. doi:10.1186/1471-2105-10-48

219. Supek F, Bošnjak M, ˇ Kunca S, ˇ Muc S. Summarizes and Visualizes Long Lists of Gene Ontology Terms. *PLoS One*. 2011;6(7):21800. doi:10.1371/journal.pone.0021800

220. Heinz S, Benner C, Spann N, et al. Simple Combinations of Lineage-Determining Transcription Factors Prime cis-Regulatory Elements Required for Macrophage and B Cell Identities. *Mol Cell*. 2010;38(4):576-589. doi:10.1016/j.molcel.2010.05.004

221. Huang DW, Sherman BT, Lempicki RA. Systematic and integrative analysis of large gene lists using DAVID bioinformatics resources. *Nat Protoc*. 2009;4(1):44-57. doi:10.1038/nprot.2008.211

222. Huang DW, Sherman BT, Lempicki RA. Bioinformatics enrichment tools: paths toward the comprehensive functional analysis of large gene lists. *Nucleic Acids Res*. 2009;37(1):1-13. doi:10.1093/nar/gkn923

223. Geiss GK, Bumgarner RE, Birditt B, et al. Direct multiplexed measurement of gene expression with color-coded probe pairs. *Nat Biotechnol*. 2008;26(3):317-325. doi:10.1038/nbt1385

224. Warnes G, Bolker B, Bonebakker L, et al. gplots: Various R Programming Tools for Plotting Data. 2020.

225. Doench JG, Fusi N, Sullender M, et al. Optimized sgRNA design to maximize activity and minimize off-target effects of CRISPR-Cas9. *Nat Biotechnol*. 2016;34(2):184-191. doi:10.1038/nbt.3437

226. Hsu PD, Scott DA, Weinstein JA, et al. DNA targeting specificity of RNA-guided Cas9 nucleases. *Nat Biotechnol*. 2013;31(9):827-832. doi:10.1038/nbt.2647

227. Song Y, Lai L, Li Z. Large-scale genomic deletions mediated by CRISPR/Cas9 system. *Oncotarget*. 2017;8(4):5647-5647. doi:10.18632/oncotarget.14543

228. Westerfield M. *The Zebrafish Book: A Guide for the Laboratory Use of Zebrafish (Brachydanio Rerio)*. Vol 3th editor. 4th editio. Eugene, OR: University of Oregon Press; 2000. https://zfin.org/zf_info/zfbook/zfbk.html.

229. Lindeman L, Vogt-Kielland L, Alestrom P, Collas P. Fish'n ChIPs: chromatin immunoprecipitation in the zebrafish embryo. *Methods Mol Biol*. 2009;567:75-86.

230. Reddy TE, Gertz J, Crawford GE, Garabedian MJ, Myers RM. The Hypersensitive Glucocorticoid Response Specifically Regulates Period 1 and Expression of Circadian Genes. 2012. doi:10.1128/MCB.00062-12

231. Blair LJ, Criado-Marrero M, Rein T, Binder EB, Porter JT, Iii JK. Hsp90 and FKBP51: complex regulators of psychiatric diseases. doi:10.1098/rstb.2016.0532

232. Facchinello N, Skobo T, Meneghetti G, et al. Nr3c1 null mutant zebrafish are viable and reveal DNA-binding-independent activities of the glucocorticoid receptor. *Sci Rep*. 2017;7(1):1-13. doi:10.1038/s41598-017-04535-6

233. Lee HB, Schwab TL, Sigafoos AN, et al. Novel zebrafish behavioral assay to identify modifiers of the rapid, nongenomic stress response. 2018. doi:10.1111/gbb.12549

234. Griffiths BB, Schoonheim PJ, Ziv L, et al. A zebrafish model of glucocorticoid resistance shows serotonergic modulation of the stress response. 2012. doi:10.3389/fnbeh.2012.00068

235. Lu NZ, Cidlowski JA. Translational regulatory mechanisms generate N-terminal glucocorticoid receptor isoforms with unique transcriptional target genes. *Mol Cell*. 2005;18(3):331-342. doi:10.1016/j.molcel.2005.03.025

236. Morita M, Kobayashi A, Yamashita T, et al. Functional Analysis of Basic Transcription Element Binding Protein by Gene Targeting Technology. *Mol Cell Biol*. 2003;23(7):2489-2500. doi:10.1128/mcb.23.7.2489-2500.2003

237. Simmen RCM, Heard ME, Simmen AM, et al. The krüppel-like factors in female reproductive system pathologies. *J Mol Endocrinol*. 2015;54(2):R89-R101. doi:10.1530/JME-14-0310

238. Pabona JMP, Zhang D, Ginsburg DS, Simmen FA, Simmen RCM. Prolonged pregnancy in women is associated with attenuated myometrial expression of progesterone receptor co regulator krüppel like factor 9. *J Clin Endocrinol Metab*. 2015;100(1):166-174. doi:10.1210/jc.2014-2846

239. Najafabadi HS, Mnaimneh S, Schmitges FW, et al. C2H2 zinc finger proteins greatly expand the human regulatory lexicon. *Nat Biotechnol*. 2015;33(5):555-562. doi:10.1038/nbt.3128

240. Ying M, Tilghman J, Wei Y, et al. Kruppel-like Factor-9 (KLF9) Inhibits Glioblastoma Stemness through Global Transcription Repression and Integrin α6 Inhibition*. *J Biol Chem*. 2014;289(47):32742-32756. doi:10.1074/jbc.M114.588988

241. Zhang J-S, Moncrieffe MC, Kaczynski J, Ellenrieder V, Prendergast FG, Urrutia R. A Conserved -Helical Motif Mediates the Interaction of Sp1-Like Transcriptional Repressors with the Corepressor mSin3A. *Mol Cell Biol*. 2001;21(15):5041-5049. doi:10.1128/MCB.21.15.5041-5049.2001

242. Scammell JG, Denny WB, Valentine DL, Smith DF. Overexpression of the FK506-Binding Immunophilin FKBP51 Is the Common Cause of Glucocorticoid Resistance in Three New World Primates. 2001. doi:10.1006/gcen.2001.7696

243. Denny WB, Valentine DL, Reynolds PD, Smith DF, Scammell JG. Squirrel Monkey Immunophilin FKBP51 Is a Potent Inhibitor of Glucocorticoid Receptor Binding [1]. *Endocrinology*. 2000;141(11):4107-4113. doi:10.1210/endo.141.11.7785

244. Li H, Su P, Lai TKY, et al. The glucocorticoid receptor-FKBP51 complex contributes to fear conditioning and posttraumatic stress disorder. *J Clin Invest*. 2020;130(2):877-889. doi:10.1172/JCI130363

245. Binder EB, Salyakina D, Lichtner P, et al. Polymorphisms in FKBP5 are associated with increased recurrence of depressive episodes and rapid response to antidepressant treatment. *Nat Genet*. 2004;36(12):1319-1325. doi:10.1038/ng1479

246. Binder EB. The role of FKBP5, a co-chaperone of the glucocorticoid receptor in the pathogenesis and therapy of affective and anxiety disorders. *Psychoneuroendocrinology*. 2009;34 Suppl 1:S186-95. doi:10.1016/j.psyneuen.2009.05.021

247. Klengel T, Mehta D, Anacker C, et al. Allele-specific FKBP5 DNA demethylation mediates gene-childhood trauma interactions. *Nat Neurosci*. 2013;16(1):33-41. doi:10.1038/nn.3275

248. Thisse B, Thisse C. Fast Release Clones: A High Throughput Expression Analysis. *ZFIN Direct Data Submiss*. 2004. http://zfin.org.

249. Zhang Y, Xue Y, Cao C, et al. Thyroid hormone regulates hematopoiesis via the TR-KLF9 axis. *Blood*. 2017;130(20):2161-2170. doi:10.1182/blood-2017-05-783043

250. Steindal IAF, Whitmore D. biology Circadian Clocks in Fish-What Have We Learned so far? 2019. doi:10.3390/biology8010017

251. Morbiato, Frigato, Dinarello, et al. Feeding Entrainment of the Zebrafish Circadian Clock Is Regulated by the Glucocorticoid Receptor. *Cells*. 2019;8(11):1342. doi:10.3390/cells8111342

252. Weger BD, Weger M, Görling B, et al. Extensive Regulation of Diurnal Transcription and Metabolism by Glucocorticoids. Oster H, ed. *PLOS Genet*. 2016;12(12):e1006512. doi:10.1371/journal.pgen.1006512

253. Fan H, Zhang Y, Zhang J, et al. Cold-Inducible Klf9 Regulates Thermogenesis of Brown and Beige Fat. *Diabetes*. 2020;69(12):db191153. doi:10.2337/db19-1153

254. Jia D, Lu M, Jung KH, et al. Elucidating cancer metabolic plasticity by coupling gene regulation with metabolic pathways. *Proc Natl Acad Sci U S A*. 2019;116(9):3909-3918. doi:10.1073/pnas.1816391116

255. Cvoro A, Devito L, Milton FA, et al. A thyroid hormone receptor/KLF9 axis in human hepatocytes and pluripotent stem cells. *Stem Cells*. 2015;33(2):416—428. doi:10.1002/stem.1875

256. Sun J, Wang B, Liu Y, et al. Transcription factor KLF9 suppresses the growth of hepatocellular carcinoma cells in vivo and positively regulates p53 expression. *Cancer Lett*. 2014;355(1):25—33. doi:10.1016/j.canlet.2014.09.022

257. Zhong Z, Zhou F, Wang D, et al. Expression of KLF9 in pancreatic cancer and its effects on the invasion, migration, apoptosis, cell cycle distribution, and proliferation of pancreatic cancer cell lines. *Oncol Rep*. 2018;40(6):3852-3860. doi:10.3892/or.2018.6760

258. Lee DC, Sohn HA, Park ZY, et al. A lactate-induced response to hypoxia. *Cell*. 2015;161(3):595-609. doi:10.1016/j.cell.2015.03.011

259. Cui X-G, Han Z-T, He S-H, et al. HIF1/2α mediates hypoxia-induced LDHA expression in human pancreatic cancer cells. *Oncotarget*. 2017;8(15):24840—24852. doi:10.18632/oncotarget.15266

260. Bagamasbad PD, Bonett RM, Sachs L, et al. Deciphering the regulatory logic of an ancient, ultraconserved nuclear receptor enhancer module. *Mol Endocrinol*. 2015;29(6):856-872. doi:10.1210/me.2014-1349

261. Mangan S, Itzkovitz S, Zaslaver A, Alon U. The incoherent feed-forward loop accelerates the response-time of the gal system of Escherichia coli. *J Mol Biol*. 2006;356(5):1073-1081. doi:10.1016/j.jmb.2005.12.003

262. Alon U. *An Introduction to Systems Biology: Design Principles of Biological Circuits*. 2nd ed. Chapman and Hall/CRC; 2019.

263. Viola A, Munari F, Sánchez-Rodríguez R, Scolaro T, Castegna A. The metabolic signature of macrophage responses. *Front Immunol*. 2019;10(JULY):1462. doi:10.3389/fimmu.2019.01462

264. Palmer CS, Ostrowski M, Balderson B, et al. Glucose metabolism regulates T cell activation, differentiation, and functions. 2015. doi:10.3389/fimmu.2015.00001

265. Early JO, Curtis AM. Immunometabolism: Is it under the eye of the clock? *Semin Immunol*. 2016;28(5):478-490. doi:10.1016/j.smim.2016.10.006

266. Jones W, Bianchi K. Aerobic glycolysis: Beyond proliferation. *Front Immunol*. 2015;6(MAY):1. doi:10.3389/fimmu.2015.00227

267. Rabinowitz JD, Enerbäck S. Lactate: the ugly duckling of energy metabolism. *Nat Metab*. 2020;2(7):566-571. doi:10.1038/s42255-020-0243-4

268. Magistretti PJ, Allaman I. Lactate in the brain: From metabolic end-product to signalling molecule. *Nat Rev Neurosci*. 2018;19(4):235-249. doi:10.1038/nrn.2018.19

269. Rogatzki MJ, Ferguson BS, Goodwin ML, Gladden LB. Lactate is always the end product of glycolysis. *Front Neurosci*. 2015;9(FEB). doi:10.3389/fnins.2015.00022

270. Adeva-Andany M, López-Ojén M, Funcasta-Calderón R, et al. Comprehensive review on lactate metabolism in human health. *Mitochondrion*. 2014;17:76-100. doi:10.1016/j.mito.2014.05.007

271. Van Der Windt GJW, Pearce EL. Metabolic switching and fuel choice during T-cell differentiation and memory development. *Immunol Rev*. 2012;249(1):27-42. doi:10.1111/j.1600-065X.2012.01150.x

272. Ying M, Sang Y, Li Y, et al. Krüppel-like family of transcription factor 9, a differentiation-associated transcription factor, suppresses Notch1 signaling and inhibits glioblastoma-initiating stem cells. *Stem Cells*. 2011;29(1):20-31. doi:10.1002/stem.561

273. Tsogtbaatar E, Landin C, Minter-Dykhouse K, Folmes CDL. Energy Metabolism Regulates Stem Cell Pluripotency. *Front Cell Dev Biol*. 2020;8. doi:10.3389/fcell.2020.00087

274. Guo N, Mcdermott KD, Shih Y, et al. Running title: Klf9 regulates neural stem cell expansion in the adult hippocampus. *BioRxiv*. 2021. https://www.biorxiv.org/content/10.1101/2021.07.14.452351v1.

275. Lunt SY, Vander Heiden MG. Aerobic glycolysis: Meeting the metabolic requirements of cell proliferation. *Annu Rev Cell Dev Biol*. 2011;27:441-464. doi:10.1146/annurev-cellbio-092910-154237

276. Chen L, Zhang Z, Hoshino A, et al. NADPH production by the oxidative pentose-phosphate pathway supports folate metabolism. *Nat Metab*. 2019;1(3):404-415. doi:10.1038/s42255-019-0043-x

277. Zhao GN, Jiang DS, Li H. Interferon regulatory factors: At the crossroads of immunity, metabolism, and disease. *Biochim Biophys Acta - Mol Basis Dis*. 2015;1852(2):365-378. doi:10.1016/j.bbadis.2014.04.030

278. den Brok MH, Raaijmakers TK, Collado-Camps E, Adema GJ. Lipid Droplets as Immune Modulators in Myeloid Cells. *Trends Immunol*. 2018;39(5):380-392. doi:10.1016/j.it.2018.01.012

279. Hara Y, Miura S, Komoto S, et al. Exposure to fatty acids modulates interferon production by intraepithelial lymphocytes. *Immunol Lett*. 2003;86(2):139-148. doi:10.1016/S0165-2478(03)00007-5

280. Zucker SN, Fink EE, Bagati A, et al. Nrf2 amplifies oxidative stress via induction of Klf9. *Mol Cell*. 2014;53(6):916-928. doi:10.1016/j.molcel.2014.01.033

281. Ge T, Yang J, Zhou S, Wang Y, Li Y, Tong X. The Role of the Pentose Phosphate Pathway in Diabetes and Cancer. *Front Endocrinol (Lausanne)*. 2020;11:365. doi:10.3389/fendo.2020.00365

282. Ohradanova-Repic A, Ghaemmaghami AM, Carmo AM, et al. The Metabolic Signature of Macrophage Responses. *Front Immunol | www.frontiersin.org*. 2019;1:1462. doi:10.3389/fimmu.2019.01462

283. Yang Y, Wang H, Kouadir M, Song H, Shi F. Recent advances in the mechanisms of NLRP3 inflammasome activation and its inhibitors. *Cell Death Dis*. 2019;10(2). doi:10.1038/s41419-019-1413-8

284. Sanman LE, Qian Y, Eisele NA, et al. Disruption of glycolytic flux is a signal for inflammasome signaling and pyroptotic cell death. *Elife*. 2016;5(MARCH2016). doi:10.7554/eLife.13663

285. Kraan GPB, Dullaart RPF, Pratt JJ, Wolthers BG, Drayer NM, De Bruin R. *The Daily Cortisol Production Reinvestigated in Healthy Men. The Serum and Urinary Cortisol Production Rates Are Not Significantly Different**. Vol 83.; 1998. https://academic.oup.com/jcem/article/83/4/1247/2865411.

286. Conway-Campbell BL, Sarabdjitsingh # RA, Mckenna MA, et al. Glucocorticoid Ultradian Rhythmicity Directs Cyclical Gene Pulsing of the Clock Gene Period 1 in Rat Hippocampus Europe PMC Funders Group. *J Neuroendocr*. 2010;22(10):1093-1100. doi:10.1111/j.1365-2826.2010.02051.x

287. Sarabdjitsingh RA, Isenia S, Polman A, et al. Disrupted Corticosterone Pulsatile Patterns Attenuate Responsiveness to Glucocorticoid Signaling in Rat Brain. *Endocrinology*. 2010;151:1177-1186. doi:10.1210/en.2009-1119

288. Frøland Steindal IA, Whitmore D. Circadian clocks in fish-what have we learned so far? *Biology (Basel)*. 2019;8(1). doi:10.3390/biology8010017

289. Chan LY, Mugler CF, Heinrich S, Vallotton P, Weis K. Non-invasive measurement of mRNA decay reveals translation initiation as the major determinant of mRNA stability. Hinnebusch AG, Manley JL, Parker R, eds. *Elife*. 2018;7:e32536. doi:10.7554/eLife.32536

290. Baudrimont A, Voegeli S, Calero Viloria E, et al. Multiplexed gene control reveals rapid mRNA turnover. 2017. http://advances.sciencemag.org/. Accessed August 19, 2021.

291. Frank MG, Watkins LR, Maier SF. The permissive role of glucocorticoids in neuroinflammatory priming: Mechanisms and insights. *Curr Opin Endocrinol Diabetes Obes*. 2015;22(4):300-305. doi:10.1097/MED.0000000000000168

292. Knoedler JR, Sáenz de Miera C, Subramani A, Denver RJ. An Intact Krüppel-like factor 9 Gene Is Required for Acute Liver Period 1 mRNA Response to Restraint Stress. *Endocrinology*. 2021;162(9). doi:10.1210/endocr/bqab083

293. Zhang D, Zhang X-L, Michel FJ, Blum JL, Simmen FA, Simmen RCM. *Direct Interaction of the Krü Ppel-like Family (KLF) Member, BTEB1, and PR Mediates Progesterone-Responsive Gene Expression in Endometrial Epithelial Cells*.; 2002. https://academic.oup.com/endo/article/143/1/62/2988947.

294. Zhang XL, Zhang D, Michel FJ, Blum JL, Simmen FA, Simmen RCM. Selective interactions of Krüppel-like factor 9/basic transcription element-binding protein with progesterone receptor isoforms A and B determine transcriptional activity of progesterone-responsive genes in endometrial epithelial cells. *J Biol Chem*. 2003;278(24):21474-21482. doi:10.1074/jbc.M212098200

295. Johnson TA, Azvan R, Chereji V, et al. Conventional and pioneer modes of glucocorticoid receptor interaction with enhancer chromatin in vivo. *Nucleic Acids Res*. 2018;46(1):203-214. doi:10.1093/nar/gkx1044

296. Ewald ER, Wand GS, Seifuddin F, et al. Alterations in DNA methylation of Fkbp5 as a determinant of blood-brain correlation of glucocorticoid exposure. *Psychoneuroendocrinology*. 2014;44:112-122. doi:10.1016/j.psyneuen.2014.03.003

297. Lee RS, Tamashiro KLK, Yang X, et al. A measure of glucocorticoid load provided by DNA methylation of Fkbp5 in mice. *Psychopharmacology (Berl)*. 2011;218(1):303-312. doi:10.1007/s00213-011-2307-3

298. Häusl AS, Brix LM, Hartmann J, et al. The co-chaperone Fkbp5 shapes the acute stress response in the paraventricular nucleus of the hypothalamus of male mice. *Mol Psychiatry*. 2021. doi:10.1038/s41380-021-01044-x

299. Walker SE, Zanoletti O, Guillot de Suduiraut I, Sandi C. Constitutive differences in glucocorticoid responsiveness to stress are related to variation in aggression and anxiety-related behaviors. *Psychoneuroendocrinology*. 2017;84:1-10. doi:10.1016/j.psyneuen.2017.06.011

300. Doi M, Hirayama J, Sassone-Corsi P. Circadian Regulator CLOCK Is a Histone Acetyltransferase. *Cell*. 2006;125(3):497-508. doi:10.1016/j.cell.2006.03.033

301. Karmodiya K, Krebs AR, Oulad-Abdelghani M, Kimura H, Tora L. H3K9 and H3K14 acetylation co-occur at many gene regulatory elements, while H3K14ac marks a subset of inactive inducible promoters in mouse embryonic stem cells. *BMC Genomics*. 2012;13(1):424. doi:10.1186/1471-2164-13-424

302. Besnard A, Langberg T, Levinson S, David Leonardo E, Boldrini M, Sahay Correspondence A. Targeting Kruppel-like Factor 9 in Excitatory Neurons Protects against Chronic Stress-Induced Impairments in Dendritic Spines and Fear Responses. *Cell Rep*. 2018;23:3183-3196. doi:10.1016/j.celrep.2018.05.040

303. Scharf SH, Liebl C, Binder EB, Schmidt M V, Müller MB. Expression and regulation of the Fkbp5 gene in the adult mouse brain. *PLoS One*. 2011;6(2). doi:10.1371/journal.pone.0016883

304. Mathieson T, Franken H, Kosinski J, et al. Systematic analysis of protein turnover in primary cells. doi:10.1038/s41467-018-03106-1

305. Sandoval PC, Slentz DH, Pisitkun T, Saeed F, Hoffert JD, Knepper MA. Proteome-wide measurement of protein half-lives and translation rates in vasopressin-sensitive collecting duct cells. *J Am Soc Nephrol*. 2013;24(11):1793-1805. doi:10.1681/ASN.2013030279

306. Bulynko YA, O'Malley BW. Nuclear Receptor Coactivators: Structural and Functional Biochemistry. *Biochemistry*. 2011;50(3):313-328. doi:10.1021/bi101762x

307. Lee DY, Kim E, Choi MH. Technical and clinical aspects of cortisol as a biochemical marker of chronic stress. *BMB Rep*. 2015;48(4):209-216. doi:10.5483/BMBRep.2015.48.4.275

308. Thisse B, Heyer V, Lux A, et al. Spatial and temporal expression of the zebrafish genome by large-scale in situ hybridization screening. *Methods Cell Biol*. 2004;2004(77):505-519. doi:10.1016/s0091-679x(04)77027-2

309. Vandevyver S, Dejager L, Libert C. On the Trail of the Glucocorticoid Receptor: Into the Nucleus and Back. *Traffic*. 2012;13(3):364-374. doi:10.1111/j.1600-0854.2011.01288.x

310. Balsevich G, Häusl AS, Meyer CW, et al. Stress-responsive FKBP51 regulates AKT2-AS160 signaling and metabolic function. *Nat Commun*. 2017;8(1). doi:10.1038/s41467-017-01783-y

311. Kirschke E, Goswami D, Southworth D, Griffin PR, Agard DA. Glucocorticoid receptor function regulated by coordinated action of the Hsp90 and Hsp70 chaperone cycles. *Cell*. 2014;157(7):1685-1697. doi:10.1016/j.cell.2014.04.038

312. Denver RJ, Knoedler JR, Ávila-Mendoza J, Subramani A. The Paralogous Krüppel-like Factors 9 and 13 Regulate the Mammalian Cellular Circadian Clock Output Gene Dbp. *J Biol Rhythms*. 2020;35(3):257-274. doi:10.1177/0748730420913205

313. Rein T. FK506 binding protein 51 integrates pathways of adaptation: FKBP51 shapes the reactivity to environmental change. *BioEssays*. 2016;38(9):894-902. doi:10.1002/bies.201600050

314. Gassen NC, Fries GR, Zannas AS, et al. Chaperoning epigenetics: FKBP51 decreases the activity of DNMT1 and mediates epigenetic effects of the antidepressant paroxetine. *Sci Signal*. 2015;8(404):1-13. doi:10.1126/scisignal.aac7695

315. Gassen NC, Hartmann J, Zschocke J, et al. Association of FKBP51 with Priming of Autophagy Pathways and Mediation of Antidepressant Treatment Response: Evidence in Cells, Mice, and Humans. *PLOS Med*. 2014;11(11):e1001755. https://doi.org/10.1371/journal.pmed.1001755.

316. Ruiz-Estevez M, Staats J, Paatela E, Kobayashi H, Asakura A, Kikyo N. Promotion of Myoblast Differentiation by Fkbp5 via Cdk4 Isomerization. *CellReports*. 2018;25:2537-2551.e8. doi:10.1016/j.celrep.2018.11.006

317. Hanes SD. Prolyl isomerases in gene transcription. *Biochim Biophys Acta - Gen Subj*. 2015;1850(10):2017-2034. doi:10.1016/j.bbagen.2014.10.028

318. Lu KP, Finn G, Lee TH, Nicholson LK. Prolyl cis-trans isomerization as a molecular timer. *Nat Chem Biol*. 2007;3(10):619-629. doi:10.1038/nchembio.2007.35

319. Taipale M, Jarosz DF, Lindquist S. HSP90 at the hub of protein homeostasis: Emerging mechanistic insights. *Nat Rev Mol Cell Biol*. 2010;11(7):515-528. doi:10.1038/nrm2918

320. Sidibeh CO, Pereira MJ, Abalo XM, et al. FKBP5 expression in human adipose tissue: potential role in glucose and lipid metabolism, adipogenesis and type 2 diabetes. *Endocrine*. 2018;62(1):116-128. doi:10.1007/s12020-018-1674-5

321. Peña E, Caixàs A, Arenas C, et al. Role of the FKBP5 polymorphism rs1360780, age, sex, and type of surgery in weight loss after bariatric surgery: a follow-up study. *Surg Obes Relat Dis*. 2020;16(4):581-589. doi:10.1016/j.soard.2019.12.002

322. Touma C, Gassen NC, Herrmann L, et al. FK506 binding protein 5 shapes stress responsiveness: Modulation of neuroendocrine reactivity and coping behavior. *Biol Psychiatry*. 2011;70(10):928-936. doi:10.1016/j.biopsych.2011.07.023

323. JC OL, Zhang B, Koren J, Blair L, CA D. The Role of FKBP5 in Mood Disorders: Action of FKBP5 on Steroid Hormone Receptors Leads to Questions About its Evolutionary Importance. *CNS Neurol Disord - Drug Targets*. 2013;999(999):11-12. doi:10.2174/187152731131200121

324. Tu BP, Mohler RE, Liu JC, et al. Cyclic changes in metabolic state during the life of a yeast cell. *Proc Natl Acad Sci U S A*. 2007;104(43):16886-16891. doi:10.1073/pnas.0708365104

325. Chen Z, Odstrcil EA, Tu BP, McKnight SL. Restriction of DNA replication to the reductive phase of the metabolic cycle protects genome integrity. *Science (80- )*. 2007;316(5833):1916-1919. doi:10.1126/science.1140958

326. Slavov N, Airoldi EM, Van Oudenaarden A, Botstein D. A conserved cell growth cycle can account for the environmental stress responses of divergent eukaryotes. *Mol Biol Cell*. 2012;23(10):1986-1997. doi:10.1091/mbc.E11-11-0961

327. Wang J, Liu W, Uno T, Tonozuka H, Mitsui K, Tsurugi K. *Cellular Stress Responses Oscillate in Synchronization with the Ultradian Oscillation of Energy Metabolism in the Yeast Saccharomyces Cerevisiae*. doi:10.1111/j.1574-6968.2000.tb09198.x

328. Janes KA, Wang CC, Holmberg KJ, Cabral K, Brugge JS. Identifying single-cell molecular programs by stochastic profiling. *Nat Methods*. 2010;7(4):311-317. doi:10.1038/nmeth.1442

329. Murray JI, Whitfield ML, Trinklein ND, Myers RM, Brown PO, Botstein D. Diverse and Specific Gene Expression Responses to Stresses in Cultured Human Cells. *Mol Biol Cell*. 2004;15(5):2361-2374. doi:10.1091/mbc.E03-11-0799

330. Özbudak EM, Tassy O, Pourquié O. Spatiotemporal compartmentalization of key physiological processes during muscle precursor differentiation. *Proc Natl Acad Sci U S A*. 2010;107(9):4224-4229. doi:10.1073/pnas.0909375107

www.nature.com/scientificreports

SCIENTIFIC REPORTS
nature research



OPEN

# Klf9 is a key feedforward regulator of the transcriptomic response to glucocorticoid receptor activity

Ian Gans[1,2], Ellen I. Hartig[1], Shusen Zhu[1], Andrea R. Tilden[3], Lucie N. Hutchins[1], Nathaniel J. Maki[1], Joel H. Graber[1] & James A. Coffman[1,2]✉

**The zebrafish has recently emerged as a model system for investigating the developmental roles of glucocorticoid signaling and the mechanisms underlying glucocorticoid-induced developmental programming. To assess the role of the Glucocorticoid Receptor (GR) in such programming, we used CRISPR-Cas9 to produce a new frameshift mutation, GR$^{369-}$, which eliminates all potential in-frame initiation codons upstream of the DNA binding domain. Using RNA-seq to ask how this mutation affects the larval transcriptome under both normal conditions and with chronic cortisol treatment, we find that GR mediates most of the effects of the treatment, and paradoxically, that the transcriptome of cortisol-treated larvae is more like that of larvae lacking a GR than that of larvae with a GR, suggesting that the cortisol-treated larvae develop GR resistance. The one transcriptional regulator that was both underexpressed in GR$^{369-}$ larvae and consistently overexpressed in cortisol-treated larvae was *klf9*. We therefore used CRISPR-Cas9-mediated mutation of *klf9* and RNA-seq to assess Klf9-dependent gene expression in both normal and cortisol-treated larvae. Our results indicate that Klf9 contributes significantly to the transcriptomic response to chronic cortisol exposure, mediating the upregulation of proinflammatory genes that we reported previously.**

The vertebrate hypothalamus–pituitary–adrenal (HPA) axis orchestrates physiological, behavioral, and metabolic adjustments required for homeostasis, by dynamically regulating production and secretion of adrenal steroids known as glucocorticoids. In humans the primary glucocorticoid is cortisol, the biological activity of which is mediated by two regulatory proteins in the nuclear receptor family, the ubiquitous glucocorticoid receptor (GR) and the more tissue-restricted mineralocorticoid receptor (MR). The GR binds cortisol less avidly than the MR and is thus more dynamically regulated over the normal physiological range of cortisol fluctuations[1,2]. The GR and MR function both as transcription factors and as non-nuclear signaling proteins, including in the central nervous system where both proteins are highly expressed[1–5]. Given that the GR is more widely expressed and more dynamically regulated by cortisol, it is generally thought to be the principal mediator of cortisol-induced genomic responses to circadian rhythms and acute stress[5]. An important question for understanding GR function is what downstream transcriptional regulatory genes does it regulate, and to what end? Answering this question is not only important for understanding the physiological function and regulation of the GR, but also for deciphering the gene regulatory networks that orchestrate adaptive developmental programming in response to chronic glucocorticoid exposure such as occurs with chronic early life stress[6].

The zebrafish has recently emerged as a model system well-suited to investigating the developmental functions of glucocorticoid signaling and mechanisms underlying stress-induced developmental programming[7–11]. As in humans, the endogenous glucocorticoid in zebrafish is cortisol, which is produced by the interrenal gland, the functional equivalent of the mammalian adrenal. Thus, the zebrafish homolog of the HPA axis is the Hypothalamus-Pituitary-Interrenal (HPI) axis. Eight different zebrafish GR mutants have been described in the literature to date[12–15]. The first of these, *gr*$^{s357}$, is a missense mutation that substitutes a cysteine for an arginine in the DNA binding domain, abolishing GR DNA binding activity[12]. The other mutations, all produced by targeted mutagenesis using CRISPR-Cas9 or TALEN technology, consist of frameshift indels in exons 2 and 5[13–15], which respectively encode domains N- and C-terminal to the DNA binding domain (see Fig. 1). All of the zebrafish GR mutants manifest behavioral defects but are viable as homozygotes.

[1]MDI Biological Laboratory, Salisbury Cove, ME, USA. [2]University of Maine Graduate School of Biomedical Sciences and Engineering, Orono, ME, USA. [3]Colby College, Waterville, ME, USA. ✉email: jcoffman@mdibl.org

We showed previously that zebrafish larvae treated chronically with 1 μM cortisol upregulate proinflammatory genes and give rise to adults that maintain chronically elevated cortisol and dysregulated expression of those same genes[9]. Thus in zebrafish, chronic cortisol exposure during early development results in persistent, long-term dysregulation of the HPI axis and gene expression downstream thereof, a 'developmental programming' effect similar to what has been observed with early life stress in mammals[9,11]. To ask whether and to what extent that developmental programming depends on the GR, we used CRISPR-Cas9 technology to mutate the GR-encoding gene *nr3c1*. Here we report a new loss-of-function mutation, consisting of a deletion in *nr3c1* exon 3 that results in a frameshift and premature stop codon immediately upstream of the DNA binding domain which eliminates GR activity as a transcriptional activator. Using this mutant line, we performed an RNA-seq experiment to identify genes regulated by the GR and to parse GR-dependent and GR-independent effects of chronic cortisol treatment on larval gene expression. We found that most of the transcriptomic effects of the chronic cortisol treatment are mediated by the GR and identified *klf9*, which encodes a ubiquitously expressed[16] member of the krüppel-like family of zinc finger transcription factors, as the one regulatory gene consistently upregulated by the GR under both normal conditions and in response to chronic cortisol treatment. We therefore used CRISPR-Cas9 to mutate *klf9* and RNA-seq to interrogate its role with respect to the transcriptomic response to chronic cortisol treatment. Our results indicate that *klf9* mediates the cortisol-induced upregulation of pro-inflammatory genes that we reported previously[9], and suggest that *klf9* is a core feedforward regulator of the transcriptional response to glucocorticoid signaling.

## Results

**A frameshift deletion introduced into exon 3 of zebrafish *nr3c1* eliminates GR transcriptional function.** To mutate the GR, we employed CRISPR-Cas9 using a guide RNA (gRNA) that targets *nr3c1* exon 3 (the second coding exon; Fig. 1A). This resulted in a 20 base deletion and frameshift that introduces sixteen new amino acids after E369, followed by a premature translational stop immediately upstream of the DNA binding domain (Fig. 1B,C), a mutation hereafter referred to as $GR^{369-}$. F0 males with $GR^{369-}$ in the germline were identified and outbred to wild-type (AB) females, and siblings of that cross were mated to generate F2s, from which homozygous males and females were identified. Homozygous $GR^{369-}$ males crossed with wild-type females produced viable embryos, whereas most homozygous $GR^{369-}$ females crossed with either mutant or wild-type males produced embryos that all died within 24 h of fertilization. However, one produced 10 viable offspring that were raised to adulthood, suggesting that maternal GR is not essential for early development. However, earlier studies using morpholino antisense-mediated knockdown of the GR did suggest that maternal GR is essential for early development[17,18], so it is also possible that the mutants but not the morphants are able to compensate for loss of maternal GR as has been documented for other genes[19]. When inbred these F3 fish produced no viable offspring. However, females homozygous for $GR^{369-}$ following another generation of outcrossing produced variable numbers of viable offspring. These results suggest that loss of GR function may compromise egg quality, albeit in a context-dependent way.

The zebrafish *nr3c1* transcript has multiple AUG codons that could potentially initiate translation to allow production of alternative N-terminal isoforms from a single mRNA (Fig. 1C,D; Fig. S1), as occurs with human *nr3c1*[20] and some other transcription factors (e.g.[21]). One potential in-frame initiation codon upstream of the DNA binding domain lies downstream of all previously reported frameshift mutations in exon 2[13–15] (Fig. 1C,D), suggesting that *nr3c1* mRNA transcribed in those mutants might still allow translation of an N-terminally truncated GR isoform with an intact DNA binding domain. To assess the transcriptional activity of different N-terminal isoforms we injected homozygous $GR^{369-}$ zygotes with mRNA encoding full-length GR (FL) or GRs lacking the first 310 or 369 amino acids of the full-length GR (N310 and N369, Fig. 1D). The N310 mRNA corresponds to the shortest translation initiation variant with a DNA binding domain potentially available to the previously described exon 2 mutants[13–15], whereas the N369 corresponds to what is available in $GR^{369-}$ mutants. The embryos were collected at 6 h post fertilization (hpf) and quantitative reverse transcription and polymerase chain reaction (qRT-PCR) was used to measure the expression of the GR-target gene *fkbp5*. Unlike uninjected embryos or embryos injected with N369 or a *Xenopus* control mRNA, embryos injected with N310 mRNA upregulated *fkbp5*, indicating that N310 retains activity as a transcription factor (Fig. 1E). Zygotes injected with mRNA encoding full length GR showed ~ 50-fold stronger upregulation of *fkbp5* than those injected with N310 (Fig. 1E). We conclude that the previously described *nr3c1* exon 2 frameshift mutations[13–15] strongly abrogate but do not abolish the potential to translate a GR with transcriptional function (although for one of those mutants it was shown that *nr3c1* transcript levels were also significantly reduced, likely through nonsense-mediated decay[13]), whereas $GR^{369-}$ eliminates potential for translating a transcriptionally active GR.

**RNA-seq shows that the transcriptomic response to chronic cortisol treatment is largely GR-dependent but converges with that caused by loss of GR function.** To identify GR-dependent zygotic gene expression and assess the extent to which the GR contributes to the transcriptional effects of chronic cortisol exposure[9], we used a visual background adaptation (VBA) assay to identify homozygous $GR^{369-}$ larvae from a heterozygous cross. This assay makes use of the fact that larval melanophores mount a camouflaging response to changes in background, dispersing when larvae are transferred from the dark to a light background[12]. This response is mediated by the GR, so larvae lacking a functional GR can be identified as those in which melanophores fail to respond, remaining clustered in a dark patch after transfer to a light background. At four days post fertilization (dpf) we used the VBA screen to separate homozygous $GR^{369-}$ (VBA-) larvae from their heterozygous and wild type (VBA +) siblings developed under normal (vehicle-treated) conditions or in medium supplemented with 1 μM cortisol (Fig. 2A). In support of the screen's validity, the number of VBA- larvae was ~ 1/4 of the total number of larvae, the expected Mendelian ratio for homozygous mutants. Moreover, in a pilot

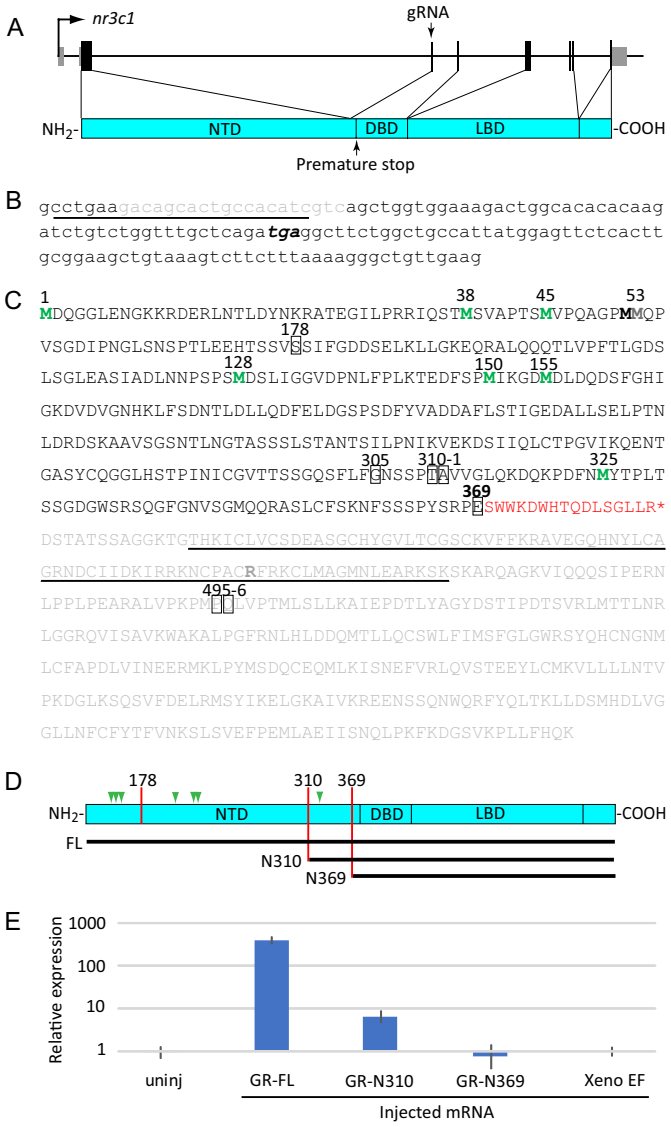


**Figure 1.** A new CRISPR-Cas9-induced mutation of the zebrafish GR. (**A**) Schematic of the *nr3c1* gene and encoded GR showing location of the targeted sequence and resulting premature stop codon with respect to the protein domains: N-terminal domain (NTD), DNA binding domain (DBD), and ligand binding domain (LBD). (**B**) Nucleotide sequence of *nr3c1* exon 3, showing sequence targeted by the gRNA (underlined), the 20 base deletion resulting from injection of that gRNA and Cas9 mRNA (gray), and the resulting premature stop codon (bold italic). (**C**) Predicted amino acid sequence of the full-length zebrafish GR, plus the extra amino acids introduced by the frameshift shown in (**B**) (red font). The sequence eliminated by the premature stop is shown in gray, with the DBD underlined. Methionines corresponding to potential alternative initiation sites are shown in green. The positions of all reported frameshift mutations (including that reported here, E369) are boxed. The arginine that is changed to a cysteine in the $gr^{s357}$ mutation is shown in orange. (**D**) Schematic of the GR showing locations of the two previously reported exon 2 frameshift mutations resulting in truncations at amino acids 178 and 310, and the one in exon 3 reported here truncating at amino acid 369, and residues included in N310 and N369 mRNA constructs produced for microinjection. (**E**) Relative expression of *fkbp5* in 6 hpf homozygous $GR^{369-}$ embryos, either uninjected or injected with mRNA encoding full-length GR (GR-FL), N-terminally truncated GR isoforms (GR-N310 and GR-N369), or a nonspecific control mRNA encoding *Xenopus* elongation factor 1α (Xeno EF).

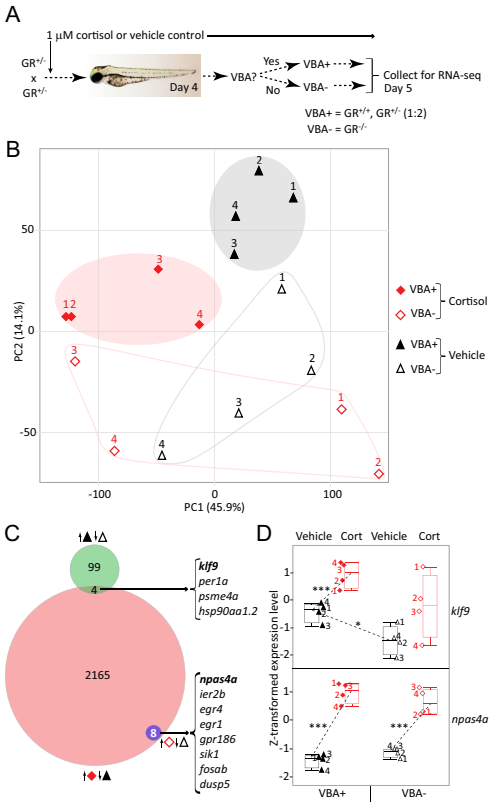


**Figure 2.** RNA-seq identifies GR-dependent and GR-independent genes and effects of chronic cortisol treatment. (**A**) Diagram of experimental design using Visual Background Adaptation (VBA) selection. (**B**) Principal component plot of the RNA-seq data, showing the location of each replicate sample with respect to the first two principal components. Cortisol-treated samples are shown in red, vehicle-treated controls in black. VBA+ samples (containing at least one functional GR allele) are filled shapes, VBA- samples are empty shapes. (**C**) Venn diagram showing numbers of genes upregulated in each of the indicated comparisons (keyed as in (**A**)): VBA+ vs. VBA- (vehicle-treated controls); cortisol-treated vs. vehicle-treated VBA+; and cortisol-treated vs. vehicle treated VBA-. Upregulated genes in common respectively between the first two and the last two comparisons are listed on the right. (**D**) Box plots of Z-transformed expression levels of *klf9* and *npas4a* obtained from the RNA-seq data. Sample numbers correspond to those in (**B**). Asterisks indicate significant differential expression (adjusted p values): ***<.0001; *<.05.

experiments high resolution melt analysis (HRMA) showed that the screen effectively segregated homozygous mutants from mixed heterozygotes and wild-type larvae at 4 dpf (data not shown), and qRT-PCR showed that the VBA- larvae underexpress *nr3c1* (Fig. S2A), likely owing to nonsense-mediated decay. The larvae developed for another day under the same conditions (vehicle- or cortisol-treated), at which time four biological replicates of each sample were collected for RNA-seq (Fig. 2A).

A principal component analysis (PCA) of the RNA-seq data indicated that 60% of the variance in gene expression among samples is captured in the first two PCs, which respectively correlate with the two treatments (chronic cortisol and absence of a GR, respectively accounting for 46% and 14% of the variance; Fig. 2B). The VBA- samples again underexpressed *nr3c1*, indicating that the VBA screen was effective in identifying homozygous mutants (Fig. S2B). The eight VBA+ (i.e. mixed wild type and heterozygous mutant) samples cluster according to whether they were treated with cortisol, with the two clusters (cortisol-treated and vehicle-treated controls) segregating toward opposite poles of PC1. This is not the case in the VBA- (i.e. homozygous $GR^{369-}$) fish, the four cortisol-treated replicates of which are widely dispersed along PC1. This indicates that the global effect of the cortisol treatment captured in PC1 is GR-dependent and suggests as well that gene expression is less constrained overall in larvae lacking a GR. PC2 correlates with the presence and absence of a GR (VBA+

vs. VBA− respectively). Interestingly, along PC2 chronic cortisol treatment displaces the VBA+ transcriptome toward the VBA- pole, suggesting that the cortisol-treated fish adapt to the exposure by developing GR resistance.

The regulatory roles of the GR were further assessed by analyzing differential gene expression (DGE) between pairs of treatments, using an adjusted *p* value (false-discovery) threshold of 0.05 as the criterion for differential expression. Comparison of VBA+ and VBA- larvae identified 405 genes affected by loss of the GR in 5-dpf larvae, 103 of which are underexpressed (Fig. 2C) and 302 of which are overexpressed in VBA- larvae compared to their VBA+ counterparts (Fig. S3A). Gene ontology (GO) analysis shows that the underexpressed genes (i.e. genes normally upregulated by the GR) are involved in sugar metabolism and response to heat, whereas the overexpressed genes (i.e. genes that are normally downregulated via the GR) are involved in basement membrane organization, epidermis development, cell adhesion, locomotion, and growth (Figs. S3 and S4; Table S1).

A DGE analysis comparing cortisol-treated VBA+ fish to their vehicle-treated VBA+ counterparts showed that in cortisol-treated larvae with a functional GR, 4,298 genes were differentially expressed (Fig. S3B), 2,177 of which were upregulated (Fig. 2C) and 2,121 of which were downregulated. GO enrichment analysis of the upregulated genes identified biological processes related to nervous system development and function as well as cell adhesion, locomotion, and growth, whereas the downregulated genes were largely involved in protein synthesis and metabolism (Figs. S5, S6; Table S2). Interestingly, the transcriptome of cortisol-treated VBA+ larvae overlapped more with that of vehicle-treated VBA- larvae than with that of vehicle treated VBA+ larvae (Fig. S3C, Table S3), and accordingly, many of the biological processes affected by the absence of GR function in VBA- larvae were similarly affected by the chronic cortisol-treatment in VBA+ larvae (Fig. S8). This again suggests that the latter larvae develop a GR resistant phenotype. This resistance is probably not associated with any effect on levels of the GR or MR in the cortisol-treated larvae, as neither *nr3c1* nor *nr3c2* displays significant differential expression in response to the cortisol treatment.

We reasoned that some of the transcriptomic effects of the cortisol treatment might stem from GR-induced upregulation of a GR target gene that functions as a feedforward transcriptional regulator of GR signaling. To the extent that basal expression of such a gene depends on the presence of a GR it might be expected to be underexpressed in VBA- larvae (which lack GR function) but upregulated in VBA+ larvae in response to chronic cortisol (i.e., opposite of the predominant trend noted above). Of the 2177 genes upregulated in cortisol-treated VBA+ larvae only four were basally underexpressed in VBA- larvae (Fig. 2C), two of which encode transcription factors: *klf9* and *per1a*. Of these, only *klf9* was also found to be significantly upregulated in our previous RNA-seq analysis of the effects of chronic cortisol treatment in wild-type fish (Fig. S3C), being one of the most highly upregulated transcription factors[9]. A plot comparing *klf9* expression in each of the conditions reveals that the GR contributes to both its normal developmental expression and its upregulation in response to the cortisol treatment (Fig. 2D), which was confirmed by qRT-PCR in another experiment (Fig. S2C). However, the plot also suggests that cortisol affects *klf9* in a GR-independent fashion, albeit more variably, as indicated by the range of expression levels in the cortisol-treated VBA- samples shown in Fig. 2D, which correlate with the spread of the cortisol-treated VBA- samples along PC1 shown in Fig. 2B.

In contrast to the situation in VBA+ larvae, only 8 genes were differentially expressed in cortisol-treated VBA- larvae compared to their vehicle-treated VBA- siblings, all of them upregulated (Fig. 2C, Fig. S3D). The genes included the immediate early genes (IEGs) *npas4a*, *egr1*, *egr4*, *fosab*, and *ier2b* (Fig. 2C, Fig. S9). The GR-independence of their cortisol-induced upregulation is clearly seen in a plot of the expression levels of the most highly upregulated gene of this set, *npas4a* (Fig. 2D), a neuronal IEG that along with the other IEGs was also found to be upregulated in our previous RNA-seq analysis of cortisol-treated larvae (Fig. S3D)[9]. This indicates that the GR mediates nearly all the transcriptomic effects of chronically elevated cortisol, except for a small subset that appears to relate to neuronal activity.

**A frameshift deletion introduced into exon 1 of zebrafish *klf9* eliminates the DNA binding domain and significantly reduces expression of the mature transcript.** The fact that *klf9* was the transcriptional regulatory gene most consistently found to be upregulated by chronic cortisol exposure in a GR-dependent way suggested that it may contribute to the transcriptomic effects of the exposure. To test this, we mutated *klf9* using CRISPR-Cas9 with a gRNA that targets exon 1 (Fig. 3A,B). This resulted in a frameshift mutation upstream of the DNA binding domain (Fig. 3A,B), producing a transcript encoding a truncated protein predicted to lack function as a transcription factor. *Klf9* loss-of-function mutations are viable in mice[22] and similarly, the *klf9* mutant fish were viable and fertile when bred to homozygosity, although mutant embryos survive at a lower rate than wild type (data not shown).

To ask how the mutation affects *klf9* expression we used qRT-PCR to compare *klf9* transcript levels in wild type and *klf9* homozygous mutant (hereafter referred to as *klf9*$^{-/-}$) larvae under both normal conditions and in response to chronic cortisol treatment. This provided further confirmation that the cortisol treatment leads to upregulation of *klf9* and revealed that *klf9* mRNA levels are significantly reduced in the *klf9*$^{-/-}$ larvae, probably due to nonsense-mediated decay triggered by the premature stop codon (Fig. 3C). In support of this possibility, there was no significant effect on *klf9* pre-mRNA levels, measured by qRT-PCR of the intron (Fig. 3C). We conclude from these experiments that the frameshift mutation introduced into *klf9* exon 1 abrogates Klf9 function.

**RNA-seq shows that *klf9* is required for the pro-inflammatory transcriptomic effects of chronic cortisol treatment.** To identify Klf9 target genes and ask whether Klf9 contributes to the transcriptomic response to cortisol treatment we used RNA-seq to query gene expression in 5-dpf wild type and *klf9*$^{-/-}$ mutant larvae from sibling parents, developed both normally and in the presence of 1 µM cortisol. Samples were collected at the same time on day 5 post-fertilization as in the previous GR knockout experiment and processed similarly. However, PCA revealed the largest source of variance in this experiment was not due to genotype or

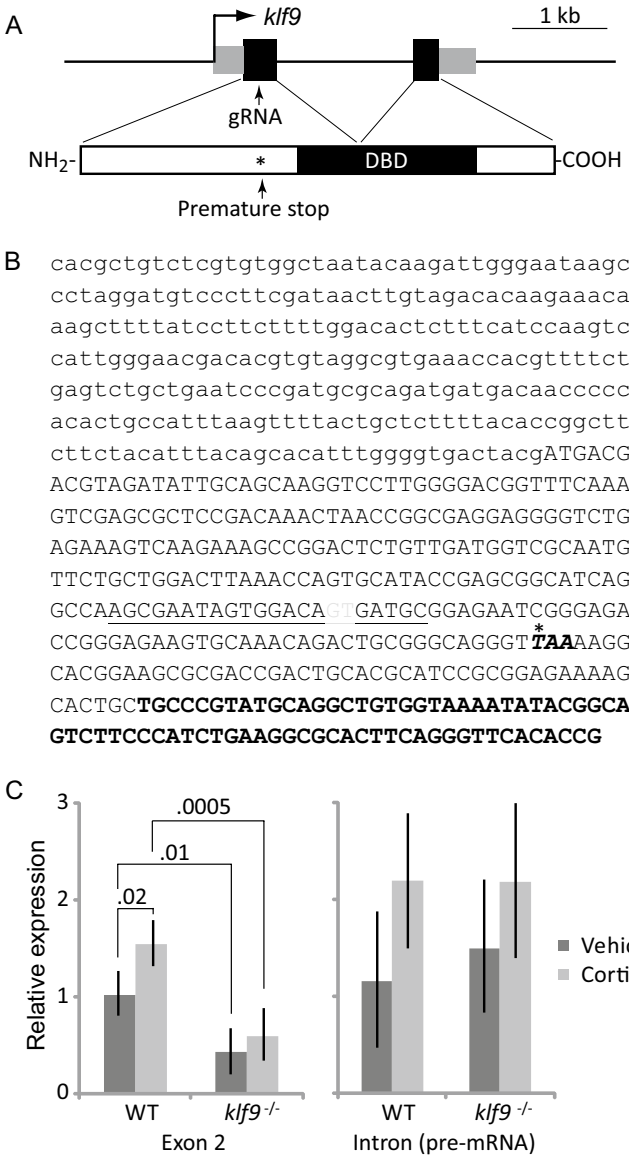


**Figure 3.** CRISPR-Cas9-mediated disruption of zebrafish *klf9*. (**A**) Schematic of the *klf9* locus and encoded protein showing location of the gRNA target in exon 1, which introduces a premature stop codon upstream of the DNA binding domain. (**B**) Sequence of *klf9* exon 1, with 5′ untranslated region in small case and coding sequence in upper case. The location of the 2 base pair deletion generated by CRISPR is shown in gray font; the gRNA target sequence is underlined; and the premature stop codon introduced by frameshift is noted with an asterisk. (**C**) Effect of chronic cortisol treatment and the frameshift mutation on relative levels of *klf9* mRNA and pre-mRNA, measured by qRT-PCR. The results show the averages and SEM of three biological replicates; significance values were obtained by ANOVA.

treatment, but rather the order in which the samples were collected and processed (Fig. S10A). GO analysis of genes correlated with the first principal component showed that the later samples (replicates 3 and 4) had

increased synaptic signaling and decreased translation (Table S4), suggestive of a physiological stress response (e.g. to the stress of capture). However, a further confound is that PC1 also correlates with preparation of the RNA in two batches on separate days, suggesting that it may also reflect technical variance in sample preparation (see Materials and Methods). Reassuringly, after normalizing for this variation the samples segregate along two principal components representing genotype and treatment (Fig. S10B). For subsequent DGE analysis we therefore treated the batch effect as a categorical covariate.

DGE analysis using a false-discovery rate of 0.05 identified 239 genes affected by loss of *klf9* function in vehicle-treated larvae, 100 of which were upregulated and 139 of which were downregulated. Gene ontology term enrichment analysis shows that the upregulated genes are largely involved in complement activation (e.g. *c3b*, *c3c*, *c4*, *cfb* ), glucose and carbohydrate metabolism (e.g. *pgm1*, *tpi1b*, and *pfkmb*), and nucleosome positioning (e.g., *h1fx*, *h1f0*, and *smarca5*; Fig. S11, Table S5). Genes downregulated in response to loss of *klf9* function are largely involved in sterol metabolism (e.g. *faxdc2*, *sqlea*, *tm7sf2*, *sc5d*, *cyp51*, *lss*, and *msmo1*; Fig. S12, Table S5). Interestingly, several of the processes associated with carbohydrate metabolism that we identified as being positively regulated by the GR are negatively regulated by *klf9* (Fig. S13).

To ask how loss of *kf9* function affects the transcriptomic response to cortisol treatment, we compared the response in wild-type embryos to that in *klf9*$^{-/-}$ larvae (Fig. 4A). Strikingly, with a false discovery threshold of 0.05 the major difference between the two responses was that ~ 70% (408) of the genes upregulated in by cortisol treatment in wild type embryos were not upregulated by the treatment in *klf9*$^{-/-}$ embryos, which instead upregulated a mostly different set of genes, albeit less strongly (Fig. 4A,B). This indicates that Klf9 is a key regulator of the transcriptomic response to cortisol. Of the 408 genes upregulated by the cortisol-treatment in a *klf9*-dependent way (Fig. 4A,B), about a quarter (91) were also identified in our previous study[9] as being significantly upregulated by chronic cortisol exposure (Table S6). Examples of the latter include *irg1l* and *marco* (Fig. 4C and Fig. S14), as well as *irg1*, *irf1a*, *ifi35*, *mpeg1.1*, *mpeg1.2*, *mxc*, *socs1a*, *socs3b*, *stat1b*, and *stat4* (Table S6). Gene ontology term enrichment analysis of the 408 genes upregulated by chronic cortisol treatment in wild-type but not *klf9*$^{-/-}$ embryos revealed significant enrichment for genes involved in defense and immunity (Fig. 4D, Table S7), the same biological processes that we previously found to be the most strongly affected by the chronic cortisol treatment[9], whereas these processes were not associated with either the 176 genes upregulated in both wild-type and *klf9*$^{-/-}$ embryos, or the 903 genes upregulated in *klf9*$^{-/-}$ embryos but not wild-type (Table S7). Notably the set of genes upregulated by cortisol in wild-type but not *klf9*$^{-/-}$ embryos included four interferon regulatory factors (*irf1a*, *irf8*, *irf9*, and *irf10*), two interleukins (*il1b* and *il34*), and four interleukin receptors (*il4r.1*, *il6r*, *il13ra1*, and *il20ra*). These results indicate that Klf9 contributes in a significant way to the pro-inflammatory gene expression induced by chronic cortisol exposure.

**Genes found to be consistently upregulated by chronic cortisol treatment in multiple RNA-seq experiments depend on *klf9* for that upregulation.** As a final analysis we assessed the overlap between the transcriptomic effects of chronic cortisol treatment across all our RNA-seq experiments with wild-type and VBA+ (mixed wild-type and heterozygous GR$^{369-}$) larvae, including the experiment published previously[9], in order to identify a set of high-confidence genes that consistently respond the cortisol treatment and then ask how loss of *klf9* function affects that response. To eliminate any technical artifacts emanating from the use of different parameters in the different analyses the sequence reads from all the experiments were reanalyzed from scratch using a common pipeline (see Materials and Methods). A PCA of the variance across all experiments produced several interesting observations. First, it showed that the effect of chronic cortisol treatment across all experiments was subtle, found only in PCs 4, 5, and 6 accounting for 14.3% of the total variance. PC5 captures a cortisol-treatment effect common to all three experiments (accounting for 2.77% of the total variance) and when plotted against PC4 clearly shows segregation of the cortisol-treated and control (vehicle-treated) samples (Fig. 5A). Gratifyingly, GO analysis of a single gene list ranked by upregulation along PC5 showed the same biological response to chronic cortisol as that which we reported previously[9], i.e. upregulation of processes related to defense, inflammation and immunity (Fig. 5B, Table S8). The fourth principal component, accounting for 8.95% of the total variance, shows a cortisol treatment effect in the two experiments reported here, but not in that which we reported previously[9] (Fig. 5A and Fig. S15). This suggests that PC4 represents cortisol-treatment effects that are dependent on the circadian light–dark cycle under which embryos in this study developed, which was absent in our previous study in which embryos developed in the dark[23] (see below, Discussion). The sixth PC (2.57%) is the complement of PC4, suggesting cortisol-induced effects that are only apparent in the larvae that were developed in the dark (Fig. S15).

The spread of the cortisol treatment effects across three principal components likely reflects differing biological responses to the treatment among different experiments. That the effects are somewhat different under total dark compared with light–dark cycles is not surprising given what is known about the interplay of GC signaling and the circadian clock[23–26]. Indeed GO analysis of PC2, which segregates our previously published experiment[9] from the two reported here (accounting for 18.5% of the variance), clearly shows that effects on circadian and light-responsive gene expression (Table S9). Additional sources of variance are less clear. The first PC, which segregates the wild-type samples in the last (*klf9*$^{-/-}$ vs. wild-type) experiment from the wild-type samples in our previous experiment as well as the VBA + samples described here (accounting for 37.6% of the variance, Fig. S15), is heavily loaded with genes involved in synaptic signaling and neurogenesis (Table S10) suggestive of differences in neurodevelopment and/or responsiveness to stress in those samples. The third PC (14.2% of the variance) segregates replicates 1 and 2 of the Klf9 experiment from all other samples, possibly reflecting the batch effect in sample preparation noted above.

Unsurprisingly given the large amount of gene expression variance across experimental samples unrelated to the cortisol treatment (i.e. noise), only 12 genes were found to be consistently upregulated by the cortisol

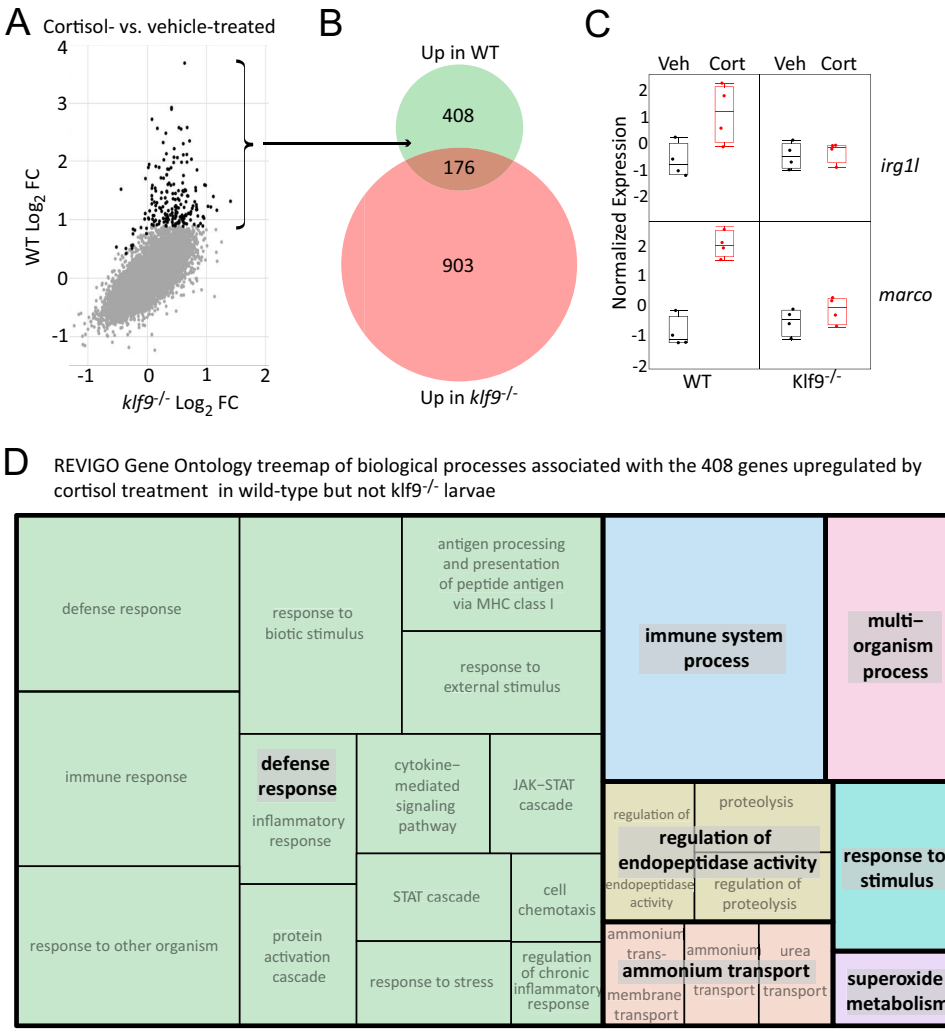


**Figure 4.** RNA-seq identifies *klf9*-dependent transcriptomic effects of chronic cortisol exposure. (**A**) Scatter plot comparing differential gene expression in response to chronic cortisol treatment in wild type (WT) and *klf9*$^{-/-}$ larvae. (**B**) Venn diagram comparing numbers of genes upregulated by cortisol treatment in wild type and *klf9*$^{-/-}$ larvae, and overlap. (**C**) Examples of two of the genes upregulated by chronic cortisol in a *klf9*-dependent fashion that were also identified in our previous analysis. (**D**) Treemap generated by REVIGO[57] (https://revigo.irb.hr/) of gene ontology biological process terms found by GOrilla[34] to be enriched in the set of 408 genes upregulated by chronic cortisol in a *klf9*-dependent way.

treatment in all the experiments with statistical significance (adjusted $p < 0.05$), whereas none were consistently downregulated in all experiments (Fig. 6A). The consistently upregulated set included *klf9*, the only gene in that set that encodes a transcription factor. We reasoned that many more genes are affected by the treatment, albeit not consistently with statistical significance owing to the abovementioned noise (see Discussion). This was borne out by plotting the estimated fold-change of the 149 genes that were upregulated by cortisol-treatment in at least two of the three experiments (Fig. 6B, Table S11), which also revealed that the upregulation of those genes is *klf9*-dependent. Furthermore, this plot shows that the cortisol treatment effect is stronger in the wild-type larvae than in the VBA+ (1:2 wild-type:heterozygous GR$^{+/-369-}$), suggesting haploinsufficiency of the GR for some of the effect. Query of this set for enrichment of GO biological process terms indicated chronic cortisol exposure upregulates genes associated with response to organic substance (including response to stress, defense response,

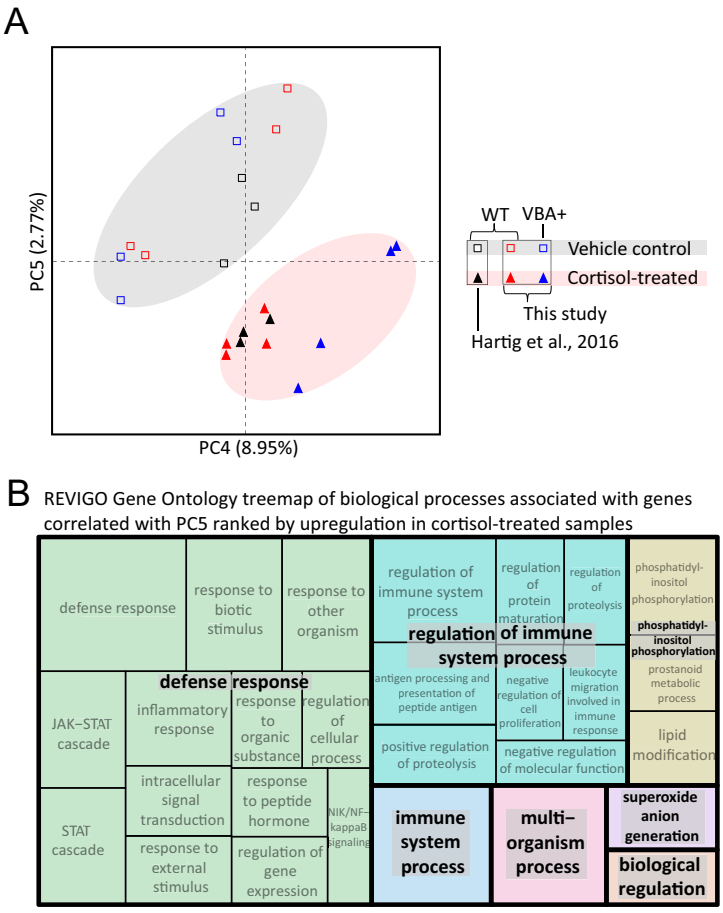


**Figure 5.** Combined analysis of three different RNA-seq datasets examining the transcriptomic effects of chronic cortisol exposure. (**A**) Principal component plot showing the location of each wild-type or VBA+ sample from all three RNA-seq experiments with respect to PCs 4 and 5. (**B**) Treemap generated by REVIGO[57] (https://revigo.irb.hr/) of GO biological process terms found by GOrilla[34] to be associated with PC5 ranked by upregulation in response to chronic cortisol treatment.

response to external biotic stimulus, and inflammatory response to wounding), similar to what we reported previously[9], and gluconeogenesis (Fig. 6C, Table S12).

Finally, we used HOMER motif enrichment analysis[27] to ask what transcription factor binding sites are enriched in flanking regions of the set of 149 genes upregulated by cortisol-treatment in at least two of the three experiments. The resulting set of motifs included sites for the various krüppel-like factors as well as the GR (Table S13). The most significantly enriched motif, the Klf14 binding motif RGKGGGCGKGGC, matches the Klf9 consensus motif in the JASPAR database[28,29] and would be expected to bind Klf9, which is in the same KLF subfamily as Klf14[30,31]. In contrast, HOMER analysis of the 408 genes identified as klf9-dependent in Fig. 4 recovered a somewhat different list of motifs that included binding sites for several immunoregulatory transcription factors (Table S13; note that there are 65 genes in common between the 408 identified in Fig. 4 and the 149 identified in Fig. 6), suggesting that the larger set includes more indirect targets of feedforward regulation downstream of Klf9. Consistent with this, the latter set of motifs includes sites for two immunoregulatory genes, *irf1* and *stat4* that are both consistently upregulated by chronic cortisol treatment (i.e. in the common list of 149 genes identified in Fig. 6) and dependent on *klf9* for that upregulation (i.e. in the list of 408 genes identified in Fig. 4). Altogether these results underscore the conclusion that *klf9* is a feedforward regulator of GR signaling that mediates the pro-inflammatory transcriptomic response to chronic cortisol exposure, likely involving both

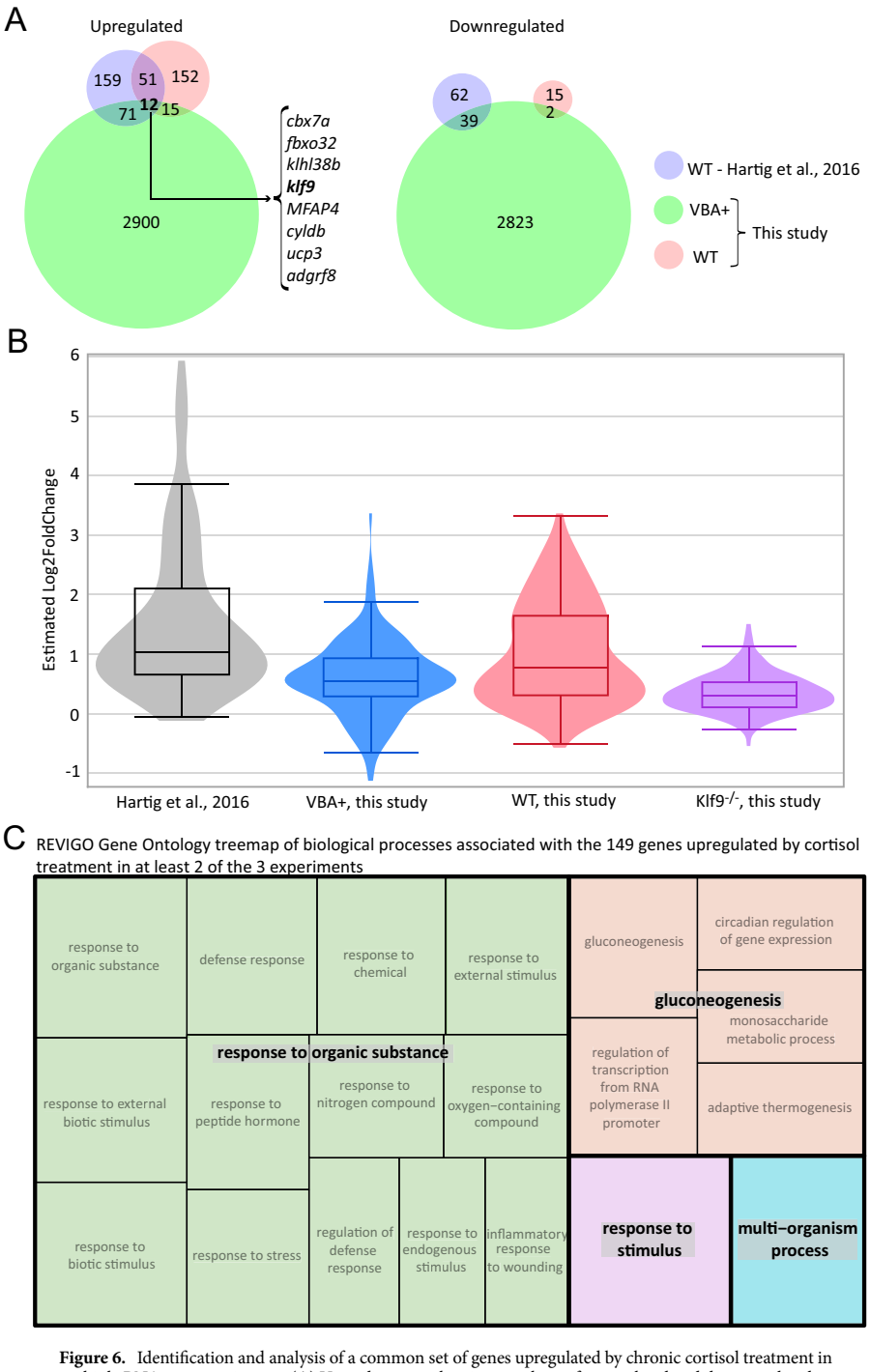


**Figure 6.** Identification and analysis of a common set of genes upregulated by chronic cortisol treatment in multiple RNA-seq experiments. (**A**) Venn diagrams showing numbers of upregulated and downregulated genes

following reanalysis of the data from all three experiments and their overlap. Only 8 of the 12 genes in common between all experiments were annotated with gene names (listed). (**B**) Violin and box plots of estimated fold change of the 149 genes that are upregulated in at least 2 of the three experiments shown in (**A**); the differences between each experiment are statistically significant (Table S14). (**C**) Treemap generated by REVIGO[57] (https://revigo.irb.hr/) of GO biological process terms found by GOrilla[34] to be associated with the 149 genes upregulated by chronic cortisol treatment in at least two out of the three experiments.

direct engagement of Klf9 with its transcriptional regulatory targets and downstream effects that those targets in turn have on the genes that they regulate.

## Discussion

Several previously published studies have characterized loss-of-function mutations of the zebrafish GR, including four frameshifting indels that introduce a premature stop codon in exon 2[13–15] (Fig. 1C). Here we report a new frameshift deletion ($GR^{369-}$) within exon 3 (Fig. 1A,B), which unlike the previous mutations removes all possible in-frame initiation codons upstream of the DNA binding domain (Fig. 1C), eliminating the transcriptional function of the mutant gene (Fig. 1E). We used RNA-seq to determine how this loss of GR function affects the larval transcriptome, both in larvae developed under normal conditions and in larvae treated chronically with cortisol. To overcome the low survival of embryos from homozygous mutant females and avoid nonspecific maternal effects that might be associated with poor egg quality, we took advantage of a visual background adaptation (VBA) screen to identify homozygous $GR^{369-}$ progeny of a heterozygous cross, as those larvae lack a VBA response (VBA- larvae). Based on the observation that VBA− larvae comprised ~ ¼ of the population, as expected for a recessive Mendelian trait, larvae that successfully mount a VBA response (VBA+ larvae) are predicted to consist of a 1:2 mixture of homozygous wild-type and heterozygous $GR^{369-}$ mutants, and hence to contain at least one intact *nr3c1* allele encoding a functional GR. A principal component analysis of the RNA-seq data revealed that absence of a functional GR has a profound effect on gene expression in both normal and cortisol-treated larvae, such that transcriptomes from larvae lacking a GR are clearly distinguished from those that have one, and that cortisol treatment produces a coherent effect only in larvae with a functional GR (Fig. 2A). A pair-wise comparison of gene expression between VBA+ and VBA− larvae (accounting for PC2) identified with statistical significance about four hundred genes that are regulated by the GR in 5-dpf larvae at the time they were collected (midmorning). GO term enrichment analysis indicated that genes upregulated by the GR at that time are involved in metabolism and stress response, as would be expected, while genes downregulated by the GR are involved in epidermis development, cell adhesion, growth, and basement membrane formation, suggesting that the GR may function as a switch to downregulate those morphogenetic processes in late development, or to temporally segregate them to a certain time of day given the circadian dynamic of glucocorticoid signaling. Interestingly, numerous biological processes and individual genes affected by loss of GR function were similarly affected by chronic cortisol treatment in larvae with a GR. This suggests that one effect of the chronic treatment is to promote development of GR resistance, and moreover, that it does so via the GR. Such resistance might be construed as an adaptive response to the chronic exposure.

Comparing gene expression in VBA+ larvae treated with cortisol versus vehicle (accounting for PC1 in that experiment) identified over four thousand genes that are differentially expressed in response to chronic cortisol treatment. This latter number is substantially larger than the 555 differentially expressed genes identified in our previous analysis[9] of the effects of chronic cortisol treatment and yielded a somewhat different result when subjected to GO term enrichment analysis (Figs. S5, S6). One major difference between the analyses reported here and that reported previously[9] is that in the latter the embryos and larvae were cultured in the dark, whereas in the present study we cultured them from fertilization in a diurnal light–dark cycle. In zebrafish larvae the circadian clock is not synchronized until the fish are exposed to a light–dark cycle[32,33], so our previous results may have had circadian asynchrony as a confounding variable. Indeed, the impact of this difference on the transcriptome is clearly seen in the PCA of the combined analysis of all three RNA-seq experiments (Fig. S15), accounting for nearly 20% of the variance. Despite this, the RNA-seq results reported here assessing effects of chronic cortisol exposure in wild-type and $klf9^{-/-}$ larvae (Fig. 4) were from embryos developed with light–dark cycles, and in the wild type larvae produced an effect on proinflammatory gene expression similar to that of our earlier study, demonstrating that that effect was not an artifact of circadian asynchrony. Another difference between both studies using wild-type larvae and that depicted in Fig. 2 was that the latter measured transcriptomic effects of chronic cortisol treatment in a 1:2 mixture wild-type and heterozygous mutant larvae (VBA +); thus the results in VBA + larvae would be expected to be less sensitive to any effects of the chronic exposure for which the GR is haploinsufficient, a possibility supported by the comparison shown in Fig. 6B. Further work is required to more fully assess the effects of GR gene dosage on the transcriptome under both normal conditions and in response to chronic cortisol exposure.

The meta-analysis comparing all our RNA-seq experiments examining the transcriptomic effects of chronic cortisol treatment in wild-type or VBA + larvae (Figs. 5 and 6 and Fig. S15) provides some important insights that are broadly relevant to RNA-seq data interpretation. One is that different experiments that examine the effects of a single variable under somewhat different conditions and in a limited number of biological replicates will often produce different lists of differentially expressed genes passing an arbitrary threshold of statistical significance (e.g. adjusted $p < 0.05$). The reason is clear enough: biological systems are highly responsive to genetic and environmental factors that vary between experiments and affect gene expression, sometimes stochastically and/or in ways that are difficult to control and measure, especially with a limited number of biological replicates. Nevertheless, GO analyses of the lists obtained from different experiments can detect consistent biological effects

even if the gene lists differ in the individual genes that they include, particularly if methods such as GOrilla[34] are used to test for statistically significant enrichment of GO terms toward one end or the other of a single list of genes ranked by some measurable criterion (e.g. a principal component that accounts for a specific condition as in Fig. 5). This underscores the important but often unappreciated point that statistical significance does not equate to biological significance, and generally is not a good sole criterion to assess the effects of a given condition on the expression of a given gene using high throughput methods such as RNA-seq. By comparing across the three experiments, we were able to identify both a small but "very high confidence" set of 12 genes as well as a larger "high confidence" set of 149 genes consistently affected by the cortisol treatment that would not have been discernible without our integrated meta-analysis (Fig. 6). Moreover, use of unbiased approaches such as PCA to parse the variance in the data can help identify robust condition-specific effects and provide insight into the biology underlying those effects when combined with GO term enrichment analysis. For the experiments reported here this approach validated our earlier finding that chronic cortisol exposure leads to upregulation of pro-inflammatory gene expression and extended that result by showing that the upregulation depends on the GR target gene *klf9*.

The set of "very high confidence" genes identified in the meta-analysis included *klf9*, one of only four genes showing GR-dependent expression in normal 5-dpf larvae that were also upregulated in VBA+ larvae in response to chronic cortisol, and only one of two that encode transcription factors, the other being *per1a* (Fig. 2B). Both *klf9* and *per1a* are involved in circadian regulation, and both have been shown to be GR targets in other vertebrate models[16,35–37]. Interestingly, *klf9* was also found to be the most commonly upregulated transcription factor gene in a recent meta-analysis of glucocorticoid-induced gene expression in the mammalian brain[38]. We have found by ATAC-seq that the promoter region of *klf9* is one of the most differentially open regions of chromatin in blood cells of adults derived from cortisol-treated embryos (Hartig et al., submitted). In mice *klf9* was recently shown to mediate glucocorticoid-induced metabolic dysregulation in liver[39]. Among other things Klf9 functions as a transcriptional repressor[40,41], and in mouse macrophages as an incoherent feedforward regulator of the GR target *klf2*[42], which functions to control inflammation[43]. Further work is needed to determine how *klf9* contributes to pro-inflammatory gene expression in response to chronic cortisol exposure, which could either be directly as a feedforward activator (possibly via effects on metabolism), indirectly as a feedforward repressor of an anti-inflammatory regulator like Klf2, or both. GO analysis also showed that genes involved in sterol biosynthesis are downregulated by loss of *klf9*, and more experiments are required to determine if *klf9* regulates the metabolism of cortisol and other steroid hormones. Our motif enrichment analysis of flanking sequences from the set of 149 genes upregulated by chronic cortisol in at least 2 of our 3 RNA-seq experiments indicated enrichment for KLF binding sites (Table S13); further work involving chromatin immunoprecipitation is needed to determine whether any of those sites are bound by Klf9 or Klf2. Additional studies are also required to determine whether loss of Klf9 alters the function of immune cells or the inflammatory response to injury or infection.

Perhaps unsurprisingly, our results (Fig. 2 and Fig. S3) indicate that the GR is required for nearly all the transcriptomic effects of chronically elevated cortisol. However, eight genes upregulated by the treatment were found in the RNA-seq analysis to be upregulated in both VBA+ and VBA− larvae (Fig. 2B), indicating that the GR is not required for their upregulation. Interestingly most of these genes are known IEGs, and include the neuronal activity-dependent gene *npas4a*, the mammalian homologue of which is directly repressed by the GR[44], as well as *egr1* which has been shown to differentially regulate GR in rat hippocampus depending on level of maternal care during development[45]. One possible explanation is that the genes are upregulated by increased MR activity, which was recently shown to contribute to stress axis regulation in zebrafish larvae[14]. Further work in MR mutant fish[14] will be needed to test this.

Finally, gene ontology analysis of genes upregulated by chronic cortisol treatment in VBA+ progeny of the $GR^{+/369-}$ cross indicated a strong effect on biological processes associated with nervous system development and function. This is consistent with a recent report that injection of cortisol into eggs leads to increased neurogenesis in the larval brain[10]. In this regard it is interesting that *klf9* is a stress-responsive gene that regulates neural differentiation and plasticity[35,46]. The long-term dysregulation of the HPA/I axis caused by early life exposure to chronic stress and/or chronically elevated cortisol suggests that the exposure perturbs brain development and activity. Given its role in regulating plasticity in brain regions relevant to neuroendocrine function, it will be interesting to determine whether *klf9* contributes to those effects.

## Materials and methods

**Zebrafish strains, husbandry, and embryo treatments.** The AB wild-type strain was used for all genetic modifications. Husbandry and procedures were as described previously[9]. All animal procedures were approved by the Institutional Animal Care and Use Committee (IACUC) of the MDI Biological Laboratory, and all methods were performed in accordance with the relevant guidelines and regulations. Embryo culture and cortisol treatments were performed as previously described[9], with one difference: embryos were cultured in a diurnal light–dark cycle (14 h light–10 h dark). Briefly, fertilized eggs were collected in the morning, disinfected and at ~4 h post fertilization placed in dishes with either 1uM cortisol or vehicle (DMSO) added to embryo media. Embryos developed in a 28.5° C incubator with a 14/10 light/dark cycle synchronized with the core fish room. Media was changed daily.

**Construction of *nr3c1* and *klf9* mutant lines.** To mutate *nr3c1* and *klf9* we used CRISPR-Cas9[47], injecting zygotes with multiple guide RNAs for each gene and mRNA encoding Cas9. Guide RNAs were designed using the CHOP-CHOP algorithm[48,49].

To generate the $GR^{369-}$ mutant line fertilized wild-type AB embryos were injected at the 1 cell stage with 1–2 nL of a gRNA cocktail targeting *nr3c1* exons 2 and 3 (final concentration 40 ng/μL for each gRNA, 230 ng/μL

Cas9 mRNA, 0.1 M KCl, and 0.01% phenol red indicator dye). Individual whole injected larvae were screened for mutations of the targeted regions by high resolution melt analysis (HRMA) of PCR amplicons containing those regions[50]. Detected mutations were then verified by Sanger sequencing of a PCR amplicon containing the targeted region. F0 adults bearing mutations were identified by HRMA of DNA extracted from tailfin clips, and germline mutations were then identified by PCR and HRMA/sequencing of sperm. F0 males with germline mutations were outcrossed to AB females, and heterozygous progeny were screened via sequencing from tailfin clips. The $GR^{369-}$ mutation was identified and selected for by breeding over 2 additional generations to yield F3 homozygous progeny. Subsequent generations were maintained as heterozygotes for health and breeding purposes.

To generate the *klf9*$^{-/-}$ mutant line fertilized wild-type AB embryos were injected at the 1-cell stage with < 20% cell volume of injection mix consisting of 200 ng/ul Cas9 mRNA, 100 ng/ul guide RNA, 0.05% phenol red dye, and 0.2 M KCl. Individual F0 larvae were screened with HRMA to confirm CRISPR efficacy. Larvae were placed into system and raised. Young adult fish were genotyped via HRMA using DNA extracted from fin clips, and mutations were confirmed by Sanger sequencing. F0 fish positive for mutation were outcrossed to wild-type (AB) fish. F1 offspring of this cross were screened by HRMA to confirm germline transmission, and Sanger sequencing identified the 2 bp frame-shift mutation in one female founder. This female was out crossed with WT AB males. The resulting F2 fish were screened as young adults via fin clip and HRMA, and males positive for mutation were back crossed to the F1 founder female. Resulting F3 generation fish were screened via fin clip HRMA and sequenced to identify homozygous mutants as well as homozygous wild-type siblings. F3 generation was Mendelian 1:2:1 wild-type:heterozygote:homozygous-mutant ratio.

**In vitro mRNA transcription and injection.** Total RNA was extracted from 5dpf wild-type larvae using Trizol. RNA was treated with DNase I (NEB), and full-length *nr3c1* cDNA was reverse transcribed using a specific primer (ggtcaaggttagtttaatgaattagtctgac) and Primescript RT kit (TaKara). Template DNA for transcripts was amplified from this cDNA using Q5 high fidelity polymerase (NEB), full-length (agtaatgcaaaatggatcaaggagg), truncated 310- (ctctttgggaacagctcgcc) or 369- (gggccagtttatgcttttcca) forward primers with upstream T7 promoters, and a common reverse primer (catcgtgtcctgctgttggg) downstream of the stop codon. Template DNA was run through an agarose gel to verify size, extracted and purified using E.Z.N.A. kit from Omega Biotek. Transcription reactions were run using mMessage mMachine Ultra T7 kit from Invitrogen, and yield quantified by spectrophotometry. Xenopus elongation factor 1a transcript from pTRI-Xef included in the mMessage mMachine kit was used as a control. Homozygous $GR^{369-}$ mutant embryos were injected at the one-cell stage with a mix containing 200 ng/ul mRNA and 0.05% phenol red dye, with an injection volume of ~ 20% cell volume. Injected embryos were snap-frozen at 6 h post fertilization for RNA extraction and qRT-PCR.

**Visual background adaptation (VBA) screen.** To identify larvae lacking a functional GR a VBA screen was performed on 4-day old larvae as described[12]. Briefly, larvae were incubated for 20 min in a dark incubator then transferred to a white background and immediately examined under a stereomicroscope with brightfield optics. Larvae that failed to mount a VBA response were identified by the failure of melanophores to disperse, remaining clustered in a dark patch on the dorsal surface[12]. Larvae were segregated as VBA+ and VBA- cohorts and returned to culture for an additional day before they were collected for RNA-seq.

**RNA-seq and data analysis.** At 3 h zeitgeber time (post lights-on) on day 5 post-fertilization four biological replicates of cortisol-treated and control embryos were collected as follows. For the first RNA-seq experiment, one by one, a dish of larvae corresponding to a single condition was removed from the incubator, and 8 larvae per replicate (4 replicates) were collected in a 1.5 mL tube with minimal water and immediately snap frozen in liquid nitrogen. All replicates from one condition were collected sequentially before moving on to the next condition. Total RNA was extracted using the Qiagen RNA-Easy Plus mini kit (Qiagen). For the second RNA-seq experiment, four replicates of n = 10 larvae were collected from a single dish for each condition and immediately snap frozen in liquid nitrogen. Collection of 16 samples occurred over 22 min. RNA was prepared as described above on two different days. On the first day (experimental replicates 1 and 2) the lysis buffer was added to all 8 frozen samples before homogenization, while on the second day the lysis buffer was added to each sample which was then immediately homogenized. This difference in sample preparation likely accounts for the large variance between samples prepared on day 1 and day 2. RNA was sent to the Oklahoma State Genomics Facility for Illumina library preparation and single-end sequencing.

RNA-seq libraries were generated with Illumina-compatible KAPA libraries and sequenced on an Illumina NextSeq 500 High Output sequencer. *klf9*$^{-/-}$ and matched control samples were sequenced as single end 75-bp reads. VBA+ and VBA- samples were sequences as paired-end 75-bp samples.

Fastq formatted read files were preprocessed with Trimmomatic[51] version 0.38 with default options, and then aligned to the Zebrafish genome version 11 as presented in Ensembl[52] version 93, using the STAR aligner[53] version 2.6.1b. The Ensembl transcriptome was preprocessed with a splice junction overhang of 100 nt. Following alignment, the resulting BAM files were processed with RSEM[54] version 1.3.0 for isoform and gene-level expression estimates. The resulting gene-level expression values were merged into a single expression matrix with an in-house python script. EDASeq[55] carried out in R version 3.6.1 was used to further normalize data for systematic effects, using gene-level length and GC-content as downloaded from Ensembl version 98 using EDAseq's included scripts. "WithinLane" normalization with GC content was judged as superior to that based on length. Final normalized gene-level counts (which = "full") were generated using GC-based WithinLaneNormalization followed by BetweenLaneNormalization. Subsequent differential expression analysis was carried out in R version 3.6.1 with the DESeq2[56] version 1.24.0, using either treatment (DMSO/cortisol) or genetics (VBA+/VBA− or *klf9*$^{-/-}$/WT) as the comparison. The *klf9*$^{-/-}$ experiment analysis also included a

two-level categorical batch covariate. DESeq2 was also used to generate a rlog-matrix which was subsequently Z-transformed to normalize each gene across all samples. The Z-transformed rlog matrix was then loaded into JMP version 15 and used for PCA (using the "Wide Method") after thresholding to an average rlog expression value of 7.5.

Both RNA-seq dataset have been deposited in the NCBI Gene Expression Omnibus database, under accession numbers GSE144884 (GR+/− experiment) and GSE144885 (Klf9+/− experiment).

The previously published RNA-seq data set was reprocessed as just described, and an overall matrix of only wild-type or VBA+ samples was generated and jointly normalized with EDASeq and then subjected to PCA as described in the previous paragraph.

DESeq2 output tables were filtered with the following restrictions for the identification of statistically significant differentially expressed genes: BaseMean ≥ 75 (average of 5 counts per sample), padj ≤ 0.05, |log2foldchange| ≥ 0.5, estimated standard error of the log2foldchange < 1.0.

The GOrilla algorithm[34] (https://cbl-gorilla.cs.technion.ac.il/) was used for Gene Ontology term enrichment analysis, and the data were visualized using REVIGO[57] (https://revigo.irb.hr/). Venn diagrams were generated using Venny 2.1 (https://bioinfogp.cnb.csic.es/tools/venny/). HOMER motif enrichment analysis[27] was used to compare incidence of known vertebrate motifs in a list of promoters of interest with incidence in a background list of all zebrafish promoters by running the findMotifs program (https://homer.ucsd.edu/homer/microarray/index.html) using default settings except that sequence from −1500 to +500 bp relative to the transcription start site was searched for motifs from 10 to 18 bp in length.

**Quantitative reverse transcription and polymerase chain reaction (qRT-PCR).** Total RNA purified from snap-frozen larvae using the Trizol method and used as template to synthesize random-primed cDNA using the Primescript cDNA synthesis kit (TaKaRa). Relative gene expression levels were measured by qRT-PCR, using the delta-delta Ct method as described previously[9], and *eif5a* as a reference gene. Examination of the results of multiple RNA-seq data sets indicated that *eif5a* activity was highly stable across treatments and genotypes. In many experiments beta-actin was also used as a reference gene, and this did not substantially change the results.

**Graphics.** RNA-seq results (PCA plots, box plots, scatter plots, and violin plot) were graphed using JMP version 15 from SAS. qRT-PCR results were graphed using Microsoft Excel. All figures were drafted using Adobe Illustrator CS4. Some of the graphs (Figs. 2B,D, 4C, and 5A) were redrawn in Illustrator exactly without modifying the depiction of the data.

Received: 7 February 2020; Accepted: 17 June 2020
Published online: 10 July 2020

## References

1. Kadmiel, M. & Cidlowski, J. A. Glucocorticoid receptor signaling in health and disease. *Trends Pharmacol. Sci.* **34**, 518–530 (2013).
2. Gomez-Sanchez, E. & Gomez-Sanchez, C. E. The multifaceted mineralocorticoid receptor. *Comp. Physiol.* **4**, 965–994 (2014).
3. McEwen, B. S. Influences of adrenocortical hormones on pituitary and brain function. *Monogr. Endocrinol.* **12**, 467–492 (1979).
4. Karst, H. *et al.* Mineralocorticoid receptors are indispensable for nongenomic modulation of hippocampal glutamate transmission by corticosterone. *Proc. Natl. Acad. Sci. USA* **102**, 19204–19207 (2005).
5. Spencer, R. L., Chun, L. E., Hartsock, M. J. & Woodruff, E. R. Glucocorticoid hormones are both a major circadian signal and major stress signal: How this shared signal contributes to a dynamic relationship between the circadian and stress systems. *Front. Neuroendocrinol.* **49**, 52–71 (2018).
6. Coffman, J. A. Chronic stress, physiological adaptation, and developmental programming of the neuroendocrine stress system. *Future Neurol.* https://doi.org/10.2217/fnl-2019-0014 (2020).
7. Nesan, D. & Vijayan, M. M. The transcriptomics of glucocorticoid receptor signaling in developing zebrafish. *PLoS ONE* **8**, e80726 (2013).
8. Nesan, D. & Vijayan, M. M. Role of glucocorticoid in developmental programming: evidence from zebrafish. *Gen. Comp. Endocrinol.* **181**, 35–44 (2013).
9. Hartig, E. I., Zhu, S., King, B. L. & Coffman, J. A. Cortisol-treated zebrafish embryos develop into pro-inflammatory adults with aberrant immune gene regulation. *Biol. Open* **5**, 1134–1141 (2016).
10. Best, C., Kurrasch, D. M. & Vijayan, M. M. Maternal cortisol stimulates neurogenesis and affects larval behaviour in zebrafish. *Sci. Rep.* **7**, 40905 (2017).
11. Wilson, K. S. *et al.* Early-life glucocorticoids programme behaviour and metabolism in adulthood in zebrafish. *J. Endocrinol.* **230**, 125–142 (2016).
12. Griffiths, B. B. *et al.* A zebrafish model of glucocorticoid resistance shows serotonergic modulation of the stress response. *Front. Behav. Neurosci.* **6**, 68 (2012).
13. Facchinello, N. *et al.* nr3c1 null mutant zebrafish are viable and reveal DNA-binding-independent activities of the glucocorticoid receptor. *Sci. Rep.* **7**, 4371 (2017).
14. Faught, E. & Vijayan, M. M. The mineralocorticoid receptor is essential for stress axis regulation in zebrafish larvae. *Sci. Rep.* **8**, 18081 (2018).
15. Lee, H. B. *et al.* Novel zebrafish behavioral assay to identify modifiers of the rapid, nongenomic stress response. *Genes Brain Behav.* **18**, e12549 (2019).
16. Shewade, L. H., Schneider, K. A., Brown, A. C. & Buchholz, D. R. In-vivo regulation of Kruppel-like factor 9 by corticosteroids and their receptors across tissues in tadpoles of Xenopus tropicalis. *Gen. Comp. Endocrinol.* **248**, 79–86 (2017).
17. Nesan, D. *et al.* Glucocorticoid receptor signaling is essential for mesoderm formation and muscle development in zebrafish. *Endocrinology* **153**, 1288–1300. https://doi.org/10.1210/en.2011-1559 (2012).
18. Pikulkaew, S. *et al.* The knockdown of maternal glucocorticoid receptor mRNA alters embryo development in zebrafish. *Dev. Dyn.* **240**, 874–889. https://doi.org/10.1002/dvdy.22586 (2011).
19. Rossi, A. *et al.* Genetic compensation induced by deleterious mutations but not gene knockdowns. *Nature* **524**, 230–233. https://doi.org/10.1038/nature14580 (2015).

20. Lu, N. Z. & Cidlowski, J. A. Translational regulatory mechanisms generate N-terminal glucocorticoid receptor isoforms with unique transcriptional target genes. *Mol. Cell* **18**, 331–342 (2005).
21. Zeller, R. W., Coffman, J. A., Harrington, M. G., Britten, R. J. & Davidson, E. H. SpGCF1, a sea urchin embryo DNA-binding protein, exists as five nested variants encoded by a single mRNA. *Dev. Biol.* **169**, 713–727 (1995).
22. Morita, M. *et al.* Functional analysis of basic transcription element binding protein by gene targeting technology. *Mol. Cell Biol.* **23**, 2489–2500. https://doi.org/10.1128/mcb.23.7.2489-2500.2003 (2003).
23. Dickmeis, T. Glucocorticoids and the circadian clock. *J. Endocrinol.* **200**, 3–22 (2009).
24. Dickmeis, T. *et al.* Glucocorticoids play a key role in circadian cell cycle rhythms. *PLoS Biol.* **5**, e78 (2007).
25. Dickmeis, T., Weger, B. D. & Weger, M. The circadian clock and glucocorticoids–interactions across many time scales. *Mol. Cell Endocrinol.* **380**, 2–15 (2013).
26. Weger, B. D. *et al.* Extensive regulation of diurnal transcription and metabolism by glucocorticoids. *PLoS Genet.* **12**, e1006512 (2016).
27. Heinz, S. *et al.* Simple combinations of lineage-determining transcription factors prime cis-regulatory elements required for macrophage and B cell identities. *Mol. Cell* **38**, 576–589 (2010).
28. Fornes, O. *et al.* JASPAR 2020: update of the open-access database of transcription factor binding profiles. *Nucl. Acids Res* https://doi.org/10.1093/nar/gkz1001 (2020).
29. Sandelin, A., Alkema, W., Engstrom, P., Wasserman, W. W. & Lenhard, B. JASPAR: an open-access database for eukaryotic transcription factor binding profiles. *Nucl. Acids Res* **32**, D91-94. https://doi.org/10.1093/nar/gkh012 (2004).
30. de Assuncao, T. M. *et al.* New role for Kruppel-like factor 14 as a transcriptional activator involved in the generation of signaling lipids. *J. Biol. Chem.* **289**, 15798–15809. https://doi.org/10.1074/jbc.M113.544346 (2014).
31. Pearson, R., Fleetwood, J., Eaton, S., Crossley, M. & Bao, S. Kruppel-like transcription factors: a functional family. *Int. J. Biochem. Cell Biol.* **40**, 1996–2001. https://doi.org/10.1016/j.biocel.2007.07.018 (2008).
32. Kaneko, M. & Cahill, G. M. Light-dependent development of circadian gene expression in transgenic zebrafish. *PLoS Biol.* **3**, e34 (2005).
33. Dekens, M. P. & Whitmore, D. Autonomous onset of the circadian clock in the zebrafish embryo. *Embo J.* **27**, 2757–2765 (2008).
34. Eden, E., Navon, R., Steinfeld, I., Lipson, D. & Yakhini, Z. GOrilla: a tool for discovery and visualization of enriched GO terms in ranked gene lists. *BMC Bioinform.* **10**, 48 (2009).
35. Bonett, R. M., Hu, F., Bagamasbad, P. & Denver, R. J. Stressor and glucocorticoid-dependent induction of the immediate early gene kruppel-like factor 9: implications for neural development and plasticity. *Endocrinology* **150**, 1757–1765 (2009).
36. Sporl, F. *et al.* Kruppel-like factor 9 is a circadian transcription factor in human epidermis that controls proliferation of keratinocytes. *Proc. Natl. Acad. Sci. USA* **109**, 10903–10908 (2012).
37. Reddy, T. E., Gertz, J., Crawford, G. E., Garabedian, M. J. & Myers, R. M. The hypersensitive glucocorticoid response specifically regulates period 1 and expression of circadian genes. *Mol. Cell Biol.* **32**, 3756–3767 (2012).
38. Juszczak, G. R. & Stankiewicz, A. M. Glucocorticoids, genes and brain function. *Prog. Neuropsychopharmacol. Biol. Psychiatry* **82**, 136–168 (2018).
39. Cui, A. *et al.* Dexamethasone-induced Kruppel-like factor 9 expression promotes hepatic gluconeogenesis and hyperglycemia. *J. Clin. Invest.* **130**, 2266–2278 (2019).
40. Knoedler, J. R., Subramani, A. & Denver, R. J. The Kruppel-like factor 9 cistrome in mouse hippocampal neurons reveals predominant transcriptional repression via proximal promoter binding. *BMC Genom.* **18**, 299 (2017).
41. Ying, M. *et al.* Kruppel-like factor-9 (KLF9) inhibits glioblastoma stemness through global transcription repression and integrin alpha6 inhibition. *J. Biol. Chem.* **289**, 32742–32756 (2014).
42. Chinenov, Y., Coppo, M., Gupte, R., Sacta, M. A. & Rogatsky, I. Glucocorticoid receptor coordinates transcription factor-dominated regulatory network in macrophages. *BMC Genom.* **15**, 656 (2014).
43. Nayak, L. *et al.* Kruppel-like factor 2 is a transcriptional regulator of chronic and acute inflammation. *Am. J. Pathol.* **182**, 1696–1704 (2013).
44. Furukawa-Hibi, Y., Yun, J., Nagai, T. & Yamada, K. Transcriptional suppression of the neuronal PAS domain 4 (Npas4) gene by stress via the binding of agonist-bound glucocorticoid receptor to its promoter. *J. Neurochem.* **123**, 866–875 (2012).
45. Weaver, I. C. *et al.* Epigenetic programming by maternal behavior. *Nat. Neurosci.* **7**, 847–854 (2004).
46. Besnard, A. *et al.* Targeting Kruppel-like factor 9 in excitatory neurons protects against chronic stress-induced impairments in dendritic spines and fear responses. *Cell Rep.* **23**, 3183–3196 (2018).
47. Hwang, W. Y. *et al.* Efficient genome editing in zebrafish using a CRISPR-Cas system. *Nat. Biotechnol.* **31**, 227–229. https://doi.org/10.1038/nbt.2501 (2013).
48. Labun, K., Montague, T. G., Gagnon, J. A., Thyme, S. B. & Valen, E. CHOPCHOP v2: a web tool for the next generation of CRISPR genome engineering. *Nucleic Acids Res.* **44**, W272-276. https://doi.org/10.1093/nar/gkw398 (2016).
49. Montague, T. G., Cruz, J. M., Gagnon, J. A., Church, G. M. & Valen, E. CHOPCHOP: a CRISPR/Cas9 and TALEN web tool for genome editing. *Nucleic Acids Res.* **42**, W401-407. https://doi.org/10.1093/nar/gku410 (2014).
50. Parant, J. M., George, S. A., Pryor, R., Wittwer, C. T. & Yost, H. J. A rapid and efficient method of genotyping zebrafish mutants. *Dev. Dyn.* **238**, 3168–3174. https://doi.org/10.1002/dvdy.22143 (2009).
51. Bolger, A. M., Lohse, M. & Usadel, B. Trimmomatic: a flexible trimmer for Illumina sequence data. *Bioinformatics* **30**, 2114–2120 (2014).
52. Zerbino, D. R. *et al.* Ensembl 2018. *Nucl. Acids Res.* **46**, D754–D761. https://doi.org/10.1093/nar/gkx1098 (2018).
53. Dobin, A. *et al.* STAR: ultrafast universal RNA-seq aligner. *Bioinformatics* **29**, 15–21. https://doi.org/10.1093/bioinformatics/bts635 (2013).
54. Li, B. & Dewey, C. N. RSEM: accurate transcript quantification from RNA-Seq data with or without a reference genome. *BMC Bioinform.* **12**, 323 (2011).
55. Risso, D., Schwartz, K., Sherlock, G. & Dudoit, S. GC-content normalization for RNA-Seq data. *BMC Bioinform.* **12**, 480. https://doi.org/10.1186/1471-2105-12-480 (2011).
56. Love, M. I., Huber, W. & Anders, S. Moderated estimation of fold change and dispersion for RNA-seq data with DESeq2. *Genome Biol.* **15**, 550. https://doi.org/10.1186/s13059-014-0550-8 (2014).
57. Supek, F., Bosnjak, M., Skunca, N. & Smuc, T. REVIGO summarizes and visualizes long lists of gene ontology terms. *PLoS ONE* **6**, e21800 (2011).


## Acknowledgements

This work was supported by Grants from the National Institutes of Health (R03- HD099468, P20-GM104318, and P20-GM103423), by a Morris Scientific Discovery Award to JAC, and by a gift from The Linde Packman Lab for Biosciences Innovation to Colby College.

## Author contributions

IG and EIH performed most of the experiments and did the matings, microinjections and husbandry to establish the *klf9* and *nr3c1* mutant zebrafish strains; SZ designed the gRNAs and performed the initial PCR and sequencing analyses to identify fish containing the desired *nr3c1* mutations; IG performed the mRNA injection experiments, qRT-PCR, RNA-seq data analysis, and HOMER motif enrichment analysis; ART contributed to the RNA-seq experimental design and data analysis; LNH wrote the code used in the RNA-seq data analysis; NJM performed the initial analysis of the RNA-seq data; JHG directed the computational analyses and performed the PCA and DGE analyses; JAC conceived the study, contributed to analysis of the data and drafted the manuscript.

## Competing interests

The authors declare no competing interests.

## Additional information

**Supplementary information** is available for this paper at https://doi.org/10.1038/s41598-020-68040-z.

**Correspondence** and requests for materials should be addressed to J.A.C.

**Reprints and permissions information** is available at www.nature.com/reprints.

**Publisher's note** Springer Nature remains neutral with regard to jurisdictional claims in published maps and institutional affiliations.

**APPENDIX B: Gans, et al., Frontiers in Cell and Developmental Biology, 2021‡**

frontiers in Cell and Developmental Biology

BRIEF RESEARCH REPORT
published: 06 October 2021
doi: 10.3389/fcell.2021.727037

# Glucocorticoid-Responsive Transcription Factor Krüppel-Like Factor 9 Regulates *fkbp5* and Metabolism

*Ian M. Gans[1,2], Janelle Grendler[1], Remy Babich[3], Nishad Jayasundara[4] and James A. Coffman[1,2]**

[1] MDI Biological Laboratory, Bar Harbor, ME, United States, [2] Graduate School of Biomedical Science and Engineering, University of Maine, Orono, ME, United States, [3] The School of Marine Sciences, University of Maine, Orono, ME, United States, [4] Nicholas School of the Environment, Duke University, Durham, NC, United States

OPEN ACCESS

**Edited by:**
Venkaiah Betapudi,
United States Department of Homeland Security, United States

**Reviewed by:**
Frank A. Simmen,
University of Arkansas for Medical Sciences, United States
Joyce Lloyd,
Virginia Commonwealth University, United States
Akira Muto,
Toho University, Japan
Mathilakath Vijayan,
University of Calgary, Canada

***Correspondence:**
James A. Coffman
jcoffman@mdibl.org

**Specialty section:**
This article was submitted to Cellular Biochemistry, a section of the journal Frontiers in Cell and Developmental Biology

**Received:** 17 June 2021
**Accepted:** 15 September 2021
**Published:** 06 October 2021

**Citation:**
Gans IM, Grendler J, Babich R, Jayasundara N and Coffman JA (2021) Glucocorticoid-Responsive Transcription Factor Krüppel-Like Factor 9 Regulates fkbp5 and Metabolism. Front. Cell Dev. Biol. 9:727037. doi: 10.3389/fcell.2021.727037

Krüppel-like factor 9 (Klf9) is a feedforward regulator of glucocorticoid receptor (GR) signaling. Here we show that in zebrafish *klf9* is expressed with GR-dependent oscillatory dynamics in synchrony with *fkbp5*, a GR target that encodes a negative feedback regulator of GR signaling. We found that *fkbp5* transcript levels are elevated in *klf9*$^{-/-}$ mutants and that Klf9 associates with chromatin at the *fkbp5* promoter, which becomes hyperacetylated in *klf9*$^{-/-}$ mutants, suggesting that the GR regulates *fkbp5* via an incoherent feedforward loop with *klf9*. As both the GR and Fkbp5 are known to regulate metabolism, we asked how loss of Klf9 affects metabolic rate and gene expression. We found that *klf9*$^{-/-}$ mutants have a decreased oxygen consumption rate (OCR) and upregulate glycolytic genes, the promoter regions of which are enriched for potential Klf9 binding motifs. Our results suggest that Klf9 functions downstream of the GR to regulate cellular glucocorticoid responsivity and metabolic homeostasis.

**Keywords: glucocorticoid receptor, Krüppel-like factor 9, *fkbp5*, cortisol, metabolism, zebrafish, RNA-seq, gene expression**

## INTRODUCTION

Glucocorticoids, the terminal hormonal output of the vertebrate hypothalamus-pituitary-adrenal (HPA) axis, function to maintain homeostasis by regulating diverse aspects of physiology, including metabolism and the immune system. Endogenous glucocorticoids (cortisol in humans and fish, corticosterone in rodents) are crucial for mounting physiological responses to stimuli that are either predictable (e.g., day/night cycles, feeding schedule) or unexpected (e.g., during the fight/flight response to acute threat). Basal circulating glucocorticoid (GC) levels oscillate with a circadian rhythm, peaking in the hours just before an animal's active phase (early morning in diurnal species, evening in nocturnal species). This circadian fluctuation is produced by amplitude modulation of shorter ultradian (i.e., ∼hourly) pulses of hormone secretion (Veldhuis et al., 1989; Jasper and Engeland, 1991; Stavreva et al., 2009). Ultradian GC pulses cause cycles of glucocorticoid receptor (GR) activation and association with chromatin that produce ultradian pulses of transcription



‡ This article was published between initial submittal of written dissertation and oral defense. Material contained in this article are used throughout this dissertation without reference to this article.

(Stavreva et al., 2009). Acute stressors also activate the HPA axis and pulsed GC release, and the magnitude of the physiological response depends on whether the stressor occurs during the rising or falling phase of the ultradian rhythm (Windle et al., 1998).

Because the GR is ubiquitously expressed and binds thousands of genomic sites in a given tissue (Sacta et al., 2016), changes in circulating GC levels produce broad changes in gene expression, and hence in physiology and behavior. Temporal gene regulation is one way in which organisms optimize usage of resources (Liu et al., 1995; Klevecz et al., 2004; Lloyd and Murray, 2005; Tu et al., 2005), and conditions that disrupt GC dynamics—e.g., chronic/repeated stress, interference with circadian cues, or Cushing's Disease (hypercortisolemia)—are associated with multi-systemic disorders, including immune, psychological and metabolic syndromes (Silverman and Sternberg, 2012). We have previously reported that treatment of zebrafish larvae with chronic 1 μM cortisol leads to aberrant immune gene expression as well as long-term effects on the dynamics of the hypothalamus-pituitary-interrenal (HPI, equivalent to the mammalian HPA) axis and immune gene expression (Hartig et al., 2016, 2020).

GC signaling dynamics are controlled by negative feedback at both systemic and intracellular levels. Systemically, negative feedback of circulating GC on the pituitary is key to the generation of ultradian GC pulses (Walker et al., 2010, 2012; Spiga et al., 2011). Within cells, a negative feedback loop exists between the GR and its co-chaperone Fkbp5: transcription of *fkbp5* is activated by the GR and translated Fkbp5 inactivates the GR by sequestering it in the cytoplasm, increasing resistance to further activation by GC (Denny et al., 2000; Scammell et al., 2001). Elevated *FKBP5* expression contributes to HPA dysfunction and associated diseases (Binder et al., 2004; Binder, 2009; Klengel et al., 2012; Li et al., 2020), including diabetes and obesity (Pereira et al., 2014; Pena et al., 2020). However, our knowledge of *fkbp5* transcriptional regulation is incomplete.

Krüppel-like Factors (KLFs) are zinc-finger transcription factors that co-regulate nuclear receptor signaling (Knoedler and Denver, 2014) and fine-tune transcription through competitive binding to regulatory DNA (Ilsley et al., 2017). *Klf9* is a GR target that is ubiquitously expressed, including in the brain (Bonett et al., 2009; Bagamasbad et al., 2012; Juszczak and Stankiewicz, 2018) wherein it directs a maladaptive response to chronic stress (Besnard et al., 2018), and in the liver where its overexpression contributes to hyperglycemia (Cui et al., 2019). GR-*klf9* feedforward regulation was documented in human skin and murine macrophages (Chinenov et al., 2014; Lili et al., 2019), and by our lab in zebrafish (Gans et al., 2020), a model organism well-suited for studies of GC signaling (Dickmeis et al., 2007; Griffiths et al., 2012; Nesan and Vijayan, 2013). Here we extend our previous report that Klf9 mediates transcriptomic effects of chronic GC exposure by asking if Klf9 contributes to the regulation of *fkbp5* and metabolism, key targets of GC signaling. We found that *klf9* and *fkbp5* are synchronously expressed with GR-dependent dynamics that differ from those of other GC-responsive genes; that *fkbp5* activity is elevated in *klf9*$^{-/-}$ mutants; and that Klf9 protein interacts with chromatin at the *fkbp5* promoter. We also show that metabolism is altered in *klf9*$^{-/-}$ mutants, as indicated by decreased oxygen consumption rate (OCR) and upregulation of glycolytic genes.

# MATERIALS AND METHODS

## Zebrafish Strains, Husbandry, and Embryo Treatments

The AB strain was used for all genetic modifications. Husbandry and procedures were carried out as described previously (Hartig et al., 2016) and in the **Supplementary Methods**. All animal procedures were approved by the Institutional Animal Care and Use Committee (IACUC) of the MDI Biological Laboratory, and all methods were performed in accordance with the relevant guidelines and regulations.

The Klf9-AMtag line was created using CRISPR-Cas9 and homology-directed repair as described in the **Supplementary Methods**, using a donor sequence encoding the AM epitope tag (**Supplementary Figure 10**) recognized by the Active Motif anti-AM antibody (Active Motif, Carlsbad, CA).

## Analysis of Gene Expression

Quantitative reverse transcription and polymerase chain reaction (qRT-PCR) was carried out as described previously (Hartig et al., 2016) and in the **Supplementary Methods**. For time-course experiments, each timepoint sample consisted of 3–6 larvae cultured in an individual Petri dish, and the dishes were arranged in the incubator so as to minimize disturbance during sampling. Sinusoid models were fit to time-course expression data using the equation y = m + a*exp(-b*x)*sin(c*(x-d)), where m = MESOR, a = amplitude, b = decay rate, c = 2*pi*frequency, and d = phase shift. Non-linear least squares regression was performed using either the *nls* function in the R Stats package or in Microsoft Excel using the Solver function (Kemmer and Keller, 2010); both methods generated the same solutions. Initial values for constants were chosen to generate a reasonable qualitative fit before iterative fitting programs were run. When generating random data sets and model fits (see section "Results"), initial constants were set to the best fit of data combined from both conditions (either VEH- and CORT-treated, or wildtype and *klf9*$^{-/-}$, depending on the experiment).

RNA-seq data were obtained from our previous study (Gans et al., 2020). The generation and analysis of the data are described in the **Supplementary Methods**.

The NanoString PlexSet assay for 24 probe sets (21 genes of interest plus 3 reference genes) was performed according to the manufacturer's instructions (NanoString Technologies, Seattle, WA) and as described in the **Supplementary Methods**. Probe sets were designed by NanoString with direction and approval of the authors (see **Supplementary Table 1**). Normalized counts were exported from the NanoString nSolver program (Geiss et al., 2008), and heat maps were generated from Z-transformed log2 counts data using the *heatmap.2* function in gplots 3.1.1 package (Warnes et al., 2020) in R. Hierarchical clustering was determined using the *hclust* function in the R stats package and the "complete" method with distance between rows calculated by the *dist* function and Euclidean method.

## Cortisol Measurement

Cortisol was assayed using the Neogen Cortisol ELISA kit, as described previously (Hartig et al., 2016) and in the **Supplementary Methods**.

## Chromatin Immunoprecipitation

Chromatin Immunoprecipitation (ChIP) was performed as described by Lindeman et al. (2009) and in the **Supplementary Methods**.

## Oxygen Consumption Rate

Oxygen consumption rate was analyzed using an XF96$^e$ Extracellular Flux Analyzer (Agilent Technologies) as described in the **Supplementary Methods**. The first data point is typically inconsistent in these runs and was therefore excluded from the analysis. The remaining 11 data points were imported to GraphPad Prism 8.0 (GraphPad Software, San Diego, CA, United States) and plotted as a function of time (**Supplementary Figure 12A**). Linear regression of time-series data was used to determine the slope (rate of change in OCR over time) and Y-intercept, which is indicative of basal metabolic rate. Statistical significance between treatment groups for the slopes and Y-intercepts were calculated by two-factor ANOVA (treatment and genetic background as the two variable, **Supplementary Figure 12B**) followed by Šídák's multiple comparisons test (GraphPad Prism 8.0). A possible confound that we cannot exclude is that CORT and VEH treatment solutions could have differences in oxygen solubility.

# RESULTS

## *Klf9* and *fkbp5* Share Synchronous and Glucocorticoid Receptor-Dependent Temporal Expression Dynamics

Treatment of zebrafish embryos with chronic 1 μM cortisol (CORT) produces a modest but significant elevation in whole-body cortisol and GR activity at 5 days post-fertilization (dpf) (Hartig et al., 2016). The CORT-treated larvae upregulate immune-related genes, an effect dependent on both the GR and Klf9 (Gans et al., 2020), and give rise to adults in which *fkbp5* and *klf9* transcripts are persistently elevated in blood cells on average, although not in every instance (Hartig et al., 2020). We hypothesized that such inconsistency could be an artifact of measuring dynamic gene expression with insufficient temporal resolution, and therefore undertook high-density time-course sampling to measure *fkbp5* and *klf9* expression in 5 dpf larvae, by which stage the HPI axis is fully developed (Alsop and Vijayan, 2008) and both genes are actively transcribed (**Supplementary Figure 1**). Although bulk analysis of larval gene expression lacks spatial resolution, we reasoned that such an analysis would be informative since both *fkbp5* and *klf9* are ubiquitously expressed (Thisse and Thisse, 2004; Zhang et al., 2017), and transcription in peripheral zebrafish tissues is highly entrained to circadian rhythms via GC signaling (Frøland Steindal and Whitmore, 2019; Morbiato et al., 2019). For the time-courses, care was taken not to disturb larvae during sampling (see section "Materials and Methods") to minimize stress-responsive expression. The results revealed that *klf9* and *fkbp5* are expressed with synchronous oscillations on both the circadian and ultradian time scales (**Figure 1A** and **Supplementary Figure 1C**). Transcript levels of both genes peaked just prior to zeitgeber time 0 (ZT 0, corresponding to lights-on in the incubator), falling sharply thereafter. The data for both genes could be fit by non-linear regression to sinusoidal models, with wavelengths of 8.2 and 9.5 h for *fkbp5* and *klf9* respectively (ANOVA $p < 0.0001$, **Supplementary Figure 2**).

Since the 10-h sampling window was too narrow to draw conclusions about circadian periodicity, we measured expression of *klf9*, *fkbp5* and the circadian gene *per1a* over a 24-h period. While *per1a* had a prototypical 24-h oscillation, *klf9* and *fkbp5* had a shorter periodicity and lower amplitude oscillation (**Supplementary Figure 3**). Nevertheless, transcript levels of all three genes peaked synchronously just before ZT 0 and dropped precipitously thereafter (**Supplementary Figure 3**). We interpret this as coordination of GR activity with the circadian clock, as whole-larva cortisol levels show a similar diurnal drop (**Supplementary Figure 4**) and GCs drive circadian cell cycle and metabolic rhythms in zebrafish larvae (Dickmeis et al., 2007; Weger et al., 2016). We verified the GR-dependence and diurnal dynamics of *klf9* and *fkbp5* activity by comparing transcript levels in wild-type larvae and GR$^{-/-}$ mutants at ZT −0.25 and ZT 3. In the GR$^{-/-}$ mutants, both genes were lowly and flatly expressed, being significantly under-expressed at the wildtype (WT) expression peak of ZT −0.25 and remaining below WT at the 3.25 ZT expression nadir (**Figure 1B**).

To determine if the temporal dynamics shared by *klf9* and *fkbp5* are common to GC-responsive genes in general we re-measured one replicate (40 samples of pooled larvae) of our time-course using the NanoString platform and a probe set (**Supplementary Table 1**) representing 21 genes known to be direct GR targets and/or that we have experimentally identified as consistently responding to CORT treatment, including *klf9* and *fkbp5* (Gans et al., 2020). Hierarchical clustering of these NanoString data distinguished two main time-dependent clusters of genes (**Figure 1C**). The tight correlation between *klf9* and *fkbp5* was underscored by their clustering together on their own branch, which in turn clustered with other genes whose expression peaked in early morning hours, including circadian regulators *per1a* and *nr1d2a*, as well as *rhcga* and *ncf1*. Conversely, for the second main cluster, which included the GR target *tsc22d3* as well as several immune genes, expression was low in the early morning when endogenous CORT is high, then rose after ZT 0.

We next assessed the effect of chronic CORT exposure, shown by our previous studies to elevate *klf9* transcript levels at the 5 dpf mid-morning (∼ZT 3) timepoint when samples were collected (Hartig et al., 2016; Gans et al., 2020). Overall, the treatment resulted in a significant elevation of *klf9* and *fkbp5* transcripts across all timepoints ($p < 0.005$, paired *t*-tests), albeit with instances of lower levels at some timepoints (**Figure 2A**). To rigorously test whether the exposure significantly increased the average expression of these genes we also computationally

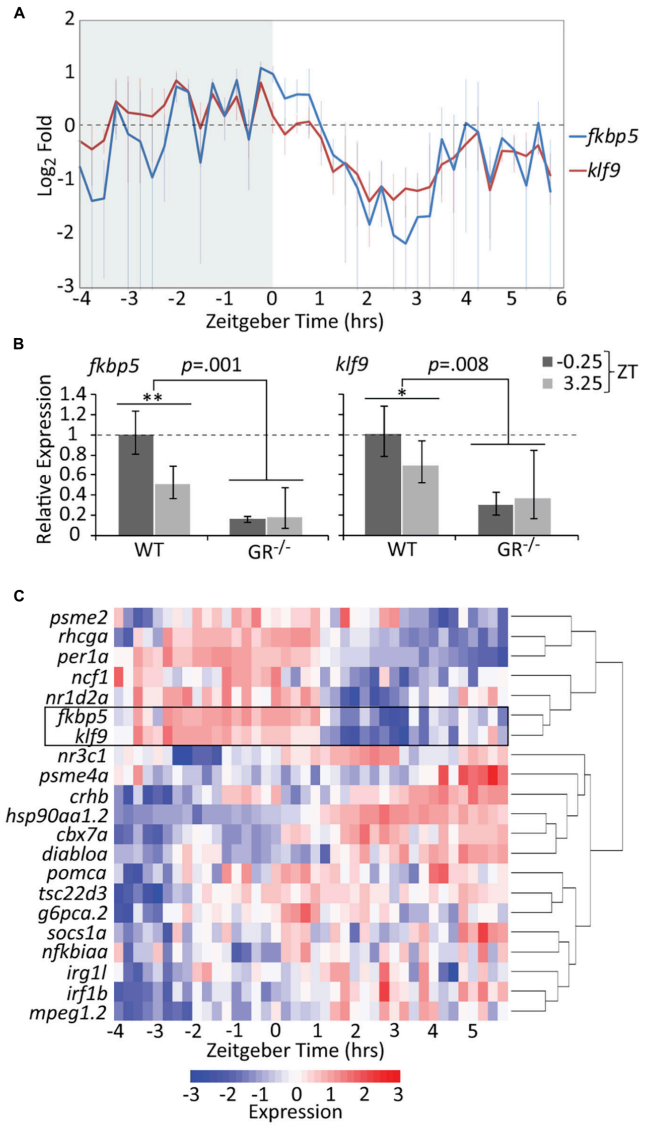


**FIGURE 1 |** The temporal activities of the GR targets *klf9* and *fkbp5* are dynamic and synchronous. **(A)** Average relative levels of *klf9* and *fkbp5* transcripts in three biological replicates of pooled ($n$ = 3–6) 5 dpf larvae snap-frozen every 15 min from −4 to 6 h zeitgeber time (ZT). Error bars are standard error of the mean of three biological replicates. **(B)** Relative expression of *klf9* and *fkbp5* in WT and *nr3c1*$^{-/-}$ (GR$^{369-}$, Gans et al., 2020) mutant larvae at −0.25 and +3.25 ZT, time points that, respectively, correspond to the activity peak and nadir of both genes in WT larvae. Error bars represent 95% confidence intervals of three biological replicates of pooled larvae ($n$ = 9 per sample). Significance calculated by two-factor (time and genotype) ANOVA, and one-tailed $t$-tests to assess the effect of time within each genotype; $^{**}p$ = 0.01; $^{*}p$ = 0.05. **(C)** Heat map of expression of *klf9*, *fkbp5*, and additional targets/regulators of glucocorticoid (GC) signaling as measured on the NanoString platform. Gene panel includes well-known glucocorticoid receptor (GR) targets as well as targets identified by our lab as consistently over-expressed in chronic CORT treated (Gans et al., 2020). Counts data are normalized to reference genes (*actb2*, *rpl13a*, and *eif5a*) and scaled within each gene to normalize for different absolute levels of expression.

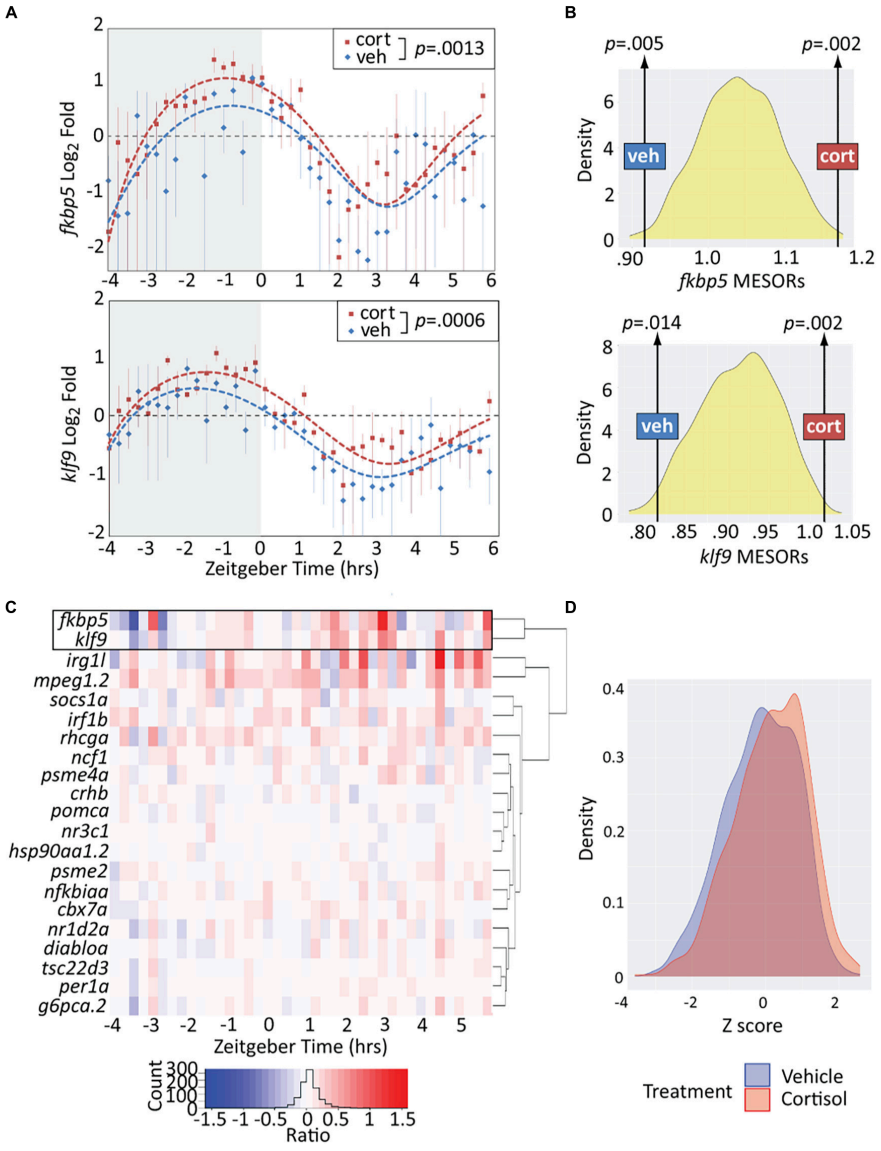


**FIGURE 2 |** Chronic cortisol treatment similarly upregulates *klf9* and *fkbp5*. **(A)** Sinusoid models fit to *fkbp5* (top) and *klf9* (bottom) qPCR relative expression data. Each data point represents the average of three biological replicates of pooled larvae (3–6 larvae per pooled sample; VEH-treated datapoints are the same as in **Figure 1**). *P*-values calculated using paired *t*-test (data paired at each timepoint). Fit of the model to the data was tested by ANOVA ($P < 0.0001$ in each case, see **Supplementary Figure 2**). **(B)** Distributions of Midline Estimated Statistics Of Rhythmicity (MESORs, a rhythm-adjusted mean) of datasets generated by randomly selecting expression data from VEH or CORT samples at each timepoint in experiments shown in panel **(A)**. MESORs of VEH and CORT datasets sit at either extreme. **(C)** Heat map of the expression ratio in CORT/VEH samples (log2 transformed) of *klf9*, *fkbp5*, and other targets of glucocorticoid (GC) signaling in our Nanostring data set. **(D)** Density plot of Z-scored expression of all genes measured with Nanostring indicates an overall increase in expression due to chronic CORT treatment.

generated 1,000 time series in which either VEH or CORT measurements were randomly selected at each timepoint in the experimental data. We then fit sinusoid models to each randomized time series. Each sinusoid equation includes five constants (see section "Materials and Methods"), including the Midline Estimating Statistic Of Rhythm (MESOR, a rhythm-adjusted mean value). For both *fkbp5* and *klf9*, the MESORs of models fit to either VEH or CORT experimental data were located at opposite extremes of approximately normal distributions of MESORs from all randomized models ($p < 0.02$, **Figure 2B**), providing confirmation that chronic CORT exposure produced a statistically significant increase in *klf9* and *fkbp5* transcript levels.

Finally, to determine how the response of *klf9* and *fkbp5* to chronic CORT compares to that of the other GR targets in our NanoString panel we calculated the expression ratio of CORT- to VEH-treated samples at each timepoint for each gene. The CORT response of *klf9* and *fkbp5* was correlated, clustering separately from that of all other genes and manifesting a stronger effect than most (**Figure 2C**). The immune genes *mpeg1.2* and *irg1l* responded similarly in magnitude, but with different timing (rising rather than falling after ZT 0). The overall effect of the treatment across all genes was a subtle increase in transcript levels (**Figure 2D**).

## Krüppel-Like Factor 9 Negatively Regulates *fkbp5* and Binds *fkbp5* Promoter-Proximal Chromatin

We performed additional time-courses to compare *fkbp5* mRNA levels in WT and *klf9*$^{-/-}$ larvae. Absent Klf9, the diurnal oscillation in *fkbp5* activity was conserved, but *fkbp5* activity was elevated on average (**Figure 3A**, $p = 0.007$, paired *t*-test), and sinusoid models fit to both WT and *klf9*$^{-/-}$ time-course data indicated a significant elevation of the *fkbp5* MESOR in the mutants (**Figure 3B** and **Supplementary Figure 5**). In addition, the circa-dawn peak of *fkbp5* activity was delayed by ∼35 min in *klf9*$^{-/-}$ larvae, occurring ∼30 min before lights-on in WT but several minutes after lights-on in mutants, and the time from peak to nadir was subsequently compressed from ∼3 h in WT to ∼2 h in mutants (**Supplementary Figure 6**). Combining chronic CORT treatment with the *klf9*$^{-/-}$ mutation cumulatively increased *fkbp5* transcript levels, which were further increased by inhibiting Fkbp5 activity with FK506 (as expected due to loss of Fkbp5-mediated inhibition of the GR), although the magnitude of the latter effect was lower in *klf9*$^{-/-}$ larvae (**Supplementary Figure 7**).

The qRT-PCR data described above suggested that Klf9 negatively regulates *fkbp5*. To determine if Klf9 physically interacts with *fkbp5*, we performed ChIP-qPCR using primers encompassing putative Klf9 binding motifs identified via JASPAR in the *fkbp5* promoter region (**Figure 3C** and **Supplementary Figure 8**). A commercial anti-Klf9 antibody recovered significantly more *fkbp5* promoter region DNA than did a non-specific IgG, and this signal was reduced in *klf9*$^{-/-}$ mutants (**Supplementary Figure 9**). However, the commercial antibody recognizes an amino acid sequence that is conserved in zebrafish Klf13. We therefore constructed a new zebrafish CRISPR line in which a C-terminal AM epitope tag was introduced into the endogenous *klf9* locus (**Supplementary Figure 10** and **Supplementary Methods**), allowing us to perform Klf9-specific ChIP with the anti-AM antibody. This antibody produced a *fkbp5* ChIP-qPCR signal specific to chromatin from the AM-tagged line (**Figure 3D**). Together these data indicate that Klf9 interacts physically with the *fkbp5* promoter region.

Because our previous gene ontology analysis suggested that Klf9 regulates steroid metabolism (Gans et al., 2020), we also asked whether the elevation of *fkbp5* transcripts observed in *klf9*$^{-/-}$ larvae might be due to mutants having higher endogenous cortisol levels. We did not, however, detect any difference in either baseline cortisol concentration or diurnal variation in 5 dpf *klf9*$^{-/-}$ larvae, and in fact the cortisol response to an acute stressor was if anything decreased in mutants (**Supplementary Figure 4**). Thus, the elevated *fkbp5* activity in *klf9*$^{-/-}$ larvae is unlikely to be due to systemically elevated cortisol.

While Klf9 has been implicated in both transcriptional activation and repression in different contexts (Mitchell and Dimario, 2010), it functions predominantly as a repressor in mouse hippocampus, where it binds promoter-proximal DNA enriched for circadian E-Box motifs (Knoedler et al., 2017). HOMER motif enrichment analysis of 149 genes consistently upregulated by chronic CORT (Gans et al., 2020) revealed that 86% of those genes had promoter-proximal KLF and circadian E-Box motifs (while only 46% had glucocorticoid response elements, **Supplementary Figure 11** and **Supplementary Table 2**), with *fkbp5* having E-boxes at +154 and −1,840 bp. As the N-terminal domain of mammalian Klf9 interacts with the Sin3a histone de-acetylation complex (Zhang et al., 2001), we hypothesized Klf9 might repress *fkbp5* via de-acetylation of histone H3 at the *fkbp5* promoter. Using an antibody to H3K14ac and ChIP-qPCR, we found a ∼threefold increase in *fkbp5* promoter DNA recovery in *klf9*$^{-/-}$ larvae compared with WT ($p < 0.05$, **Figure 3E**). This provides additional evidence that Klf9 directly represses *fkbp5*, forming a circuit predicted to regulate GR activity dynamics through a combination of Fkbp5-mediated negative feedback and Klf9-mediated incoherent feed-forward regulatory logic (**Figure 3F**).

## Loss of *klf9* Decreases Oxygen Consumption Rate and Alters Metabolic Gene Expression

The GR, Fkbp5, and Klf9 have all been previously implicated in the regulation of metabolism. To ask if loss of Klf9 affects metabolism in developing zebrafish, we first measured the OCR of 1 dpf embryos and found a 10% decrease in *klf9*$^{-/-}$ mutants compared to WT (**Figure 4A** and **Supplementary Figure 12**). We also found a significant interaction between genotype and chronic CORT treatment, which decreased OCR in WT but not mutant larvae, although OCR was still significantly decreased in the mutants compared to WT under chronic CORT (**Figure 4A** and **Supplementary Figure 12**).

For additional insight we interrogated our published RNA-seq dataset comparing WT and *klf9*$^{-/-}$ larvae (Gans et al., 2020) by

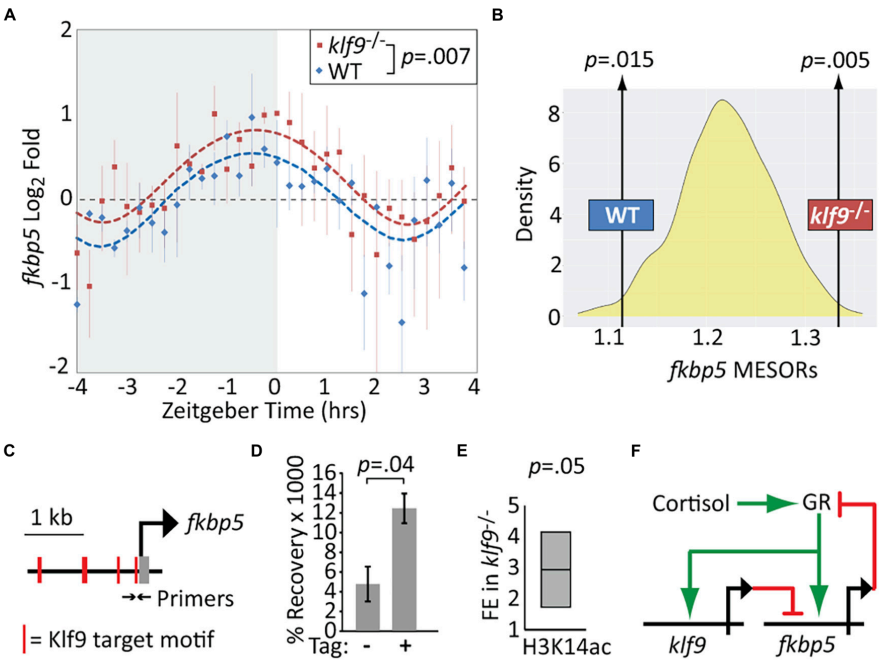


**FIGURE 3 |** Krüppel-like factor 9 (Klf9) regulates *fkbp5*. **(A)** Sinusoid modeling of *fkbp5* time-course data obtained by quantitative reverse transcription and polymerase chain reaction (qRT-PCR) of RNA extracted from wildtype (WT) and *klf9*$^{-/-}$ larvae. Each data point represents the average of three biological replicates of pooled larvae. *P*-value calculated by paired *t*-test (data paired at each timepoint). Error bars represent standard error of the mean. Model fits tested by ANOVA ($P < 0.0001$, see **Supplementary Figure 4**). **(B)** Distribution of Midline Estimated Statistics Of Rhythmicity (MESORs) of datasets generated by random sampling as described in **Figure 2** and Methods. MESORs of measured WT and *klf9*$^{-/-}$ data sit at either extreme. **(C)** Schematic of putative Klf9 target motifs in the *fkbp5* promoter region. Black arrows indicate sites of primers used in panels **(D,E)**. **(D)** Recovery of *fkbp5* promoter DNA from WT (-) and Klf9-AM tagged (+) larvae by ChIP with anti-AM tag antibody. **(E)** Fold enrichment (FE) of *fkbp5* promoter DNA recovered in *klf9*$^{-/-}$ mutants with ChIP using antibody to acetyled-H3K14. **(F)** Proposed gene regulatory circuit containing the glucocorticoid receptor (GR), *fkbp5*, and *klf9*. Activation is denoted by green arrows, repression by red lines.

performing a focused principal component analysis (PCA) on two gene lists (**Supplementary Table 3**) comprising targets of Hif1 and AMPK signaling, which respectively regulate glycolysis and oxidative metabolism. These gene lists were previously shown to accurately reflect changes in metabolic phenotype of cancer cells, which rely more heavily on glycolysis as they become more malignant (i.e., the Warburg Effect) (Jia et al., 2019). The first principal components (PC) of both datasets (respectively, accounting for 28 and 27% of the variance) represented the effect of chronic CORT treatment, and plotting them against each other reveals correlation between the two pathways (**Supplementary Figure 13A**). Top genes contributing to AMPK PC1 included insulin regulator *mafa* at the VEH pole, while the CORT-treated pole was weighted by the GC target *g6pca*, two members of the stress-responsive *gadd45* family, and *acadm*, which encodes a catalyst of mitochondrial beta-oxidation. Klf9$^{-/-}$ mutant samples showed a shift away from the CORT pole of AMPK PC1, suggesting less influence of CORT on expression of these genes in mutants. Plotting PC1 vs. PC2 within either the Hif1 or AMPK dataset segregated the samples by treatment and genotype (**Supplementary Figure 13B**). Hif1 PC2 (12% of variance) segregated WT from *klf9*$^{-/-}$ mutant samples; examples of genes at either end of this axis included the Hif1a regulator *egln3*, upregulated in mutants (**Figure 4B**), and *eprs1*, downregulated in mutants. Lactate dehydrogenase (*ldha*), a noted Hif1 target (Lee et al., 2015; Cui et al., 2017), was also upregulated in *klf9*$^{-/-}$ mutants (**Figure 4B**). Wild-type samples spanned AMPK PC2 (19% of variance), whereas *klf9*$^{-/-}$ samples were restricted to one pole (**Supplementary Figure 13B**), indicating less variation in expression in mutants of these genes, which included *pck1* and *pck2*.

We previously reported that genes involved in glycolysis and pyruvate metabolism were reciprocally regulated in *klf9*$^{-/-}$ and GR$^{-/-}$ mutants, being upregulated in the former and downregulated in the latter (Gans et al., 2020). KEGG pathway analysis of the full set of genes significantly affected in *klf9*$^{-/-}$ larvae under all conditions (FDR $q < 0.05$, **Supplementary Table 4**) showed enrichment for genes involved

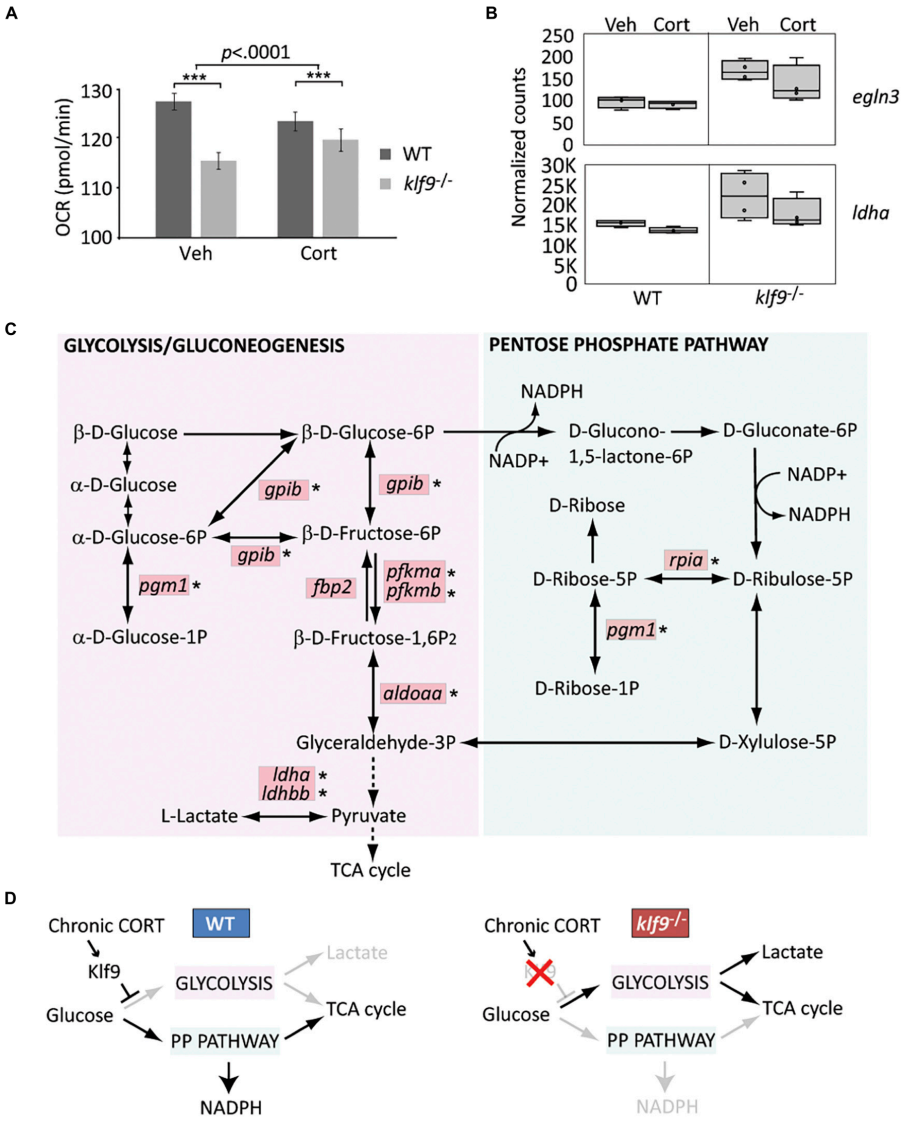


**FIGURE 4 |** *Klf9* regulates metabolism. **(A)** Oxygen consumption rate (OCR) at 1 dpf, as measured by Seahorse XF96 extracellular flux analyzer. The averages of three experimental replicates are shown, each with 20 embryos per condition measured individually and simultaneously over the course of at least 85 min (thus $n = 60$ total for each condition). The bars represent the average Y-intercept of linear fits of the averaged time-course data (see **Supplementary Figure 12**), ±standard error. Two-way ANOVA indicated significant effects of both genotype (WT vs. $klf9^{-/-}$, $p < 0.0001$) and treatment (VEH vs. CORT, $p = 0.04$), as well as a significant interaction ($p < 0.0001$). ***Adjusted $p < 0.0001$ by Šídák's multiple comparisons test. **(B)** Normalized counts of Hif1a target *egln3* and glycolytic gene *ldha* (from Gans et al., 2020). **(C)** Krüppel-like factor 9 (Klf9) downregulates multiple genes in the glycolysis/gluconeogenesis pathway. Red boxes indicate genes significantly over expressed (FDR < 0.05) in RNA-seq of $klf9^{-/-}$ larvae compared to wild type (Gans et al., 2020). Asterisks denote genes in which putative Klf9 binding sites were identified using HOMER. **(D)** Model for Klf9-mediated regulation of metabolic flux. In response to stress, Klf9 is predicted to inhibit glycolysis, shunting flux through the Pentose Phosphate Pathway (PPP).

in glycolysis/gluconeogenesis as well as the adjacent pentose phosphate pathway (PPP) (**Figure 4C**, FDR < 0.01). We further parsed this by separate Gene Ontology comparisons between WT and *klf9*$^{-/-}$ larvae in VEH or chronic CORT conditions. Processes up-regulated in CORT-treated *klf9*$^{-/-}$ vs. CORT-treated WT larvae again included glycolysis and pyruvate metabolism (**Supplementary Figure 14** and **Supplementary Table 4**), while processes upregulated in mutants under VEH conditions were instead largely involved in innate immunity as reported previously (Gans et al., 2020). These data suggest that chronic CORT exposure activates a metabolic stress response that unmasks the role of Klf9 in regulating genes involved in glycolysis and related processes. We used HOMER to look for enriched transcription factor binding motifs within 2,000 bp of the transcription start site (TSS) of genes upregulated in mutants treated with CORT. The consensus motif for Klf9 was the highest scoring motif on the list (**Supplementary Figure 14**), and seven of the top ten were highly similar binding motifs for other KLF factors that Klf9 could also be expected to bind (Ilsley et al., 2017). Notably, except for *fbp2*, all the glycolytic and PPP genes overexpressed in *klf9*$^{-/-}$ mutants had potential KLF sites (**Figure 4C**). In contrast, genes downregulated in mutants showed no enrichment for KLF motifs, and were instead enriched for motifs for IRFs, HNF4a, CREB5, and the retinoic acid receptor. These data suggest that Klf9 functions predominantly as a repressor as previously reported (Knoedler et al., 2017), leading us to hypothesize that it regulates metabolism in part by repressing glycolytic genes, with a predicted effect of shunting flux through the PPP (**Figure 4D**). Further studies are required to test this hypothesis, using ChIP to assay Klf9 binding to putative KLF sites in metabolic genes, and analysis of metabolites to test predicted effects of *klf9* mutation.

## DISCUSSION

We have shown that in zebrafish the GC-responsive genes *klf9* and *fkbp5* are expressed with synchronous oscillatory dynamics that are distinct from those of other GC-responsive genes we examined. *FKBP5* is a gene of high biomedical interest given its role in GR regulation, maladaptation to stress, and mental and metabolic health (Hausl et al., 2019; Zimmer et al., 2020). *Klf9* has also been linked to a maladaptive stress response (Besnard et al., 2018), and our results suggest that the GR, *klf9*, and *fkbp5* comprise a "hardwired" genetic circuit. *FKBP5* was previously reported to be repressed by KLF9 in human epidermis (Sporl et al., 2012), and we show here that loss of Klf9 function in zebrafish leads to elevated *fkbp5* transcript levels and hyperacetylation of chromatin at the *fkbp5* promoter, and that Klf9 physically associates with that chromatin, supporting that *fkbp5* is a target of Klf9-mediated repression. The proposed GR-*klf9*-*fkbp5* regulatory circuit (**Figure 3F**) combines negative feedback and incoherent feedforward loops, motifs predicted to facilitate adaptation to repeated or chronic stimuli (Ma et al., 2009; Shi et al., 2017; Alon, 2019). Further study is necessary to test this hypothesis and explore its ramifications for specific cell and tissue types under different conditions affecting GC signaling, and to determine how the transcript dynamics reported here relate to protein dynamics.

The evidence reported here and in our previous study (Gans et al., 2020) that *klf9* both responds to and regulates GC signaling, together with our observation that *klf9*$^{-/-}$ mutants have reduced OCR at 1 dpf and increased expression of glycolytic genes at 5 dpf, suggests that *klf9* is instrumental in regulating metabolism and metabolic responses to cortisol (Denver et al., 1999; Bagamasbad et al., 2015; Pabona et al., 2015). Repression of glycolytic genes by Klf9 fits with its reported inhibition of growth and regeneration (Apara et al., 2017; Galvao et al., 2018) and regulation of stem-cell metabolism (Cvoro et al., 2015) and could also contribute to its role in tumor suppression (Sun et al., 2014; Zhong et al., 2018), given the reliance of cancer cells on glycolysis. Shunting flux through the PPP is predicted to increase NADPH, which fits with the known role of Klf9 as a regulator of redox homeostasis (Zucker et al., 2014). It is important to emphasize, however, that we do not yet know the mechanisms underlying the effects of either the *klf9*$^{-/-}$ mutation or chronic CORT on the OCR in 1 dpf embryos. A previous study reported that morpholino knockdown of *klf9* disrupts erythropoiesis in zebrafish (Zhang et al., 2017), suggesting decreased OCR in *klf9*$^{-/-}$ larvae could result from a deficit in red blood cells. However, in that study primitive hematopoiesis was unaffected, and no differences observed prior to 2 dpf (whereas we measured OCR at 1 dpf), which makes that explanation unlikely. While our gene expression results suggest that loss of *klf9* function produces a metabolic shift toward glycolysis, those results were obtained in 5 dpf larvae, and may not be directly relatable to the differences in OCR observed at 1 dpf, given the significant development that occurs between 1 and 5 dpf. Our results are nonetheless consistent with evidence of cell autonomous metabolic regulation in mice, where over-expression of *klf9* increased oxygen consumption and the number of mitochondria in cultured adipocytes (Fan et al., 2020). Similarly, elimination of *fkbp5* elevates resting metabolic rate while protecting against obesity and increasing glucose tolerance (Balsevich et al., 2017). *FKBP5* expression and blood glucose/insulin resistance are positively correlated in humans (Sidibeh et al., 2018), and a mutation causing elevated *FKBP5* is associated with reduced weight loss following bariatric surgery (Pena et al., 2020).

Induction of hepatic *klf9* by dexamethasone promotes gluconeogenesis and hyperglycemia via PPAR activation, while *klf9* knockout animals display hypoglycemia (Cui et al., 2019). PPAR promotes PPP flux as well as *de novo* lipogenesis (Summermatter et al., 2010). Interestingly, we found that promoters of genes under-expressed in *klf9*$^{-/-}$ mutants are enriched for sequence motifs recognized by the retinoic acid receptor, known to dimerize with PPAR (Keller et al., 1993). Lipid signaling may be an indirect means by which Klf9 regulates gene expression, which may account for the enrichment for IRF motifs among genes upregulated by CORT treatment in WT but not *klf9*$^{-/-}$ larvae (Gans et al., 2020) as lipid signaling regulates interferon levels (Hara et al., 2003; Den Brok et al., 2018). The Klf9-dependency of GC-induced immune gene expression (Gans et al., 2020) may be secondary to metabolic differences in *klf9*$^{-/-}$

mutants, as reactive oxygen species, disruption of glycolytic flux, and the accompanying drop in NADH promote inflammasome activation (Sanman et al., 2016; Yang et al., 2019). Further studies are required to test these possibilities.

## DATA AVAILABILITY STATEMENT

The datasets presented in this study can be found in online repositories. The names of the repository/repositories and accession number(s) can be found below: https://www.ncbi.nlm.nih.gov/, GSE144885.

## ETHICS STATEMENT

The animal study was reviewed and approved by the Institutional Animal Use and Care Committee, MDI Biological Laboratory.

## AUTHOR CONTRIBUTIONS

IG and JC: conceptualization, writing—original draft, and visualization. IG, RB, NJ, and JC: methodology and writing—review and editing. IG, JG, and RB: investigation. NJ: resources. JC and NJ: supervision. JC: project administration and funding acquisition. All authors contributed to the article and approved the submitted version.

## FUNDING

Funding and infrastructure support for this work was provided by grants from the National Institutes of Health (R03-HD099468, P20-GM104318, and P20-GM103423) and the MDI Biological Laboratory.

## ACKNOWLEDGMENTS

We thank Joel Graber (MDI Biological Laboratory) for helpful discussions and advice on the analysis of gene expression data.

## SUPPLEMENTARY MATERIAL

The Supplementary Material for this article can be found online at: https://www.frontiersin.org/articles/10.3389/fcell.2021.727037/full#supplementary-material

## REFERENCES

Alon, U. (2019). *An Introduction to Systems Biology: Design Principles of Biological Circuits*, 2nd Edn. London: Chapman and Hall. doi: 10.1201/9780429283321

Alsop, D., and Vijayan, M. M. (2008). Development of the corticosteroid stress axis and receptor expression in zebrafish. *Am. J. Physiol. Regul. Integr. Comp. Physiol.* 294, R711–R719. doi: 10.1152/ajpregu.00671.2007

Apara, A., Galvao, J., Wang, Y., Blackmore, M., Trillo, A., Iwao, K., et al. (2017). KLF9 and JNK3 interact to suppress axon regeneration in the adult CNS. *J. Neurosci.* 37, 9632–9644. doi: 10.1523/JNEUROSCI.0643-16.2017

Bagamasbad, P., Ziera, T., Borden, S. A., Bonett, R. M., Rozeboom, A. M., Seasholtz, A., et al. (2012). Molecular basis for glucocorticoid induction of the Kruppel-like factor 9 gene in hippocampal neurons. *Endocrinology* 153, 5334–5345. doi: 10.1210/en.2012-1303

Bagamasbad, P. D., Bonett, R. M., Sachs, L., Buisine, N., Raj, S., Knoedler, J. R., et al. (2015). Deciphering the regulatory logic of an ancient, ultraconserved nuclear receptor enhancer module. *Mol. Endocrinol.* 29, 856–872. doi: 10.1210/me.2014-1349

Balsevich, G., Hausl, A. S., Meyer, C. W., Karamihalev, S., Feng, X., Pohlmann, M. L., et al. (2017). Stress-responsive FKBP51 regulates AKT2-AS160 signaling and metabolic function. *Nat. Commun.* 8:1725. doi: 10.1038/s41467-017-01783-y

Besnard, A., Langberg, T., Levinson, S., Chu, D., Vicidomini, C., Scobie, K. N., et al. (2018). Targeting Kruppel-like factor 9 in excitatory neurons protects against chronic stress-induced impairments in dendritic spines and fear responses. *Cell Rep.* 23, 3183–3196. doi: 10.1016/j.celrep.2018.05.040

Binder, E. B. (2009). The role of FKBP5, a co-chaperone of the glucocorticoid receptor in the pathogenesis and therapy of affective and anxiety disorders. *Psychoneuroendocrinology* 34(Suppl. 1), S186–S195. doi: 10.1016/j.psyneuen.2009.05.021

Binder, E. B., Salyakina, D., Lichtner, P., Wochnik, G. M., Ising, M., Putz, B., et al. (2004). Polymorphisms in FKBP5 are associated with increased recurrence of depressive episodes and rapid response to antidepressant treatment. *Nat. Genet.* 36, 1319–1325. doi: 10.1038/ng1479

Bonett, R. M., Hu, F., Bagamasbad, P., and Denver, R. J. (2009). Stressor and glucocorticoid-dependent induction of the immediate early gene kruppel-like factor 9: implications for neural development and plasticity. *Endocrinology* 150, 1757–1765. doi: 10.1210/en.2008-1441

Chinenov, Y., Coppo, M., Gupte, R., Sacta, M. A., and Rogatsky, I. (2014). Glucocorticoid receptor coordinates transcription factor-dominated regulatory network in macrophages. *BMC Genomics* 15:656. doi: 10.1186/1471-2164-15-656

Cui, A., Fan, H., Zhang, Y., Zhang, Y., Niu, D., Liu, S., et al. (2019). Dexamethasone-induced Kruppel-like factor 9 expression promotes hepatic gluconeogenesis and hyperglycemia. *J. Clin. Invest.* 130, 2266–2278. doi: 10.1172/JCI66062

Cui, X. G., Han, Z. T., He, S. H., Wu, X. D., Chen, T. R., Shao, C. H., et al. (2017). HIF1/2alpha mediates hypoxia-induced LDHA expression in human pancreatic cancer cells. *Oncotarget* 8, 24840–24852. doi: 10.18632/oncotarget.15266

Cvoro, A., Devito, L., Milton, F. A., Noli, L., Zhang, A., Filippi, C., et al. (2015). A thyroid hormone receptor/KLF9 axis in human hepatocytes and pluripotent stem cells. *Stem Cells* 33, 416–428. doi: 10.1002/stem.1875

Den Brok, M. H., Raaijmakers, T. K., Collado-Camps, E., and Adema, G. J. (2018). Lipid droplets as immune modulators in myeloid cells. *Trends Immunol.* 39, 380–392. doi: 10.1016/j.it.2018.01.012

Denny, W. B., Valentine, D. L., Reynolds, P. D., Smith, D. F., and Scammell, J. G. (2000). Squirrel monkey immunophilin FKBP51 is a potent inhibitor of glucocorticoid receptor binding. *Endocrinology* 141, 4107–4113. doi: 10.1210/endo.141.11.7785

Denver, R. J., Ouellet, L., Furling, D., Kobayashi, A., Fujii-Kuriyama, Y., and Puymirat, J. (1999). Basic transcription element-binding protein (BTEB) is a thyroid hormone-regulated gene in the developing central nervous system. Evidence for a role in neurite outgrowth. *J. Biol. Chem.* 274, 23128–23134. doi: 10.1074/jbc.274.33.23128

Dickmeis, T., Lahiri, K., Nica, G., Vallone, D., Santoriello, C., Neumann, C. J., et al. (2007). Glucocorticoids play a key role in circadian cell cycle rhythms. *PLoS Biol.* 5:e78. doi: 10.1371/journal.pbio.0050078

Fan, H., Zhang, Y., Zhang, J., Yao, Q., Song, Y., Shen, Q., et al. (2020). Cold-inducible Klf9 regulates thermogenesis of brown and beige fat. *Diabetes* 69, 2603–2618. doi: 10.2337/db19-1153

Frøland Steindal, I. A., and Whitmore, D. (2019). Circadian clocks in fish-what have we learned so far? *Biology (Basel)* 8:17. doi: 10.3390/biology8010017

Galvao, J., Iwao, K., Apara, A., Wang, Y., Ashouri, M., Shah, T. N., et al. (2018). The Kruppel-like factor gene target dusp14 regulates axon growth and regeneration. *Invest. Ophthalmol. Vis. Sci.* 59, 2736–2747. doi: 10.1167/iovs.17-23319

Gans, I., Hartig, E. I, Zhu, S., Tilden, A., Hutchins, L., Maki, N., et al. (2020). Klf9 is a key feedforward regulator of the transcriptomic response to glucocorticoid receptor activity. *Sci. Rep.* 10:11415. doi: 10.1038/s41598-020-68040-z

Geiss, G. K., Bumgarner, R. E., Birditt, B., Dahl, T., Dowidar, N., Dunaway, D. L., et al. (2008). Direct multiplexed measurement of gene expression with color-coded probe pairs. *Nat. Biotechnol.* 26, 317–325. doi: 10.1038/nbt1385

Griffiths, B. B., Schoonheim, P. J., Ziv, L., Voelker, L., Baier, H., and Gahtan, E. (2012). A zebrafish model of glucocorticoid resistance shows serotonergic modulation of the stress response. *Front. Behav. Neurosci.* 6:68. doi: 10.3389/fnbeh.2012.00068

Hara, Y., Miura, S., Komoto, S., Inamura, T., Koseki, S., Watanabe, C., et al. (2003). Exposure to fatty acids modulates interferon production by intraepithelial lymphocytes. *Immunol. Lett.* 86, 139–148. doi: 10.1016/S0165-2478(03)00007-5

Hartig, E. I., Zhu, S., King, B. L., and Coffman, J. A. (2016). Cortisol-treated zebrafish embryos develop into pro-inflammatory adults with aberrant immune gene regulation. *Biol. Open* 5, 1134–1141. doi: 10.1242/bio.020065

Hartig, E. I, Zhu, S., King, B. L., and Coffman, J. A. (2020). Chronic cortisol exposure in early development leads to neuroendocrine dysregulation in adulthood. *BMC Res. Notes* 13:366. doi: 10.1186/s13104-020-05208-w

Hausl, A. S., Balsevich, G., Gassen, N. C., and Schmidt, M. V. (2019). Focus on FKBP51: a molecular link between stress and metabolic disorders. *Mol. Metab.* 29, 170–181. doi: 10.1016/j.molmet.2019.09.003

Ilsley, M. D., Gillinder, K. R., Magor, G. W., Huang, S., Bailey, T. L., Crossley, M., et al. (2017). Kruppel-like factors compete for promoters and enhancers to fine-tune transcription. *Nucleic Acids Res.* 45, 6572–6588. doi: 10.1093/nar/gkx441

Jasper, M. S., and Engeland, W. C. (1991). Synchronous ultradian rhythms in adrenocortical secretion detected by microdialysis in awake rats. *Am. J. Physiol.* 261, R1257–R1268. doi: 10.1152/ajpregu.1991.261.5.R1257

Jia, D., Lu, M., Jung, K. H., Park, J. H., Yu, L., Onuchic, J. N., et al. (2019). Elucidating cancer metabolic plasticity by coupling gene regulation with metabolic pathways. *Proc. Natl. Acad. Sci. U. S. A.* 116, 3909–3918. doi: 10.1073/pnas.1816391116

Juszczak, G. R., and Stankiewicz, A. M. (2018). Glucocorticoids, genes and brain function. *Prog. Neuropsychopharmacol. Biol. Psychiatry* 82, 136–168. doi: 10.1016/j.pnpbp.2017.11.020

Keller, H., Dreyer, C., Medin, J., Mahfoudi, A., Ozato, K., and Wahli, W. (1993). Fatty acids and retinoids control lipid metabolism through activation of peroxisome proliferator-activated receptor-retinoid X receptor heterodimers. *Proc. Natl. Acad. Sci. U. S. A.* 90, 2160–2164. doi: 10.1073/pnas.90.6.2160

Kemmer, G., and Keller, S. (2010). Nonlinear least-squares data fitting in Excel spreadsheets. *Nat. Protoc.* 5, 267–281. doi: 10.1038/nprot.2009.182

Klengel, T., Mehta, D., Anacker, C., Rex-Haffner, M., Pruessner, J. C., Pariante, C. M., et al. (2012). Allele-specific FKBP5 DNA demethylation mediates gene-childhood trauma interactions. *Nat. Neurosci.* 16, 33–41. doi: 10.1038/nn.3275

Klevecz, R. R., Bolen, J., Forrest, G., and Murray, D. B. (2004). A genomewide oscillation in transcription gates DNA replication and cell cycle. *Proc. Natl. Acad. Sci. U. S. A.* 101, 1200–1205. doi: 10.1073/pnas.0306490101

Knoedler, J. R., and Denver, R. J. (2014). Kruppel-like factors are effectors of nuclear receptor signaling. *Gen. Comp. Endocrinol.* 203, 49–59. doi: 10.1016/j.ygcen.2014.03.003

Knoedler, J. R., Subramani, A., and Denver, R. J. (2017). The Kruppel-like factor 9 cistrome in mouse hippocampal neurons reveals predominant transcriptional repression via proximal promoter binding. *BMC Genomics* 18:299. doi: 10.1186/s12864-017-3640-7

Lee, D. C., Sohn, H. A., Park, Z. Y., Oh, S., Kang, Y. K., Lee, K. M., et al. (2015). A lactate-induced response to hypoxia. *Cell* 161, 595–609. doi: 10.1016/j.cell.2015.03.011

Li, H., Su, P., Lai, T. K., Jiang, A., Liu, J., Zhai, D., et al. (2020). The glucocorticoid receptor-FKBP51 complex contributes to fear conditioning and posttraumatic stress disorder. *J. Clin. Invest.* 130, 877–889. doi: 10.1172/JCI130363

Lili, L. N., Klopot, A., Readhead, B., Baida, G., Dudley, J. T., and Budunova, I. (2019). Transcriptomic network interactions in human skin treated with topical glucocorticoid clobetasol propionate. *J. Invest. Dermatol.* 139, 2281–2291. doi: 10.1016/j.jid.2019.04.021

Lindeman, L. C., Vogt-Kielland, L. T., Alestrom, P., and Collas, P. (2009). Fish'n ChIPs: chromatin immunoprecipitation in the zebrafish embryo. *Methods Mol. Biol.* 567, 75–86. doi: 10.1007/978-1-60327-414-2_5

Liu, Y., Tsinoremas, N. F., Johnson, C. H., Lebedeva, N. V., Golden, S. S., Ishiura, M., et al. (1995). Circadian orchestration of gene expression in cyanobacteria. *Genes Dev.* 9, 1469–1478. doi: 10.1101/gad.9.12.1469

Lloyd, D., and Murray, D. B. (2005). Ultradian metronome: timekeeper for orchestration of cellular coherence. *Trends Biochem. Sci.* 30, 373–377. doi: 10.1016/j.tibs.2005.05.005

Ma, W., Trusina, A., El-Samad, H., Lim, W. A., and Tang, C. (2009). Defining network topologies that can achieve biochemical adaptation. *Cell* 138, 760–773. doi: 10.1016/j.cell.2009.06.013

Mitchell, D. L., and Dimario, J. X. (2010). Bimodal, reciprocal regulation of fibroblast growth factor receptor 1 promoter activity by BTEB1/KLF9 during myogenesis. *Mol. Biol. Cell* 21, 2780–2787. doi: 10.1091/mbc.e10-04-0290

Morbiato, E., Frigato, E., Dinarello, A., Maradonna, F., Facchinello, N., Argenton, F., et al. (2019). Feeding entrainment of the zebrafish circadian clock is regulated by the glucocorticoid receptor. *Cells* 8:1342. doi: 10.3390/cells8111342

Nesan, D., and Vijayan, M. M. (2013). Role of glucocorticoid in developmental programming: evidence from zebrafish. *Gen. Comp. Endocrinol.* 181, 35–44. doi: 10.1016/j.ygcen.2012.10.006

Pabona, J. M., Zhang, D., Ginsburg, D. S., Simmen, F. A., and Simmen, R. C. (2015). Prolonged pregnancy in women is associated with attenuated myometrial expression of progesterone receptor co-regulator Kruppel-like Factor 9. *J. Clin. Endocrinol. Metab.* 100, 166–174. doi: 10.1210/jc.2014-2846

Pena, E., Caixas, A., Arenas, C., Rigla, M., Crivilles, S., Cardoner, N., et al. (2020). Role of the FKBP5 polymorphism rs1360780, age, sex, and type of surgery in weight loss after bariatric surgery: a follow-up study. *Surg. Obes. Relat. Dis.* 16, 581–589. doi: 10.1016/j.soard.2019.12.002

Pereira, M. J., Palming, J., Svensson, M. K., Rizell, M., Dalenback, J., Hammar, M., et al. (2014). FKBP5 expression in human adipose tissue increases following dexamethasone exposure and is associated with insulin resistance. *Metabolism* 63, 1198–1208. doi: 10.1016/j.metabol.2014.05.015

Sacta, M. A., Chinenov, Y., and Rogatsky, I. (2016). Glucocorticoid signaling: an update from a genomic perspective. *Annu. Rev. Physiol.* 78, 155–180. doi: 10.1146/annurev-physiol-021115-105323

Sanman, L. E., Qian, Y., Eisele, N. A., Ng, T. M., Van Der Linden, W. A., Monack, D. M., et al. (2016). Disruption of glycolytic flux is a signal for inflammasome signaling and pyroptotic cell death. *Elife* 5:e13663. doi: 10.7554/eLife.13663.040

Scammell, J. G., Denny, W. B., Valentine, D. L., and Smith, D. F. (2001). Overexpression of the FK506-binding immunophilin FKBP51 is the common cause of glucocorticoid resistance in three New World primates. *Gen. Comp. Endocrinol.* 124, 152–165. doi: 10.1006/gcen.2001.7696

Shi, W., Ma, W., Xiong, L., Zhang, M., and Tang, C. (2017). Adaptation with transcriptional regulation. *Sci. Rep.* 7:42648. doi: 10.1038/srep42648

Sidibeh, C. O., Pereira, M. J., Abalo, X. M., J Boersma, G., Skrtic, S., Lundkvist, P., et al. (2018). FKBP5 expression in human adipose tissue: potential role in glucose and lipid metabolism, adipogenesis and type 2 diabetes. *Endocrine* 62, 116–128. doi: 10.1007/s12020-018-1674-5

Silverman, M. N., and Sternberg, E. M. (2012). Glucocorticoid regulation of inflammation and its functional correlates: from HPA axis to glucocorticoid receptor dysfunction. *Ann. N. Y. Acad. Sci.* 1261, 55–63. doi: 10.1111/j.1749-6632.2012.06633.x

Spiga, F., Waite, E. J., Liu, Y., Kershaw, Y. M., Aguilera, G., and Lightman, S. L. (2011). ACTH-dependent ultradian rhythm of corticosterone secretion. *Endocrinology* 152, 1448–1457. doi: 10.1210/en.2010-1209

Sporl, F., Korge, S., Jurchott, K., Wunderskirchner, M., Schellenberg, K., Heins, S., et al. (2012). Kruppel-like factor 9 is a circadian transcription factor in human epidermis that controls proliferation of keratinocytes. *Proc. Natl. Acad. Sci. U. S. A.* 109, 10903–10908. doi: 10.1073/pnas.1118641109

Stavreva, D. A., Wiench, M., John, S., Conway-Campbell, B. L., Mckenna, M. A., Pooley, J. R., et al. (2009). Ultradian hormone stimulation induces glucocorticoid receptor-mediated pulses of gene transcription. *Nat. Cell Biol.* 11, 1093–1102. doi: 10.1038/ncb1922

Summermatter, S., Baum, O., Santos, G., Hoppeler, H., and Handschin, C. (2010). Peroxisome proliferator-activated receptor {gamma} coactivator 1{alpha}

(PGC-1{alpha}) promotes skeletal muscle lipid refueling *in vivo* by activating de novo lipogenesis and the pentose phosphate pathway. *J. Biol. Chem.* 285, 32793–32800. doi: 10.1074/jbc.M110.145995

Sun, J., Wang, B., Liu, Y., Zhang, L., Ma, A., Yang, Z., et al. (2014). Transcription factor KLF9 suppresses the growth of hepatocellular carcinoma cells *in vivo* and positively regulates p53 expression. *Cancer Lett.* 355, 25–33. doi: 10.1016/j.canlet.2014.09.022

Thisse, B., and Thisse, C. (2004). *Fast Release Clones: A High Throughput Expression Analysis (ZFIN Direct Data Submission)*. Available online at: http://zfin.org (accessed March, 2021).

Tu, B. P., Kudlicki, A., Rowicka, M., and Mcknight, S. L. (2005). Logic of the yeast metabolic cycle: temporal compartmentalization of cellular processes. *Science* 310, 1152–1158. doi: 10.1126/science.1120499

Veldhuis, J. D., Iranmanesh, A., Lizarralde, G., and Johnson, M. L. (1989). Amplitude modulation of a burstlike mode of cortisol secretion subserves the circadian glucocorticoid rhythm. *Am. J. Physiol.* 257, E6–E14. doi: 10.1152/ajpendo.1989.257.1.E6

Walker, J. J., Spiga, F., Waite, E., Zhao, Z., Kershaw, Y., Terry, J. R., et al. (2012). The origin of glucocorticoid hormone oscillations. *PLoS Biol.* 10:e1001341. doi: 10.1371/journal.pbio.1001341

Walker, J. J., Terry, J. R., and Lightman, S. L. (2010). Origin of ultradian pulsatility in the hypothalamic-pituitary-adrenal axis. *Proc. Biol. Sci.* 277, 1627–1633. doi: 10.1098/rspb.2009.2148

Warnes, G. R., Bolker, B., Bonebakker, L., Gentleman, R., Huber, W., Liaw, A., et al. (2020). *gplots: Various R Programming Tools for Plotting Data. R package version 3.1.1*.

Weger, B. D., Weger, M., Gorling, B., Schink, A., Gobet, C., Keime, C., et al. (2016). Extensive regulation of diurnal transcription and metabolism by glucocorticoids. *PLoS Genet.* 12:e1006512. doi: 10.1371/journal.pgen.1006512

Windle, R. J., Wood, S. A., Lightman, S. L., and Ingram, C. D. (1998). The pulsatile characteristics of hypothalamo-pituitary-adrenal activity in female Lewis and Fischer 344 rats and its relationship to differential stress responses. *Endocrinology* 139, 4044–4052. doi: 10.1210/endo.139.10.6238

Yang, Y., Wang, H., Kouadir, M., Song, H., and Shi, F. (2019). Recent advances in the mechanisms of NLRP3 inflammasome activation and its inhibitors. *Cell Death Dis.* 10:128. doi: 10.1038/s41419-019-1413-8

Zhang, J. S., Moncrieffe, M. C., Kaczynski, J., Ellenrieder, V., Prendergast, F. G., and Urrutia, R. (2001). A conserved alpha-helical motif mediates the interaction of Sp1-like transcriptional repressors with the corepressor mSin3A. *Mol. Cell Biol.* 21, 5041–5049. doi: 10.1128/MCB.21.15.5041-5049.2001

Zhang, Y., Xue, Y., Cao, C., Huang, J., Hong, Q., Hai, T., et al. (2017). Thyroid hormone regulates hematopoiesis via the TR-KLF9 axis. *Blood* 130, 2161–2170. doi: 10.1182/blood-2017-05-783043

Zhong, Z., Zhou, F., Wang, D., Wu, M., Zhou, W., Zou, Y., et al. (2018). Expression of KLF9 in pancreatic cancer and its effects on the invasion, migration, apoptosis, cell cycle distribution, and proliferation of pancreatic cancer cell lines. *Oncol. Rep.* 40, 3852–3860. doi: 10.3892/or.2018.6760

Zimmer, C., Hanson, H. E., Wildman, D. E., Uddin, M., and Martin, L. B. (2020). FKBP5: a key mediator of how vertebrates flexibly cope with adversity. *BioScience* 70, 1127–1138. doi: 10.1093/biosci/biaa114

Zucker, S. N., Fink, E. E., Bagati, A., Mannava, S., Bianchi-Smiraglia, A., Bogner, P. N., et al. (2014). Nrf2 amplifies oxidative stress via induction of Klf9. *Mol. Cell* 53, 916–928. doi: 10.1016/j.molcel.2014.01.033

**Conflict of Interest:** The authors declare that the research was conducted in the absence of any commercial or financial relationships that could be construed as a potential conflict of interest.

**Publisher's Note:** All claims expressed in this article are solely those of the authors and do not necessarily represent those of their affiliated organizations, or those of the publisher, the editors and the reviewers. Any product that may be evaluated in this article, or claim that may be made by its manufacturer, is not guaranteed or endorsed by the publisher.

## APPENDIX C: Potential CRISPR off-target sites

See Table 2.3 for sgRNA sequences and additional information.

**Table C.1. Klf9KO sgRNA 1 off-target sites**

| Sequence | PAM | Score | Gene | Chromosome | Strand | Position | Mis-matches |
|---|---|---|---|---|---|---|---|
| TTGATCCAGTGCATACTGAG | GAG | 1.39 | | chr1 | -1 | 50582045 | 3 |
| TTAAACCAATGCATGCCGAG | GGG | 1.10 | | chr4 | -1 | 15420023 | 2 |
| TATTACAAGTGCATACCGAG | TGG | 0.95 | | chr8 | -1 | 52995421 | 4 |
| TCAAAACTGTGCATACAGAG | CAG | 0.43 | | chr11 | -1 | 35102185 | 4 |
| TGAAACCTGTGTATACCGAC | CAG | 0.43 | | chr2 | 1 | 54743967 | 4 |
| TCAAAGCAGGGCATACTGAG | TAG | 0.41 | | chr23 | 1 | 41249467 | 4 |
| TTGAGCCAGTCCATACTGAG | CGG | 0.40 | | chr18 | -1 | 10385571 | 4 |
| TTAACCCAGTGCACACCGAC | TGG | 0.24 | | chr21 | -1 | 6365654 | 3 |
| TTAACCCAGTACATACTGAA | AGG | 0.17 | | chr23 | 1 | 31365669 | 4 |
| TTAATCCAGCGCATATGGAG | AGG | 0.11 | myo7ab, ENSDARG00000044632 | chr21 | 1 | 22245912 | 4 |
| TTAAAACAGAACATACCAAG | CGG | 0.10 | dazap1, ENSDARG00000070846 | chr11 | -1 | 5905518 | 4 |
| TTAAACCTGTGTATTCCGAA | TGG | 0.09 | | chr5 | 1 | 58900669 | 4 |
| TTAAACAAGGACATATCGAG | AAG | 0.09 | | chr12 | -1 | 3548030 | 4 |
| TTAAACCAGTGGATAAAGAG | GAG | 0.08 | | chr1 | -1 | 7945585 | 3 |
| TTACACCAGTGCATTCAGTG | AAG | 0.06 | | chr22 | -1 | 9772098 | 4 |
| TTACACCAGTACACACAGAG | CAG | 0.06 | | KN150170.1 | -1 | 54995 | 4 |
| TTACACCAGTACACACAGAG | CAG | 0.06 | | KN150170.1 | 1 | 45707 | 4 |
| TCAAACCAGTGAATTCCCAG | TGG | 0.05 | | chr25 | 1 | 30424616 | 4 |
| TTAAAAGAGTGGAAACCGAG | AGG | 0.05 | | chr19 | 1 | 37933226 | 4 |
| TTAAATCAGTACATACAAAG | AAG | 0.04 | | chr23 | -1 | 6204750 | 4 |
| TTTAATCAGTGCATATCCAG | TAG | 0.04 | | chr21 | -1 | 7935277 | 4 |
| TTATACCAGTGCATGCGCAG | TGG | 0.04 | | chr11 | 1 | 10931038 | 4 |
| TTAAATCAGTTCATCCCAAG | AAG | 0.03 | | chr13 | -1 | 10069399 | 4 |
| TTAAACCAGTCAAAACAGAG | GAG | 0.02 | | chr2 | -1 | 36536373 | 4 |
| TTAAACCAGTAAAAACAGAG | AAG | 0.02 | | chr2 | -1 | 36384951 | 4 |
| TTAATCCAGTGCAGAATGAG | AGG | 0.02 | | chr10 | 1 | 42844656 | 4 |
| TTAAACAAGTGCGGACCCAG | GAG | 0.01 | neflb, ENSDARG00000012426 | chr8 | -1 | 6833529 | 4 |
| TTAAACCAGTGCAGCCCGTA | TGG | 0.01 | | chr23 | -1 | 35879759 | 4 |

**Table C.2. Klf9KO sgRNA 2 off-target sites**

| Sequence | PAM | Score | Gene | Chromosome | Strand | Position | Mis-matches |
|---|---|---|---|---|---|---|---|
| TAGAATAGAGGACAGTGATG | GAG | 1.75 | march4, ENSDARG00000056439 | chr9 | -1 | 52999944 | 3 |
| GCAAATTGTGCACAGTGATG | AAG | 1.07 | | chr17 | -1 | 26480391 | 3 |
| TCTAATTTTGGACAGTGATG | TAG | 1.02 | | chr1 | 1 | 40067265 | 4 |
| GCTGATAGCTGACAGTGATG | TGG | 0.85 | | chr15 | -1 | 24458602 | 4 |
| GCTTGTAGTGTACAGTGATG | CAG | 0.83 | | chr8 | 1 | 3843612 | 4 |
| GTGATTAGTATACAGTGATG | CAG | 0.82 | | chr1 | 1 | 22959459 | 4 |
| TAAAATAGTGGACAGTGAAG | AAG | 0.63 | | chr5 | 1 | 44479790 | 4 |
| GCGCATTGATGACAGTGATG | GAG | 0.56 | | chr7 | 1 | 65626771 | 4 |
| TCGAACATTGAACAGTGATG | AGG | 0.54 | | chr18 | -1 | 50831979 | 4 |
| GGGATCAGTGAACAGTGATG | AAG | 0.52 | | chr12 | -1 | 12226909 | 4 |
| GGGAATAGTGGAGAGTGAAG | CAG | 0.52 | | chr9 | -1 | 46496463 | 3 |
| ACGAATAATGGCCAGTGATT | TAG | 0.45 | | chr19 | 1 | 34558856 | 4 |
| GTGAAAAATGGACAGTTATG | CAG | 0.43 | | chr19 | -1 | 25059156 | 4 |
| GTAAATAGTGGACAGTAATT | TGG | 0.38 | | chr2 | -1 | 52959026 | 4 |
| GCGCATAGAAGACAGTAATG | GAG | 0.38 | | chr1 | 1 | 58004851 | 4 |
| ATGAATAGTGGTGAGTGATG | AGG | 0.35 | | chr5 | 1 | 5343706 | 4 |
| GCTAATTGAGGACAGTGATT | CAG | 0.34 | | chr14 | -1 | 48367352 | 4 |
| CTGAATAATGGACAGAGATG | TAG | 0.33 | | chr2 | 1 | 32227090 | 4 |
| GGCAGTAGTGGACAGAGATG | CAG | 0.31 | | chr25 | -1 | 13642619 | 4 |
| GTGAATACTGCACACTGATG | AGG | 0.26 | | chr5 | 1 | 70484864 | 4 |
| GAGAAGAGTGTAAAGTGATG | CGG | 0.22 | | chr10 | 1 | 27616110 | 4 |
| GCCAGTAGTGGACACTTATG | CAG | 0.20 | | chr6 | 1 | 22411830 | 4 |
| GAGAATAGAGTACATTGATG | AAG | 0.16 | | chr16 | 1 | 23821989 | 4 |
| CCGAAAAGTGGACAATGATA | AGG | 0.16 | | chr17 | -1 | 11918474 | 4 |
| GCGAATATTGGATTGTGATG | AGG | 0.15 | | chr16 | -1 | 9038433 | 3 |
| GGGAATAGAGGATAGTGAGG | GGG | 0.15 | | chr2 | 1 | 12328104 | 4 |
| ACAAATAGTGGACAGAGAAG | TGG | 0.13 | | chr1 | -1 | 45746355 | 4 |
| GCGAAAGGTGGAGAGTGATT | AAG | 0.13 | | chr9 | -1 | 33790807 | 4 |
| GAGAATAATGGAAAGAGATG | GAG | 0.12 | | chr18 | 1 | 46438335 | 4 |
| GCAAACAGTGGACATTGAAG | TGG | 0.10 | | chr9 | 1 | 40413648 | 4 |

**Table C.2. Klf9KO sgRNA2 off-target sites, continued**

| | | | | | | | |
|---|---|---|---|---|---|---|---|
| GTGAATAGTGGTCAGTGTTT | TAG | 0.09 | | chr8 | -1 | 50831964 | 4 |
| GCGTATAATGGACAAAGATG | TGG | 0.08 | | chr9 | 1 | 33465561 | 4 |
| GCGAATTGTGGACAGGGGTG | GGG | 0.07 | | chr6 | 1 | 16454219 | 3 |
| GCGATTAGGGGATAGGGATG | AGG | 0.07 | | chr16 | -1 | 24737366 | 4 |
| GCAAATAGGGGAAGGTGATG | TGG | 0.06 | | chr10 | 1 | 5192439 | 4 |
| GCGAATTGTGTTCAGAGATG | AAG | 0.05 | | chr8 | -1 | 52940901 | 4 |
| GTGAACAGTGGACAGGGGTG | GAG | 0.04 | | chr20 | 1 | 48806402 | 4 |
| ACGAATAGTGGAACGTGAAG | AAG | 0.04 | exoc3l1, ENSDARG00000051899 | chr25 | -1 | 14334531 | 4 |
| GCGAATAGTGGAGTCTGATG | TGG | 0.04 | tjp1a, ENSDARG00000077506 | chr7 | 1 | 30840581 | 3 |
| GCGAATGGTGAACACTGCTG | GAG | 0.03 | topbp1, ENSDARG00000059322 | chr24 | 1 | 9566552 | 4 |
| GCGTATAGTGGAGAGGGGTG | GGG | 0.02 | | chr7 | 1 | 22447071 | 4 |
| GCGAATAGTCGACAGAGGTC | AAG | 0.02 | | chr13 | -1 | 38213982 | 4 |
| GCGAATAATGGAATGGGATG | TGG | 0.02 | | chr21 | 1 | 11344215 | 4 |

**Table C.3. Klf9KO sgRNA3 off-target sites**

| Sequence | PAM | Score | Gene | Chromosome | Strand | Position | Mis-matches |
|---|---|---|---|---|---|---|---|
| GGCCCTGCTGTATACTGGGG | AAG | 0.53 | | chr18 | 1 | 15128210 | 4 |
| TAACCTGGAGCATAGTGGGA | AGG | 0.27 | unc80, ENSDARG00000098290 | chr6 | 1 | 16415320 | 4 |
| GAGACTGGAGCCTACAGGGG | GAG | 0.16 | | chr1 | -1 | 37789854 | 4 |
| GAAACTGGAGCATGCTGGGA | AGG | 0.13 | dla, ENSDARG00000010791 | chr1 | 1 | 53363035 | 4 |
| GACTCTGGGGCAGATTGGGG | CGG | 0.11 | lin54, ENSDARG00000063194 | chr10 | 1 | 11389791 | 4 |
| GACACTGGAGATTACAGGGG | AAG | 0.08 | | chr3 | -1 | 1198556 | 4 |
| GTCACTGGAGCATTATGGGG | TGG | 0.08 | mylipa, ENSDARG00000008859 | chr19 | 1 | 26785321 | 4 |
| GAACCTGGAGCAGAGTTGGG | TGG | 0.07 | pygo2, ENSDARG00000036772 | chr19 | -1 | 7712407 | 4 |
| GACCCTGTAGCTTAGTGGTG | GGG | 0.07 | | chr4 | -1 | 38103190 | 4 |
| AACCCTGGAGCAGAATGGAG | GAG | 0.07 | | chr20 | 1 | 41205917 | 4 |
| GACTCTGGAGCTGACTGCGG | GAG | 0.07 | aspscr1, ENSDARG00000105321 | chr11 | 1 | 44178745 | 4 |
| GACACTGGGGCATTCTGGTG | AGG | 0.06 | | chr5 | -1 | 54471849 | 4 |
| GACCGTAGAGCATCCTGAGG | GAG | 0.04 | | chr18 | 1 | 23171560 | 4 |
| GACACTGGCGCATGCTGAGG | TGG | 0.03 | | chr3 | 1 | 55301187 | 4 |
| GACCCTGGAGCTAATTGGGA | AAG | 0.03 | | chr1 | -1 | 7091712 | 4 |
| GACTCTGGAGCAGAGCGGGG | CAG | 0.03 | | chr2 | -1 | 25743421 | 4 |
| GACCCTGGAGAAGAGTGAGG | GAG | 0.02 | | chr16 | 1 | 54775970 | 4 |
| GACCCTGGTGCATGCCGTGG | AAG | 0.00 | sf1, ENSDARG00000008188 | chr7 | -1 | 22547505 | 4 |

**Table C.4. Klf9KO sgRNA4 off-target sites**

| Sequence | PAM | Score | Gene | Chromosome | Strand | Position | Mis-matches |
|---|---|---|---|---|---|---|---|
| GACGTCACCCTGGAGCAGAC | TGG | 0.48 | ambra1a, ENSDARG00000008322 | chr7 | -1 | 39081293 | 3 |
| CATGTGACCCTGGAGCACAC | AGG | 0.38 | | chr15 | 1 | 239606 | 4 |
| GGCCTGAAACTGGAGCATTC | TGG | 0.36 | | chr3 | 1 | 13020230 | 4 |
| GGTGAAACCCTGGAGAATAC | TAG | 0.18 | | chr5 | 1 | 65835640 | 4 |
| AGTGTGACCCTGGAGCTGAC | CAG | 0.17 | fat3, ENSDARG00000087709 | chr10 | -1 | 25150717 | 4 |
| GGCGTGATCATGGAGCACAA | TGG | 0.14 | | chr3 | -1 | 43723877 | 4 |
| GCAGTGACCCTGGTGCTTAC | CAG | 0.12 | | chr2 | 1 | 34419117 | 4 |
| GGCGTGAGGCTGGAGCTCAC | TGG | 0.08 | | chr15 | 1 | 43718923 | 4 |
| GGCGTCTCCCTGAAGCAGAC | TGG | 0.06 | dna2, ENSDARG00000078759 | chr13 | -1 | 22706024 | 4 |
| GGTGTGACCCTATTGCATAC | CAG | 0.05 | | chr16 | -1 | 52738608 | 4 |
| GGCTTGACCCTGGAGTCTGC | AAG | 0.04 | | chr10 | 1 | 44951491 | 4 |
| GGCGTGGCCCTGGAGCGCAG | CGG | 0.04 | ext1c, ENSDARG00000035649 | chr19 | 1 | 47741824 | 4 |
| GGCGAGACCCTGGAGTGTTC | CGG | 0.04 | btbd11b, ENSDARG00000063040 | chr18 | -1 | 15132443 | 4 |
| GGCGCGACCCTGGGGCGCAC | CGG | 0.02 | tnfrsf11b, ENSDARG00000098377 | chr19 | -1 | 142284 | 4 |
| GGCGTGACCTTGGAGGTCAC | GAG | 0.02 | | chr1 | -1 | 38830460 | 4 |

**Table C.5. AM Tag sgRNA1 off-target sites**

| Sequence | PAM | Score | Gene | Chromo-some | Strand | Position | Mis-matches |
|---|---|---|---|---|---|---|---|
| TCGAACGATCAGATGTCTGC | AGG | 1.44 | | chr9 | 1 | 16880566 | 3 |
| TTCAGTGATCATATGTATGC | TGG | 0.89 | fat2, ENSDARG00000018923 | chr14 | 1 | 25807239 | 3 |
| TGCTGCGCTCAGATGTCTGC | TGG | 0.81 | | chr17 | -1 | 7801999 | 4 |
| TCGGACGATCAAATGTCTGC | TGG | 0.75 | | chr4 | -1 | 26262567 | 4 |
| TCGGACGATCAGATGTCTGC | AGG | 0.75 | | chr20 | 1 | 14592014 | 4 |
| TATAGCGATAATATGTATGC | AAG | 0.69 | | chr2 | 1 | 1294802 | 4 |
| AACAGCAATCATATGTCTGT | CGG | 0.63 | | chr7 | 1 | 10081441 | 4 |
| TTGAGCGATCATTTGTCTGA | CAG | 0.36 | | chr14 | -1 | 34423761 | 4 |
| TCCACCGTTCATATGTGTGT | AGG | 0.32 | insrb, ENSDARG00000071524 | chr22 | 1 | 10898254 | 4 |
| CCCAGGGACCAGATGTCTGC | TGG | 0.30 | map3k5, ENSDARG00000005416 | chr20 | 1 | 3013368 | 4 |
| TGCAGCGACCTTATGTGTGC | GAG | 0.24 | | chr5 | 1 | 42207105 | 4 |
| TGCAGCGATTGTATTTCTGC | TAG | 0.24 | | chr17 | 1 | 1589175 | 4 |
| ACCAGAGATCATATGTTTGA | CAG | 0.23 | | chr19 | 1 | 39883391 | 4 |
| TCCAGCTGTCAGATGTGTGC | AAG | 0.21 | | chr5 | 1 | 71407460 | 4 |
| TCCAGTGTTCTTCTGTCTGC | TAG | 0.20 | | chr10 | -1 | 23489733 | 4 |
| TCCAGTGGTCAGATGTGTGC | CAG | 0.19 | | chr6 | 1 | 15933697 | 4 |
| GGCAGCCATCATAAGTCTGC | AAG | 0.18 | | chr19 | -1 | 26566866 | 4 |
| TCAAGCGTTCATATCTCTTC | AGG | 0.17 | | chr7 | -1 | 24437192 | 4 |
| TCCAGCTCTCATTTGTATGC | TAG | 0.17 | | chr1 | 1 | 45630345 | 4 |
| GCCAGGGATCTTATATCTGC | GGG | 0.17 | | chr17 | -1 | 28546492 | 4 |
| TCTAGCGTTCCTATGGCTGC | CAG | 0.17 | | chr4 | -1 | 24998619 | 4 |
| TCTAGCGATCAGATGTGTGA | TGG | 0.16 | | chr25 | 1 | 5469868 | 4 |
| TCCAGACATCCTGTGTCTGC | AGG | 0.13 | apex1, ENSDARG00000045843 | chr4 | 1 | 5329265 | 4 |
| TCCTGCGATCCTGTGTCTTC | CAG | 0.13 | | chr6 | -1 | 55116913 | 4 |
| TCCAGGGATTAAATATCTGC | CGG | 0.12 | | chr21 | -1 | 2788088 | 4 |
| TCCAGCGAATATGTTTCTGC | GAG | 0.09 | si:dkeyp-110a12.4, ENSDARG00000087784 | chr17 | 1 | 7451124 | 4 |
| TCCAGCGGTAATAAGTATGC | CAG | 0.08 | shroom2, ENSDARG00000076416 | chr6 | -1 | 30385658 | 4 |
| TCCAGTGTTCATTTGACTGC | TGG | 0.07 | | chr16 | -1 | 2985346 | 4 |
| TCCAGCGATGCTATGGCTGT | CAG | 0.06 | si:ch211-152f22.2, ENSDARG00000104543 | chr12 | 1 | 37096021 | 4 |
| TCCAGCCATCCTGTGCCTGC | GAG | 0.04 | | chr25 | 1 | 14734610 | 4 |
| TCCAGCTGTCATACGTCCGC | AAG | 0.03 | | chr25 | -1 | 16295689 | 4 |
| TCCAGGGTTCATACGGCTGC | TGG | 0.03 | | chr6 | 1 | 59925865 | 4 |
| TCCAGGGATCATCTGCATGC | CAG | 0.03 | cth1, ENSDARG00000057328 | chr7 | -1 | 17697972 | 4 |
| TCCAGCGATCATATACATGA | AGG | 0.01 | sidt2, ENSDARG00000045976 | chr15 | -1 | 47064334 | 4 |

## APPENDIX D: Klf9 AM-tag CRISPR design

This appendix contains sequences of oligos used with CRISPR/Cas9 to synthesize templates for short guide RNA (sgRNA) transcription and homologous recombination (HR), used to insert an AM-tag sequence in frame at the end of the coding region of Klf9 exon 2. Fusion PCR protocol for template synthesis is included the end of this appendix.

### PART I: HR TEMPLATE SEQUENCES

**Klf9 c-terminal sequence (CODING/noncoding):**
AGACGACACTCTTCAACATCCACATCCTCCTCTGGCTCCAGCGATCATATGTCTGCTGGTGTTTAAGCAttt
tgactgtcctcctacctgacacaacacgttcaggagtctctgctagtgagttggtg

**+ Strand sgRNA Target:**
TCCAGCGATCATATGTCTGCTGG

**- Strand sgRNA Target:**
cctcctacctgacacaacacgtt
(aacgtgttgtgtcaggtagg agg

**AM Tag Seq (102bp):**

TGCCAAGATCCTCAACGCAAAGGCAACGTGATACTCTCTCAGGCTTACGGGTGCCAAGATCCTCAACGC
AAAGGCAACGTGATACTCTCTCAGGCTTACTAG

**HR full template sequence (primers) (designed mutations to avoid CRISPR re-editing) (228bp):**

AGACGACACTCTTCAACATCCACATCCTCCTCTGGCTCCAGCGATCAAATGagcGCTGGTGTTTGCCAAGA
TCCTCAACGCAAAGGCAACGTGATACTCTCTCAGGCTTACGGGTGCCAAGATCCTCAACGCAAAGGCAA
CGTGATACTCTCTCAGGCTTACTAAGCAttttgactgtcTctcctacctgacacaacacgttcaggagtctctgctagtgagtt
ggtg

**Partial HR template oligos to anneal:**

FWD ("klf9AMtemp FWD"):
AGA CGA CAC TCT TCA ACA TCC ACA TCC TCC TCT GGC TCC AGC GAT CAA ATG agc GCT GGT GTT
TGC CAA GAT CCT CAA CGC AAA GGC AAC GTG ATA CTC TCT CAG GCT TAC GGG TGC CAA GAT
CCT CAA CGC AAA GGC AAC GTG ATA CTC TCT CAG GC Tm=71.6C

RVS (“klf9AMtemp RVS”):
cac caa ctc act agc aga gac tcc tga acg tgt tgt gtc agg tag gag Aga cag tca aaa TGC TTA GTA AGC CTG AGA GAG TAT CAC GTT GCC Tm=70.9C

*(Reverse complement of:*
*GGCAACGTGATACTCTCTCAGGCTTACTAAGCAttttgactgtcTctcctacctgacacaacacgttcaggagtctctgct agtgagttggtg)*

overlap region Tm=59.5C
GGC AAC GTG ATA CTC TCT CAG GC

**PART II: GUIDE RNA SYNTHESIS**

**Constant Antisense Scaffold Oligo (FE modified, i.e. Flipped A-U pair and Extended hairpin):**
AAAAGCACCGACTCGGTGCCACTTTTTCAAGTTGATAACGGACTAGCCTTATTTAAACTTGCTATGCTGTT TCCAGCATAGCTCTTAAAC

**Short Guide Oligo w/ T7 promoter for RNA polymerase (overlap with constant scaffold):**

Generic:
GTAATACGACTCACTATAGG**NNNNNNNNNNNNNNNNNNN**GTTTAAGAGCTATGCTGGAA

Guide 1:
GTA ATA CGA CTC ACT ATA GGT CCA GCG ATC ATA TGT CTG CGT TTA AGA GCT ATG CTG GAA

Guide 2:
GTA ATA CGA CTC ACT ATA GGa acg tgt tgt gtc agg tag gGT TTA AGA GCT ATG CTG GAA

Full-length gRNA template = 130 bp, amplification optimal TA=63ºC

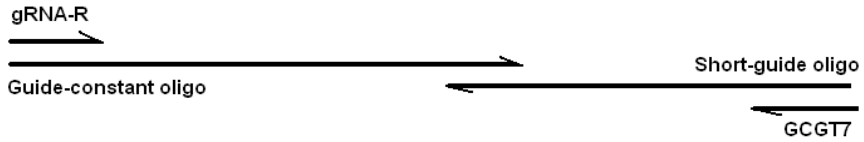

**PART III: FUSION PCR PROTOCOL**

**Mix:**

| | |
|---|---|
| 10 x PCR buffer | 5 µl |
| 10-100 nM short-guide oligo | 1 µl (final conc. 0.2-2 nM) |
| 10-100 nM constant oligo | 1 µl (final conc. 0.2-2 nM) |
| 10 µM dNTP | 1.5 µl |
| 25 mM MgCl2 | 4 µl |
| DMSO | 1.5 µl |
| Taq pol (NEB) | 0.75 µl |
| H2O | 30.25 µl |
| | 45 µl |

**Annealing:**

| | |
|---|---|
| 95 ºC | 10 second |
| 95 ºC to 85 ºC | -2 ºC /second |
| 85 ºC to 40 ºC | -0.1 ºC /second |
| 40 ºC | 10 second |
| 63 ºC | 1 min |

**Add:**

| | |
|---|---|
| 5 µM primer F | 2.5 µl (final conc. 250 nM) |
| 5 µM primer R | 2.5 µl (final conc. 250 nM) |

**Amplification**:

| | | |
|---|---|---|
| 95 ºC | 1 min | |
| 95 ºC | 15 sec | x 40 cycles |
| 62 ºC | 30 sec | |
| 68 ºC | 20 sec | |
| 68 ºC | 5 min | |

Note that similar fusion protocol is used for sgRNA and HR templates. sgRNA template is subsequently used with T7 *in vitro* transcription kit according to manufacturer's instructions.

## APPENDIX E: GO processes dysregulated across replicate order

(i.e. WT/Klf9$^{-/-}$ RNA-seq PC1, before "batch" normalization)

**Table E.1. Processes upregulated with replicate order**

| GO Term | Upregulated Process Description | P-value | FDR q-value | Enrichment |
|---|---|---|---|---|
| GO:0006811 | ion transport | 2.09E-11 | 1.29E-07 | 1.94 |
| GO:0023052 | signaling | 2.54E-11 | 7.84E-08 | 2.62 |
| GO:0006812 | cation transport | 2.78E-11 | 5.71E-08 | 2.26 |
| GO:0065007 | biological regulation | 3.73E-10 | 5.75E-07 | 1.22 |
| GO:0030001 | metal ion transport | 1.65E-09 | 2.03E-06 | 2.28 |
| GO:0043269 | regulation of ion transport | 3.30E-09 | 3.39E-06 | 2.61 |
| GO:0034765 | regulation of ion transmembrane transport | 4.73E-09 | 4.17E-06 | 2.79 |
| GO:0007267 | cell-cell signaling | 5.08E-09 | 3.91E-06 | 2.75 |
| GO:0022610 | biological adhesion | 6.60E-09 | 4.52E-06 | 2.43 |
| GO:0007155 | cell adhesion | 6.60E-09 | 4.07E-06 | 2.43 |
| GO:0034762 | regulation of transmembrane transport | 1.15E-08 | 6.46E-06 | 2.73 |
| GO:0034220 | ion transmembrane transport | 1.30E-08 | 6.68E-06 | 2.06 |
| GO:0099536 | synaptic signaling | 1.97E-08 | 9.33E-06 | 2.72 |
| GO:0051049 | regulation of transport | 1.97E-08 | 8.69E-06 | 2.06 |
| GO:0098609 | cell-cell adhesion | 2.44E-08 | 1.00E-05 | 2.9 |
| GO:0098916 | anterograde trans-synaptic signaling | 4.05E-08 | 1.56E-05 | 2.7 |
| GO:0007268 | chemical synaptic transmission | 4.05E-08 | 1.47E-05 | 2.7 |
| GO:0050789 | regulation of biological process | 4.49E-08 | 1.54E-05 | 1.22 |
| GO:0098660 | inorganic ion transmembrane transport | 4.57E-08 | 1.48E-05 | 2.2 |
| GO:0098662 | inorganic cation transmembrane transport | 5.37E-08 | 1.66E-05 | 2.26 |
| GO:0099537 | trans-synaptic signaling | 5.49E-08 | 1.61E-05 | 2.67 |
| GO:0098655 | cation transmembrane transport | 5.64E-08 | 1.58E-05 | 2.22 |
| GO:0007154 | cell communication | 9.19E-08 | 2.47E-05 | 2.42 |
| GO:0007214 | gamma-aminobutyric acid signaling pathway | 2.41E-07 | 6.20E-05 | 14.48 |
| GO:0098742 | cell-cell adhesion via plasma-membrane adhesion molecules | 2.44E-07 | 6.03E-05 | 2.99 |
| GO:0006810 | transport | 7.49E-07 | 1.78E-04 | 1.4 |
| GO:0060078 | regulation of postsynaptic membrane potential | 1.40E-06 | 3.19E-04 | 9.11 |
| GO:0051234 | establishment of localization | 1.52E-06 | 3.34E-04 | 1.39 |
| GO:0007156 | homophilic cell adhesion via plasma membrane adhesion molecules | 1.62E-06 | 3.44E-04 | 2.95 |
| GO:0017157 | regulation of exocytosis | 2.44E-06 | 5.02E-04 | 3.14 |
| GO:0099003 | vesicle-mediated transport in synapse | 2.93E-06 | 5.84E-04 | 3.62 |
| GO:0032879 | regulation of localization | 3.18E-06 | 6.13E-04 | 1.68 |
| GO:0055085 | transmembrane transport | 4.58E-06 | 8.57E-04 | 1.74 |
| GO:0050806 | positive regulation of synaptic transmission | 4.81E-06 | 8.72E-04 | 7.08 |

**Table E.1 continued**

| GO Term | Upregulated Process Description | P-value | FDR q-value | Enrichment |
|---|---|---|---|---|
| GO:0006816 | calcium ion transport | 8.41E-06 | 1.48E-03 | 2.6 |
| GO:0099177 | regulation of trans-synaptic signaling | 1.49E-05 | 2.55E-03 | 2.67 |
| GO:0050804 | modulation of chemical synaptic transmission | 1.49E-05 | 2.48E-03 | 2.67 |
| GO:0051179 | localization | 1.56E-05 | 2.53E-03 | 1.33 |
| GO:0070838 | divalent metal ion transport | 1.70E-05 | 2.69E-03 | 2.52 |
| GO:0072511 | divalent inorganic cation transport | 1.70E-05 | 2.62E-03 | 2.52 |
| GO:0070588 | calcium ion transmembrane transport | 2.32E-05 | 3.49E-03 | 2.64 |
| GO:0050794 | regulation of cellular process | 2.45E-05 | 3.59E-03 | 1.19 |
| GO:0031114 | regulation of microtubule depolymerization | 2.65E-05 | 3.80E-03 | 10.6 |
| GO:0006898 | receptor-mediated endocytosis | 3.34E-05 | 4.69E-03 | 3.29 |
| GO:0050808 | synapse organization | 3.39E-05 | 4.65E-03 | 2.86 |
| GO:0098657 | import into cell | 3.52E-05 | 4.72E-03 | 2.12 |
| GO:0015672 | monovalent inorganic cation transport | 4.21E-05 | 5.52E-03 | 2.18 |
| GO:0007411 | axon guidance | 5.35E-05 | 6.87E-03 | 2.55 |
| GO:0006897 | endocytosis | 5.57E-05 | 7.01E-03 | 2.28 |
| GO:0010975 | regulation of neuron projection development | 5.59E-05 | 6.90E-03 | 3.52 |
| GO:0097485 | neuron projection guidance | 7.26E-05 | 8.78E-03 | 2.51 |
| GO:0099590 | neurotransmitter receptor internalization | 7.96E-05 | 9.45E-03 | 5.57 |
| GO:0051960 | regulation of nervous system development | 8.47E-05 | 9.86E-03 | 2.06 |
| GO:0060079 | excitatory postsynaptic potential | 1.05E-04 | 1.19E-02 | 8.1 |
| GO:0042391 | regulation of membrane potential | 1.51E-04 | 1.69E-02 | 2.59 |
| GO:0051963 | regulation of synapse assembly | 1.58E-04 | 1.74E-02 | 9.94 |
| GO:0010976 | positive regulation of neuron projection development | 1.67E-04 | 1.80E-02 | 5.47 |
| GO:0016192 | vesicle-mediated transport | 2.41E-04 | 2.56E-02 | 1.59 |
| GO:0045664 | regulation of neuron differentiation | 3.51E-04 | 3.67E-02 | 4.17 |
| GO:0060627 | regulation of vesicle-mediated transport | 3.71E-04 | 3.81E-02 | 2.33 |
| GO:0035249 | synaptic transmission, glutamatergic | 3.86E-04 | 3.90E-02 | 3.34 |
| GO:0019226 | transmission of nerve impulse | 3.86E-04 | 3.84E-02 | 5.46 |
| GO:0099560 | synaptic membrane adhesion | 4.07E-04 | 3.99E-02 | 78.69 |
| GO:0140238 | presynaptic endocytosis | 4.12E-04 | 3.97E-02 | 4.19 |
| GO:0048488 | synaptic vesicle endocytosis | 4.12E-04 | 3.91E-02 | 4.19 |
| GO:0048489 | synaptic vesicle transport | 4.43E-04 | 4.14E-02 | 4.61 |
| GO:0097480 | establishment of synaptic vesicle localization | 4.43E-04 | 4.08E-02 | 4.61 |
| GO:0097479 | synaptic vesicle localization | 4.43E-04 | 4.02E-02 | 4.61 |
| GO:0120035 | regulation of plasma membrane bounded cell projection organization | 5.38E-04 | 4.81E-02 | 2.97 |
| GO:0031344 | regulation of cell projection organization | 5.38E-04 | 4.74E-02 | 2.97 |
| GO:0051962 | positive regulation of nervous system development | 5.84E-04 | 5.07E-02 | 2.48 |
| GO:0120039 | plasma membrane bounded cell projection morphogenesis | 6.12E-04 | 5.24E-02 | 2.1 |

**Table E.1 continued**

| GO Term | Upregulated Process Description | P-value | FDR q-value | Enrichment |
|---|---|---|---|---|
| GO:0048858 | cell projection morphogenesis | 6.12E-04 | 5.17E-02 | 2.1 |
| GO:0048812 | neuron projection morphogenesis | 6.12E-04 | 5.10E-02 | 2.1 |
| GO:0051899 | membrane depolarization | 6.59E-04 | 5.42E-02 | 10.99 |
| GO:0086010 | membrane depolarization during action potential | 6.59E-04 | 5.35E-02 | 10.99 |
| GO:0031623 | receptor internalization | 6.76E-04 | 5.42E-02 | 3.82 |
| GO:0099072 | regulation of postsynaptic membrane neurotransmitter receptor levels | 6.77E-04 | 5.35E-02 | 3.82 |
| GO:0021517 | ventral spinal cord development | 7.38E-04 | 5.76E-02 | 13.73 |
| GO:0032990 | cell part morphogenesis | 7.56E-04 | 5.83E-02 | 2.07 |

**Table E.2. Processes downregulated with replicate order**

| GO Term | Downregulated Process Description | P-value | FDR q-value | Enrichment |
|---|---|---|---|---|
| GO:0006518 | peptide metabolic process | 2.58E-18 | 1.81E-14 | 2.74 |
| GO:0043603 | cellular amide metabolic process | 4.74E-17 | 1.67E-13 | 2.43 |
| GO:0043604 | amide biosynthetic process | 1.47E-16 | 3.45E-13 | 2.65 |
| GO:0043043 | peptide biosynthetic process | 1.73E-16 | 3.04E-13 | 2.79 |
| GO:0006412 | translation | 2.01E-16 | 2.82E-13 | 2.81 |
| GO:1901566 | organonitrogen compound biosynthetic process | 1.46E-09 | 1.71E-06 | 1.82 |
| GO:0034645 | cellular macromolecule biosynthetic process | 9.76E-09 | 9.80E-06 | 1.86 |
| GO:0044271 | cellular nitrogen compound biosynthetic process | 2.84E-08 | 2.49E-05 | 1.7 |
| GO:0009059 | macromolecule biosynthetic process | 3.21E-07 | 2.50E-04 | 1.74 |
| GO:0008544 | epidermis development | 9.66E-06 | 6.78E-03 | 6 |
| GO:0006749 | glutathione metabolic process | 2.46E-05 | 1.57E-02 | 19.45 |
| GO:0010499 | proteasomal ubiquitin-independent protein catabolic process | 4.31E-05 | 2.52E-02 | 4.92 |
| GO:0017144 | drug metabolic process | 4.46E-05 | 2.41E-02 | 2.14 |
| GO:0009058 | biosynthetic process | 7.61E-05 | 3.82E-02 | 1.39 |
| GO:0051186 | cofactor metabolic process | 7.67E-05 | 3.59E-02 | 3.95 |
| GO:0045454 | cell redox homeostasis | 8.32E-05 | 3.65E-02 | 3.61 |
| GO:0022900 | electron transport chain | 1.04E-04 | 4.28E-02 | 3.47 |
| GO:1901576 | organic substance biosynthetic process | 1.19E-04 | 4.63E-02 | 1.38 |
| GO:0044249 | cellular biosynthetic process | 1.23E-04 | 4.55E-02 | 1.4 |
| GO:0001708 | cell fate specification | 1.62E-04 | 5.68E-02 | 53.63 |
| GO:0022904 | respiratory electron transport chain | 3.45E-04 | 1.15E-01 | 3.32 |
| GO:0022618 | ribonucleoprotein complex assembly | 3.51E-04 | 1.12E-01 | 2.24 |
| GO:0009887 | animal organ morphogenesis | 3.70E-04 | 1.13E-01 | 16.74 |
| GO:0009790 | embryo development | 4.01E-04 | 1.17E-01 | 2.5 |
| GO:0051216 | cartilage development | 4.43E-04 | 1.24E-01 | 19.38 |
| GO:0071826 | ribonucleoprotein complex subunit organization | 8.93E-04 | 2.41E-01 | 2.13 |
| GO:0006123 | mitochondrial electron transport, cytochrome c to oxygen | 9.48E-04 | 2.47E-01 | 6.92 |
| GO:0019646 | aerobic electron transport chain | 9.48E-04 | 2.38E-01 | 6.92 |

## APPENDIX F: Differentially Expressed Genes in *klf9*$^{-/-}$ Larvae

### Table F.1. Upregulated genes in vehicle treated Klf9 mutants

| #geneID | Upregulated gene | base mean | log2 fold change | p-value | FDR |
|---|---|---|---|---|---|
| ENSDARG00000056386 | TMC1 | 64.14016 | 2.383065 | 1.39E-24 | 7.95E-21 |
| ENSDARG00000100095 | anxa1b | 544.7187 | 1.573788 | 1.77E-18 | 5.07E-15 |
| ENSDARG00000035018 | thy1 | 161.2853 | 1.503206 | 2.71E-18 | 6.91E-15 |
| ENSDARG00000087359 | c3a.2 | 434.3324 | 1.112235 | 2.63E-17 | 6.04E-14 |
| ENSDARG00000022832 | bnip4 | 165.7345 | 1.28385 | 3.00E-14 | 4.91E-11 |
| ENSDARG00000023656 | he1.1 | 38.54385 | 2.520366 | 3.12E-13 | 4.48E-10 |
| ENSDARG00000038559 | h1f0 | 4105.112 | 0.800699 | 4.68E-13 | 6.32E-10 |
| ENSDARG00000054058 | h1fx | 766.1531 | 0.647735 | 7.87E-11 | 8.60E-08 |
| ENSDARG00000098013 | si:ch211-130m23.5 | 121.0294 | 1.230553 | 1.90E-10 | 1.78E-07 |
| ENSDARG00000035562 | mpdu1a | 127.8187 | 0.925333 | 1.53E-09 | 1.13E-06 |
| ENSDARG00000090850 | serpina1l | 4481.798 | 0.53227 | 4.60E-09 | 2.85E-06 |
| ENSDARG00000016319 | c9 | 1767.94 | 0.684395 | 8.41E-09 | 4.82E-06 |
| ENSDARG00000011824 | pbxip1b | 886.2065 | 0.581219 | 1.58E-08 | 8.41E-06 |
| ENSDARG00000035569 | cyp1d1 | 184.3977 | 0.769169 | 2.67E-08 | 1.33E-05 |
| ENSDARG00000055705 | f5 | 349.2945 | 0.650294 | 2.63E-08 | 1.33E-05 |
| ENSDARG00000038424 | si:dkey-8k3.2 | 150.4916 | 0.789798 | 1.13E-07 | 4.99E-05 |
| ENSDARG00000116586 | zgc:92066 | 244.819 | 0.912009 | 1.76E-07 | 7.20E-05 |
| ENSDARG00000042533 | gstm.1 | 519.3929 | 0.641382 | 1.88E-07 | 7.44E-05 |
| ENSDARG00000052207 | c3a.3 | 617.9246 | 0.624885 | 3.65E-07 | 0.000135 |
| ENSDARG00000103260 | si:ch211-57b15.1 | 29.85401 | 1.557837 | 1.30E-06 | 0.00042 |
| ENSDARG00000039347 | rps24 | 41217.16 | 0.723353 | 1.38E-06 | 0.000438 |
| ENSDARG00000078618 | inpp5kb | 440.0779 | 0.480439 | 1.64E-06 | 0.000508 |
| ENSDARG00000021004 | c5 | 544.2652 | 0.529965 | 1.78E-06 | 0.000532 |
| ENSDARG00000054597 | cnot6l | 743.4654 | 0.48364 | 3.00E-06 | 0.000809 |
| ENSDARG00000103760 | cfhl2 | 142.2487 | 0.955803 | 3.18E-06 | 0.000839 |
| ENSDARG00000078114 | si:ch73-237c6.1 | 588.0229 | 0.510015 | 3.50E-06 | 0.000893 |
| ENSDARG00000035329 | capns1a | 1420.783 | 0.580403 | 4.11E-06 | 0.001026 |
| ENSDARG00000033227 | lect2l | 145.5139 | 0.788984 | 8.23E-06 | 0.001951 |
| ENSDARG00000019122 | he1.2 | 11.59556 | 2.816693 | 8.60E-06 | 0.002012 |
| ENSDARG00000112648 | si:dkeyp-82b4.2 | 70.29532 | 1.441216 | 9.35E-06 | 0.002166 |
| ENSDARG00000078411 | hspb15 | 138.3928 | 0.677401 | 9.60E-06 | 0.002201 |
| ENSDARG00000100406 | zgc:112265 | 1848.532 | 0.405696 | 1.12E-05 | 0.00251 |
| ENSDARG00000035309 | entpd3 | 205.6335 | 0.730603 | 1.20E-05 | 0.002679 |
| ENSDARG00000007024 | uox | 842.7825 | 0.486551 | 1.22E-05 | 0.002685 |
| ENSDARG00000101481 | rbp5 | 758.5103 | 0.412983 | 2.17E-05 | 0.004494 |
| ENSDARG00000095557 | BX664610.1 | 131.532 | 0.867819 | 2.47E-05 | 0.00497 |
| ENSDARG00000013561 | pgm1 | 2641.712 | 0.339989 | 2.58E-05 | 0.0051 |

**Table F.1 continued**

| #geneID | Upregulated gene | base mean | log2 fold change | p-value | FDR |
|---|---|---|---|---|---|
| ENSDARG00000092493 | si:dkeyp-44a8.2 | 1044.875 | 0.475074 | 2.70E-05 | 0.005256 |
| ENSDARG00000100442 | cfh | 251.6577 | 0.633614 | 2.79E-05 | 0.005328 |
| ENSDARG00000104654 | leap2 | 177.2018 | 0.68611 | 2.95E-05 | 0.00555 |
| ENSDARG00000057498 | habp2 | 280.4272 | 0.511818 | 3.10E-05 | 0.005786 |
| ENSDARG00000068262 | vamp5 | 144.502 | 0.716844 | 3.34E-05 | 0.006178 |
| ENSDARG00000057903 | si:ch211-266g18.10 | 2714.697 | 0.54148 | 3.51E-05 | 0.006367 |
| ENSDARG00000045947 | hrc | 1424.369 | 0.435995 | 3.59E-05 | 0.006385 |
| ENSDARG00000041060 | lgals9l3 | 86.20587 | 0.930777 | 3.68E-05 | 0.006486 |
| ENSDARG00000059883 | trpv1 | 54.15539 | 0.915727 | 3.75E-05 | 0.006563 |
| ENSDARG00000040988 | tpi1b | 7013.502 | 0.397868 | 4.39E-05 | 0.007418 |
| ENSDARG00000041257 | smtnl1 | 59.84584 | 0.908152 | 5.31E-05 | 0.008746 |
| ENSDARG00000103495 | zgc:173714 | 11.70188 | 2.30866 | 5.79E-05 | 0.009217 |
| ENSDARG00000030311 | tmc2b | 16.05267 | 1.612489 | 5.76E-05 | 0.009217 |
| ENSDARG00000052039 | caspb | 339.102 | 0.773688 | 6.05E-05 | 0.009446 |
| ENSDARG00000023111 | plg | 2405.395 | 0.431809 | 6.05E-05 | 0.009446 |
| ENSDARG00000002369 | UBB | 2047.219 | 0.362195 | 6.26E-05 | 0.009703 |
| ENSDARG00000095142 | si:ch211-208h16.4 | 91.69251 | 0.765936 | 6.46E-05 | 0.00995 |
| ENSDARG00000012776 | smarca1 | 263.219 | 0.472984 | 6.67E-05 | 0.010195 |
| ENSDARG00000053476 | lipca | 41.35953 | 1.013062 | 6.84E-05 | 0.010383 |
| ENSDARG00000103826 | gpib | 1066.238 | 0.348931 | 7.36E-05 | 0.011104 |
| ENSDARG00000093572 | lamc3 | 470.0309 | 0.414333 | 8.61E-05 | 0.012573 |
| ENSDARG00000007480 | rpe65a | 3198.203 | 0.391357 | 8.57E-05 | 0.012573 |
| ENSDARG00000102456 | cfhl4 | 1376.199 | 0.505869 | 9.12E-05 | 0.013245 |
| ENSDARG00000038025 | cbx7a | 453.8307 | 0.594211 | 9.97E-05 | 0.014028 |
| ENSDARG00000101766 | ptmab | 7208.844 | 0.384481 | 0.000114 | 0.015881 |
| ENSDARG00000021113 | ptmaa | 5505.346 | 0.506018 | 0.000118 | 0.016267 |
| ENSDARG00000073936 | BX511021.1 | 241.6633 | 0.788253 | 0.00012 | 0.01643 |
| ENSDARG00000042980 | cyp2p7 | 217.9266 | 0.685211 | 0.000122 | 0.016523 |
| ENSDARG00000077504 | si:ch211-103n10.5 | 23.1332 | 1.617428 | 0.000126 | 0.016936 |
| ENSDARG00000076448 | serpinf2a | 344.5886 | 0.502317 | 0.000142 | 0.018544 |
| ENSDARG00000059719 | fam169aa | 175.5422 | 0.634921 | 0.000149 | 0.019182 |
| ENSDARG00000055120 | ctsba | 943.1379 | 0.582215 | 0.000163 | 0.020536 |
| ENSDARG00000070960 | si:ch211-288g17.4 | 115.0754 | 0.652499 | 0.000168 | 0.020672 |
| ENSDARG00000015065 | c4 | 30.25022 | 1.105303 | 0.000193 | 0.02278 |
| ENSDARG00000098537 | spata22 | 174.898 | 0.539229 | 0.0002 | 0.023461 |
| ENSDARG00000014975 | irge1 | 13.94034 | 1.846166 | 0.000235 | 0.026828 |
| ENSDARG00000092770 | si:ch211-253p18.2 | 17.91622 | 1.635956 | 0.000256 | 0.028147 |
| ENSDARG00000033760 | pmelb | 474.1198 | 0.434502 | 0.000256 | 0.028147 |
| ENSDARG00000052905 | zgc:165423 | 838.3998 | 0.416904 | 0.000253 | 0.028147 |

**Table F.1 continued**

| #geneID | Upregulated gene | base mean | log2 fold change | p-value | FDR |
|---|---|---|---|---|---|
| ENSDARG00000097877 | si:ch211-167b20.8 | 649.1454 | 0.410081 | 0.000256 | 0.028147 |
| ENSDARG00000008306 | rdh5 | 603.7632 | 0.363422 | 0.000256 | 0.028147 |
| ENSDARG00000044626 | ccdc90b | 38.23185 | 1.079205 | 0.000275 | 0.029717 |
| ENSDARG00000078069 | rrm2 | 935.9859 | 0.504901 | 0.000286 | 0.030808 |
| ENSDARG00000034933 | chchd3b | 106.8861 | 0.58604 | 0.000295 | 0.031396 |
| ENSDARG00000015862 | rpl5b | 21838.73 | 0.38928 | 0.000297 | 0.031396 |
| ENSDARG00000098989 | CU459012.1 | 80.88583 | 0.714954 | 0.000299 | 0.031484 |
| ENSDARG00000069432 | plscr3b | 1214.034 | 0.319398 | 0.000325 | 0.033394 |
| ENSDARG00000096829 | blvrb | 126.9907 | 0.54879 | 0.000359 | 0.036475 |
| ENSDARG00000042684 | serpinc1 | 857.2663 | 0.40627 | 0.000364 | 0.036587 |
| ENSDARG00000019492 | shbg | 385.3129 | 0.463381 | 0.000373 | 0.037317 |
| ENSDARG00000099885 | trim105 | 56.98115 | 0.862385 | 0.000383 | 0.03805 |
| ENSDARG00000055278 | cfb | 500.439 | 0.393528 | 0.000391 | 0.038539 |
| ENSDARG00000097720 | BX005129.3 | 11.93893 | 1.832288 | 0.00043 | 0.041603 |
| ENSDARG00000102884 | si:ch211-145h19.5 | 3.358286 | 4.427668 | 0.000464 | 0.043765 |
| ENSDARG00000105545 | si:dkey-165a24.10 | 6.47176 | 2.513261 | 0.000493 | 0.044867 |
| ENSDARG00000073786 | cmbl | 396.0786 | 0.445208 | 0.000491 | 0.044867 |
| ENSDARG00000060797 | pfkmb | 298.0049 | 0.540481 | 0.000504 | 0.045478 |
| ENSDARG00000057571 | pgam2 | 2322.113 | 0.354372 | 0.000509 | 0.045728 |
| ENSDARG00000044280 | opn1mw2 | 166.0227 | 0.769 | 0.000515 | 0.045762 |
| ENSDARG00000105039 | phka1b | 172.4235 | 0.628473 | 0.000548 | 0.04853 |
| ENSDARG00000096804 | si:dkey-219e21.4 | 21.15657 | 1.175202 | 0.000558 | 0.049169 |
| ENSDARG00000074201 | flna | 3279.297 | 0.276057 | 0.000559 | 0.049169 |
| ENSDARG00000086571 | kcna7 | 68.10377 | 0.696301 | 0.000567 | 0.049672 |

**Table F.2. Downregulated genes in vehicle treated Klf9 mutants**

| #geneID | Downregulated gene | base mean | log2 fold change | p-value | FDR |
|---|---|---|---|---|---|
| ENSDARG00000035519 | histh1l | 2768.665 | -1.86339 | 2.89E-73 | 6.63E-69 |
| ENSDARG00000035438 | myhc4 | 1880.458 | -5.9945 | 3.16E-22 | 1.45E-18 |
| ENSDARG00000036481 | tcn2 | 652.4145 | -0.8027 | 1.39E-16 | 2.89E-13 |
| ENSDARG00000052779 | zgc:153932 | 262.1276 | -1.23939 | 7.83E-16 | 1.38E-12 |
| ENSDARG00000070057 | si:dkey-69o16.5 | 108.537 | -1.38794 | 4.55E-14 | 6.95E-11 |
| ENSDARG00000020711 | rrm2 | 439.901 | -1.39052 | 1.70E-12 | 2.17E-09 |
| ENSDARG00000068088 | tcnl | 216.8114 | -1.01027 | 6.86E-12 | 8.28E-09 |
| ENSDARG00000021059 | alas1 | 2669.096 | -0.63889 | 1.41E-10 | 1.47E-07 |
| ENSDARG00000045414 | elovl2 | 624.9931 | -0.80142 | 1.53E-10 | 1.53E-07 |
| ENSDARG00000105644 | zgc:172079 | 380.1255 | -0.69585 | 1.95E-10 | 1.78E-07 |
| ENSDARG00000099558 | NPC1L1 | 261.2222 | -0.90562 | 4.28E-10 | 3.77E-07 |
| ENSDARG00000003902 | ctsl.1 | 1112.789 | -0.77403 | 4.75E-10 | 4.04E-07 |
| ENSDARG00000094929 | BX004983.1 | 310.5673 | -1.00411 | 5.93E-10 | 4.86E-07 |
| ENSDARG00000020866 | apoa4b.2 | 3842.331 | -0.78421 | 1.01E-09 | 7.97E-07 |
| ENSDARG00000102249 | pepd | 642.3329 | -0.65329 | 1.16E-09 | 8.86E-07 |
| ENSDARG00000003197 | wdr21 | 29.83967 | -1.88224 | 2.48E-09 | 1.72E-06 |
| ENSDARG00000068194 | klf9 | 168.7448 | -1.12272 | 3.44E-09 | 2.32E-06 |
| ENSDARG00000060679 | kdm1a | 1983.014 | -0.49922 | 4.39E-09 | 2.85E-06 |
| ENSDARG00000095863 | afp4 | 3493.26 | -0.82452 | 4.58E-09 | 2.85E-06 |
| ENSDARG00000031336 | hsd20b2 | 218.3645 | -0.73921 | 4.90E-09 | 2.96E-06 |
| ENSDARG00000009612 | chia.3 | 243.1291 | -1.0698 | 6.63E-09 | 3.90E-06 |
| ENSDARG00000103025 | hmgcs1 | 681.1838 | -0.67705 | 8.69E-09 | 4.86E-06 |
| ENSDARG00000007955 | iars | 923.4237 | -0.55248 | 1.38E-08 | 7.56E-06 |
| ENSDARG00000026726 | anxa1a | 3250.504 | -0.97678 | 2.79E-08 | 1.36E-05 |
| ENSDARG00000093606 | si:dkey-159f12.2 | 169.2184 | -0.96385 | 3.40E-08 | 1.62E-05 |
| ENSDARG00000034368 | hexb | 405.6381 | -0.58543 | 5.88E-08 | 2.70E-05 |
| ENSDARG00000055754 | smc1a | 74.17655 | -1.25434 | 9.18E-08 | 4.13E-05 |
| ENSDARG00000035610 | zgc:113208 | 194.02 | -0.7375 | 1.18E-07 | 5.13E-05 |
| ENSDARG00000009280 | smyd1a | 2388.335 | -0.55804 | 1.62E-07 | 6.89E-05 |
| ENSDARG00000098063 | alp3 | 118.0563 | -0.96557 | 1.73E-07 | 7.20E-05 |
| ENSDARG00000102442 | FOLR2 | 257.8307 | -0.68403 | 1.79E-07 | 7.20E-05 |
| ENSDARG00000103295 | cyp3a65 | 4324.851 | -0.45809 | 2.18E-07 | 8.47E-05 |
| ENSDARG00000045367 | tuba1b | 999.3486 | -0.68108 | 2.83E-07 | 0.000108 |
| ENSDARG00000036864 | slc34a2b | 235.7654 | -0.71809 | 6.25E-07 | 0.000228 |
| ENSDARG00000061120 | slc43a2b | 4052.023 | -0.52488 | 7.56E-07 | 0.000268 |
| ENSDARG00000036359 | riox2 | 178.0987 | -0.72739 | 7.60E-07 | 0.000268 |
| ENSDARG00000079946 | sqlea | 126.1469 | -1.21204 | 8.19E-07 | 0.000284 |
| ENSDARG00000003032 | eif4a1b | 6058.099 | -0.51401 | 1.08E-06 | 0.00036 |
| ENSDARG00000060879 | slc28a1 | 244.3711 | -0.77969 | 1.08E-06 | 0.00036 |

**Table F.2 continued**

| #geneID | Downregulated gene | base mean | log2 fold change | p-value | FDR |
|---|---|---|---|---|---|
| ENSDARG00000012387 | pdha1a | 2619.283 | -0.40335 | 1.27E-06 | 0.000416 |
| ENSDARG00000092404 | si:dkey-79p17.3 | 61.44082 | -1.10458 | 1.51E-06 | 0.000475 |
| ENSDARG00000100315 | slc15a1a | 348.0006 | -0.72875 | 1.69E-06 | 0.000518 |
| ENSDARG00000026759 | ldlrb | 162.7448 | -0.76171 | 1.79E-06 | 0.000532 |
| ENSDARG00000044642 | sc5d | 158.4746 | -0.81389 | 2.03E-06 | 0.000596 |
| ENSDARG00000021882 | fbxl3b | 149.6257 | -0.82607 | 2.17E-06 | 0.000631 |
| ENSDARG00000086848 | atad3 | 154.3654 | -0.73494 | 2.30E-06 | 0.000652 |
| ENSDARG00000052734 | hmgcra | 1875.458 | -1.81771 | 2.47E-06 | 0.000692 |
| ENSDARG00000101051 | ctsbb | 240.4093 | -0.63244 | 2.65E-06 | 0.000733 |
| ENSDARG00000105829 | CR788316.4 | 196.6503 | -1.04511 | 2.75E-06 | 0.000751 |
| ENSDARG00000055539 | epdl2 | 948.6487 | -0.59093 | 3.05E-06 | 0.000814 |
| ENSDARG00000099946 | fam189a2 | 140.6069 | -0.74187 | 3.23E-06 | 0.000841 |
| ENSDARG00000042641 | cyp51 | 641.8636 | -1.41146 | 3.27E-06 | 0.000843 |
| ENSDARG00000053215 | me1 | 177.62 | -0.65275 | 3.98E-06 | 0.001002 |
| ENSDARG00000100635 | chia.1 | 1527.249 | -0.61901 | 4.49E-06 | 0.001109 |
| ENSDARG00000077960 | si:ch211-186e20.7 | 65.95029 | -0.95914 | 5.51E-06 | 0.001345 |
| ENSDARG00000095200 | si:ch211-197e7.1 | 34.69832 | -1.32398 | 8.25E-06 | 0.001951 |
| ENSDARG00000057973 | dph1 | 129.3977 | -0.68003 | 1.01E-05 | 0.002292 |
| ENSDARG00000097080 | si:ch73-181m17.1 | 32.68139 | -1.54296 | 1.29E-05 | 0.002826 |
| ENSDARG00000041848 | rh50 | 92.06114 | -0.81118 | 1.36E-05 | 0.002937 |
| ENSDARG00000071592 | aqp8a.2 | 428.9828 | -0.50882 | 1.45E-05 | 0.003115 |
| ENSDARG00000087013 | cubn | 207.9272 | -0.57249 | 1.60E-05 | 0.00339 |
| ENSDARG00000010936 | abcb4 | 1458.282 | -0.66106 | 1.89E-05 | 0.003973 |
| ENSDARG00000023820 | faxdc2 | 1872.401 | -0.55773 | 1.93E-05 | 0.004024 |
| ENSDARG00000029587 | msra | 184.2666 | -0.62553 | 2.20E-05 | 0.004513 |
| ENSDARG00000069977 | myg1 | 359.5154 | -0.54219 | 2.29E-05 | 0.004645 |
| ENSDARG00000099764 | CR855389.1 | 21.62847 | -1.61664 | 2.52E-05 | 0.005032 |
| ENSDARG00000110614 | ugt2a7 | 3.728411 | -5.13511 | 2.63E-05 | 0.005152 |
| ENSDARG00000000103 | myh10 | 1240.932 | -0.38228 | 2.75E-05 | 0.005301 |
| ENSDARG00000092680 | si:dkey-58f10.12 | 3.354211 | -5.14873 | 2.87E-05 | 0.005444 |
| ENSDARG00000001870 | atp1a1a.4 | 3861.153 | -0.41739 | 3.47E-05 | 0.006367 |
| ENSDARG00000063438 | srebf2 | 937.7128 | -0.43104 | 3.53E-05 | 0.006367 |
| ENSDARG00000087805 | FP236735.1 | 90.89468 | -0.76969 | 3.58E-05 | 0.006385 |
| ENSDARG00000103825 | galnt10 | 117.3432 | -0.7194 | 3.83E-05 | 0.00666 |
| ENSDARG00000079361 | abcg2b | 268.2522 | -0.62147 | 4.34E-05 | 0.007418 |
| ENSDARG00000104359 | anxa1c | 709.8119 | -1.20774 | 5.06E-05 | 0.008414 |
| ENSDARG00000068387 | slc6a18 | 67.02408 | -0.80018 | 5.34E-05 | 0.008746 |
| ENSDARG00000096445 | si:ch211-214p16.3 | 833.4699 | -0.59877 | 5.47E-05 | 0.008861 |
| ENSDARG00000067966 | fem1a | 176.2754 | -0.98181 | 5.86E-05 | 0.009267 |

**Table F.2 continued**

| #geneID | Downregulated gene | base mean | log2 fold change | p-value | FDR |
|---|---|---|---|---|---|
| ENSDARG00000002355 | shpk | 12.19937 | -1.94657 | 7.58E-05 | 0.011292 |
| ENSDARG00000115015 | PSTK | 53.45122 | -0.90525 | 7.63E-05 | 0.011295 |
| ENSDARG00000103277 | cyp24a1 | 375.1038 | -0.83885 | 9.30E-05 | 0.013423 |
| ENSDARG00000070021 | cyp3c4 | 240.3419 | -0.60283 | 9.48E-05 | 0.013513 |
| ENSDARG00000098481 | ANXA1_(1_of_many) | 166.3025 | -0.80574 | 9.44E-05 | 0.013513 |
| ENSDARG00000022261 | pdzk1 | 1191.857 | -0.54944 | 9.76E-05 | 0.013813 |
| ENSDARG00000012881 | slc4a1a | 385.9588 | -0.41917 | 0.000103 | 0.014344 |
| ENSDARG00000103799 | kars | 2715.921 | -0.36277 | 0.000122 | 0.016523 |
| ENSDARG00000013475 | cct4 | 4966.35 | -0.41475 | 0.000122 | 0.016523 |
| ENSDARG00000020364 | fbp1b | 2265.203 | -0.35224 | 0.000134 | 0.017925 |
| ENSDARG00000098949 | mslna | 105.3115 | -0.90505 | 0.000137 | 0.018206 |
| ENSDARG00000037533 | mep1b | 148.3307 | -0.60767 | 0.000139 | 0.018295 |
| ENSDARG00000103464 | pggt1b | 355.2972 | -0.54424 | 0.000143 | 0.018544 |
| ENSDARG00000061355 | aoc1 | 772.7346 | -0.50888 | 0.000154 | 0.019677 |
| ENSDARG00000035549 | uprt | 359.3888 | -0.39507 | 0.000156 | 0.019828 |
| ENSDARG00000103226 | dhcr7 | 593.4361 | -0.45878 | 0.000165 | 0.020611 |
| ENSDARG00000032816 | tm7sf2 | 187.5734 | -0.53822 | 0.000165 | 0.020611 |
| ENSDARG00000042124 | si:dkey-4e7.3 | 299.4002 | -0.49052 | 0.000167 | 0.020672 |
| ENSDARG00000092730 | enam | 218.6128 | -0.62782 | 0.00017 | 0.020709 |
| ENSDARG00000055876 | msmo1 | 739.6583 | -1.24368 | 0.000169 | 0.020709 |
| ENSDARG00000099313 | naga | 388.4939 | -0.44622 | 0.000177 | 0.021417 |
| ENSDARG00000071090 | actn2b | 318.7622 | -0.45145 | 0.000177 | 0.021417 |
| ENSDARG00000040683 | si:ch73-40a17.3 | 188.545 | -0.613 | 0.000189 | 0.022574 |
| ENSDARG00000068374 | si:ch211-132b12.7 | 1719.118 | -0.39834 | 0.000192 | 0.02278 |
| ENSDARG00000067976 | ar | 60.46118 | -0.83571 | 0.000197 | 0.023191 |
| ENSDARG00000074571 | gpaa1 | 175.1277 | -0.58036 | 0.000204 | 0.023776 |
| ENSDARG00000055647 | ftr82 | 350.4402 | -0.40289 | 0.000216 | 0.024915 |
| ENSDARG00000015111 | ddx39ab | 2283.753 | -0.51683 | 0.000216 | 0.024915 |
| ENSDARG00000035120 | gldc | 775.91 | -0.4758 | 0.000227 | 0.026024 |
| ENSDARG00000012468 | aacs | 295.9771 | -0.4557 | 0.000238 | 0.02701 |
| ENSDARG00000042221 | mthfd1l | 94.04474 | -0.76515 | 0.000245 | 0.027717 |
| ENSDARG00000101062 | fdft1 | 137.1911 | -0.56277 | 0.000249 | 0.028003 |
| ENSDARG00000103296 | nup54 | 462.5089 | -0.48685 | 0.000265 | 0.028979 |
| ENSDARG00000101089 | gart | 187.5208 | -0.53022 | 0.000274 | 0.029717 |
| ENSDARG00000030494 | hjv | 177.8493 | -0.65599 | 0.000293 | 0.031396 |
| ENSDARG00000046091 | si:ch211-283g2.1 | 66.65205 | -1.10965 | 0.000296 | 0.031396 |
| ENSDARG00000054334 | dctpp1 | 7.44147 | -2.65357 | 0.000309 | 0.032331 |
| ENSDARG00000001897 | man2b1 | 516.3698 | -0.36987 | 0.000312 | 0.032579 |
| ENSDARG00000052816 | shmt1 | 709.1141 | -0.35026 | 0.000321 | 0.033291 |

**Table F.2 continued**

| #geneID | Downregulated gene | base mean | log2 fold change | p-value | FDR |
|---|---|---|---|---|---|
| ENSDARG00000053448 | si:ch211-251f6.6 | 180.3523 | -0.71722 | 0.000322 | 0.033291 |
| ENSDARG00000103266 | ogal | 381.9023 | -0.43031 | 0.000334 | 0.034241 |
| ENSDARG00000093044 | si:ch211-161h7.5 | 1353.777 | -0.46191 | 0.000355 | 0.036187 |
| ENSDARG00000098118 | trappc10 | 447.9254 | -0.43072 | 0.000362 | 0.036542 |
| ENSDARG00000102004 | apoea | 3521.724 | -0.44291 | 0.000378 | 0.037718 |
| ENSDARG00000002917 | gls2b | 118.439 | -0.60388 | 0.000389 | 0.038453 |
| ENSDARG00000079664 | zgc:172341 | 43.08202 | -0.92333 | 0.000408 | 0.039994 |
| ENSDARG00000101239 | hsd17b4 | 638.4174 | -0.42261 | 0.000419 | 0.040887 |
| ENSDARG00000022410 | rrp12 | 1350.096 | -0.32575 | 0.000426 | 0.041365 |
| ENSDARG00000095150 | si:dkey-114c15.5 | 7.691941 | -2.52437 | 0.000436 | 0.04198 |
| ENSDARG00000035809 | col1a1b | 31881.1 | -0.56294 | 0.00044 | 0.04221 |
| ENSDARG00000104848 | cdkal1 | 162.7989 | -0.52402 | 0.000449 | 0.042879 |
| ENSDARG00000045297 | phb2a | 1157.652 | -0.33204 | 0.000464 | 0.043765 |
| ENSDARG00000089888 | daglb | 355.0618 | -0.50969 | 0.000461 | 0.043765 |
| ENSDARG00000076554 | cdkn1a | 113.2197 | -0.56089 | 0.000466 | 0.043816 |
| ENSDARG00000102798 | mcm2 | 1000.735 | -0.38652 | 0.000474 | 0.044332 |
| ENSDARG00000059059 | emsy | 555.0022 | -0.47999 | 0.000484 | 0.044823 |
| ENSDARG00000003615 | slc26a3.2 | 408.8037 | -0.53114 | 0.000489 | 0.044823 |
| ENSDARG00000103167 | si:dkey-245n4.2 | 90.53049 | -0.63535 | 0.000488 | 0.044823 |
| ENSDARG00000061274 | lss | 78.31014 | -0.85661 | 0.000486 | 0.044823 |
| ENSDARG00000001777 | nup155 | 426.9367 | -0.40747 | 0.000502 | 0.045478 |
| ENSDARG00000101180 | mcm7 | 718.8041 | -0.39558 | 0.000511 | 0.045728 |

## APPENDIX G: Genes most significantly dysregulated by chronic cortisol in WT and *klf9*$^{-/-}$ larvae

### Table G.1. Genes upregulated by CORT in WT larvae

| #geneID | Upregulated gene | Base Mean | log2 Fold Change | pvalue | FDR |
|---|---|---|---|---|---|
| ENSDARG00000109648 | si:ch211-147m6.1 | 183.8033 | 2.572598 | 4.22E-41 | 8.75E-37 |
| ENSDARG00000043249 | irf1b | 312.7757 | 2.889045 | 1.06E-34 | 1.10E-30 |
| ENSDARG00000090352 | CR855311.1 | 482.9401 | 2.574487 | 1.67E-31 | 1.16E-27 |
| ENSDARG00000090783 | mfap4 | 150.0106 | 2.476785 | 4.33E-31 | 2.24E-27 |
| ENSDARG00000069844 | acod1 | 57.90671 | 3.842765 | 6.57E-29 | 2.72E-25 |
| ENSDARG00000024789 | mxc | 120.4908 | 3.676099 | 1.24E-27 | 4.28E-24 |
| ENSDARG00000074322 | si:ch211-194m7.3 | 173.8251 | 2.549077 | 9.86E-25 | 2.92E-21 |
| ENSDARG00000088745 | MFAP4_(1_of_many) | 193.2504 | 2.29722 | 1.57E-23 | 4.07E-20 |
| ENSDARG00000026049 | mxf | 70.74042 | 5.164147 | 2.18E-23 | 5.01E-20 |
| ENSDARG00000056615 | cybb | 108.2924 | 1.7044 | 8.95E-23 | 1.76E-19 |
| ENSDARG00000033227 | lect2l | 213.6467 | 1.601246 | 9.35E-23 | 1.76E-19 |
| ENSDARG00000058731 | slc2a6 | 60.07606 | 2.715882 | 3.85E-22 | 6.14E-19 |
| ENSDARG00000036767 | urgcp | 470.9223 | 2.316574 | 4.77E-20 | 7.07E-17 |
| ENSDARG00000093936 | si:dkeyp-1h4.6 | 511.7943 | 2.057517 | 5.73E-20 | 7.91E-17 |
| ENSDARG00000038424 | si:dkey-8k3.2 | 283.0238 | 2.128589 | 4.56E-19 | 5.90E-16 |
| ENSDARG00000038668 | gbp1 | 62.14689 | 2.124016 | 2.33E-18 | 2.85E-15 |
| ENSDARG00000033587 | CABZ01088134.1 | 30.00041 | 4.679085 | 8.20E-18 | 9.44E-15 |
| ENSDARG00000007769 | sult5a1 | 112.7194 | 2.560444 | 9.70E-18 | 1.06E-14 |
| ENSDARG00000076182 | stat1b | 40.61663 | 2.917481 | 1.04E-17 | 1.08E-14 |
| ENSDARG00000054610 | coro1a | 228.9183 | 1.299886 | 1.17E-17 | 1.16E-14 |
| ENSDARG00000053836 | si:ch211-284o19.8 | 32.14647 | 3.048544 | 4.94E-17 | 4.45E-14 |
| ENSDARG00000113076 | si:ch211-182p11.1 | 60.17462 | 1.97414 | 4.85E-17 | 4.45E-14 |
| ENSDARG00000090889 | si:ch211-132p1.3 | 43.56367 | 3.609922 | 1.05E-16 | 9.10E-14 |
| ENSDARG00000033144 | psme2 | 123.2381 | 1.856847 | 1.15E-16 | 9.55E-14 |
| ENSDARG00000025903 | lgals9l1 | 85.53969 | 1.765223 | 2.57E-16 | 2.05E-13 |
| ENSDARG00000040445 | si:ch211-219a4.3 | 139.3815 | 1.234196 | 6.44E-16 | 4.94E-13 |
| ENSDARG00000003523 | itln3 | 110.7729 | 1.337828 | 8.40E-16 | 6.22E-13 |
| ENSDARG00000023188 | lcp1 | 295.2901 | 1.040461 | 7.60E-15 | 5.43E-12 |
| ENSDARG00000056874 | lygl1 | 214.7887 | 1.978463 | 2.49E-14 | 1.72E-11 |
| ENSDARG00000090730 | cfbl | 51.96144 | 1.889906 | 4.15E-14 | 2.75E-11 |
| ENSDARG00000076483 | zgc:198241 | 53.27327 | 1.861296 | 4.25E-14 | 2.75E-11 |
| ENSDARG00000033735 | ncf1 | 93.45246 | 1.481076 | 5.87E-14 | 3.69E-11 |
| ENSDARG00000117407 | AL954191.1 | 88.67542 | 1.404593 | 6.12E-14 | 3.73E-11 |
| ENSDARG00000043093 | mpeg1.2 | 454.8752 | 1.597342 | 2.20E-13 | 1.31E-10 |
| ENSDARG00000079227 | plekhs1 | 265.61 | 2.064915 | 2.73E-13 | 1.56E-10 |

**Table G.1 continued**

| #geneID | Upregulated gene | Base Mean | log2 Fold Change | pvalue | FDR |
|---|---|---|---|---|---|
| ENSDARG00000102758 | FO704661.1 | 101.9056 | 1.884338 | 2.79E-13 | 1.56E-10 |
| ENSDARG00000113315 | zgc:153932 | 81.80156 | 2.210676 | 3.24E-13 | 1.77E-10 |
| ENSDARG00000031588 | si:dkey-239b22.1 | 1551.79 | 1.504327 | 4.07E-13 | 2.16E-10 |
| ENSDARG00000010729 | CABZ01073795.1 | 23.92005 | 3.069448 | 5.61E-13 | 2.91E-10 |
| ENSDARG00000074150 | si:ch211-226h7.5 | 57.79296 | 1.980892 | 7.28E-13 | 3.68E-10 |
| ENSDARG00000068939 | xaf1 | 38.4684 | 2.019841 | 8.01E-13 | 3.95E-10 |
| ENSDARG00000019521 | mpx | 143.6125 | 1.342574 | 8.27E-13 | 3.99E-10 |
| ENSDARG00000004748 | zgc:100868 | 1107.495 | 1.481627 | 1.31E-12 | 6.16E-10 |
| ENSDARG00000034063 | unm_sa911 | 50.51132 | 2.105165 | 2.77E-12 | 1.27E-09 |
| ENSDARG00000094104 | AL929237.1 | 100.8443 | 2.344335 | 3.44E-12 | 1.55E-09 |
| ENSDARG00000100900 | si:ch211-183d5.2 | 22.29367 | 3.306727 | 4.20E-12 | 1.85E-09 |
| ENSDARG00000097909 | si:dkey-195m11.11 | 21.67183 | 2.996893 | 1.59E-11 | 6.87E-09 |
| ENSDARG00000040921 | zmp:0000000606 | 53.667 | 1.940688 | 1.85E-11 | 7.81E-09 |
| ENSDARG00000078093 | zgc:172065 | 74.28101 | 1.760948 | 3.67E-11 | 1.52E-08 |
| ENSDARG00000103634 | CU914622.2 | 1139.146 | 1.295211 | 4.20E-11 | 1.71E-08 |
| ENSDARG00000052779 | zgc:153932 | 648.3197 | 1.390303 | 5.84E-11 | 2.33E-08 |
| ENSDARG00000086337 | si:dkey-102g19.3 | 18.17167 | 3.351288 | 6.49E-11 | 2.54E-08 |
| ENSDARG00000055504 | si:ch211-212k18.7 | 765.8241 | 0.766327 | 8.89E-11 | 3.41E-08 |
| ENSDARG00000099476 | zgc:174863 | 236.2642 | 1.07454 | 9.74E-11 | 3.67E-08 |
| ENSDARG00000004954 | grna | 55.03268 | 1.581297 | 1.06E-10 | 3.94E-08 |
| ENSDARG00000053136 | b2m | 60.49399 | 1.583452 | 1.62E-10 | 5.88E-08 |
| ENSDARG00000029720 | si:dkeyp-9d4.2 | 11.7239 | 6.927567 | 1.75E-10 | 6.24E-08 |
| ENSDARG00000093857 | si:dkey-79f11.10 | 10.59999 | 6.793985 | 4.54E-10 | 1.54E-07 |
| ENSDARG00000107486 | CR855320.3 | 26.03745 | 2.250252 | 4.82E-10 | 1.61E-07 |
| ENSDARG00000059294 | marco | 31.78962 | 1.908414 | 4.93E-10 | 1.62E-07 |
| ENSDARG00000092191 | CR318588.1 | 24.75314 | 3.385857 | 6.35E-10 | 2.06E-07 |
| ENSDARG00000101785 | laptm5 | 66.32603 | 1.542723 | 8.00E-10 | 2.55E-07 |
| ENSDARG00000021250 | slc25a48 | 398.7547 | 0.659392 | 8.60E-10 | 2.70E-07 |
| ENSDARG00000093303 | ifitm1 | 235.3227 | 1.048649 | 9.00E-10 | 2.78E-07 |
| ENSDARG00000075643 | ifi35 | 73.14728 | 1.45964 | 9.33E-10 | 2.84E-07 |
| ENSDARG00000097080 | si:ch73-181m17.1 | 124.9265 | 2.030835 | 1.07E-09 | 3.20E-07 |
| ENSDARG00000045561 | dram1 | 40.97148 | 2.111662 | 1.19E-09 | 3.51E-07 |
| ENSDARG00000090873 | ccl34a.4 | 24.22967 | 3.371059 | 1.45E-09 | 4.23E-07 |
| ENSDARG00000013771 | ctss2.2 | 226.2963 | 1.193864 | 1.62E-09 | 4.66E-07 |
| ENSDARG00000042816 | mmp9 | 183.1288 | 1.476405 | 1.70E-09 | 4.83E-07 |
| ENSDARG00000038669 | gbp2 | 49.91573 | 1.492152 | 1.73E-09 | 4.84E-07 |
| ENSDARG00000016457 | irf9 | 122.9381 | 0.925429 | 2.00E-09 | 5.52E-07 |
| ENSDARG00000039351 | ccl19b | 215.5503 | 1.398821 | 2.58E-09 | 7.02E-07 |
| ENSDARG00000077069 | srgn | 290.2578 | 0.831893 | 2.83E-09 | 7.61E-07 |

**Table G.1 continued**

| #geneID | Upregulated gene | Base Mean | log2 Fold Change | pvalue | FDR |
|---|---|---|---|---|---|
| ENSDARG00000056407 | irf8 | 46.31907 | 1.442397 | 2.98E-09 | 7.91E-07 |
| ENSDARG00000002165 | psme1 | 180.9624 | 1.137586 | 3.06E-09 | 8.03E-07 |
| ENSDARG00000061222 | uba7 | 23.54679 | 2.125064 | 3.42E-09 | 8.86E-07 |
| ENSDARG00000001303 | psmb8a | 14.69413 | 3.720836 | 3.68E-09 | 9.43E-07 |
| ENSDARG00000104399 | tppp | 33.96042 | 1.750979 | 4.23E-09 | 1.07E-06 |
| ENSDARG00000052515 | calcoco2 | 133.6723 | 0.986606 | 4.49E-09 | 1.12E-06 |
| ENSDARG00000041294 | noxo1a | 57.81667 | 1.485256 | 6.49E-09 | 1.60E-06 |
| ENSDARG00000039393 | si:ch211-240l19.5 | 199.3735 | 1.203307 | 8.02E-09 | 1.96E-06 |
| ENSDARG00000095830 | serpinb1l1 | 30.75702 | 1.797572 | 9.31E-09 | 2.24E-06 |
| ENSDARG00000024815 | ogfrl2 | 39.84304 | 1.532348 | 9.72E-09 | 2.29E-06 |
| ENSDARG00000036171 | rnasel3 | 144.0015 | 1.078074 | 9.67E-09 | 2.29E-06 |
| ENSDARG00000102456 | cfhl4 | 1503.556 | 0.854835 | 1.13E-08 | 2.61E-06 |
| ENSDARG00000069566 | mucms1 | 114.1643 | 1.491034 | 1.16E-08 | 2.64E-06 |
| ENSDARG00000015278 | plxnc1 | 114.281 | 1.007578 | 1.25E-08 | 2.82E-06 |
| ENSDARG00000043436 | si:dkey-5n18.1 | 129.838 | 1.006511 | 1.37E-08 | 3.05E-06 |
| ENSDARG00000067797 | spi1a | 70.84552 | 1.153924 | 1.77E-08 | 3.90E-06 |
| ENSDARG00000098204 | CU984600.2 | 39.13438 | 1.515663 | 1.84E-08 | 4.02E-06 |
| ENSDARG00000036588 | mhc1zba | 1593.16 | 1.095211 | 1.89E-08 | 4.08E-06 |
| ENSDARG00000045999 | saa | 12.19949 | 4.569064 | 2.33E-08 | 4.94E-06 |
| ENSDARG00000092778 | si:ch73-338o16.4 | 24.80999 | 2.733067 | 2.32E-08 | 4.94E-06 |
| ENSDARG00000104077 | fcer1gl | 71.28688 | 1.439811 | 2.40E-08 | 5.02E-06 |
| ENSDARG00000054160 | zgc:113625 | 72.89916 | 1.88845 | 2.73E-08 | 5.65E-06 |
| ENSDARG00000079402 | tapbp.1 | 43.95969 | 1.367622 | 2.87E-08 | 5.88E-06 |
| ENSDARG00000067672 | card9 | 21.54264 | 2.122326 | 3.13E-08 | 6.26E-06 |
| ENSDARG00000009702 | ascl1b | 39.84551 | 1.4882 | 3.14E-08 | 6.26E-06 |
| ENSDARG00000074390 | tmem176l.4 | 1061.712 | 0.980317 | 3.10E-08 | 6.26E-06 |
| ENSDARG00000040278 | klhl38b | 250.8579 | 0.757015 | 3.30E-08 | 6.50E-06 |
| ENSDARG00000010312 | cp | 1521.425 | 0.898024 | 3.60E-08 | 6.96E-06 |
| ENSDARG00000076196 | si:ch211-226h7.6 | 38.59109 | 1.494659 | 3.67E-08 | 7.03E-06 |
| ENSDARG00000051914 | slc14a2 | 124.2715 | 1.09334 | 3.84E-08 | 7.30E-06 |
| ENSDARG00000091906 | rbp7a | 211.3611 | 1.417225 | 3.98E-08 | 7.50E-06 |
| ENSDARG00000019253 | rhag | 3789.628 | 0.639873 | 4.50E-08 | 8.41E-06 |
| ENSDARG00000095409 | si:ch211-226h7.8 | 42.54639 | 1.624316 | 4.92E-08 | 9.10E-06 |
| ENSDARG00000018283 | cyba | 128.2687 | 0.951189 | 5.04E-08 | 9.24E-06 |
| ENSDARG00000109626 | si:ch211-226h7.3 | 414.1301 | 1.353471 | 5.65E-08 | 1.03E-05 |
| ENSDARG00000105562 | si:dkey-23i12.7 | 17.16477 | 3.114676 | 9.59E-08 | 1.73E-05 |
| ENSDARG00000086654 | cbln11 | 41.80395 | 1.619878 | 9.90E-08 | 1.77E-05 |
| ENSDARG00000045530 | si:ch211-244b2.4 | 78.60943 | 1.01986 | 1.00E-07 | 1.78E-05 |
| ENSDARG00000100095 | anxa1b | 443.9386 | 1.081684 | 1.12E-07 | 1.96E-05 |

**Table G.1 continued**

| #geneID | Upregulated gene | Base Mean | log2 Fold Change | pvalue | FDR |
|---|---|---|---|---|---|
| ENSDARG00000052905 | zgc:165423 | 920.1826 | 0.681024 | 1.15E-07 | 2.01E-05 |
| ENSDARG00000067741 | itpkcb | 390.0302 | 0.706077 | 1.41E-07 | 2.41E-05 |
| ENSDARG00000028731 | stat4 | 88.85503 | 0.933402 | 1.76E-07 | 2.98E-05 |
| ENSDARG00000057789 | lyz | 471.7913 | 1.022577 | 1.77E-07 | 2.99E-05 |
| ENSDARG00000033446 | tap2t | 84.88074 | 0.971002 | 1.82E-07 | 3.05E-05 |
| ENSDARG00000021859 | erap1b | 64.57774 | 1.024132 | 1.90E-07 | 3.15E-05 |
| ENSDARG00000095245 | si:ch211-157j23.2 | 20.65048 | 2.061273 | 2.29E-07 | 3.76E-05 |
| ENSDARG00000055278 | cfb | 665.9172 | 1.154987 | 2.41E-07 | 3.93E-05 |
| ENSDARG00000094485 | si:dkey-27h10.2 | 15.20104 | 2.314264 | 2.45E-07 | 3.96E-05 |
| ENSDARG00000027658 | irf10 | 18.4188 | 2.473993 | 2.55E-07 | 4.09E-05 |
| ENSDARG00000079727 | selenop2 | 1078.166 | 0.588469 | 3.01E-07 | 4.72E-05 |
| ENSDARG00000039243 | zgc:152791 | 17.79617 | 2.442949 | 3.07E-07 | 4.79E-05 |
| ENSDARG00000003113 | ada | 4311.399 | 0.676793 | 3.72E-07 | 5.72E-05 |
| ENSDARG00000068233 | zgc:64051 | 44.32473 | 1.27519 | 3.79E-07 | 5.77E-05 |
| ENSDARG00000020866 | apoa4b.2 | 6142.337 | 0.639827 | 3.91E-07 | 5.88E-05 |
| ENSDARG00000013024 | erap1a | 66.35327 | 1.005412 | 3.98E-07 | 5.93E-05 |
| ENSDARG00000003203 | rhcga | 808.1989 | 1.022489 | 4.16E-07 | 6.16E-05 |
| ENSDARG00000015887 | b2ml | 1781.119 | 0.657335 | 4.54E-07 | 6.67E-05 |
| ENSDARG00000094935 | si:dkey-58f10.11 | 9.854471 | 4.740639 | 4.66E-07 | 6.80E-05 |
| ENSDARG00000074656 | ctss2.1 | 49.6226 | 1.402906 | 4.88E-07 | 7.07E-05 |
| ENSDARG00000090882 | si:rp71-36a1.5 | 15.47458 | 2.585342 | 5.01E-07 | 7.20E-05 |
| ENSDARG00000095533 | si:ch211-198c19.3 | 30.48871 | 1.490858 | 5.78E-07 | 8.20E-05 |
| ENSDARG00000075164 | mylk5 | 595.7918 | 0.655869 | 6.05E-07 | 8.52E-05 |
| ENSDARG00000036282 | rnaset2 | 254.3274 | 0.841852 | 6.31E-07 | 8.83E-05 |
| ENSDARG00000045835 | si:dkey-14d8.6 | 882.8699 | 1.283726 | 6.91E-07 | 9.61E-05 |
| ENSDARG00000104380 | si:dkey-238k10.2 | 113.4772 | 0.860801 | 6.99E-07 | 9.65E-05 |
| ENSDARG00000100969 | tmprss13a | 142.9274 | 1.044825 | 7.38E-07 | 0.000101 |
| ENSDARG00000005481 | nfkbiaa | 309.5964 | 1.046337 | 7.53E-07 | 0.000103 |
| ENSDARG00000068784 | vsir | 79.10146 | 1.116378 | 7.85E-07 | 0.000106 |
| ENSDARG00000089724 | cyldb | 110.4385 | 1.074872 | 8.01E-07 | 0.000108 |
| ENSDARG00000052039 | caspb | 386.9069 | 1.066524 | 8.27E-07 | 0.00011 |
| ENSDARG00000069988 | arid6 | 148.7751 | 0.865158 | 8.23E-07 | 0.00011 |
| ENSDARG00000038185 | gh1 | 143.8439 | 0.848641 | 8.33E-07 | 0.00011 |
| ENSDARG00000103480 | BX640512.3 | 19.30459 | 1.825501 | 8.47E-07 | 0.000111 |
| ENSDARG00000077138 | zgc:195173 | 103.4174 | 0.980456 | 8.83E-07 | 0.000115 |
| ENSDARG00000097019 | dhrs13b | 29.26156 | 1.689121 | 9.39E-07 | 0.000122 |
| ENSDARG00000092283 | cxl34b.11 | 716.7648 | 1.35118 | 9.89E-07 | 0.000127 |
| ENSDARG00000101169 | grap2b | 45.13531 | 1.215825 | 1.03E-06 | 0.000132 |
| ENSDARG00000062788 | irg1l | 103.7971 | 1.534314 | 1.13E-06 | 0.000144 |

**Table G.1 continued**

| #geneID | Upregulated gene | Base Mean | log2 Fold Change | pvalue | FDR |
|---|---|---|---|---|---|
| ENSDARG00000067566 | sftpbb | 52.14353 | 1.14368 | 1.41E-06 | 0.000178 |
| ENSDARG00000016188 | si:ch73-63e15.2 | 382.1953 | 0.530038 | 1.43E-06 | 0.000179 |
| ENSDARG00000014975 | irge1 | 16.31034 | 2.12461 | 1.51E-06 | 0.000188 |
| ENSDARG00000041060 | lgals9l3 | 97.47142 | 1.184831 | 1.57E-06 | 0.000195 |
| ENSDARG00000070426 | chac1 | 3738.056 | 0.606355 | 1.60E-06 | 0.000197 |
| ENSDARG00000033285 | gsto2 | 1141.409 | 0.704987 | 1.76E-06 | 0.000216 |
| ENSDARG00000062221 | arap1a | 164.4186 | 1.163585 | 2.02E-06 | 0.000246 |
| ENSDARG00000040277 | fbxo32 | 310.8871 | 0.797587 | 2.03E-06 | 0.000246 |
| ENSDARG00000089043 | ptpn6 | 116.0833 | 0.761901 | 2.08E-06 | 0.00025 |
| ENSDARG00000051912 | zgc:152945 | 119.8982 | 0.913712 | 2.13E-06 | 0.000255 |
| ENSDARG00000042613 | crp3 | 715.6651 | 0.638715 | 2.38E-06 | 0.000284 |
| ENSDARG00000087402 | tpm1 | 3334.528 | 0.493449 | 2.51E-06 | 0.000297 |
| ENSDARG00000077308 | gpr84 | 10.83091 | 2.898602 | 2.79E-06 | 0.000327 |
| ENSDARG00000016939 | itgb2 | 93.35063 | 0.858923 | 3.01E-06 | 0.000348 |
| ENSDARG00000076978 | pmchl | 99.04605 | 1.054693 | 3.11E-06 | 0.000358 |
| ENSDARG00000069244 | si:ch211-244b2.3 | 50.02496 | 1.067156 | 3.14E-06 | 0.000359 |
| ENSDARG00000076789 | cx32.2 | 30.52103 | 1.427708 | 3.24E-06 | 0.000369 |
| ENSDARG00000070651 | prkcdb | 621.205 | 0.620346 | 3.37E-06 | 0.000381 |
| ENSDARG00000093316 | adgrf8 | 156.3467 | 0.991984 | 3.45E-06 | 0.000389 |
| ENSDARG00000095147 | krt96 | 786.2942 | 0.779171 | 3.88E-06 | 0.000434 |
| ENSDARG00000074378 | junba | 216.8258 | 0.802416 | 4.29E-06 | 0.000479 |
| ENSDARG00000090635 | kcnj1a.4 | 92.16537 | 0.930965 | 4.76E-06 | 0.000527 |
| ENSDARG00000070669 | cxcr3.3 | 145.3721 | 0.78389 | 5.01E-06 | 0.000553 |
| ENSDARG00000010625 | clic2 | 123.4041 | 0.837847 | 5.06E-06 | 0.000553 |
| ENSDARG00000038359 | enosf1 | 341.4614 | 0.594058 | 5.07E-06 | 0.000553 |
| ENSDARG00000008275 | klhl24b | 1072.665 | 0.559972 | 5.18E-06 | 0.000559 |
| ENSDARG00000098736 | si:dkey-201i2.4 | 13.83629 | 2.110572 | 5.34E-06 | 0.000574 |
| ENSDARG00000038199 | cdab | 231.1404 | 0.67639 | 5.67E-06 | 0.000605 |
| ENSDARG00000018569 | tnfrsf1a | 291.6441 | 0.773871 | 5.72E-06 | 0.000608 |
| ENSDARG00000021677 | phf11 | 18.30455 | 1.681447 | 5.83E-06 | 0.000617 |
| ENSDARG00000102076 | zgc:158852 | 105.2217 | 0.949898 | 6.17E-06 | 0.00064 |
| ENSDARG00000095090 | tspan37 | 100.3635 | 0.888178 | 6.14E-06 | 0.00064 |
| ENSDARG00000022712 | stat3 | 448.485 | 0.4941 | 6.19E-06 | 0.00064 |
| ENSDARG00000004301 | rhogb | 131.3023 | 1.006517 | 6.29E-06 | 0.000645 |
| ENSDARG00000015662 | pla2g12b | 1377.067 | 0.510645 | 6.33E-06 | 0.000646 |
| ENSDARG00000087706 | dicp3.3 | 19.91159 | 1.699935 | 6.62E-06 | 0.000672 |
| ENSDARG00000075504 | si:dkey-40c23.2 | 26.51904 | 1.411598 | 6.77E-06 | 0.000684 |
| ENSDARG00000007244 | acp2 | 459.5427 | 0.692455 | 7.62E-06 | 0.000767 |
| ENSDARG00000044094 | gfpt2 | 282.0701 | 0.720315 | 8.43E-06 | 0.000844 |

**Table G.1 continued**

| #geneID | Upregulated gene | Base Mean | log2 Fold Change | pvalue | FDR |
|---|---|---|---|---|---|
| ENSDARG00000068431 | si:ch211-195h23.3 | 248.0224 | 0.706942 | 8.74E-06 | 0.000871 |
| ENSDARG00000075785 | si:ch73-190m4.1 | 8.231604 | 3.350774 | 8.96E-06 | 0.000885 |
| ENSDARG00000103687 | sycn.2 | 869.5098 | 0.812971 | 8.97E-06 | 0.000885 |
| ENSDARG00000100461 | CABZ01078737.1 | 29.49431 | 1.275758 | 9.02E-06 | 0.000886 |
| ENSDARG00000104325 | plek | 40.96059 | 1.358933 | 9.83E-06 | 0.000956 |
| ENSDARG00000105052 | cfhl5 | 63.72555 | 1.100523 | 6.51E-05 | 0.004378 |
| ENSDARG00000039900 | si:ch73-168d20.1 | 12.60058 | 2.05698 | 6.58E-05 | 0.004414 |
| ENSDARG00000040076 | pycard | 308.2686 | 0.924073 | 6.76E-05 | 0.004504 |
| ENSDARG00000039579 | cfd | 1554.413 | 0.758554 | 6.75E-05 | 0.004504 |
| ENSDARG00000029290 | stx11b.1 | 215.3912 | 0.93702 | 6.91E-05 | 0.004589 |
| ENSDARG00000069461 | rnaseka | 216.3192 | 0.803255 | 6.96E-05 | 0.004606 |
| ENSDARG00000094678 | si:dkey-9i23.6 | 35.93057 | 1.147303 | 7.00E-05 | 0.004618 |
| ENSDARG00000016319 | c9 | 1675.694 | 0.684172 | 7.18E-05 | 0.004721 |
| ENSDARG00000029587 | msra | 318.9237 | 0.789129 | 7.31E-05 | 0.004762 |
| ENSDARG00000106669 | CABZ01068358.1 | 142.6194 | 0.69325 | 7.80E-05 | 0.005037 |
| ENSDARG00000077874 | vwa10.1 | 70.32654 | 1.25502 | 8.16E-05 | 0.005252 |
| ENSDARG00000011519 | myl4 | 329.0297 | 0.598772 | 8.63E-05 | 0.005504 |
| ENSDARG00000036848 | slc43a2a | 582.5648 | 0.436693 | 8.69E-05 | 0.005525 |
| ENSDARG00000054968 | cd40 | 26.88343 | 1.335252 | 8.78E-05 | 0.005568 |
| ENSDARG00000090890 | cmklr1 | 25.61643 | 1.294985 | 8.89E-05 | 0.005614 |
| ENSDARG00000101495 | ugt5b2 | 145.3916 | 0.700465 | 8.91E-05 | 0.005614 |
| ENSDARG00000053858 | crip1 | 1388.778 | 0.679956 | 8.96E-05 | 0.005629 |
| ENSDARG00000093546 | ms4a17a.10 | 61.69524 | 1.073963 | 9.62E-05 | 0.006004 |
| ENSDARG00000086100 | cd302 | 174.8626 | 0.680712 | 9.83E-05 | 0.0061 |
| ENSDARG00000045887 | mmp30 | 844.3355 | 0.554946 | 9.88E-05 | 0.006112 |
| ENSDARG00000030915 | cpa1 | 672.6076 | 1.012477 | 0.000101 | 0.006226 |
| ENSDARG00000028096 | cldn23a | 319.406 | 0.8104 | 0.000101 | 0.006226 |
| ENSDARG00000105498 | si:ch211-220e11.3 | 85.26038 | 0.837398 | 0.000102 | 0.006234 |
| ENSDARG00000037281 | fgg | 2060.844 | 0.658663 | 0.000109 | 0.0066 |
| ENSDARG00000070331 | muc5.1 | 774.7429 | 0.594469 | 0.000111 | 0.006645 |
| ENSDARG00000003281 | pik3ip1 | 840.2665 | 0.405241 | 0.000111 | 0.006645 |
| ENSDARG00000040258 | si:ch73-340m8.2 | 68.00526 | 0.834116 | 0.000113 | 0.006696 |
| ENSDARG00000079255 | zgc:174935 | 140.5816 | 0.829868 | 0.000113 | 0.006696 |
| ENSDARG00000031954 | rbck1 | 130.4467 | 0.587562 | 0.000112 | 0.006696 |
| ENSDARG00000098293 | si:dkey-27i16.2 | 81.93384 | 0.770868 | 0.000115 | 0.00679 |
| ENSDARG00000009779 | mcl1a | 1757.412 | 0.723966 | 0.000116 | 0.006837 |
| ENSDARG00000055436 | ftr97 | 49.76731 | 0.858094 | 0.000117 | 0.006867 |
| ENSDARG00000015495 | klf3 | 346.8624 | 0.405853 | 0.000117 | 0.006874 |
| ENSDARG00000038025 | cbx7a | 441.3008 | 0.549487 | 0.00012 | 0.006981 |

**Table G.1 continued**

| #geneID | Upregulated gene | Base Mean | log2 Fold Change | pvalue | FDR |
|---|---|---|---|---|---|
| ENSDARG00000035178 | gna14 | 354.743 | 0.789877 | 0.000122 | 0.007092 |
| ENSDARG00000055290 | mpeg1.1 | 73.03198 | 0.834984 | 0.000123 | 0.007169 |
| ENSDARG00000105117 | sdad1 | 1262.171 | 0.478909 | 0.000127 | 0.007325 |
| ENSDARG00000111840 | cxcl18a.1 | 31.07463 | 1.403989 | 0.000128 | 0.007345 |
| ENSDARG00000103483 | litaf | 216.3076 | 0.715842 | 0.000127 | 0.007345 |
| ENSDARG00000092653 | si:dkey-1h24.6 | 18.28991 | 1.458782 | 0.00013 | 0.007467 |
| ENSDARG00000076146 | zgc:172075 | 75.7153 | 0.967937 | 0.000138 | 0.007875 |
| ENSDARG00000105142 | tcirg1b | 273.4634 | 0.488656 | 0.000143 | 0.008146 |
| ENSDARG00000088641 | grn2 | 71.48058 | 1.211005 | 0.000145 | 0.008191 |
| ENSDARG00000043729 | plac8.1 | 1073.993 | 0.683361 | 0.000146 | 0.00826 |
| ENSDARG00000071216 | si:ch211-133n4.9 | 28.65668 | 1.204645 | 0.000148 | 0.008317 |
| ENSDARG00000000804 | rassf6 | 133.3712 | 0.692757 | 0.00015 | 0.008448 |
| ENSDARG00000038683 | MFAP4_(1_of_many) | 43.77511 | 1.22136 | 0.000155 | 0.008685 |
| ENSDARG00000077982 | elf3 | 606.2731 | 0.881509 | 0.000161 | 0.008977 |
| ENSDARG00000095633 | si:ch211-133l5.7 | 702.9712 | 0.420572 | 0.000171 | 0.009527 |
| ENSDARG00000043770 | si:dkey-192d15.2 | 119.2418 | 0.773827 | 0.000172 | 0.009528 |
| ENSDARG00000038561 | klf6b | 29.21789 | 1.114652 | 0.000173 | 0.009545 |
| ENSDARG00000089844 | scarb2c | 197.9489 | 0.541914 | 0.000173 | 0.009551 |
| ENSDARG00000007080 | rhcgl1 | 1055.087 | 0.618497 | 0.000174 | 0.009562 |
| ENSDARG00000053761 | si:dkey-187j14.4 | 164.9086 | 0.864448 | 0.000177 | 0.009654 |
| ENSDARG00000009939 | micu2 | 322.8228 | 0.410181 | 0.000179 | 0.009756 |
| ENSDARG00000103199 | si:dkey-247k7.2 | 2534.908 | 1.582384 | 0.000183 | 0.009892 |
| ENSDARG00000076914 | lacc1 | 24.38059 | 1.298572 | 0.000182 | 0.009892 |
| ENSDARG00000026611 | socs3b | 243.7919 | 0.594993 | 0.000183 | 0.009892 |

**Table G.2. Genes downregulated by CORT in WT larvae**

| #geneID | Downregulated gene | Base Mean | log2 Fold Change | p-value | FDR |
|---|---|---|---|---|---|
| ENSDARG00000055723 | hsp70l | 546.7091 | -0.81154 | 4.09E-10 | 1.44E-07 |
| ENSDARG00000024746 | hsp90aa1.2 | 4296.206 | -0.66537 | 4.26E-10 | 1.47E-07 |
| ENSDARG00000010478 | hsp90aa1.1 | 1623.901 | -0.76474 | 1.11E-08 | 2.58E-06 |
| ENSDARG00000024829 | tnn | 3412.689 | -0.53827 | 1.22E-07 | 2.11E-05 |
| ENSDARG00000011020 | hnrnpa1a | 1870.918 | -0.60346 | 2.93E-07 | 4.63E-05 |
| ENSDARG00000056160 | hspd1 | 3663.657 | -0.81004 | 3.88E-07 | 5.86E-05 |
| ENSDARG00000031483 | col9a1b | 7214.68 | -0.97459 | 5.22E-07 | 7.46E-05 |
| ENSDARG00000031795 | abcf1 | 1642.913 | -0.54233 | 2.83E-06 | 0.00033 |
| ENSDARG00000097008 | opn1mw1 | 4394.881 | -0.49519 | 5.12E-06 | 0.000556 |
| ENSDARG00000096257 | si:ch73-367p23.2 | 14695.34 | -0.63239 | 6.15E-06 | 0.00064 |
| ENSDARG00000008433 | unc45b | 417.9777 | -0.73809 | 6.21E-06 | 0.00064 |
| ENSDARG00000035809 | col1a1b | 29061.61 | -0.97359 | 9.21E-06 | 0.0009 |
| ENSDARG00000044861 | opn1lw2 | 5504.249 | -0.97006 | 1.02E-05 | 0.000992 |
| ENSDARG00000041252 | gemin4 | 35.51873 | -1.19211 | 1.24E-05 | 0.001154 |
| ENSDARG00000010472 | atp1a2a | 3100.567 | -0.47132 | 1.83E-05 | 0.001583 |
| ENSDARG00000026165 | col11a1a | 12926.96 | -0.6842 | 1.82E-05 | 0.001583 |
| ENSDARG00000103846 | hspa5 | 5629.632 | -0.44279 | 2.23E-05 | 0.001892 |
| ENSDARG00000012422 | col11a2 | 3277.633 | -0.40197 | 3.10E-05 | 0.00245 |
| ENSDARG00000037691 | pcdh2ab2 | 41.34133 | -1.23959 | 3.48E-05 | 0.002719 |
| ENSDARG00000055527 | cmn | 2203.104 | -0.63635 | 4.28E-05 | 0.003192 |
| ENSDARG00000092467 | si:ch73-46j18.5 | 1890.728 | -0.507 | 4.54E-05 | 0.003346 |
| ENSDARG00000001889 | tuba1a | 3717.643 | -0.37239 | 5.24E-05 | 0.003691 |
| ENSDARG00000042535 | actc1a | 6453.287 | -0.42588 | 6.06E-05 | 0.004119 |
| ENSDARG00000037997 | tubb5 | 2818.7 | -0.75825 | 7.28E-05 | 0.004758 |
| ENSDARG00000102362 | slc25a12 | 1103.604 | -0.40025 | 7.38E-05 | 0.004796 |
| ENSDARG00000002403 | nusap1 | 163.1077 | -0.68255 | 7.72E-05 | 0.005002 |
| ENSDARG00000104436 | zgc:153426 | 1916.44 | -0.67362 | 8.24E-05 | 0.005286 |
| ENSDARG00000070537 | stmn2b | 1132.949 | -0.43677 | 8.53E-05 | 0.005455 |
| ENSDARG00000020482 | nono | 1165.81 | -0.36805 | 9.34E-05 | 0.005848 |
| ENSDARG00000103837 | MYH6_(1_of_many) | 298.2776 | -0.53989 | 0.000102 | 0.006245 |
| ENSDARG00000011665 | aldoaa | 8685.712 | -0.33477 | 0.000103 | 0.006287 |
| ENSDARG00000045677 | opn1sw1 | 35207.02 | -0.82316 | 0.000109 | 0.006616 |
| ENSDARG00000074745 | zmp:0000000760 | 1637.445 | -0.5522 | 0.000111 | 0.006645 |
| ENSDARG00000078654 | tpx2 | 254.7152 | -0.56313 | 0.000141 | 0.008052 |
| ENSDARG00000077187 | impg1a | 169.6942 | -0.74244 | 0.000176 | 0.009654 |

**Table G.3. Genes upregulated by CORT in Klf9 mutant larvae**

| #geneID | Upregulated gene | Base Mean | log2 Fold Change | p-value | FDR |
|---|---|---|---|---|---|
| ENSDARG00000026726 | anxa1a | 3280.766 | 0.918698 | 3.29E-18 | 5.50E-14 |
| ENSDARG00000058371 | krt5 | 72173.03 | 0.973768 | 1.91E-16 | 1.60E-12 |
| ENSDARG00000094041 | krt17 | 52077.67 | 1.18166 | 2.18E-13 | 5.46E-10 |
| ENSDARG00000052779 | zgc:153932 | 251.4699 | 1.117693 | 2.61E-13 | 5.46E-10 |
| ENSDARG00000016691 | cd9b | 718.9376 | 0.834182 | 4.76E-13 | 7.95E-10 |
| ENSDARG00000034836 | si:dkey-222n6.2 | 803.5529 | 0.795187 | 4.62E-13 | 7.95E-10 |
| ENSDARG00000018637 | sec61g | 3267.609 | 0.710579 | 9.04E-12 | 1.08E-08 |
| ENSDARG00000004658 | zgc:101810 | 615.9247 | 0.693238 | 3.15E-11 | 3.29E-08 |
| ENSDARG00000078042 | il10rb | 501.2969 | 0.698075 | 4.74E-11 | 4.40E-08 |
| ENSDARG00000053858 | crip1 | 1336.582 | 0.710789 | 6.79E-11 | 5.67E-08 |
| ENSDARG00000023082 | krt1-19d | 2459.91 | 0.57053 | 8.48E-11 | 6.75E-08 |
| ENSDARG00000042829 | si:dkey-30j22.1 | 482.4749 | 0.769334 | 1.29E-10 | 9.77E-08 |
| ENSDARG00000105829 | CR788316.4 | 215.3995 | 1.17663 | 1.51E-10 | 1.05E-07 |
| ENSDARG00000022165 | mgst1.2 | 1320.948 | 0.752839 | 3.00E-10 | 1.81E-07 |
| ENSDARG00000009779 | mcl1a | 1499.018 | 0.64736 | 2.82E-10 | 1.81E-07 |
| ENSDARG00000040628 | zgc:110333 | 390.2532 | 0.804541 | 4.12E-10 | 2.37E-07 |
| ENSDARG00000098949 | mslna | 119.7335 | 1.168097 | 4.47E-10 | 2.49E-07 |
| ENSDARG00000040045 | cldn1 | 326.699 | 0.893628 | 5.21E-10 | 2.81E-07 |
| ENSDARG00000100952 | wu:fj16a03 | 527.069 | 0.688436 | 5.65E-10 | 2.95E-07 |
| ENSDARG00000090268 | krtt1c19e | 36826.58 | 0.851816 | 6.69E-10 | 3.19E-07 |
| ENSDARG00000021787 | abcb5 | 6345.886 | 0.742529 | 6.55E-10 | 3.19E-07 |
| ENSDARG00000068589 | vimr1 | 1057.587 | 0.673571 | 7.55E-10 | 3.50E-07 |
| ENSDARG00000042055 | fam129aa | 297.1694 | 0.776593 | 8.10E-10 | 3.62E-07 |
| ENSDARG00000100588 | rpl36 | 7816.252 | 0.473833 | 8.72E-10 | 3.73E-07 |
| ENSDARG00000039381 | ch25hl1.1 | 347.6442 | 0.700776 | 1.16E-09 | 4.60E-07 |
| ENSDARG00000101794 | atp6v0e1 | 486.613 | 0.675094 | 1.13E-09 | 4.60E-07 |
| ENSDARG00000009250 | etfb | 3117.548 | 0.545325 | 2.08E-09 | 7.89E-07 |
| ENSDARG00000094300 | nupr1a | 564.0208 | 0.752303 | 3.34E-09 | 1.15E-06 |
| ENSDARG00000104537 | cox7c | 2343.672 | 0.622983 | 3.37E-09 | 1.15E-06 |
| ENSDARG00000054060 | pof1b | 934.5372 | 0.59492 | 3.37E-09 | 1.15E-06 |
| ENSDARG00000094210 | zgc:109934 | 1893.308 | 0.63316 | 3.83E-09 | 1.26E-06 |
| ENSDARG00000012341 | capn9 | 359.1312 | 0.753619 | 3.93E-09 | 1.26E-06 |
| ENSDARG00000041483 | paqr6 | 534.5361 | 0.658462 | 5.30E-09 | 1.64E-06 |
| ENSDARG00000093628 | s100a11 | 804.7141 | 0.821529 | 6.89E-09 | 1.99E-06 |
| ENSDARG00000102435 | plekhf1 | 366.1218 | 0.737877 | 6.83E-09 | 1.99E-06 |
| ENSDARG00000036840 | krt15 | 6577.517 | 0.526672 | 6.71E-09 | 1.99E-06 |
| ENSDARG00000035326 | nccrp1 | 469.7927 | 0.645952 | 7.34E-09 | 2.04E-06 |
| ENSDARG00000043154 | ucp2 | 3654.183 | 0.540522 | 7.48E-09 | 2.04E-06 |
| ENSDARG00000027984 | gstz1 | 458.2283 | 0.692311 | 8.44E-09 | 2.21E-06 |

**Table G.3 continued**

| #geneID | Upregulated gene | Base Mean | log2 Fold Change | p-value | FDR |
|---|---|---|---|---|---|
| ENSDARG00000039832 | gsta.2 | 376.1378 | 0.671065 | 9.06E-09 | 2.33E-06 |
| ENSDARG00000026322 | dhrs13a.1 | 346.2039 | 0.693447 | 9.22E-09 | 2.33E-06 |
| ENSDARG00000069476 | spint2 | 1437.895 | 0.610836 | 9.82E-09 | 2.41E-06 |
| ENSDARG00000097157 | si:ch211-207n23.2 | 560.7747 | 0.841756 | 1.19E-08 | 2.87E-06 |
| ENSDARG00000091138 | actr3 | 1200.943 | 0.599404 | 1.38E-08 | 3.25E-06 |
| ENSDARG00000104200 | BX901923.2 | 515.7654 | 0.738298 | 1.48E-08 | 3.42E-06 |
| ENSDARG00000075014 | sqstm1 | 1142.005 | 0.649316 | 1.56E-08 | 3.52E-06 |
| ENSDARG00000019778 | rps6 | 25909.94 | 0.753608 | 1.92E-08 | 4.17E-06 |
| ENSDARG00000055514 | icn2 | 1788.426 | 0.7328 | 1.97E-08 | 4.17E-06 |
| ENSDARG00000035890 | fuca1.1 | 774.2099 | 0.619987 | 1.93E-08 | 4.17E-06 |
| ENSDARG00000003203 | rhcga | 666.5547 | 0.959943 | 2.36E-08 | 4.70E-06 |
| ENSDARG00000033170 | sult2st1 | 360.6829 | 0.783444 | 2.34E-08 | 4.70E-06 |
| ENSDARG00000043102 | lxn | 526.5027 | 0.780995 | 2.32E-08 | 4.70E-06 |
| ENSDARG00000079175 | si:ch211-79k12.1 | 361.5794 | 0.667891 | 2.41E-08 | 4.75E-06 |
| ENSDARG00000091801 | serpinb14 | 492.4033 | 0.608772 | 2.58E-08 | 5.02E-06 |
| ENSDARG00000055046 | ponzr5 | 301.9423 | 0.719197 | 2.65E-08 | 5.06E-06 |
| ENSDARG00000102986 | csf1ra | 400.1724 | 0.682651 | 2.67E-08 | 5.06E-06 |
| ENSDARG00000060682 | agr1 | 1047.326 | 0.628817 | 2.80E-08 | 5.25E-06 |
| ENSDARG00000037790 | pvalb8 | 1781.592 | 0.538844 | 2.83E-08 | 5.25E-06 |
| ENSDARG00000005926 | ak2 | 1388.901 | 0.532766 | 3.90E-08 | 6.83E-06 |
| ENSDARG00000109310 | im:7150988 | 224.237 | 1.161263 | 4.63E-08 | 7.98E-06 |
| ENSDARG00000036044 | rps20 | 15622.93 | 0.422245 | 5.64E-08 | 9.42E-06 |
| ENSDARG00000007080 | rhcgl1 | 793.4592 | 0.679438 | 5.73E-08 | 9.48E-06 |
| ENSDARG00000096721 | si:rp71-1c10.11 | 290.8427 | 0.653302 | 6.45E-08 | 1.03E-05 |
| ENSDARG00000113977 | zgc:194125 | 2020.26 | 0.550788 | 6.99E-08 | 1.10E-05 |
| ENSDARG00000045514 | atp5f1c | 4932.979 | 0.465782 | 7.17E-08 | 1.12E-05 |
| ENSDARG00000007739 | atp1a1a.2 | 2121.818 | 0.720085 | 8.33E-08 | 1.27E-05 |
| ENSDARG00000025254 | s100a10b | 1227.483 | 0.539212 | 9.07E-08 | 1.35E-05 |
| ENSDARG00000093303 | ifitm1 | 178.7251 | 0.948295 | 9.85E-08 | 1.46E-05 |
| ENSDARG00000104069 | rnf170 | 432.5467 | 0.735396 | 1.09E-07 | 1.60E-05 |
| ENSDARG00000011245 | esrp1 | 732.6923 | 0.580144 | 1.30E-07 | 1.88E-05 |
| ENSDARG00000027750 | dpp7 | 492.2575 | 0.542011 | 1.39E-07 | 1.99E-05 |
| ENSDARG00000100969 | tmprss13a | 125.0188 | 0.942869 | 1.47E-07 | 2.08E-05 |
| ENSDARG00000011693 | ttc36 | 198.3207 | 0.834792 | 1.82E-07 | 2.49E-05 |
| ENSDARG00000053448 | si:ch211-251f6.6 | 191.7542 | 0.833517 | 2.05E-07 | 2.76E-05 |
| ENSDARG00000056378 | ifi30 | 340.8921 | 0.630144 | 2.12E-07 | 2.81E-05 |
| ENSDARG00000073905 | zgc:92481 | 462.6369 | 0.60379 | 2.33E-07 | 3.02E-05 |
| ENSDARG00000014496 | trpv6 | 1637.182 | 0.823715 | 2.54E-07 | 3.24E-05 |
| ENSDARG00000039579 | cfd | 1298.05 | 0.653425 | 2.58E-07 | 3.24E-05 |

**Table G.3 continued**

| #geneID | Upregulated gene | Base Mean | log2 Fold Change | p-value | FDR |
|---|---|---|---|---|---|
| ENSDARG00000005108 | oclna | 727.4432 | 0.594423 | 2.80E-07 | 3.49E-05 |
| ENSDARG00000014047 | cldn7b | 845.7909 | 0.607859 | 2.91E-07 | 3.58E-05 |
| ENSDARG00000093584 | zgc:193505 | 352.2222 | 0.595243 | 2.92E-07 | 3.58E-05 |
| ENSDARG00000102591 | btr30 | 249.8119 | 0.879248 | 3.21E-07 | 3.88E-05 |
| ENSDARG00000035018 | thy1 | 319.5186 | 0.700807 | 3.31E-07 | 3.94E-05 |
| ENSDARG00000040747 | tm4sf4 | 1893.226 | 0.487526 | 3.33E-07 | 3.94E-05 |
| ENSDARG00000057437 | apodb | 797.0636 | 0.604388 | 4.71E-07 | 5.35E-05 |
| ENSDARG00000099902 | il17rc | 370.213 | 0.600369 | 4.65E-07 | 5.35E-05 |
| ENSDARG00000076836 | gpx4b | 2086.664 | 0.552581 | 5.37E-07 | 5.98E-05 |
| ENSDARG00000090462 | mrpl20 | 249.843 | 0.856314 | 5.60E-07 | 6.20E-05 |
| ENSDARG00000021366 | fbp1a | 670.3167 | 0.539974 | 5.72E-07 | 6.29E-05 |
| ENSDARG00000098724 | rgrb | 846.469 | 0.814261 | 5.87E-07 | 6.41E-05 |
| ENSDARG00000041505 | itm2bb | 967.3922 | 0.469962 | 6.01E-07 | 6.48E-05 |
| ENSDARG00000032405 | ckap4 | 829.0893 | 0.763357 | 6.47E-07 | 6.88E-05 |
| ENSDARG00000009978 | icn | 4175.041 | 0.500339 | 6.70E-07 | 6.99E-05 |
| ENSDARG00000003091 | oclnb | 371.5721 | 0.645252 | 7.03E-07 | 7.25E-05 |
| ENSDARG00000095400 | si:ch73-52f15.5 | 180.2961 | 0.74188 | 7.18E-07 | 7.31E-05 |
| ENSDARG00000071626 | ptgdsb.2 | 2944.678 | 0.410089 | 7.63E-07 | 7.73E-05 |
| ENSDARG00000029069 | tnni2a.4 | 23712.62 | 0.587153 | 7.83E-07 | 7.88E-05 |
| ENSDARG00000094760 | si:dkey-125i10.3 | 239.9625 | 0.646261 | 9.15E-07 | 9.10E-05 |
| ENSDARG00000093957 | si:dkey-251i10.2 | 303.8125 | 0.842579 | 9.47E-07 | 9.36E-05 |
| ENSDARG00000076221 | zgc:198419 | 2859.424 | 0.578076 | 1.06E-06 | 0.000102 |
| ENSDARG00000090185 | si:dkeyp-73b11.8 | 1214.062 | 0.441324 | 1.05E-06 | 0.000102 |
| ENSDARG00000079745 | si:ch211-166a6.5 | 8489.529 | 0.584481 | 1.09E-06 | 0.000104 |
| ENSDARG00000043442 | zgc:153665 | 194.8664 | 0.814089 | 1.13E-06 | 0.000106 |
| ENSDARG00000040076 | pycard | 272.252 | 0.667795 | 1.14E-06 | 0.000106 |
| ENSDARG00000015123 | dnase1l4.1 | 300.1371 | 0.607471 | 1.14E-06 | 0.000106 |
| ENSDARG00000052705 | pkp1b | 218.9248 | 0.698982 | 1.16E-06 | 0.000106 |
| ENSDARG00000033364 | mgst3b | 1540.193 | 0.565311 | 1.16E-06 | 0.000106 |
| ENSDARG00000091116 | pkhd1l1 | 704.2367 | 0.726883 | 1.22E-06 | 0.000109 |
| ENSDARG00000018404 | krt18 | 4899.164 | 0.449489 | 1.24E-06 | 0.00011 |
| ENSDARG00000089645 | si:ch1073-406l10.2 | 234.7907 | 0.766265 | 1.26E-06 | 0.000111 |
| ENSDARG00000053217 | cox7a2a | 1460.056 | 0.573562 | 1.26E-06 | 0.000111 |
| ENSDARG00000037425 | s100a10a | 757.0633 | 0.489266 | 1.32E-06 | 0.000115 |
| ENSDARG00000069920 | cox17 | 683.3919 | 0.635035 | 1.46E-06 | 0.000126 |
| ENSDARG00000114245 | zgc:158619 | 541.7742 | 0.593093 | 1.45E-06 | 0.000126 |
| ENSDARG00000043453 | rps5 | 26791.6 | 0.629983 | 1.49E-06 | 0.000128 |
| ENSDARG00000038666 | igfbp1b | 201.0025 | 0.773861 | 1.52E-06 | 0.000129 |
| ENSDARG00000015128 | rpl27 | 16596.93 | 0.586153 | 1.58E-06 | 0.000133 |

**Table G.3 continued**

| #geneID | Upregulated gene | Base Mean | log2 Fold Change | p-value | FDR |
|---|---|---|---|---|---|
| ENSDARG00000057984 | eps8l1a | 239.6344 | 0.654661 | 1.63E-06 | 0.000134 |
| ENSDARG00000115271 | zgc:171772 | 22529.35 | 0.689708 | 1.85E-06 | 0.000149 |
| ENSDARG00000036942 | gpd1c | 654.1379 | 0.552396 | 1.91E-06 | 0.000153 |
| ENSDARG00000067958 | sh3gl1a | 212.2214 | 0.618714 | 1.92E-06 | 0.000154 |
| ENSDARG00000004748 | zgc:100868 | 778.4416 | 0.605082 | 2.01E-06 | 0.000158 |
| ENSDARG00000040764 | id1 | 2116.43 | 0.452307 | 2.29E-06 | 0.000178 |
| ENSDARG00000090369 | zgc:86896 | 2557.403 | 0.487776 | 2.38E-06 | 0.000183 |
| ENSDARG00000041947 | styk1b | 252.5459 | 0.646587 | 2.44E-06 | 0.000187 |
| ENSDARG00000113599 | hbbe1.1 | 3430.593 | 0.80076 | 2.54E-06 | 0.000193 |
| ENSDARG00000086842 | dap1b | 758.9604 | 0.573265 | 2.71E-06 | 0.000203 |
| ENSDARG00000054610 | coro1a | 173.4598 | 0.802986 | 2.77E-06 | 0.000207 |
| ENSDARG00000086216 | prr13 | 312.9745 | 0.557979 | 2.78E-06 | 0.000207 |
| ENSDARG00000070437 | rpl22 | 5662.554 | 0.432377 | 2.82E-06 | 0.000209 |
| ENSDARG00000061391 | grhl1 | 403.9754 | 0.684297 | 2.92E-06 | 0.000213 |
| ENSDARG00000100513 | rps27l | 333.5692 | 0.607267 | 2.91E-06 | 0.000213 |
| ENSDARG00000043128 | cldne | 833.8417 | 0.5514 | 2.94E-06 | 0.000213 |
| ENSDARG00000043848 | sod1 | 1766.971 | 0.388415 | 2.93E-06 | 0.000213 |
| ENSDARG00000054696 | psmb4 | 1327.561 | 0.469759 | 3.02E-06 | 0.000218 |
| ENSDARG00000042707 | cx30.3 | 469.4395 | 0.6099 | 3.04E-06 | 0.000218 |
| ENSDARG00000042245 | myl13 | 6524.085 | 0.492861 | 3.09E-06 | 0.00022 |
| ENSDARG00000036671 | tnni4b.2 | 1477.587 | 0.541064 | 3.34E-06 | 0.000235 |
| ENSDARG00000040513 | zgc:92313 | 296.5934 | 0.575224 | 3.55E-06 | 0.000247 |
| ENSDARG00000038577 | cox6c | 1920.221 | 0.374382 | 3.77E-06 | 0.000259 |
| ENSDARG00000009544 | cldnb | 514.2274 | 0.666589 | 3.94E-06 | 0.000269 |
| ENSDARG00000104233 | dynlrb1 | 207.7963 | 0.922346 | 3.97E-06 | 0.00027 |
| ENSDARG00000070057 | si:dkey-69o16.5 | 91.62713 | 1.137838 | 4.02E-06 | 0.000272 |
| ENSDARG00000077934 | tegt | 1247.521 | 0.498731 | 4.34E-06 | 0.000291 |
| ENSDARG00000098746 | dhrs13l1 | 932.6283 | 0.592455 | 4.60E-06 | 0.000306 |
| ENSDARG00000116628 | BX908782.3 | 73.65363 | 0.940997 | 4.76E-06 | 0.000313 |
| ENSDARG00000003216 | anxa2a | 2979.549 | 0.544841 | 4.73E-06 | 0.000313 |
| ENSDARG00000101892 | ino80e | 360.0157 | 0.529484 | 5.04E-06 | 0.000329 |
| ENSDARG00000038694 | zgc:101744 | 794.6652 | 0.481295 | 5.15E-06 | 0.000332 |
| ENSDARG00000100223 | gpa33a | 851.3221 | 0.501015 | 5.23E-06 | 0.000335 |
| ENSDARG00000042866 | cx35.4 | 179.8878 | 0.62194 | 5.29E-06 | 0.000337 |
| ENSDARG00000102051 | mtbl | 341.0597 | 0.638396 | 5.39E-06 | 0.000339 |
| ENSDARG00000091996 | si:ch211-117m20.5 | 966.365 | 0.635204 | 5.38E-06 | 0.000339 |
| ENSDARG00000009447 | atp5mc3b | 7899.511 | 0.373755 | 5.35E-06 | 0.000339 |
| ENSDARG00000068088 | tcnl | 193.5228 | 0.736869 | 5.54E-06 | 0.000345 |
| ENSDARG00000045143 | hbbe2 | 1657.141 | 0.684429 | 5.55E-06 | 0.000345 |

**Table G.3 continued**

| #geneID | Upregulated gene | Base Mean | log2 Fold Change | p-value | FDR |
|---|---|---|---|---|---|
| ENSDARG00000034677 | scel | 1276.971 | 0.561091 | 5.61E-06 | 0.000346 |
| ENSDARG00000078619 | pnp5a | 969.9164 | 0.556997 | 5.64E-06 | 0.000346 |
| ENSDARG00000055592 | capn2b | 281.0653 | 0.707475 | 5.69E-06 | 0.000347 |
| ENSDARG00000095897 | atp5f1e | 1205.348 | 0.52252 | 5.70E-06 | 0.000347 |
| ENSDARG00000068478 | gpx4a | 6028.37 | 0.460691 | 5.93E-06 | 0.000358 |
| ENSDARG00000074869 | si:ch1073-291c23.2 | 372.1164 | 0.549067 | 6.00E-06 | 0.00036 |
| ENSDARG00000076121 | smpd1 | 247.8247 | 0.573726 | 6.08E-06 | 0.000364 |
| ENSDARG00000055395 | foxq1b | 183.4449 | 0.747939 | 6.12E-06 | 0.000365 |
| ENSDARG00000063435 | trpm4b.2 | 191.0543 | 0.687971 | 6.26E-06 | 0.000372 |
| ENSDARG00000028098 | fut9d | 1090.591 | 0.581504 | 6.39E-06 | 0.000377 |
| ENSDARG00000033285 | gsto2 | 952.9609 | 0.576058 | 6.55E-06 | 0.000383 |
| ENSDARG00000025403 | ftr83 | 302.9105 | 0.628463 | 6.62E-06 | 0.000384 |
| ENSDARG00000102291 | eef1da | 7233.301 | 0.430877 | 6.61E-06 | 0.000384 |
| ENSDARG00000103929 | ildr1a | 368.0728 | 0.640744 | 6.84E-06 | 0.000395 |
| ENSDARG00000103296 | nup54 | 486.8859 | 0.604959 | 7.01E-06 | 0.000401 |
| ENSDARG00000060980 | atp8b1 | 317.8065 | 0.788611 | 7.15E-06 | 0.000408 |
| ENSDARG00000074390 | tmem176l.4 | 842.5302 | 0.604666 | 7.39E-06 | 0.000419 |
| ENSDARG00000018814 | esrp2 | 499.9383 | 0.500633 | 7.39E-06 | 0.000419 |
| ENSDARG00000076623 | col14a1b | 1270.125 | 0.549695 | 7.88E-06 | 0.00044 |
| ENSDARG00000099448 | sh3d21 | 397.6538 | 0.51897 | 8.29E-06 | 0.000457 |
| ENSDARG00000078797 | dennd3a | 224.9658 | 0.621316 | 8.58E-06 | 0.000472 |
| ENSDARG00000102364 | si:dkey-202l22.6 | 121.9753 | 0.798238 | 8.93E-06 | 0.000483 |
| ENSDARG00000032079 | acsl3a | 174.6879 | 0.663387 | 8.90E-06 | 0.000483 |
| ENSDARG00000003526 | psma5 | 784.1273 | 0.519638 | 8.88E-06 | 0.000483 |
| ENSDARG00000039499 | soul2 | 567.0256 | 0.569979 | 8.99E-06 | 0.000484 |
| ENSDARG00000014556 | serpinb1l3 | 923.7275 | 0.458178 | 9.12E-06 | 0.000487 |
| ENSDARG00000005481 | nfkbiaa | 265.2361 | 0.595178 | 9.36E-06 | 0.000496 |
| ENSDARG00000115557 | cox7b | 3136.345 | 0.465053 | 9.48E-06 | 0.0005 |
| ENSDARG00000037960 | lrrc17 | 421.387 | 0.5238 | 9.89E-06 | 0.000513 |
| ENSDARG00000100582 | si:ch211-195b11.3 | 1679.886 | 0.659231 | 1.00E-05 | 0.000516 |
| ENSDARG00000041400 | ndufa3 | 869.6834 | 0.612325 | 1.08E-05 | 0.000551 |
| ENSDARG00000055093 | cdh27 | 227.9451 | 0.608631 | 1.10E-05 | 0.000561 |
| ENSDARG00000029064 | uqcrq | 1682.87 | 0.438619 | 1.10E-05 | 0.000561 |
| ENSDARG00000090552 | si:dkey-7j14.6 | 428.5925 | 0.503979 | 1.12E-05 | 0.000564 |
| ENSDARG00000077533 | eif3f | 3965.899 | 0.468572 | 1.14E-05 | 0.000573 |
| ENSDARG00000089187 | wfdc2 | 189.7914 | 0.654746 | 1.16E-05 | 0.000578 |
| ENSDARG00000077360 | zgc:173593 | 246.0061 | 0.720835 | 1.19E-05 | 0.000589 |
| ENSDARG00000035028 | lpcat4 | 240.366 | 0.596245 | 1.29E-05 | 0.000636 |
| ENSDARG00000096003 | atp5md | 925.9758 | 0.570593 | 1.32E-05 | 0.000647 |

**Table G.3 continued**

| #geneID | Upregulated gene | Base Mean | log2 Fold Change | p-value | FDR |
|---|---|---|---|---|---|
| ENSDARG00000095796 | si:dkey-87o1.2 | 220.8512 | 0.623629 | 1.32E-05 | 0.000648 |
| ENSDARG00000076673 | wu:fi04e12 | 1027.631 | 0.507514 | 1.33E-05 | 0.00065 |
| ENSDARG00000075164 | mylk5 | 495.4604 | 0.491502 | 1.34E-05 | 0.000651 |
| ENSDARG00000111240 | dhrs13a.2 | 181.2838 | 0.950822 | 1.36E-05 | 0.000661 |
| ENSDARG00000116617 | spaca4l | 1106.453 | 0.689667 | 1.40E-05 | 0.000665 |
| ENSDARG00000087402 | tpm1 | 3093.157 | 0.399846 | 1.42E-05 | 0.000673 |
| ENSDARG00000095826 | smdt1a | 134.2467 | 0.762937 | 1.44E-05 | 0.000681 |
| ENSDARG00000004875 | tmc6b | 504.8069 | 0.46719 | 1.46E-05 | 0.000687 |
| ENSDARG00000017388 | gstt1b | 490.6493 | 0.465392 | 1.48E-05 | 0.000691 |
| ENSDARG00000097959 | si:dkey-248g15.3 | 430.8317 | 0.574213 | 1.55E-05 | 0.000719 |
| ENSDARG00000075468 | vwa1 | 322.9317 | 0.561629 | 1.57E-05 | 0.000727 |
| ENSDARG00000062221 | arap1a | 89.52311 | 0.831173 | 1.60E-05 | 0.000738 |
| ENSDARG00000052712 | suclg1 | 3605.475 | 0.437904 | 1.66E-05 | 0.000758 |
| ENSDARG00000021984 | ndufa2 | 612.5223 | 0.537181 | 1.71E-05 | 0.000778 |
| ENSDARG00000044073 | fuca2 | 513.6839 | 0.515189 | 1.76E-05 | 0.000795 |
| ENSDARG00000012972 | cfl1l | 3340.519 | 0.445596 | 1.83E-05 | 0.000815 |
| ENSDARG00000020929 | fam49ba | 265.0916 | 0.551054 | 1.89E-05 | 0.000839 |
| ENSDARG00000035329 | capns1a | 2032.465 | 0.44195 | 1.89E-05 | 0.000839 |
| ENSDARG00000059841 | exosc1 | 270.4478 | 0.536203 | 1.94E-05 | 0.000859 |
| ENSDARG00000025350 | prdx2 | 5965.38 | 0.397701 | 2.10E-05 | 0.000917 |
| ENSDARG00000099117 | si:dkey-33i11.4 | 713.8102 | 0.596132 | 2.16E-05 | 0.000941 |
| ENSDARG00000058206 | si:ch211-153b23.5 | 421.4994 | 0.482808 | 2.16E-05 | 0.000941 |
| ENSDARG00000029500 | rpl34 | 13294.49 | 0.407432 | 2.20E-05 | 0.00095 |
| ENSDARG00000035400 | btf3 | 11052.1 | 0.32608 | 2.19E-05 | 0.00095 |
| ENSDARG00000056836 | si:ch211-125o16.4 | 2139.646 | 0.672869 | 2.21E-05 | 0.000955 |
| ENSDARG00000036876 | zgc:153284 | 180.6052 | 0.64262 | 2.27E-05 | 0.000974 |
| ENSDARG00000041623 | mt2 | 1093.172 | 0.482751 | 2.36E-05 | 0.001013 |
| ENSDARG00000007244 | acp2 | 403.674 | 0.445902 | 2.50E-05 | 0.001064 |
| ENSDARG00000017034 | sqor | 394.1507 | 0.491471 | 2.54E-05 | 0.001079 |
| ENSDARG00000037867 | atp5mf | 1553.011 | 0.428291 | 2.55E-05 | 0.001079 |
| ENSDARG00000013475 | cct4 | 4809.234 | 0.340121 | 2.55E-05 | 0.001079 |
| ENSDARG00000099351 | igfbp1a | 335.1117 | 0.561266 | 2.57E-05 | 0.00108 |
| ENSDARG00000055416 | serpinb1 | 760.0758 | 0.389263 | 2.57E-05 | 0.00108 |
| ENSDARG00000062171 | olfml3b | 362.9969 | 0.484366 | 2.67E-05 | 0.00112 |
| ENSDARG00000076386 | epdl1 | 589.9244 | 0.454664 | 2.80E-05 | 0.001161 |
| ENSDARG00000012467 | spint1b | 226.508 | 0.654783 | 2.85E-05 | 0.001175 |
| ENSDARG00000041051 | mid1ip1a | 596.6958 | 0.525587 | 2.92E-05 | 0.001195 |
| ENSDARG00000041595 | ces3 | 458.368 | 0.57274 | 2.96E-05 | 0.001202 |
| ENSDARG00000074507 | rmdn1 | 448.4813 | 0.600826 | 3.13E-05 | 0.001259 |

**Table G.3 continued**

| #geneID | Upregulated gene | Base Mean | log2 Fold Change | p-value | FDR |
|---|---|---|---|---|---|
| ENSDARG00000101406 | rplp2 | 8201.748 | 0.533729 | 3.15E-05 | 0.001261 |
| ENSDARG00000103220 | slc10a3 | 240.5313 | 0.604279 | 3.16E-05 | 0.001262 |
| ENSDARG00000019845 | pdlim1 | 361.0612 | 0.535885 | 3.19E-05 | 0.001273 |
| ENSDARG00000100788 | trip10b | 70.56885 | 0.899145 | 3.21E-05 | 0.001274 |
| ENSDARG00000070480 | agr2 | 557.4797 | 0.773967 | 3.21E-05 | 0.001274 |
| ENSDARG00000090969 | cbln18 | 94.26156 | 0.835021 | 3.22E-05 | 0.001274 |
| ENSDARG00000045262 | gsnb | 501.0169 | 0.497624 | 3.26E-05 | 0.001281 |
| ENSDARG00000004745 | lmbr1l | 302.295 | 0.495522 | 3.32E-05 | 0.001297 |
| ENSDARG00000099672 | capgb | 456.5585 | 0.468857 | 3.32E-05 | 0.001297 |
| ENSDARG00000079119 | si:ch211-229d2.5 | 346.1516 | 0.481013 | 3.37E-05 | 0.001307 |
| ENSDARG00000023820 | faxdc2 | 1730.971 | 0.470616 | 3.56E-05 | 0.001374 |
| ENSDARG00000038608 | sdhc | 1082.301 | 0.430625 | 3.60E-05 | 0.001384 |
| ENSDARG00000105223 | pmp22a | 1187.967 | 0.415899 | 3.68E-05 | 0.001409 |
| ENSDARG00000042561 | lpar2b | 108.6828 | 0.751679 | 3.69E-05 | 0.001412 |
| ENSDARG00000024540 | tspan36 | 795.5373 | 0.415376 | 3.83E-05 | 0.001456 |
| ENSDARG00000104138 | igfbp7 | 395.3971 | 0.632055 | 3.86E-05 | 0.001464 |
| ENSDARG00000089368 | hopx | 378.7718 | 0.551075 | 4.15E-05 | 0.001561 |
| ENSDARG00000037350 | rpl9 | 23936.27 | 0.54174 | 4.22E-05 | 0.001576 |
| ENSDARG00000056119 | eef1g | 27546.61 | 0.448999 | 4.21E-05 | 0.001576 |
| ENSDARG00000016867 | rnf128a | 821.205 | 0.408845 | 4.21E-05 | 0.001576 |
| ENSDARG00000101910 | pcdh20 | 273.2198 | 0.50297 | 4.23E-05 | 0.001577 |
| ENSDARG00000031317 | ppdpfb | 3510.369 | 0.314598 | 4.24E-05 | 0.001577 |
| ENSDARG00000100815 | srsf3a | 84.49106 | 0.919143 | 4.44E-05 | 0.001639 |
| ENSDARG00000090156 | pttg1ipa | 257.0056 | 0.541172 | 4.58E-05 | 0.001687 |
| ENSDARG00000076572 | crygm2d7 | 5531.527 | 0.494989 | 4.72E-05 | 0.001728 |
| ENSDARG00000063631 | VIT | 489.2739 | 0.561262 | 4.76E-05 | 0.00174 |
| ENSDARG00000006202 | erbb3a | 494.3357 | 0.462614 | 4.79E-05 | 0.001747 |
| ENSDARG00000035198 | gcnt4a | 180.0924 | 0.620847 | 4.89E-05 | 0.001776 |
| ENSDARG00000031929 | stard14 | 231.7343 | 0.526039 | 5.01E-05 | 0.001817 |
| ENSDARG00000042777 | ndufa11 | 788.2465 | 0.517713 | 5.06E-05 | 0.001817 |
| ENSDARG00000100133 | cnmd | 1017.439 | 0.393643 | 5.03E-05 | 0.001817 |
| ENSDARG00000006008 | dct | 1550.048 | 0.356417 | 5.06E-05 | 0.001817 |
| ENSDARG00000102452 | eif3ha | 1855.297 | 0.460906 | 5.19E-05 | 0.001852 |
| ENSDARG00000110357 | txndc15 | 225.0579 | 0.788989 | 5.30E-05 | 0.001884 |
| ENSDARG00000093316 | adgrf8 | 100.2797 | 0.733331 | 5.56E-05 | 0.001958 |
| ENSDARG00000110700 | COX7A2_(1_of_many) | 97.13202 | 0.724333 | 5.57E-05 | 0.001958 |
| ENSDARG00000019033 | tmem59 | 670.0033 | 0.433313 | 5.64E-05 | 0.001981 |
| ENSDARG00000068148 | arrdc1a | 170.5099 | 0.584197 | 5.66E-05 | 0.001981 |
| ENSDARG00000051914 | slc14a2 | 117.4326 | 0.733301 | 5.83E-05 | 0.00203 |

**Table G.3 continued**

| #geneID | Upregulated gene | Base Mean | log2 Fold Change | p-value | FDR |
|---|---|---|---|---|---|
| ENSDARG00000109678 | dap1b | 609.7888 | 0.392095 | 6.17E-05 | 0.00213 |
| ENSDARG00000023713 | aqp1a.1 | 713.7493 | 0.380722 | 6.17E-05 | 0.00213 |
| ENSDARG00000009285 | rpl15 | 17379.82 | 0.47383 | 6.34E-05 | 0.002184 |
| ENSDARG00000078918 | comtd1 | 196.6471 | 0.547882 | 6.56E-05 | 0.00224 |
| ENSDARG00000103271 | pla2g15 | 1345.436 | 0.439548 | 6.58E-05 | 0.002241 |
| ENSDARG00000042613 | crp3 | 813.3173 | 0.616694 | 6.66E-05 | 0.00226 |
| ENSDARG00000014313 | atp5pf | 1650.434 | 0.410256 | 6.67E-05 | 0.00226 |
| ENSDARG00000087476 | cbln20 | 135.2834 | 0.628307 | 6.69E-05 | 0.002261 |
| ENSDARG00000018146 | gpx1a | 697.9837 | 0.429249 | 6.72E-05 | 0.002264 |
| ENSDARG00000070787 | jupa | 1349.878 | 0.386231 | 6.76E-05 | 0.002269 |
| ENSDARG00000027867 | paplna | 232.0944 | 0.57084 | 6.84E-05 | 0.00228 |
| ENSDARG00000027345 | mpzl2b | 250.0581 | 0.51915 | 6.81E-05 | 0.00228 |
| ENSDARG00000057714 | cmah | 216.9422 | 0.507876 | 6.85E-05 | 0.00228 |
| ENSDARG00000095863 | afp4 | 3215.06 | 0.604136 | 6.96E-05 | 0.002312 |
| ENSDARG00000013822 | anapc16 | 258.9999 | 0.56918 | 7.17E-05 | 0.002361 |
| ENSDARG00000097902 | si:ch73-204p21.2 | 353.9723 | 0.500228 | 7.25E-05 | 0.002378 |
| ENSDARG00000098171 | zgc:162193 | 345.6147 | 0.480068 | 7.33E-05 | 0.002401 |
| ENSDARG00000101023 | msx2b | 94.00157 | 0.824041 | 7.44E-05 | 0.00242 |
| ENSDARG00000109902 | tmem254 | 95.81575 | 0.683493 | 7.44E-05 | 0.00242 |
| ENSDARG00000078882 | slc22a31 | 216.4258 | 0.569847 | 7.45E-05 | 0.00242 |
| ENSDARG00000013804 | capns1b | 1062.624 | 0.522189 | 7.59E-05 | 0.002446 |
| ENSDARG00000099803 | pik3c2g | 57.40869 | 0.952884 | 7.65E-05 | 0.002457 |
| ENSDARG00000055589 | s100t | 614.3325 | 0.370097 | 7.64E-05 | 0.002457 |
| ENSDARG00000092124 | cox14 | 234.2874 | 0.620809 | 7.90E-05 | 0.002519 |
| ENSDARG00000056630 | angptl5 | 141.9829 | 0.610676 | 7.93E-05 | 0.002523 |
| ENSDARG00000069279 | elovl7a | 360.129 | 0.553566 | 8.10E-05 | 0.002549 |
| ENSDARG00000088711 | lgals1l1 | 345.4349 | 0.834247 | 8.47E-05 | 0.002626 |
| ENSDARG00000038151 | zgc:92360 | 408.7935 | 0.475799 | 8.46E-05 | 0.002626 |
| ENSDARG00000004877 | rock2b | 316.966 | 0.462984 | 8.47E-05 | 0.002626 |
| ENSDARG00000070386 | krtcap2 | 228.8002 | 0.547664 | 8.53E-05 | 0.002639 |
| ENSDARG00000088641 | grn2 | 38.83351 | 1.075515 | 8.64E-05 | 0.002659 |
| ENSDARG00000031588 | si:dkey-239b22.1 | 916.657 | 0.639651 | 8.71E-05 | 0.002674 |
| ENSDARG00000020232 | eif6 | 586.0966 | 0.473291 | 8.86E-05 | 0.002703 |
| ENSDARG00000024775 | si:ch211-129c21.1 | 273.1484 | 0.527446 | 8.94E-05 | 0.002705 |
| ENSDARG00000054930 | tpra1 | 383.6323 | 0.447471 | 8.95E-05 | 0.002705 |
| ENSDARG00000070043 | dars | 1982.249 | 0.347158 | 8.97E-05 | 0.002705 |
| ENSDARG00000043242 | si:dkey-222f2.1 | 323.9371 | 0.468401 | 8.99E-05 | 0.002705 |
| ENSDARG00000006422 | esyt3 | 118.1377 | 0.707695 | 9.06E-05 | 0.002721 |
| ENSDARG00000002593 | slc45a2 | 749.8554 | 0.36571 | 9.21E-05 | 0.002762 |

**Table G.3 continued**

| #geneID | Upregulated gene | Base Mean | log2 Fold Change | p-value | FDR |
|---|---|---|---|---|---|
| ENSDARG00000074266 | si:ch1073-314i13.4 | 93.72954 | 0.780175 | 9.33E-05 | 0.002779 |
| ENSDARG00000058946 | CU856539.2 | 312.1485 | 0.462158 | 9.33E-05 | 0.002779 |
| ENSDARG00000100823 | selenok | 285.9129 | 0.518676 | 9.68E-05 | 0.002859 |
| ENSDARG00000033738 | MYL6_(1_of_many) | 2305.855 | 0.349785 | 9.87E-05 | 0.002902 |
| ENSDARG00000027600 | pdlim5b | 234.0909 | 0.581807 | 0.0001 | 0.002938 |
| ENSDARG00000056532 | serinc2 | 475.4029 | 0.4664 | 0.0001 | 0.002938 |
| ENSDARG00000004539 | ptgs2a | 155.7529 | 0.570561 | 0.000102 | 0.00297 |
| ENSDARG00000017255 | tmed1b | 116.6171 | 0.699726 | 0.000102 | 0.002981 |
| ENSDARG00000101631 | etfa | 1949.302 | 0.300998 | 0.000103 | 0.002989 |
| ENSDARG00000076618 | tm2d3 | 211.0007 | 0.58408 | 0.000103 | 0.002992 |
| ENSDARG00000063572 | perp | 1873.55 | 0.517076 | 0.000104 | 0.003016 |
| ENSDARG00000078552 | grhl3 | 189.7644 | 0.52899 | 0.000106 | 0.003034 |
| ENSDARG00000040455 | unc50 | 160.4217 | 0.554295 | 0.000106 | 0.003035 |
| ENSDARG00000090635 | kcnj1a.4 | 85.6669 | 0.901337 | 0.000107 | 0.003042 |
| ENSDARG00000010160 | rps15a | 7135.342 | 0.35723 | 0.000107 | 0.003042 |
| ENSDARG00000058005 | hgd | 1185.039 | 0.465716 | 0.000111 | 0.00315 |
| ENSDARG00000038359 | enosf1 | 331.7955 | 0.4363 | 0.000112 | 0.00316 |
| ENSDARG00000098481 | ANXA1_(1_of_many) | 162.967 | 0.698036 | 0.000114 | 0.003199 |
| ENSDARG00000076838 | apom | 1834.835 | 0.563656 | 0.000115 | 0.003218 |
| ENSDARG00000035914 | tmem167a | 317.8173 | 0.612344 | 0.000116 | 0.003242 |
| ENSDARG00000076568 | sec61b | 779.9749 | 0.42639 | 0.000117 | 0.00328 |
| ENSDARG00000042021 | mapk12a | 305.6062 | 0.448914 | 0.000118 | 0.00329 |
| ENSDARG00000101627 | ssr1 | 818.0494 | 0.397958 | 0.000119 | 0.00331 |
| ENSDARG00000051965 | btr01 | 70.55758 | 0.782404 | 0.000119 | 0.003316 |
| ENSDARG00000094277 | mrpl44 | 264.7998 | 0.502315 | 0.00012 | 0.003319 |
| ENSDARG00000014676 | bckdhb | 688.2579 | 0.403377 | 0.000121 | 0.003342 |
| ENSDARG00000078659 | tmem176 | 374.954 | 0.456668 | 0.000122 | 0.003356 |
| ENSDARG00000093448 | mpc1 | 839.2411 | 0.451467 | 0.000123 | 0.003362 |
| ENSDARG00000037071 | rps26 | 4672.06 | 0.433823 | 0.000123 | 0.003362 |
| ENSDARG00000105341 | si:dkey-9l20.3 | 861.1491 | 0.696371 | 0.000124 | 0.003373 |
| ENSDARG00000039346 | ndufa5 | 688.7495 | 0.405252 | 0.000125 | 0.003391 |
| ENSDARG00000103983 | slc30a10 | 106.891 | 0.664716 | 0.000125 | 0.003397 |
| ENSDARG00000026655 | tspo | 739.3339 | 0.355998 | 0.000128 | 0.003467 |
| ENSDARG00000068503 | gbgt1l4 | 347.0073 | 0.511099 | 0.000131 | 0.003543 |
| ENSDARG00000096616 | si:ch211-255p10.3 | 1683.949 | 0.684501 | 0.000132 | 0.003548 |
| ENSDARG00000078522 | si:ch211-80h18.1 | 829.9663 | 0.480762 | 0.000132 | 0.003548 |
| ENSDARG00000103464 | pggt1b | 356.6671 | 0.549118 | 0.000133 | 0.003574 |
| ENSDARG00000008363 | mcl1b | 725.2676 | 0.458013 | 0.000135 | 0.00361 |
| ENSDARG00000079372 | si:ch211-264f5.6 | 346.9584 | 0.783688 | 0.000136 | 0.003627 |

**Table G.3 continued**

| #geneID | Upregulated gene | Base Mean | log2 Fold Change | p-value | FDR |
|---|---|---|---|---|---|
| ENSDARG00000041492 | si:ch211-196f5.2 | 190.1324 | 0.624255 | 0.00014 | 0.003696 |
| ENSDARG00000071475 | aox5 | 222.2795 | 0.525767 | 0.000139 | 0.003696 |
| ENSDARG00000044809 | fpgs | 384.7036 | 0.402698 | 0.000139 | 0.003696 |
| ENSDARG00000058348 | scinlb | 341.0515 | 0.475742 | 0.000144 | 0.003792 |
| ENSDARG00000056379 | si:ch73-86n18.1 | 280.5867 | 0.465996 | 0.000145 | 0.003807 |
| ENSDARG00000015662 | pla2g12b | 1296.995 | 0.46585 | 0.000146 | 0.003813 |
| ENSDARG00000006290 | ndufs5 | 1067.937 | 0.479582 | 0.000149 | 0.003869 |
| ENSDARG00000103720 | zgc:162730 | 936.2789 | 0.426992 | 0.000149 | 0.003869 |
| ENSDARG00000036865 | slc2a12 | 222.3232 | 0.516584 | 0.000154 | 0.00397 |
| ENSDARG00000100095 | anxa1b | 1033.957 | 0.652797 | 0.000154 | 0.003971 |
| ENSDARG00000062568 | mrpl2 | 503.2395 | 0.456171 | 0.000154 | 0.003971 |
| ENSDARG00000056510 | gstk1 | 713.6936 | 0.380023 | 0.000156 | 0.003991 |
| ENSDARG00000028096 | cldn23a | 270.2003 | 0.550798 | 0.000156 | 0.003993 |
| ENSDARG00000003808 | aqp3a | 1585.55 | 0.455371 | 0.000159 | 0.004065 |
| ENSDARG00000102772 | klhdc3 | 309.061 | 0.520623 | 0.000161 | 0.004082 |
| ENSDARG00000043182 | hhla2a.1 | 288.3723 | 0.483692 | 0.000162 | 0.004082 |
| ENSDARG00000104647 | surf4 | 343.4758 | 0.471551 | 0.000162 | 0.004082 |
| ENSDARG00000040180 | slc35a1 | 285.4796 | 0.471059 | 0.000161 | 0.004082 |
| ENSDARG00000069583 | zgc:114181 | 1382.615 | 0.394383 | 0.000161 | 0.004082 |
| ENSDARG00000056767 | itgb3a | 300.0613 | 0.496517 | 0.000165 | 0.00415 |
| ENSDARG00000035622 | xbp1 | 2297.1 | 0.307935 | 0.000166 | 0.00415 |
| ENSDARG00000053232 | itgb1b.1 | 549.5559 | 0.571855 | 0.000168 | 0.004178 |
| ENSDARG00000051861 | pkp3a | 1040.853 | 0.38784 | 0.000169 | 0.004206 |
| ENSDARG00000102020 | pnpla3 | 431.6563 | 0.481329 | 0.00017 | 0.004211 |
| ENSDARG00000101199 | rbp4 | 10128.49 | 0.320192 | 0.000171 | 0.004225 |
| ENSDARG00000099022 | faua | 10122.28 | 0.350591 | 0.000173 | 0.00426 |
| ENSDARG00000103101 | si:ch211-235e9.6 | 305.3588 | 0.568172 | 0.000175 | 0.004294 |
| ENSDARG00000028618 | zgc:77517 | 2141.438 | 0.342326 | 0.000176 | 0.004305 |
| ENSDARG00000036282 | rnaset2 | 274.6675 | 0.449666 | 0.000178 | 0.004344 |
| ENSDARG00000024032 | coch | 140.8084 | 0.645872 | 0.000178 | 0.004349 |
| ENSDARG00000104068 | gstp1 | 5422.302 | 0.535156 | 0.000179 | 0.004349 |
| ENSDARG00000075015 | soul5 | 1711.524 | 0.47975 | 0.000179 | 0.004349 |
| ENSDARG00000104775 | ly6m2 | 50.73418 | 0.856137 | 0.000182 | 0.004424 |
| ENSDARG00000016156 | fam53b | 460.7113 | 0.442572 | 0.000184 | 0.004434 |
| ENSDARG00000077114 | arhgef16 | 280.9975 | 0.464391 | 0.000185 | 0.004464 |
| ENSDARG00000069540 | si:dkey-30c15.2 | 57.32293 | 0.794851 | 0.000187 | 0.004489 |
| ENSDARG00000098296 | gnsb | 157.2732 | 0.589277 | 0.000187 | 0.004489 |
| ENSDARG00000116586 | zgc:92066 | 400.7784 | 0.519008 | 0.000187 | 0.004489 |
| ENSDARG00000044094 | gfpt2 | 223.4642 | 0.650584 | 0.000189 | 0.004509 |

**Table G.3 continued**

| #geneID | Upregulated gene | Base Mean | log2 Fold Change | p-value | FDR |
|---|---|---|---|---|---|
| ENSDARG00000010244 | rpl22l1 | 2688.76 | 0.521271 | 0.00019 | 0.004511 |
| ENSDARG00000073936 | BX511021.1 | 419.049 | 0.657373 | 0.000194 | 0.00458 |
| ENSDARG00000043211 | ripk4 | 143.0901 | 0.603939 | 0.000196 | 0.004608 |
| ENSDARG00000091609 | spink4 | 172.4045 | 0.530077 | 0.000196 | 0.004608 |
| ENSDARG00000086481 | mogat3a | 175.2721 | 0.559024 | 0.000197 | 0.004622 |
| ENSDARG00000093476 | si:dkey-175d9.2 | 83.2041 | 0.729587 | 0.000198 | 0.004638 |
| ENSDARG00000027916 | fntb | 453.1307 | 0.456842 | 0.000199 | 0.004648 |
| ENSDARG00000087873 | eevs | 781.641 | 0.396941 | 0.000202 | 0.004711 |
| ENSDARG00000103981 | bhlha9 | 56.17062 | 0.946723 | 0.000203 | 0.004719 |
| ENSDARG00000087093 | si:ch211-157c3.4 | 773.0018 | 0.50405 | 0.000204 | 0.004722 |
| ENSDARG00000101749 | zgc:92161 | 158.9495 | 0.544334 | 0.000206 | 0.004769 |
| ENSDARG00000094557 | nupr1b | 1252.785 | 0.332092 | 0.000206 | 0.004769 |
| ENSDARG00000056239 | tmem45b | 406.397 | 0.472023 | 0.000207 | 0.004779 |
| ENSDARG00000006207 | gpx1b | 199.1956 | 0.549625 | 0.000212 | 0.004876 |
| ENSDARG00000069461 | rnaseka | 178.4541 | 0.668367 | 0.000215 | 0.004911 |
| ENSDARG00000071558 | fblim1 | 265.3693 | 0.520062 | 0.000215 | 0.004911 |
| ENSDARG00000040534 | epcam | 2544.989 | 0.455678 | 0.000215 | 0.004911 |
| ENSDARG00000017489 | zgc:123068 | 85.54903 | 0.864917 | 0.000219 | 0.004959 |
| ENSDARG00000043562 | zgc:65997 | 360.6755 | 0.508551 | 0.000219 | 0.004959 |
| ENSDARG00000099663 | cox5ab | 1305.771 | 0.411001 | 0.000221 | 0.005001 |
| ENSDARG00000009724 | rpn2 | 3014.775 | 0.437257 | 0.000222 | 0.00502 |
| ENSDARG00000060439 | clcn2c | 213.7501 | 0.496527 | 0.000223 | 0.00503 |
| ENSDARG00000044125 | txn | 570.1499 | 0.474155 | 0.000225 | 0.005056 |
| ENSDARG00000018903 | aimp2 | 703.3404 | 0.441133 | 0.000225 | 0.005056 |
| ENSDARG00000069977 | myg1 | 351.1331 | 0.478024 | 0.000226 | 0.005067 |
| ENSDARG00000096874 | tmem176l.3b | 417.6245 | 0.435668 | 0.000229 | 0.005112 |
| ENSDARG00000101181 | s100w | 436.5445 | 0.484375 | 0.000234 | 0.005154 |
| ENSDARG00000104722 | CABZ01076669.1 | 415.7536 | 0.439256 | 0.000233 | 0.005154 |
| ENSDARG00000026759 | ldlrb | 154.149 | 0.644805 | 0.000236 | 0.005179 |
| ENSDARG00000096905 | si:ch73-23l24.1 | 466.6893 | 0.558792 | 0.000236 | 0.005179 |
| ENSDARG00000061858 | zgc:153968 | 1127.746 | 0.393178 | 0.000241 | 0.005265 |
| ENSDARG00000070721 | vdrb | 340.9621 | 0.425383 | 0.000245 | 0.005317 |
| ENSDARG00000042934 | ctgfa | 1236.181 | 0.412864 | 0.000246 | 0.005318 |
| ENSDARG00000037267 | zgc:158263 | 253.8109 | 0.484624 | 0.000249 | 0.005372 |
| ENSDARG00000086248 | kcnj1a.3 | 67.66005 | 0.895812 | 0.000249 | 0.005377 |
| ENSDARG00000027159 | fbxo28 | 264.1245 | 0.471105 | 0.00025 | 0.005384 |
| ENSDARG00000098286 | CU695232.1 | 166.8264 | 0.558199 | 0.000253 | 0.005423 |
| ENSDARG00000019444 | ssr4 | 1074.347 | 0.369623 | 0.000254 | 0.005444 |
| ENSDARG00000100265 | rhcgb | 147.4643 | 0.641017 | 0.000256 | 0.005475 |

**Table G.3 continued**

| #geneID | Upregulated gene | Base Mean | log2 Fold Change | p-value | FDR |
|---|---|---|---|---|---|
| ENSDARG00000101393 | si:dkey-31g6.6 | 120.8977 | 0.592536 | 0.000257 | 0.005477 |
| ENSDARG00000055118 | mylipb | 549.8613 | 0.371368 | 0.00026 | 0.005513 |
| ENSDARG00000033466 | tagln2 | 976.2074 | 0.39908 | 0.000264 | 0.005595 |
| ENSDARG00000102441 | ctnna1 | 935.8542 | 0.435076 | 0.000269 | 0.005667 |
| ENSDARG00000039934 | hlcs | 184.1192 | 0.617573 | 0.000273 | 0.005728 |
| ENSDARG00000005485 | ucmab | 704.504 | 0.407188 | 0.000273 | 0.005728 |
| ENSDARG00000088091 | pfn1 | 12170.52 | 0.338704 | 0.000274 | 0.005728 |
| ENSDARG00000104359 | anxa1c | 569.6096 | 0.638535 | 0.000277 | 0.00578 |
| ENSDARG00000002909 | tjp3 | 633.9895 | 0.422481 | 0.000279 | 0.005815 |
| ENSDARG00000105239 | ecm1b | 283.4384 | 0.415995 | 0.000283 | 0.00586 |
| ENSDARG00000039077 | tyr | 722.7103 | 0.38701 | 0.000282 | 0.00586 |
| ENSDARG00000042933 | bloc1s6 | 326.948 | 0.41211 | 0.000285 | 0.005906 |
| ENSDARG00000054122 | tmem30b | 228.9554 | 0.514363 | 0.000286 | 0.005913 |
| ENSDARG00000074749 | abca12 | 1066.359 | 0.375216 | 0.000286 | 0.005913 |
| ENSDARG00000002002 | lmcd1 | 124.6308 | 0.575317 | 0.000288 | 0.005927 |
| ENSDARG00000071601 | pvalb9 | 569.1076 | 0.440107 | 0.000289 | 0.005942 |
| ENSDARG00000109626 | si:ch211-226h7.3 | 181.3191 | 0.521291 | 0.000293 | 0.005994 |
| ENSDARG00000005713 | ethe1 | 390.8663 | 0.418449 | 0.000294 | 0.006005 |
| ENSDARG00000104172 | diabloa | 608.6108 | 0.533122 | 0.000302 | 0.006125 |
| ENSDARG00000087277 | selenoj | 578.7544 | 0.39166 | 0.000304 | 0.006125 |
| ENSDARG00000041339 | zgc:92380 | 1016.677 | 0.355429 | 0.000304 | 0.006125 |
| ENSDARG00000046030 | zgc:110339 | 1336.863 | 0.344292 | 0.000303 | 0.006125 |
| ENSDARG00000055331 | aldh9a1a.2 | 210.3738 | 0.485103 | 0.000306 | 0.006154 |
| ENSDARG00000003113 | ada | 4150.087 | 0.447603 | 0.000307 | 0.006154 |
| ENSDARG00000002204 | hspb11 | 540.2416 | 0.42775 | 0.000308 | 0.006167 |
| ENSDARG00000091079 | si:zfos-1192g2.3 | 290.4354 | 0.606075 | 0.000311 | 0.0062 |
| ENSDARG00000027824 | top1mt | 375.6601 | 0.39322 | 0.000314 | 0.006248 |
| ENSDARG00000102332 | spint1a | 1130.874 | 0.452923 | 0.000316 | 0.00627 |
| ENSDARG00000070873 | ccl25b | 388.8325 | 0.433868 | 0.000316 | 0.00627 |
| ENSDARG00000068275 | ptx3a | 161.1678 | 0.843355 | 0.000328 | 0.006454 |
| ENSDARG00000056087 | ecrg4a | 208.5504 | 0.535116 | 0.000328 | 0.006454 |
| ENSDARG00000003193 | rassf7b | 143.299 | 0.530591 | 0.000332 | 0.006493 |
| ENSDARG00000040295 | apoeb | 10917.56 | 0.458568 | 0.000332 | 0.006493 |
| ENSDARG00000070427 | s100v1 | 291.3411 | 0.513546 | 0.000332 | 0.006498 |
| ENSDARG00000087401 | slc25a34 | 84.20925 | 0.730079 | 0.000333 | 0.006503 |
| ENSDARG00000115015 | PSTK | 55.43027 | 0.911508 | 0.000338 | 0.006555 |
| ENSDARG00000001414 | mctp2a | 123.9005 | 0.590232 | 0.000338 | 0.006555 |
| ENSDARG00000035178 | gna14 | 283.6255 | 0.499512 | 0.000338 | 0.006555 |
| ENSDARG00000015385 | ndufs3 | 1240.437 | 0.428204 | 0.000338 | 0.006555 |

**Table G.3 continued**

| #geneID | Upregulated gene | Base Mean | log2 Fold Change | p-value | FDR |
|---|---|---|---|---|---|
| ENSDARG00000029587 | msra | 183.7478 | 0.586586 | 0.000343 | 0.006622 |
| ENSDARG00000002745 | tdh | 8222.71 | 0.434175 | 0.000349 | 0.006701 |
| ENSDARG00000099306 | zgc:175088 | 1080.996 | 0.413904 | 0.000351 | 0.006726 |
| ENSDARG00000039099 | aep1 | 350.0902 | 0.59517 | 0.000357 | 0.006848 |
| ENSDARG00000098852 | smdt1b | 813.4015 | 0.433728 | 0.000359 | 0.006857 |
| ENSDARG00000030530 | slc22a2 | 818.0617 | 0.347238 | 0.000361 | 0.006887 |
| ENSDARG00000029204 | tyrp1a | 539.1957 | 0.520301 | 0.000369 | 0.006999 |
| ENSDARG00000095147 | krt96 | 821.732 | 0.475553 | 0.00037 | 0.006999 |
| ENSDARG00000070991 | mlpha | 365.0789 | 0.45177 | 0.00037 | 0.006999 |
| ENSDARG00000103566 | tomm20b | 1114.158 | 0.3909 | 0.000372 | 0.00703 |
| ENSDARG00000022689 | itgb1b.2 | 353.8679 | 0.466092 | 0.000376 | 0.007087 |
| ENSDARG00000018621 | slc6a19a.1 | 277.0739 | 0.638886 | 0.000381 | 0.007165 |
| ENSDARG00000038964 | traf4b | 48.1206 | 0.854596 | 0.000384 | 0.007206 |
| ENSDARG00000069027 | admb | 68.25834 | 0.704797 | 0.000388 | 0.007244 |
| ENSDARG00000030402 | twist1a | 143.5483 | 0.541633 | 0.000398 | 0.007382 |
| ENSDARG00000057882 | arpc3 | 871.7512 | 0.333415 | 0.000399 | 0.007398 |
| ENSDARG00000038787 | tmub1 | 301.6361 | 0.470968 | 0.000406 | 0.007487 |
| ENSDARG00000059234 | mrps27 | 325.9326 | 0.44976 | 0.000407 | 0.007493 |
| ENSDARG00000043865 | timm9 | 202.7882 | 0.521387 | 0.000408 | 0.007512 |
| ENSDARG00000100712 | si:dkey-19b23.12 | 316.6489 | 0.528367 | 0.000411 | 0.007556 |
| ENSDARG00000002240 | psmb6 | 725.9787 | 0.385207 | 0.000416 | 0.007621 |
| ENSDARG00000016866 | fam102ab | 268.8039 | 0.48576 | 0.00043 | 0.007802 |
| ENSDARG00000031763 | smad6b | 298.8412 | 0.431086 | 0.00043 | 0.007802 |
| ENSDARG00000097746 | si:rp71-77l1.1 | 87.70927 | 0.696442 | 0.000432 | 0.007829 |
| ENSDARG00000029230 | pnp4b | 1411.044 | 0.351846 | 0.000438 | 0.007918 |
| ENSDARG00000074552 | ndufs7 | 1408.073 | 0.330533 | 0.000445 | 0.008007 |
| ENSDARG00000051956 | isca1 | 744.5115 | 0.367228 | 0.000447 | 0.008032 |
| ENSDARG00000036074 | cebpa | 389.5211 | 0.441585 | 0.000448 | 0.008045 |
| ENSDARG00000102643 | chmp1a | 288.2635 | 0.49345 | 0.00045 | 0.008082 |
| ENSDARG00000045075 | tmem106a | 267.6287 | 0.458048 | 0.000455 | 0.008126 |
| ENSDARG00000029766 | nr1i2 | 179.2899 | 0.477036 | 0.000455 | 0.008126 |
| ENSDARG00000003444 | dhrs7 | 231.0253 | 0.449192 | 0.000456 | 0.008128 |
| ENSDARG00000037307 | gnpda1 | 182.8116 | 0.506184 | 0.000458 | 0.008154 |
| ENSDARG00000090912 | npc2 | 624.949 | 0.344967 | 0.000458 | 0.008154 |
| ENSDARG00000092895 | si:dkey-188i13.11 | 155.4111 | 0.659617 | 0.00046 | 0.008184 |
| ENSDARG00000091699 | capn2a | 1287.835 | 0.409191 | 0.000473 | 0.008396 |
| ENSDARG00000026294 | erbb2 | 213.4497 | 0.524099 | 0.000474 | 0.008411 |
| ENSDARG00000071040 | smim8 | 133.0963 | 0.659325 | 0.000477 | 0.008458 |
| ENSDARG00000058463 | ndufab1a | 913.8872 | 0.418675 | 0.000479 | 0.008474 |

**Table G.3 continued**

| #geneID | Upregulated gene | Base Mean | log2 Fold Change | p-value | FDR |
|---|---|---|---|---|---|
| ENSDARG00000019081 | zgc:101723 | 312.3559 | 0.597507 | 0.000482 | 0.008525 |
| ENSDARG00000096359 | eppk1 | 1781.327 | 0.424669 | 0.000484 | 0.008527 |
| ENSDARG00000069377 | si:dkey-242g16.2 | 72.34605 | 0.675714 | 0.000494 | 0.008692 |
| ENSDARG00000052997 | sema4e | 238.9305 | 0.443018 | 0.000495 | 0.008699 |
| ENSDARG00000067717 | tomm7 | 332.6118 | 0.452519 | 0.000496 | 0.0087 |
| ENSDARG00000037943 | cpt1cb | 88.51837 | 0.691733 | 0.0005 | 0.008764 |
| ENSDARG00000031616 | g6pca.1 | 168.8674 | 0.602258 | 0.000502 | 0.008776 |
| ENSDARG00000058656 | desma | 3550.665 | 0.359231 | 0.000502 | 0.008777 |
| ENSDARG00000086272 | si:dkey-4p15.5 | 369.9962 | 0.432799 | 0.000503 | 0.00878 |
| ENSDARG00000041592 | dcun1d2b | 351.1944 | 0.456132 | 0.000505 | 0.008808 |
| ENSDARG00000089060 | kcnj1a.5 | 109.0154 | 0.791826 | 0.00051 | 0.008883 |
| ENSDARG00000039133 | lamb4 | 545.6446 | 0.351813 | 0.00051 | 0.008883 |
| ENSDARG00000029305 | baiap2l1a | 142.4459 | 0.502834 | 0.000532 | 0.009174 |
| ENSDARG00000042793 | tpp1 | 286.9916 | 0.419118 | 0.00053 | 0.009174 |
| ENSDARG00000052371 | higd2a | 290.419 | 0.518618 | 0.000536 | 0.009246 |
| ENSDARG00000039351 | ccl19b | 124.1783 | 0.690798 | 0.000537 | 0.009249 |
| ENSDARG00000076839 | ftr86 | 56.26684 | 0.823412 | 0.000539 | 0.009256 |
| ENSDARG00000057854 | sap18 | 569.5025 | 0.3625 | 0.000544 | 0.009318 |
| ENSDARG00000042876 | abracl | 305.9278 | 0.544231 | 0.000546 | 0.009319 |
| ENSDARG00000044655 | st14b | 222.7179 | 0.532588 | 0.000547 | 0.009319 |
| ENSDARG00000027986 | slc35d1b | 217.1551 | 0.484891 | 0.000547 | 0.009319 |
| ENSDARG00000044935 | hpdb | 1094.603 | 0.462393 | 0.000546 | 0.009319 |
| ENSDARG00000024141 | cav3 | 876.2885 | 0.3753 | 0.000547 | 0.009319 |
| ENSDARG00000022727 | epha2b | 209.5662 | 0.537824 | 0.00056 | 0.009481 |
| ENSDARG00000011925 | spns1 | 520.141 | 0.403675 | 0.000563 | 0.009514 |
| ENSDARG00000014794 | uqcrc2a | 1997.552 | 0.303631 | 0.000572 | 0.009649 |
| ENSDARG00000095157 | TMEM14A | 143.4497 | 0.510746 | 0.000577 | 0.009699 |
| ENSDARG00000067966 | fem1a | 165.0353 | 0.842464 | 0.000579 | 0.009717 |
| ENSDARG00000006314 | itgav | 2433.606 | 0.461677 | 0.000579 | 0.009717 |
| ENSDARG00000034541 | tgfbr2b | 417.7178 | 0.405605 | 0.00058 | 0.009726 |
| ENSDARG00000027611 | cavin2a | 749.8761 | 0.345994 | 0.000585 | 0.00976 |
| ENSDARG00000059247 | tmem54a | 169.7242 | 0.515715 | 0.000587 | 0.009772 |
| ENSDARG00000024295 | slc11a2 | 583.188 | 0.332188 | 0.000587 | 0.009772 |
| ENSDARG00000043133 | cldnf | 96.74621 | 0.654248 | 0.000594 | 0.009825 |
| ENSDARG00000027529 | hmox1a | 97.68196 | 0.575559 | 0.000594 | 0.009825 |
| ENSDARG00000027088 | ptgdsb.1 | 7606.774 | 0.522765 | 0.000594 | 0.009825 |
| ENSDARG00000038106 | slc37a4a | 357.5124 | 0.448399 | 0.000594 | 0.009825 |
| ENSDARG00000015422 | ppil1 | 209.2136 | 0.476428 | 0.000597 | 0.009845 |
| ENSDARG00000036613 | tab1 | 239.5457 | 0.457981 | 0.000607 | 0.009977 |

**Table G.4. Genes downregulated by CORT in Klf9 mutant larvae**

| #geneID | Downregulated gene | Base Mean | log2 Fold Change | p-value | FDR |
|---|---|---|---|---|---|
| ENSDARG00000014420 | elavl3 | 3854.277 | -0.76001 | 9.20E-15 | 5.12E-11 |
| ENSDARG00000075433 | myom2a | 10825.15 | -0.60008 | 6.72E-14 | 2.65E-10 |
| ENSDARG00000077341 | ppp1r14c | 1252.045 | -0.81547 | 7.92E-14 | 2.65E-10 |
| ENSDARG00000044861 | opn1lw2 | 6162.082 | -1.04099 | 2.42E-13 | 5.46E-10 |
| ENSDARG00000096257 | si:ch73-367p23.2 | 17326.36 | -0.67577 | 4.05E-12 | 6.15E-09 |
| ENSDARG00000078748 | si:ch211-137a8.4 | 2174.572 | -0.70865 | 5.45E-12 | 7.00E-09 |
| ENSDARG00000056036 | stxbp1b | 750.3798 | -0.82372 | 5.03E-12 | 7.00E-09 |
| ENSDARG00000042529 | gnat2 | 13565.63 | -0.95177 | 1.41E-11 | 1.57E-08 |
| ENSDARG00000098392 | si:ch73-28h20.1 | 439.5446 | -0.75871 | 4.22E-11 | 4.15E-08 |
| ENSDARG00000045677 | opn1sw1 | 37731.35 | -0.93638 | 6.66E-11 | 5.67E-08 |
| ENSDARG00000025847 | sox12 | 447.3689 | -0.6983 | 1.45E-10 | 1.05E-07 |
| ENSDARG00000017673 | nova2 | 2822.332 | -0.58514 | 2.36E-10 | 1.57E-07 |
| ENSDARG00000004836 | dnajc5ab | 705.5122 | -0.71625 | 3.03E-10 | 1.81E-07 |
| ENSDARG00000042988 | slc24a2 | 813.8243 | -0.74431 | 6.52E-10 | 3.19E-07 |
| ENSDARG00000100397 | pde6c | 7209.952 | -1.09159 | 8.23E-10 | 3.62E-07 |
| ENSDARG00000097008 | opn1mw1 | 4847.951 | -0.53703 | 1.01E-09 | 4.20E-07 |
| ENSDARG00000078473 | nucks1a | 1610.592 | -0.71395 | 1.69E-09 | 6.55E-07 |
| ENSDARG00000071684 | rx1 | 337.3164 | -0.83499 | 2.19E-09 | 8.14E-07 |
| ENSDARG00000100244 | ebf3a | 1187.835 | -0.60261 | 2.93E-09 | 1.06E-06 |
| ENSDARG00000096398 | si:ch211-276a17.5 | 161.2247 | -0.91106 | 3.50E-09 | 1.17E-06 |
| ENSDARG00000056490 | zgc:110158 | 1063.661 | -0.66751 | 4.81E-09 | 1.52E-06 |
| ENSDARG00000057007 | ctbp1 | 1563.143 | -0.52149 | 6.85E-09 | 1.99E-06 |
| ENSDARG00000077256 | nat8l | 1880.195 | -0.55138 | 7.14E-09 | 2.02E-06 |
| ENSDARG00000037925 | rgs9a | 490.5767 | -0.90966 | 7.58E-09 | 2.04E-06 |
| ENSDARG00000063899 | mt-nd2 | 17924.88 | -0.50757 | 8.47E-09 | 2.21E-06 |
| ENSDARG00000055455 | gpm6aa | 35728.56 | -0.88678 | 9.64E-09 | 2.40E-06 |
| ENSDARG00000011989 | crx | 640.4066 | -0.73595 | 1.33E-08 | 3.17E-06 |
| ENSDARG00000000503 | stx1b | 6726.799 | -0.81455 | 1.50E-08 | 3.42E-06 |
| ENSDARG00000069737 | pou4f2 | 405.9651 | -0.69354 | 1.58E-08 | 3.52E-06 |
| ENSDARG00000028335 | hmga1a | 6628.224 | -0.46609 | 1.96E-08 | 4.17E-06 |
| ENSDARG00000098475 | arr3b | 3150.929 | -0.99783 | 2.00E-08 | 4.17E-06 |
| ENSDARG00000070951 | hmga1b | 891.0781 | -0.63269 | 2.15E-08 | 4.44E-06 |
| ENSDARG00000079891 | dnajc6 | 1057.639 | -0.61649 | 3.05E-08 | 5.54E-06 |
| ENSDARG00000040926 | nr2f2 | 1449.987 | -0.5255 | 3.23E-08 | 5.80E-06 |
| ENSDARG00000037997 | tubb5 | 3117.781 | -0.67785 | 3.64E-08 | 6.48E-06 |
| ENSDARG00000103937 | ndrg4 | 4188.52 | -0.98269 | 3.92E-08 | 6.83E-06 |
| ENSDARG00000057427 | sv2ba | 653.0101 | -0.68501 | 4.99E-08 | 8.50E-06 |
| ENSDARG00000023536 | nnt | 14052.79 | -0.53541 | 5.44E-08 | 9.18E-06 |
| ENSDARG00000078118 | sinhcafl | 161.9731 | -0.85855 | 5.79E-08 | 9.48E-06 |

**Table G.4 continued**

| #geneID | Downregulated gene | Base Mean | log2 Fold Change | p-value | FDR |
|---|---|---|---|---|---|
| ENSDARG00000069615 | ckmt2a | 1813.449 | -0.63239 | 6.22E-08 | 1.01E-05 |
| ENSDARG00000070959 | si:ch211-288g17.3 | 2488.177 | -0.5294 | 6.46E-08 | 1.03E-05 |
| ENSDARG00000020602 | grk7a | 2884.565 | -0.79259 | 7.45E-08 | 1.15E-05 |
| ENSDARG00000077499 | plekho1b | 524.5975 | -0.5377 | 7.97E-08 | 1.22E-05 |
| ENSDARG00000011020 | hnrnpa1a | 1820.452 | -0.58462 | 9.05E-08 | 1.35E-05 |
| ENSDARG00000078416 | zeb2b | 577.0702 | -0.66974 | 1.20E-07 | 1.74E-05 |
| ENSDARG00000011671 | pde6b | 320.5457 | -0.80079 | 1.48E-07 | 2.08E-05 |
| ENSDARG00000027495 | elovl4b | 427.7936 | -0.65072 | 1.67E-07 | 2.31E-05 |
| ENSDARG00000055618 | acta1b | 38238.82 | -0.71619 | 1.92E-07 | 2.61E-05 |
| ENSDARG00000038862 | kcnb2 | 297.8932 | -0.61289 | 2.07E-07 | 2.76E-05 |
| ENSDARG00000019752 | rom1a | 605.5187 | -0.64811 | 2.20E-07 | 2.89E-05 |
| ENSDARG00000091150 | mki67 | 688.0537 | -0.77407 | 2.25E-07 | 2.94E-05 |
| ENSDARG00000015537 | gad2 | 2246.236 | -0.61884 | 2.49E-07 | 3.20E-05 |
| ENSDARG00000062646 | tet3 | 2236.308 | -0.62536 | 2.57E-07 | 3.24E-05 |
| ENSDARG00000004643 | cdhr1a | 325.576 | -0.65482 | 2.94E-07 | 3.59E-05 |
| ENSDARG00000035870 | laptm4b | 2483.612 | -0.54781 | 3.25E-07 | 3.90E-05 |
| ENSDARG00000094965 | nfil3-5 | 305.5598 | -0.5787 | 3.81E-07 | 4.48E-05 |
| ENSDARG00000013360 | sh3gl3a | 393.9846 | -0.59675 | 3.84E-07 | 4.49E-05 |
| ENSDARG00000087616 | maptb | 1051.986 | -0.59982 | 4.23E-07 | 4.91E-05 |
| ENSDARG00000002587 | dpysl3 | 4773.834 | -0.80972 | 4.74E-07 | 5.35E-05 |
| ENSDARG00000017634 | pdcb | 1607.803 | -0.75693 | 5.91E-07 | 6.41E-05 |
| ENSDARG00000007788 | atp2b1b | 565.0741 | -0.74739 | 6.34E-07 | 6.79E-05 |
| ENSDARG00000016676 | gnao1a | 1821.428 | -0.63606 | 6.55E-07 | 6.89E-05 |
| ENSDARG00000034007 | prom1b | 672.0192 | -0.60043 | 6.96E-07 | 7.22E-05 |
| ENSDARG00000104139 | atp1a3b | 3994.57 | -0.47577 | 7.15E-07 | 7.31E-05 |
| ENSDARG00000007960 | hnrnpaba | 5309.15 | -0.4202 | 8.80E-07 | 8.80E-05 |
| ENSDARG00000102453 | slc1a2b | 10796.2 | -0.52015 | 9.54E-07 | 9.38E-05 |
| ENSDARG00000011065 | camk2b1 | 2077.464 | -0.42753 | 9.91E-07 | 9.68E-05 |
| ENSDARG00000074581 | add2 | 822.5625 | -0.59727 | 1.05E-06 | 0.000102 |
| ENSDARG00000039347 | rps24 | 42952.37 | -0.58602 | 1.09E-06 | 0.000104 |
| ENSDARG00000091756 | insm1a | 383.6349 | -0.60664 | 1.12E-06 | 0.000106 |
| ENSDARG00000032868 | pde4ba | 2397.999 | -0.53346 | 1.15E-06 | 0.000106 |
| ENSDARG00000104685 | grk1b | 627.4739 | -0.80824 | 1.20E-06 | 0.000108 |
| ENSDARG00000100494 | pbx1a | 601.1176 | -0.60493 | 1.21E-06 | 0.000109 |
| ENSDARG00000018524 | midn | 1092.946 | -0.4223 | 1.44E-06 | 0.000125 |
| ENSDARG00000038882 | smc4 | 321.6212 | -0.58895 | 1.56E-06 | 0.000132 |
| ENSDARG00000008433 | unc45b | 432.9019 | -0.57282 | 1.58E-06 | 0.000133 |
| ENSDARG00000111106 | arl3l1 | 451.211 | -0.6463 | 1.59E-06 | 0.000133 |
| ENSDARG00000019902 | rcvrn2 | 2320.016 | -0.59781 | 1.63E-06 | 0.000134 |

**Table G.4 continued**

| #geneID | Downregulated gene | Base Mean | log2 Fold Change | p-value | FDR |
|---|---|---|---|---|---|
| ENSDARG00000038018 | prph2a | 1288.313 | -0.5746 | 1.70E-06 | 0.000139 |
| ENSDARG00000045639 | elavl4 | 3192.16 | -0.63579 | 1.72E-06 | 0.000141 |
| ENSDARG00000069339 | tbc1d24 | 439.2992 | -0.56372 | 1.74E-06 | 0.000141 |
| ENSDARG00000011235 | otx2b | 498.4064 | -0.60407 | 1.95E-06 | 0.000155 |
| ENSDARG00000068745 | map4l | 1962.649 | -0.62712 | 1.98E-06 | 0.000157 |
| ENSDARG00000031768 | roraa | 816.7952 | -0.4813 | 2.08E-06 | 0.000163 |
| ENSDARG00000056519 | si:dkey-280e21.3 | 183.6819 | -0.68047 | 2.32E-06 | 0.00018 |
| ENSDARG00000086222 | nat16 | 780.8793 | -0.58686 | 2.36E-06 | 0.000183 |
| ENSDARG00000071251 | ppp1r18 | 146.0767 | -0.85303 | 2.55E-06 | 0.000193 |
| ENSDARG00000052138 | slc1a2a | 345.2535 | -0.71864 | 2.58E-06 | 0.000194 |
| ENSDARG00000042236 | atrx | 2128.94 | -0.47776 | 2.96E-06 | 0.000214 |
| ENSDARG00000061836 | nfixb | 178.4004 | -0.68156 | 3.11E-06 | 0.00022 |
| ENSDARG00000062661 | abca4b | 319.6782 | -0.70659 | 3.11E-06 | 0.00022 |
| ENSDARG00000054804 | anp32e | 3057.133 | -0.38139 | 3.36E-06 | 0.000235 |
| ENSDARG00000013615 | pbx3b | 1126.591 | -0.56507 | 3.36E-06 | 0.000235 |
| ENSDARG00000016548 | eif5b | 1015.96 | -0.44416 | 3.77E-06 | 0.000259 |
| ENSDARG00000078210 | tulp1b | 104.8198 | -0.86431 | 3.77E-06 | 0.000259 |
| ENSDARG00000044669 | hp1bp3 | 1767.898 | -0.43743 | 3.81E-06 | 0.000261 |
| ENSDARG00000059574 | fscn2a | 52.72869 | -1.23033 | 4.26E-06 | 0.000287 |
| ENSDARG00000099194 | CABZ01058261.1 | 223.0653 | -0.78244 | 4.59E-06 | 0.000306 |
| ENSDARG00000054378 | pcbp3 | 575.6343 | -0.4576 | 4.78E-06 | 0.000313 |
| ENSDARG00000001994 | stxbp1a | 5006.695 | -0.65645 | 4.78E-06 | 0.000313 |
| ENSDARG00000095930 | myha | 113.6072 | -0.76907 | 5.06E-06 | 0.000329 |
| ENSDARG00000011862 | inaa | 406.1012 | -0.7495 | 5.13E-06 | 0.000332 |
| ENSDARG00000013078 | ywhaba | 4921.534 | -0.37936 | 5.24E-06 | 0.000335 |
| ENSDARG00000058868 | apc | 2630.145 | -0.40664 | 5.39E-06 | 0.000339 |
| ENSDARG00000019000 | smc3 | 1521.798 | -0.53808 | 5.53E-06 | 0.000345 |
| ENSDARG00000070107 | six7 | 242.9741 | -0.74048 | 5.57E-06 | 0.000345 |
| ENSDARG00000071051 | cbx6a | 374.569 | -0.54518 | 5.75E-06 | 0.000349 |
| ENSDARG00000079847 | zgc:194578 | 531.5998 | -0.67203 | 5.86E-06 | 0.000355 |
| ENSDARG00000101368 | cngb3.2 | 160.2835 | -0.85666 | 6.34E-06 | 0.000376 |
| ENSDARG00000041609 | adarb1a | 555.3718 | -0.51001 | 6.44E-06 | 0.000378 |
| ENSDARG00000056605 | wbp2 | 463.0598 | -0.55907 | 6.45E-06 | 0.000378 |
| ENSDARG00000003469 | neurod4 | 289.5265 | -0.64197 | 6.89E-06 | 0.000397 |
| ENSDARG00000034195 | top2b | 1724.412 | -0.55484 | 6.94E-06 | 0.000399 |
| ENSDARG00000076532 | si:ch211-222l21.1 | 8089.804 | -0.55674 | 7.74E-06 | 0.000434 |
| ENSDARG00000031222 | lhx2b | 206.388 | -0.63833 | 7.72E-06 | 0.000434 |
| ENSDARG00000070726 | cnga3a | 273.8531 | -0.89287 | 7.92E-06 | 0.000441 |
| ENSDARG00000004735 | hnrnpub | 1291.312 | -0.42078 | 8.01E-06 | 0.000445 |

**Table G.4 continued**

| #geneID | Downregulated gene | Base Mean | log2 Fold Change | p-value | FDR |
|---|---|---|---|---|---|
| ENSDARG00000005526 | igfn1.1 | 433.9357 | -0.52642 | 8.06E-06 | 0.000446 |
| ENSDARG00000100670 | pcdh1g31 | 297.2007 | -0.594 | 8.63E-06 | 0.000473 |
| ENSDARG00000032865 | pacsin1a | 1199.144 | -0.63562 | 8.81E-06 | 0.000481 |
| ENSDARG00000043003 | pcyt2 | 874.6149 | -0.47013 | 9.07E-06 | 0.000486 |
| ENSDARG00000098368 | aplp1 | 4088.309 | -0.49511 | 9.08E-06 | 0.000486 |
| ENSDARG00000090454 | gnb1a | 3300.086 | -0.38891 | 9.32E-06 | 0.000496 |
| ENSDARG00000060434 | map1b | 730.6587 | -0.58043 | 9.49E-06 | 0.0005 |
| ENSDARG00000099695 | si:dkey-61n16.5 | 307.915 | -0.63766 | 9.59E-06 | 0.000504 |
| ENSDARG00000057317 | nexn | 791.2582 | -0.46532 | 9.76E-06 | 0.000508 |
| ENSDARG00000098164 | si:ch211-106m9.1 | 66.40486 | -1.04953 | 9.75E-06 | 0.000508 |
| ENSDARG00000017803 | gsk3b | 1011.742 | -0.42405 | 9.97E-06 | 0.000516 |
| ENSDARG00000079725 | dhx9 | 465.4531 | -0.51997 | 1.01E-05 | 0.000522 |
| ENSDARG00000007247 | ric8a | 304.5574 | -0.57983 | 1.04E-05 | 0.000533 |
| ENSDARG00000058803 | grk1a | 458.6189 | -0.62032 | 1.12E-05 | 0.000564 |
| ENSDARG00000038695 | elavl1a | 1715.505 | -0.43205 | 1.14E-05 | 0.000573 |
| ENSDARG00000054641 | tent5ab | 312.7372 | -0.61428 | 1.17E-05 | 0.000585 |
| ENSDARG00000075295 | tulp1a | 213.1708 | -0.71629 | 1.21E-05 | 0.000597 |
| ENSDARG00000009637 | rcvrn3 | 6246.262 | -0.60576 | 1.22E-05 | 0.000604 |
| ENSDARG00000041150 | slc17a6b | 1778.121 | -0.46052 | 1.38E-05 | 0.000665 |
| ENSDARG00000053301 | insm1b | 402.0154 | -0.50338 | 1.40E-05 | 0.000665 |
| ENSDARG00000004049 | marcksa | 189.5184 | -0.63943 | 1.40E-05 | 0.000665 |
| ENSDARG00000087188 | nfil3-6 | 177.0577 | -0.69238 | 1.40E-05 | 0.000665 |
| ENSDARG00000002403 | nusap1 | 151.0651 | -0.77475 | 1.38E-05 | 0.000665 |
| ENSDARG00000014746 | rbfox1 | 1289.619 | -0.40305 | 1.45E-05 | 0.000683 |
| ENSDARG00000059351 | hnrnpa3 | 175.4515 | -0.64794 | 1.47E-05 | 0.000688 |
| ENSDARG00000044545 | zgc:77262 | 491.0482 | -0.4482 | 1.49E-05 | 0.000694 |
| ENSDARG00000074396 | fscn2b | 173.5332 | -0.68207 | 1.52E-05 | 0.000707 |
| ENSDARG00000016830 | rimkla | 1755.891 | -0.49363 | 1.56E-05 | 0.000721 |
| ENSDARG00000095802 | si:ch1073-155h21.2 | 209.3513 | -0.65776 | 1.66E-05 | 0.000759 |
| ENSDARG00000055900 | zswim5 | 1049.635 | -0.37803 | 1.69E-05 | 0.000767 |
| ENSDARG00000055052 | map2 | 526.0871 | -0.50488 | 1.78E-05 | 0.000803 |
| ENSDARG00000031894 | lef1 | 324.8345 | -0.51492 | 1.79E-05 | 0.000804 |
| ENSDARG00000045014 | tuba2 | 5377.547 | -0.54586 | 1.79E-05 | 0.000804 |
| ENSDARG00000102204 | jph3 | 388.9799 | -0.58427 | 1.80E-05 | 0.000804 |
| ENSDARG00000062973 | ttll7 | 279.1502 | -0.65751 | 1.81E-05 | 0.00081 |
| ENSDARG00000104372 | gnb1b | 2024.595 | -0.37309 | 1.96E-05 | 0.000865 |
| ENSDARG00000061918 | cplx2 | 812.6976 | -0.59898 | 1.97E-05 | 0.000867 |
| ENSDARG00000088881 | si:dkeyp-69b9.3 | 130.8789 | -0.67712 | 2.07E-05 | 0.000908 |
| ENSDARG00000067995 | myhz1.2 | 74565.39 | -0.88559 | 2.25E-05 | 0.000968 |

**Table G.4 continued**

| #geneID | Downregulated gene | Base Mean | log2 Fold Change | p-value | FDR |
|---|---|---|---|---|---|
| ENSDARG00000101318 | pcdh2ab9 | 2025.952 | -0.45719 | 2.48E-05 | 0.001059 |
| ENSDARG00000040184 | syncrip | 3422.557 | -0.36065 | 2.70E-05 | 0.001131 |
| ENSDARG00000077946 | smarcc2 | 594.5361 | -0.5393 | 2.73E-05 | 0.00114 |
| ENSDARG00000052150 | pbx4 | 1346.909 | -0.39852 | 2.76E-05 | 0.001149 |
| ENSDARG00000056122 | gdi1 | 1721.695 | -0.51673 | 2.76E-05 | 0.001149 |
| ENSDARG00000095831 | si:ch211-175f12.2 | 81.43064 | -0.86556 | 2.83E-05 | 0.001171 |
| ENSDARG00000070545 | top1l | 1071.445 | -0.50238 | 2.89E-05 | 0.001186 |
| ENSDARG00000026820 | gucy2d | 710.521 | -0.6479 | 2.93E-05 | 0.001195 |
| ENSDARG00000102047 | mab21l1 | 916.3309 | -0.39972 | 2.94E-05 | 0.001197 |
| ENSDARG00000056745 | necab2 | 1031.944 | -0.60206 | 3.06E-05 | 0.001238 |
| ENSDARG00000023771 | gabrb3 | 549.6425 | -0.4809 | 3.13E-05 | 0.001259 |
| ENSDARG00000059978 | cplx4a | 794.9134 | -0.58916 | 3.13E-05 | 0.001259 |
| ENSDARG00000087413 | bean1 | 173.5456 | -0.59509 | 3.23E-05 | 0.001274 |
| ENSDARG00000024488 | top2a | 454.101 | -0.62409 | 3.24E-05 | 0.001276 |
| ENSDARG00000103672 | cirbpa | 4968.965 | -0.32056 | 3.28E-05 | 0.001285 |
| ENSDARG00000011334 | ncaldb | 445.9252 | -0.59406 | 3.35E-05 | 0.001303 |
| ENSDARG00000038859 | rgs20 | 368.7477 | -0.60854 | 3.35E-05 | 0.001303 |
| ENSDARG00000101446 | si:dkey-46i9.1 | 3283.74 | -0.36657 | 3.41E-05 | 0.001317 |
| ENSDARG00000017219 | pabpc1a | 12405.22 | -0.47942 | 3.67E-05 | 0.001408 |
| ENSDARG00000038559 | h1f0 | 4578.441 | -0.43314 | 3.72E-05 | 0.001421 |
| ENSDARG00000076312 | myot | 513.6268 | -0.46543 | 3.93E-05 | 0.001489 |
| ENSDARG00000034189 | oxsr1a | 414.8789 | -0.4756 | 4.00E-05 | 0.001513 |
| ENSDARG00000045936 | pax6b | 356.251 | -0.48186 | 4.13E-05 | 0.001559 |
| ENSDARG00000016260 | fxr2 | 1750.714 | -0.44621 | 4.26E-05 | 0.001577 |
| ENSDARG00000035861 | si:rp71-39b20.4 | 101.9324 | -0.74836 | 4.25E-05 | 0.001577 |
| ENSDARG00000032317 | tox | 859.0296 | -0.49843 | 4.35E-05 | 0.001608 |
| ENSDARG00000057519 | pcdh1g9 | 475.9772 | -0.45786 | 4.69E-05 | 0.001722 |
| ENSDARG00000005141 | camkvb | 321.1436 | -0.62389 | 4.82E-05 | 0.001753 |
| ENSDARG00000017274 | opn1sw2 | 8073.087 | -0.66246 | 5.04E-05 | 0.001817 |
| ENSDARG00000043697 | nefmb | 779.7942 | -0.45795 | 5.19E-05 | 0.001852 |
| ENSDARG00000063133 | slc4a10a | 2289.787 | -0.46388 | 5.17E-05 | 0.001852 |
| ENSDARG00000078654 | tpx2 | 241.8135 | -0.59032 | 5.28E-05 | 0.00188 |
| ENSDARG00000036698 | znf865 | 1104.237 | -0.36624 | 5.34E-05 | 0.001894 |
| ENSDARG00000101234 | nsmfb | 216.6934 | -0.53534 | 5.37E-05 | 0.0019 |
| ENSDARG00000012667 | tfap2b | 412.6411 | -0.51425 | 5.40E-05 | 0.001906 |
| ENSDARG00000102690 | rims2b | 436.3795 | -0.54997 | 5.70E-05 | 0.001994 |
| ENSDARG00000098809 | snap91 | 1141.826 | -0.52058 | 6.04E-05 | 0.002095 |
| ENSDARG00000045904 | nr2e3 | 85.0552 | -0.82367 | 6.37E-05 | 0.002188 |
| ENSDARG00000008788 | camk1gb | 681.5776 | -0.50652 | 6.47E-05 | 0.00222 |

**Table G.4 continued**

| #geneID | Downregulated gene | Base Mean | log2 Fold Change | p-value | FDR |
|---|---|---|---|---|---|
| ENSDARG00000032838 | si:dkey-206f10.1 | 210.6761 | -0.60721 | 6.49E-05 | 0.002222 |
| ENSDARG00000103900 | sept9b | 373.2307 | -0.48003 | 6.59E-05 | 0.002241 |
| ENSDARG00000063519 | PLEKHB1 | 346.8774 | -0.57122 | 6.70E-05 | 0.002262 |
| ENSDARG00000070109 | ncapg | 230.5915 | -0.57942 | 6.74E-05 | 0.002265 |
| ENSDARG00000090481 | trarg1a | 470.9268 | -0.41844 | 6.82E-05 | 0.00228 |
| ENSDARG00000018397 | hpca | 1208.17 | -0.40387 | 7.00E-05 | 0.002319 |
| ENSDARG00000053547 | jakmip2 | 569.5904 | -0.48671 | 7.01E-05 | 0.002319 |
| ENSDARG00000056050 | kctd17 | 317.9842 | -0.50977 | 7.08E-05 | 0.002339 |
| ENSDARG00000103316 | si:ch211-212k18.5 | 406.8898 | -0.58134 | 7.22E-05 | 0.002374 |
| ENSDARG00000063385 | cenpe | 288.4845 | -0.54392 | 7.41E-05 | 0.00242 |
| ENSDARG00000101959 | etv1 | 130.6694 | -0.66165 | 7.48E-05 | 0.002423 |
| ENSDARG00000005026 | tshz1 | 463.6639 | -0.43933 | 7.54E-05 | 0.002437 |
| ENSDARG00000074030 | myt1a | 955.4827 | -0.62321 | 7.66E-05 | 0.002457 |
| ENSDARG00000100560 | zfpm2b | 121.755 | -0.78411 | 7.82E-05 | 0.002501 |
| ENSDARG00000055106 | znf148 | 251.8921 | -0.48634 | 7.88E-05 | 0.002516 |
| ENSDARG00000103754 | aspm | 307.3496 | -0.50569 | 7.96E-05 | 0.002528 |
| ENSDARG00000045760 | prmt8b | 188.4789 | -0.75632 | 7.98E-05 | 0.002528 |
| ENSDARG00000024619 | foxo6b | 183.8865 | -0.66137 | 7.99E-05 | 0.00253 |
| ENSDARG00000028228 | zbtb18 | 688.1472 | -0.43407 | 8.02E-05 | 0.002534 |
| ENSDARG00000010478 | hsp90aa1.1 | 1806.329 | -0.55629 | 8.08E-05 | 0.002545 |
| ENSDARG00000056929 | kdm6bb | 1025.84 | -0.41413 | 8.20E-05 | 0.002576 |
| ENSDARG00000011602 | si:dkeyp-117h8.2 | 495.8321 | -0.55845 | 8.38E-05 | 0.002622 |
| ENSDARG00000103071 | si:ch211-244c8.4 | 469.6959 | -0.58441 | 8.38E-05 | 0.002622 |
| ENSDARG00000030614 | syt1a | 4092.675 | -0.41053 | 8.47E-05 | 0.002626 |
| ENSDARG00000058256 | draxin | 183.8527 | -0.56455 | 8.43E-05 | 0.002626 |
| ENSDARG00000004621 | gpm6ab | 6827.079 | -0.38529 | 8.58E-05 | 0.002648 |
| ENSDARG00000044375 | zgc:158291 | 394.1934 | -0.49301 | 8.64E-05 | 0.002659 |
| ENSDARG00000069402 | lrrc4.1 | 634.6354 | -0.45715 | 8.74E-05 | 0.002678 |
| ENSDARG00000003680 | runx1t1 | 817.2429 | -0.47676 | 8.82E-05 | 0.002699 |
| ENSDARG00000031283 | vamp1 | 1016.274 | -0.41264 | 8.87E-05 | 0.002703 |
| ENSDARG00000103743 | si:dkeyp-72e1.9 | 116.2484 | -0.65554 | 8.96E-05 | 0.002705 |
| ENSDARG00000018530 | mapkapk2b | 40.64507 | -1.11604 | 8.94E-05 | 0.002705 |
| ENSDARG00000008209 | myt1la | 705.2204 | -0.51813 | 9.25E-05 | 0.002768 |
| ENSDARG00000074319 | sall1a | 459.6609 | -0.41788 | 9.33E-05 | 0.002779 |
| ENSDARG00000034409 | pik3r3b | 827.6856 | -0.39319 | 9.38E-05 | 0.002788 |
| ENSDARG00000018809 | abhd3 | 256.2006 | -0.54036 | 9.57E-05 | 0.00284 |
| ENSDARG00000089458 | rp1l1a | 229.0188 | -0.568 | 9.69E-05 | 0.002859 |
| ENSDARG00000023058 | foxo3a | 1715.686 | -0.48472 | 9.80E-05 | 0.002888 |
| ENSDARG00000069600 | zgc:109889 | 596.6445 | -0.5258 | 0.000103 | 0.002992 |

**Table G.4 continued**

| #geneID | Downregulated gene | Base Mean | log2 Fold Change | p-value | FDR |
|---|---|---|---|---|---|
| ENSDARG00000070239 | knl1 | 173.8125 | -0.68227 | 0.000103 | 0.002992 |
| ENSDARG00000004415 | tcf7l2 | 1124.771 | -0.43812 | 0.000104 | 0.003009 |
| ENSDARG00000102229 | mapk8ip1a | 716.2269 | -0.46423 | 0.000105 | 0.003017 |
| ENSDARG00000013031 | mta2 | 760.4794 | -0.42757 | 0.000105 | 0.00302 |
| ENSDARG00000093413 | edil3a | 1104.714 | -0.4537 | 0.000105 | 0.003024 |
| ENSDARG00000040321 | rx2 | 77.35448 | -0.81658 | 0.000105 | 0.003024 |
| ENSDARG00000010591 | foxn4 | 77.18078 | -0.79054 | 0.000107 | 0.003042 |
| ENSDARG00000019566 | neurod1 | 838.6534 | -0.36396 | 0.000109 | 0.003086 |
| ENSDARG00000009922 | dmbx1a | 177.5255 | -0.64666 | 0.00011 | 0.003117 |
| ENSDARG00000051886 | ankrd11 | 1225.147 | -0.41767 | 0.000113 | 0.003176 |
| ENSDARG00000062335 | nudt14 | 123.0386 | -0.59744 | 0.000115 | 0.003218 |
| ENSDARG00000051981 | STX3 | 74.84644 | -0.78866 | 0.00012 | 0.00333 |
| ENSDARG00000074502 | zmiz1a | 1005.64 | -0.34352 | 0.000121 | 0.003334 |
| ENSDARG00000074057 | calm3b | 4552.075 | -0.41666 | 0.000122 | 0.003362 |
| ENSDARG00000089009 | frmpd1b | 427.0318 | -0.43828 | 0.000123 | 0.003362 |
| ENSDARG00000013855 | slc12a3 | 132.3066 | -0.61244 | 0.000123 | 0.003362 |
| ENSDARG00000056347 | rab3aa | 240.4682 | -0.4793 | 0.000126 | 0.003426 |
| ENSDARG00000037941 | syt5a | 419.3589 | -0.4596 | 0.000128 | 0.003467 |
| ENSDARG00000035910 | znf281b | 275.0817 | -0.46 | 0.000128 | 0.003467 |
| ENSDARG00000062165 | tub | 337.9615 | -0.50319 | 0.000138 | 0.003674 |
| ENSDARG00000074245 | spen | 1491.027 | -0.3605 | 0.000139 | 0.003696 |
| ENSDARG00000011141 | dpysl5a | 708.4039 | -0.60528 | 0.000139 | 0.003696 |
| ENSDARG00000062510 | bcl11ba | 928.1749 | -0.49078 | 0.00014 | 0.003701 |
| ENSDARG00000043026 | ttbk2b | 327.3552 | -0.44694 | 0.000141 | 0.003706 |
| ENSDARG00000036344 | calb2b | 919.7758 | -0.46496 | 0.000145 | 0.003808 |
| ENSDARG00000061205 | stag1a | 573.9191 | -0.38379 | 0.000147 | 0.003842 |
| ENSDARG00000031494 | prrc2a | 2113.263 | -0.38991 | 0.000148 | 0.003867 |
| ENSDARG00000075928 | hivep3a | 532.6452 | -0.52348 | 0.000149 | 0.003883 |
| ENSDARG00000103361 | tshz3b | 438.6752 | -0.47106 | 0.000151 | 0.003911 |
| ENSDARG00000053358 | basp1 | 3546.401 | -0.37856 | 0.000152 | 0.003933 |
| ENSDARG00000031795 | abcf1 | 1467.053 | -0.42863 | 0.000154 | 0.003971 |
| ENSDARG00000056175 | scrt2 | 223.7981 | -0.52384 | 0.000155 | 0.003975 |
| ENSDARG00000009480 | pdcl | 1567.797 | -0.39876 | 0.000157 | 0.004018 |
| ENSDARG00000071467 | zbtb33 | 237.5089 | -0.49179 | 0.00016 | 0.00407 |
| ENSDARG00000088181 | mpped1 | 122.3132 | -0.66856 | 0.00016 | 0.00407 |
| ENSDARG00000097897 | sgip1a | 941.2428 | -0.393 | 0.000162 | 0.004082 |
| ENSDARG00000043907 | fgf11b | 300.8673 | -0.51391 | 0.000163 | 0.004114 |
| ENSDARG00000060639 | apba2b | 915.327 | -0.4267 | 0.000164 | 0.004129 |
| ENSDARG00000079738 | znf219 | 543.171 | -0.52879 | 0.000165 | 0.00415 |

**Table G.4 continued**

| #geneID | Downregulated gene | Base Mean | log2 Fold Change | p-value | FDR |
|---|---|---|---|---|---|
| ENSDARG00000097819 | znf576.1 | 417.2758 | -0.47515 | 0.000166 | 0.00415 |
| ENSDARG00000010408 | igsf9b | 170.7251 | -0.51336 | 0.000167 | 0.004163 |
| ENSDARG00000060711 | sv2bb | 1242.312 | -0.42464 | 0.000167 | 0.00417 |
| ENSDARG00000063007 | apc2 | 1535.099 | -0.52181 | 0.000171 | 0.004225 |
| ENSDARG00000053248 | inab | 490.4481 | -0.56911 | 0.000171 | 0.004225 |
| ENSDARG00000103490 | dpysl4 | 341.0487 | -0.61879 | 0.000171 | 0.004225 |
| ENSDARG00000098644 | si:ch211-126j24.1 | 643.4516 | -0.37647 | 0.000174 | 0.00427 |
| ENSDARG00000035066 | ubtf | 846.4071 | -0.3504 | 0.000176 | 0.004305 |
| ENSDARG00000008413 | atp11a | 1304.209 | -0.31226 | 0.00018 | 0.004379 |
| ENSDARG00000089302 | hnrnpa0a | 1227.494 | -0.33189 | 0.000183 | 0.004429 |
| ENSDARG00000026482 | arhgap12b | 494.1666 | -0.45066 | 0.000183 | 0.004429 |
| ENSDARG00000013669 | napba | 676.1735 | -0.61692 | 0.000186 | 0.004486 |
| ENSDARG00000076928 | tet2 | 713.2525 | -0.38027 | 0.000188 | 0.004495 |
| ENSDARG00000079253 | plch1 | 429.497 | -0.43092 | 0.000188 | 0.004499 |
| ENSDARG00000060368 | syn1 | 995.332 | -0.57213 | 0.000189 | 0.004507 |
| ENSDARG00000079217 | bbs9 | 74.37844 | -0.88504 | 0.000189 | 0.004507 |
| ENSDARG00000115657 | prkca | 647.0088 | -0.44753 | 0.00019 | 0.004511 |
| ENSDARG00000039729 | asap1b | 442.1142 | -0.44543 | 0.000191 | 0.004525 |
| ENSDARG00000018259 | atp1a3a | 7193.488 | -0.42059 | 0.000193 | 0.004561 |
| ENSDARG00000025789 | chd4b | 2534.509 | -0.32078 | 0.000195 | 0.004606 |
| ENSDARG00000012574 | slkb | 248.9471 | -0.47338 | 0.000196 | 0.004608 |
| ENSDARG00000060354 | samd7 | 45.62876 | -0.91167 | 0.000196 | 0.004608 |
| ENSDARG00000038524 | pik3r1 | 3300.529 | -0.30928 | 0.000199 | 0.004647 |
| ENSDARG00000021794 | hmmr | 85.35269 | -0.71014 | 0.000203 | 0.004719 |
| ENSDARG00000070809 | znf516 | 351.8225 | -0.46864 | 0.000204 | 0.004722 |
| ENSDARG00000060149 | ablim1a | 225.1306 | -0.49004 | 0.000207 | 0.004772 |
| ENSDARG00000077545 | si:dkey-16p21.7 | 631.3316 | -0.43449 | 0.000208 | 0.004783 |
| ENSDARG00000077228 | ntrk3a | 552.7275 | -0.41771 | 0.000208 | 0.004786 |
| ENSDARG00000099283 | epb41a | 533.6256 | -0.50134 | 0.000213 | 0.00488 |
| ENSDARG00000056742 | crmp1 | 361.4164 | -0.60757 | 0.000214 | 0.004901 |
| ENSDARG00000060018 | si:ch1073-44g3.1 | 273.768 | -0.53431 | 0.000218 | 0.004959 |
| ENSDARG00000036295 | golga7ba | 466.1343 | -0.42988 | 0.000219 | 0.004959 |
| ENSDARG00000093357 | nyap2b | 139.8933 | -0.58562 | 0.000222 | 0.005018 |
| ENSDARG00000077405 | psip1b | 948.4055 | -0.43129 | 0.000224 | 0.005044 |
| ENSDARG00000023537 | ahr1b | 161.3085 | -0.54639 | 0.000225 | 0.00505 |
| ENSDARG00000103648 | znf536 | 681.8195 | -0.45594 | 0.000227 | 0.005086 |
| ENSDARG00000027322 | lin7c | 1055.653 | -0.45524 | 0.00023 | 0.005112 |
| ENSDARG00000017744 | smc2 | 243.6737 | -0.60074 | 0.000229 | 0.005112 |
| ENSDARG00000061543 | ccdc85b | 541.1624 | -0.39224 | 0.00023 | 0.005113 |

**Table G.4 continued**

| #geneID | Downregulated gene | Base Mean | log2 Fold Change | p-value | FDR |
|---|---|---|---|---|---|
| ENSDARG00000037397 | ssrp1a | 513.1926 | -0.4238 | 0.00023 | 0.00512 |
| ENSDARG00000070442 | si:ch211-113g11.6 | 1335.549 | -0.38033 | 0.000231 | 0.005124 |
| ENSDARG00000059945 | sv2a | 3821.082 | -0.38113 | 0.000233 | 0.005154 |
| ENSDARG00000086990 | carmil3 | 228.8908 | -0.47521 | 0.000234 | 0.005154 |
| ENSDARG00000053544 | hspa4l | 801.5594 | -0.5142 | 0.000234 | 0.005154 |
| ENSDARG00000052242 | aff2 | 238.6475 | -0.57001 | 0.000233 | 0.005154 |
| ENSDARG00000055133 | cenpf | 249.4586 | -0.68462 | 0.000234 | 0.005154 |
| ENSDARG00000059601 | map1aa | 2075.138 | -0.53043 | 0.000241 | 0.005265 |
| ENSDARG00000090232 | clpb | 228.9427 | -0.53704 | 0.000241 | 0.00527 |
| ENSDARG00000068640 | rsf1b.1 | 622.6518 | -0.44932 | 0.000243 | 0.005291 |
| ENSDARG00000079688 | tnrc6a | 2560.044 | -0.35818 | 0.000244 | 0.005302 |
| ENSDARG00000056722 | cd99l2 | 2097.598 | -0.42099 | 0.000244 | 0.005302 |
| ENSDARG00000102288 | CABZ01056321.1 | 106.2834 | -0.65344 | 0.000246 | 0.005318 |
| ENSDARG00000087249 | znf1011 | 50.93824 | -1.15318 | 0.000249 | 0.005372 |
| ENSDARG00000020231 | mapre3a | 179.6216 | -0.55835 | 0.00025 | 0.005384 |
| ENSDARG00000089109 | bcl2b | 330.8269 | -0.47945 | 0.000251 | 0.005389 |
| ENSDARG00000010948 | kif11 | 202.4166 | -0.60097 | 0.000252 | 0.005395 |
| ENSDARG00000077840 | meis2b | 1106.258 | -0.38628 | 0.00026 | 0.005513 |
| ENSDARG00000012944 | myhz2 | 52942.93 | -1.02058 | 0.000259 | 0.005513 |
| ENSDARG00000022045 | map1ab | 1336.319 | -0.55006 | 0.00026 | 0.005515 |
| ENSDARG00000011886 | pdca | 249.8302 | -0.59885 | 0.000267 | 0.005636 |
| ENSDARG00000042107 | si:dkey-44k1.5 | 215.1044 | -0.57224 | 0.000267 | 0.005637 |
| ENSDARG00000101458 | r3hdm1 | 1343.433 | -0.37502 | 0.000269 | 0.005667 |
| ENSDARG00000076371 | CABZ01080074.1 | 193.0821 | -0.60747 | 0.000271 | 0.005708 |
| ENSDARG00000008660 | coro1b | 762.9575 | -0.37966 | 0.000273 | 0.005728 |
| ENSDARG00000067964 | slc6a5 | 959.7016 | -0.40233 | 0.000276 | 0.005765 |
| ENSDARG00000067507 | kctd8 | 204.4908 | -0.60032 | 0.000278 | 0.005791 |
| ENSDARG00000004074 | bach2b | 296.7921 | -0.44159 | 0.000279 | 0.005815 |
| ENSDARG00000002656 | stxbp5a | 563.5012 | -0.45693 | 0.000283 | 0.00586 |
| ENSDARG00000076290 | calr | 1908.468 | -0.35964 | 0.000287 | 0.005913 |
| ENSDARG00000019579 | ldb2a | 263.8329 | -0.49682 | 0.000288 | 0.005931 |
| ENSDARG00000094677 | si:dkey-92j12.5 | 152.145 | -0.60527 | 0.00029 | 0.005948 |
| ENSDARG00000036675 | hnrnpa1b | 1838.668 | -0.34663 | 0.000291 | 0.005972 |
| ENSDARG00000055389 | si:dkey-67c22.2 | 759.902 | -0.34387 | 0.000293 | 0.005993 |
| ENSDARG00000012297 | cnga3b | 54.33367 | -0.87076 | 0.000294 | 0.006005 |
| ENSDARG00000062020 | gse1 | 567.5938 | -0.36921 | 0.000296 | 0.006025 |
| ENSDARG00000030758 | guca1c | 272.2239 | -0.56221 | 0.000296 | 0.006025 |
| ENSDARG00000017014 | ywhae2 | 1901.07 | -0.39521 | 0.000297 | 0.006043 |
| ENSDARG00000033234 | stmn2a | 1515.043 | -0.32229 | 0.000299 | 0.006061 |

**Table G.4 continued**

| #geneID | Downregulated gene | Base Mean | log2 Fold Change | p-value | FDR |
|---|---|---|---|---|---|
| ENSDARG00000091359 | CABZ01118678.1 | 431.8687 | -0.44275 | 0.000303 | 0.006125 |
| ENSDARG00000040110 | kif20bb | 87.7172 | -0.70321 | 0.000304 | 0.006125 |
| ENSDARG00000056483 | ssbp4 | 1282.785 | -0.33197 | 0.000307 | 0.006154 |
| ENSDARG00000077162 | nwd2 | 556.3671 | -0.40438 | 0.000307 | 0.006154 |
| ENSDARG00000098925 | prdm1b | 68.23544 | -0.7185 | 0.000307 | 0.006154 |
| ENSDARG00000090716 | cltcb | 2384.915 | -0.33859 | 0.00031 | 0.006188 |
| ENSDARG00000068582 | rnf44 | 549.7399 | -0.36916 | 0.00031 | 0.006193 |
| ENSDARG00000071497 | zic3 | 469.304 | -0.4451 | 0.000317 | 0.00628 |
| ENSDARG00000025011 | synj1 | 1008.049 | -0.43382 | 0.000321 | 0.006363 |
| ENSDARG00000059960 | plch2a | 423.9936 | -0.42102 | 0.000322 | 0.00637 |
| ENSDARG00000069438 | neurl1aa | 304.6219 | -0.4403 | 0.000326 | 0.006438 |
| ENSDARG00000027963 | camkva | 100.1132 | -0.72419 | 0.000326 | 0.006438 |
| ENSDARG00000013317 | pygmb | 2552.984 | -0.36388 | 0.000327 | 0.006441 |
| ENSDARG00000087538 | kif3a | 593.8318 | -0.47638 | 0.000329 | 0.006457 |
| ENSDARG00000077852 | samd11 | 477.4224 | -0.37636 | 0.000335 | 0.00653 |
| ENSDARG00000062056 | elmod1 | 3166.893 | -0.49617 | 0.000338 | 0.006555 |
| ENSDARG00000105447 | si:ch211-129p13.1 | 146.4574 | -0.59623 | 0.000338 | 0.006555 |
| ENSDARG00000043821 | klf7b | 687.7612 | -0.39178 | 0.00034 | 0.006583 |
| ENSDARG00000089271 | nexmifa | 770.9155 | -0.45886 | 0.000341 | 0.006597 |
| ENSDARG00000006128 | cep170aa | 359.5473 | -0.48414 | 0.000342 | 0.006597 |
| ENSDARG00000010710 | msi1 | 308.0947 | -0.41761 | 0.000347 | 0.006684 |
| ENSDARG00000101215 | sgip1b | 156.1641 | -0.57903 | 0.000349 | 0.006701 |
| ENSDARG00000007136 | gtf2h4 | 218.2447 | -0.45024 | 0.000358 | 0.006857 |
| ENSDARG00000005699 | ddx19 | 464.8238 | -0.36394 | 0.000361 | 0.006887 |
| ENSDARG00000034293 | hif1ab | 1613.61 | -0.36723 | 0.000369 | 0.006999 |
| ENSDARG00000086626 | im:7147486 | 386.0439 | -0.44483 | 0.00037 | 0.006999 |
| ENSDARG00000040123 | zfpm2a | 238.3044 | -0.66623 | 0.000369 | 0.006999 |
| ENSDARG00000032630 | neb | 33604.84 | -0.66926 | 0.00037 | 0.006999 |
| ENSDARG00000077811 | sox11a | 1216.682 | -0.35526 | 0.000376 | 0.007087 |
| ENSDARG00000036816 | pou2f2a | 261.1925 | -0.53351 | 0.000377 | 0.007099 |
| ENSDARG00000019335 | hes6 | 163.4876 | -0.49767 | 0.00038 | 0.007143 |
| ENSDARG00000063921 | mt-nd5 | 49019.25 | -1.00087 | 0.000384 | 0.007206 |
| ENSDARG00000017107 | nr2e1 | 87.74651 | -0.66397 | 0.000385 | 0.007207 |
| ENSDARG00000105441 | pcdh11 | 175.5632 | -0.59158 | 0.000385 | 0.007212 |
| ENSDARG00000075116 | sall2 | 290.3834 | -0.48737 | 0.000386 | 0.007213 |
| ENSDARG00000033009 | h3f3c | 4025.776 | -0.36399 | 0.000389 | 0.007245 |
| ENSDARG00000013343 | kif26ba | 580.8533 | -0.46996 | 0.000389 | 0.007249 |
| ENSDARG00000035907 | fam49al | 1010.877 | -0.35867 | 0.000394 | 0.007323 |
| ENSDARG00000052348 | smarca5 | 719.5481 | -0.38023 | 0.000395 | 0.007333 |

**Table G.4 continued**

| #geneID | Downregulated gene | Base Mean | log2 Fold Change | p-value | FDR |
|---|---|---|---|---|---|
| ENSDARG00000078317 | si:dkey-175m17.7 | 165.7492 | -0.56696 | 0.000395 | 0.007333 |
| ENSDARG00000079665 | gpr158b | 173.4724 | -0.52339 | 0.000401 | 0.007425 |
| ENSDARG00000054010 | scaf1 | 984.5958 | -0.37743 | 0.000403 | 0.007447 |
| ENSDARG00000034424 | atp1b2b | 462.9276 | -0.44403 | 0.000403 | 0.007447 |
| ENSDARG00000070491 | hpcal4 | 399.7947 | -0.46204 | 0.000415 | 0.007618 |
| ENSDARG00000104664 | dclk1b | 596.1157 | -0.47007 | 0.000416 | 0.007621 |
| ENSDARG00000094280 | usp21 | 172.1235 | -0.54892 | 0.000416 | 0.007621 |
| ENSDARG00000099966 | polr2a | 2365.162 | -0.31068 | 0.00042 | 0.007657 |
| ENSDARG00000056690 | mtmr1a | 322.1039 | -0.4127 | 0.000419 | 0.007657 |
| ENSDARG00000012125 | cnga1b | 91.77459 | -0.67043 | 0.00042 | 0.007657 |
| ENSDARG00000054290 | acin1a | 2908.416 | -0.34129 | 0.000424 | 0.007732 |
| ENSDARG00000045087 | cdk5r1b | 627.9467 | -0.4641 | 0.000429 | 0.007802 |
| ENSDARG00000063922 | mt-nd6 | 7672.919 | -0.50619 | 0.000431 | 0.00782 |
| ENSDARG00000015184 | mpp3a | 282.7604 | -0.44217 | 0.000433 | 0.007831 |
| ENSDARG00000068242 | cngb1a | 95.84974 | -0.64592 | 0.000435 | 0.007873 |
| ENSDARG00000036593 | kdm2ba | 1098.62 | -0.44073 | 0.000441 | 0.007959 |
| ENSDARG00000024746 | hsp90aa1.2 | 4192.634 | -0.45088 | 0.000442 | 0.007974 |
| ENSDARG00000058771 | nav1b | 738.5357 | -0.46863 | 0.000451 | 0.008083 |
| ENSDARG00000019529 | parp1 | 474.9705 | -0.46576 | 0.000452 | 0.00809 |
| ENSDARG00000017798 | bcor | 952.6854 | -0.30243 | 0.000454 | 0.008118 |
| ENSDARG00000044155 | mafaa | 295.2108 | -0.44521 | 0.000483 | 0.008525 |
| ENSDARG00000008255 | cnot6a | 1162.833 | -0.36375 | 0.000484 | 0.008527 |
| ENSDARG00000076451 | prdm2b | 547.1011 | -0.34342 | 0.000494 | 0.008689 |
| ENSDARG00000023600 | sh3gl2a | 1365.482 | -0.4866 | 0.000497 | 0.008712 |
| ENSDARG00000043835 | rab3ab | 386.3453 | -0.59614 | 0.000514 | 0.008936 |
| ENSDARG00000059781 | atcayb | 245.388 | -0.52228 | 0.00052 | 0.009018 |
| ENSDARG00000000380 | pde6a | 205.612 | -0.63101 | 0.00052 | 0.009018 |
| ENSDARG00000004588 | sox4a | 2671.945 | -0.3305 | 0.000528 | 0.009157 |
| ENSDARG00000078671 | cdk5r2b | 305.3187 | -0.44316 | 0.000531 | 0.009174 |
| ENSDARG00000051970 | smu1b | 304.4144 | -0.44782 | 0.000531 | 0.009174 |
| ENSDARG00000021193 | coro1cb | 781.6185 | -0.36835 | 0.000538 | 0.009249 |
| ENSDARG00000063535 | chd4a | 890.7613 | -0.41737 | 0.000538 | 0.009249 |
| ENSDARG00000005454 | tacc3 | 187.747 | -0.59288 | 0.000542 | 0.009302 |
| ENSDARG00000052567 | tmem35 | 1145.818 | -0.35476 | 0.000548 | 0.009319 |
| ENSDARG00000096533 | rltgr | 265.9566 | -0.53597 | 0.000546 | 0.009319 |
| ENSDARG00000103057 | zfhx3 | 1790.333 | -0.305 | 0.000556 | 0.009424 |
| ENSDARG00000044199 | gnat1 | 1355.314 | -0.45106 | 0.000556 | 0.009424 |
| ENSDARG00000075455 | soga3b | 157.7339 | -0.54797 | 0.000556 | 0.009424 |
| ENSDARG00000092119 | si:ch211-235f12.2 | 144.7601 | -0.52576 | 0.00056 | 0.009481 |

**Table G.4 continued**

| #geneID | Downregulated gene | Base Mean | log2 Fold Change | p-value | FDR |
|---|---|---|---|---|---|
| ENSDARG00000060297 | arhgap35b | 630.573 | -0.40811 | 0.000563 | 0.009514 |
| ENSDARG00000060298 | nin | 91.57482 | -0.62795 | 0.000568 | 0.009586 |
| ENSDARG00000010231 | ppm1na | 173.8836 | -0.67848 | 0.000573 | 0.009657 |
| ENSDARG00000103950 | pcdh1gc6 | 306.8749 | -0.46744 | 0.000574 | 0.009661 |
| ENSDARG00000100596 | si:ch73-43g23.1 | 768.5462 | -0.40335 | 0.000582 | 0.009736 |
| ENSDARG00000104361 | barhl2 | 234.1934 | -0.49417 | 0.000582 | 0.009736 |
| ENSDARG00000029612 | gpkow | 173.0562 | -0.48324 | 0.000583 | 0.009745 |
| ENSDARG00000008278 | rcor2 | 219.6068 | -0.57733 | 0.000587 | 0.009772 |
| ENSDARG00000031720 | clstn1 | 6764.655 | -0.33784 | 0.00059 | 0.009801 |
| ENSDARG00000004906 | stip1 | 1647.572 | -0.32018 | 0.000593 | 0.009825 |
| ENSDARG00000103413 | zgc:109949 | 160.9122 | -0.49292 | 0.000595 | 0.009827 |
| ENSDARG00000079985 | nrip2 | 201.3558 | -0.52578 | 0.000595 | 0.009827 |
| ENSDARG00000054320 | ap2a1 | 2045.976 | -0.34303 | 0.000599 | 0.009863 |
| ENSDARG00000068965 | nrip1a | 302.0727 | -0.39056 | 0.000606 | 0.009965 |
| ENSDARG00000097245 | soga3a | 395.8668 | -0.4205 | 0.000606 | 0.009965 |

## APPENDIX H: GO processes upregulated by chronic cortisol in Klf9 mutants only

**Table H.1. GO processes upregulated by CORT only in Klf9 mutants**

| GO Term | Description | P-value | FDR q-value | Enrichment |
|---|---|---|---|---|
| GO:0006518 | peptide metabolic process | 2.52E-10 | 2.06E-06 | 3.11 |
| GO:0043603 | cellular amide metabolic process | 3.84E-09 | 1.57E-05 | 2.57 |
| GO:0043604 | amide biosynthetic process | 8.25E-09 | 2.24E-05 | 2.9 |
| GO:0006412 | translation | 1.02E-08 | 2.09E-05 | 3.18 |
| GO:0043043 | peptide biosynthetic process | 2.00E-08 | 3.27E-05 | 3.09 |
| GO:0015985 | energy coupled proton transport, down electrochemical gradient | 9.18E-07 | 1.25E-03 | 9.16 |
| GO:0015986 | ATP synthesis coupled proton transport | 9.18E-07 | 1.07E-03 | 9.16 |
| GO:1901566 | organonitrogen compound biosynthetic process | 1.77E-06 | 1.80E-03 | 1.97 |
| GO:0007568 | aging | 6.71E-06 | 6.08E-03 | 10.88 |
| GO:0034645 | cellular macromolecule biosynthetic process | 1.44E-05 | 1.17E-02 | 1.98 |
| GO:0044271 | cellular nitrogen compound biosynthetic process | 1.83E-05 | 1.36E-02 | 1.79 |
| GO:0010499 | proteasomal ubiquitin-independent protein catabolic process | 2.77E-05 | 1.88E-02 | 7.25 |
| GO:0002181 | cytoplasmic translation | 3.90E-05 | 2.45E-02 | 6.92 |
| GO:0009059 | macromolecule biosynthetic process | 4.11E-05 | 2.40E-02 | 1.88 |
| GO:1902600 | proton transmembrane transport | 5.61E-05 | 3.05E-02 | 4.13 |
| GO:0006869 | lipid transport | 6.37E-05 | 3.25E-02 | 3.05 |
| GO:0006582 | melanin metabolic process | 9.67E-05 | 4.64E-02 | 21.76 |
| GO:0042438 | melanin biosynthetic process | 9.67E-05 | 4.38E-02 | 21.76 |
| GO:0097250 | mitochondrial respiratory chain supercomplex assembly | 9.67E-05 | 4.15E-02 | 21.76 |
| GO:0044249 | cellular biosynthetic process | 1.29E-04 | 5.26E-02 | 1.54 |
| GO:0098754 | detoxification | 1.49E-04 | 5.81E-02 | 6.87 |
| GO:1901576 | organic substance biosynthetic process | 2.13E-04 | 7.89E-02 | 1.5 |
| GO:0046034 | ATP metabolic process | 2.77E-04 | 9.84E-02 | 3.75 |

## APPENDIX I: Consistently overexpressed genes in larvae with wild-type GR in chronic cortisol

### Table I.1. Consistently overexpressed genes in larvae with wild-type GR in chronic cortisol

| Gene ID | Gene name | Gene_description |
|---|---|---|
| ENSDARG00000038025 | cbx7a | chromobox_homolog_7a_[Source:ZFIN;Acc:ZDB-GENE-050417-400] |
| ENSDARG00000040277 | fbxo32 | F-box_protein_32_[Source:ZFIN;Acc:ZDB-GENE-040426-1040] |
| ENSDARG00000040278 | klhl38b | kelch-like_family_member_38b_[Source:ZFIN;Acc:ZDB-GENE-120727-8] |
| ENSDARG00000068194 | klf9 | Kruppel-like_factor_9_[Source:ZFIN;Acc:ZDB-GENE-060526-244] |
| ENSDARG00000074322 | si:ch211-194m7.3 | si:ch211-194m7.3_[Source:ZFIN;Acc:ZDB-GENE-131121-19] |
| ENSDARG00000088745 | MFAP4_(1_of_many) | microfibril_associated_protein_4_[Source:HGNC_Symbol;Acc:HGNC:7035] |
| ENSDARG00000089724 | cyldb | cylindromatosis_(turban_tumor_syndrome),_b_[Source:ZFIN;Acc:ZDB-GENE-100208-1] |
| ENSDARG00000091209 | ucp3 | uncoupling_protein_3_[Source:ZFIN;Acc:ZDB-GENE-040426-1317] |
| ENSDARG00000093316 | adgrf8 | adhesion_G_protein-coupled_receptor_F8_[Source:ZFIN;Acc:ZDB-GENE-130531-41] |
| ENSDARG00000098736 | si:dkey-201i2.4 | si:dkey-201i2.4_[Source:ZFIN;Acc:ZDB-GENE-141215-24] |
| ENSDARG00000113076 | si:ch211-182p11.1 | si:ch211-182p11.1_[Source:ZFIN;Acc:ZDB-GENE-131127-323] |
| ENSDARG00000117818 | CR926130.2 | |
| ENSDARG00000004748 | zgc:100868 | zgc:100868_[Source:ZFIN;Acc:ZDB-GENE-040801-33] |
| ENSDARG00000007769 | sult5a1 | sulfotransferase_family_5A,_member_1_[Source:ZFIN;Acc:ZDB-GENE-060929-978] |
| ENSDARG00000016188 | si:ch73-63e15.2 | si:ch73-63e15.2_[Source:ZFIN;Acc:ZDB-GENE-091204-463] |
| ENSDARG00000028731 | stat4 | signal_transducer_and_activator_of_transcription_4_[Source:ZFIN;Acc:ZDB-GENE-030616-264] |
| ENSDARG00000031588 | si:dkey-239b22.1 | si:dkey-239b22.1_[Source:ZFIN;Acc:ZDB-GENE-131119-12] |
| ENSDARG00000033684 | oxgr1a.1 | oxoglutarate_(alpha-ketoglutarate)_receptor_1a,_tandem_duplicate_1_[Source:ZFIN;Acc:ZDB-GENE-060421-6734] |
| ENSDARG00000036767 | urgcp | upregulator_of_cell_proliferation_[Source:ZFIN;Acc:ZDB-GENE-120215-160] |
| ENSDARG00000038668 | gbp1 | guanylate_binding_protein_1_[Source:ZFIN;Acc:ZDB-GENE-040718-32] |
| ENSDARG00000041294 | noxo1a | NADPH_oxidase_organizer_1a_[Source:ZFIN;Acc:ZDB-GENE-030131-9700] |
| ENSDARG00000042816 | mmp9 | matrix_metallopeptidase_9_[Source:ZFIN;Acc:ZDB-GENE-040426-2132] |
| ENSDARG00000043093 | mpeg1.2 | macrophage_expressed_1,_tandem_duplicate_2_[Source:ZFIN;Acc:ZDB-GENE-050522-305] |
| ENSDARG00000043249 | irf1b | interferon_regulatory_factor_1b_[Source:ZFIN;Acc:ZDB-GENE-041114-13] |
| ENSDARG00000051914 | slc14a2 | solute_carrier_family_14_(urea_transporter),_member_2_[Source:ZFIN;Acc:ZDB-GENE-030131-4833] |
| ENSDARG00000052626 | AL954655.1 | |
| ENSDARG00000052779 | zgc:153932 | zgc:153932_[Source:ZFIN;Acc:ZDB-GENE-070209-223] |

**Table I.1 continued**

| Gene ID | Gene name | Gene_description |
|---|---|---|
| ENSDARG00000054160 | zgc:113625 | zgc:113625_[Source:ZFIN;Acc:ZDB-GENE-050320-47] |
| ENSDARG00000056874 | lygl1 | lysozyme_g-like_1_[Source:ZFIN;Acc:ZDB-GENE-040718-461] |
| ENSDARG00000059054 | pdk2b | pyruvate_dehydrogenase_kinase,_isozyme_2b_[Source:ZFIN;Acc:ZDB-GENE-040426-939] |
| ENSDARG00000062788 | irg1l | immunoresponsive_gene_1,_like_[Source:ZFIN;Acc:ZDB-GENE-061103-301] |
| ENSDARG00000067741 | itpkcb | inositol-trisphosphate_3-kinase_Cb_[Source:ZFIN;Acc:ZDB-GENE-080225-27] |
| ENSDARG00000068951 | si:ch211-219a15.4 | si:ch211-219a15.4_[Source:ZFIN;Acc:ZDB-GENE-060503-308] |
| ENSDARG00000070426 | chac1 | ChaC,_cation_transport_regulator_homolog_1_(E._coli)_[Source:ZFIN;Acc:ZDB-GENE-030131-1957] |
| ENSDARG00000074150 | si:ch211-226h7.5 | si:ch211-226h7.5_[Source:ZFIN;Acc:ZDB-GENE-130531-3] |
| ENSDARG00000074378 | junba | JunB_proto-oncogene,_AP-1_transcription_factor_subunit_a_[Source:ZFIN;Acc:ZDB-GENE-040426-2172] |
| ENSDARG00000076196 | si:ch211-226h7.6 | si:ch211-226h7.6_[Source:ZFIN;Acc:ZDB-GENE-130531-12] |
| ENSDARG00000076269 | zgc:172131 | zgc:172131_[Source:ZFIN;Acc:ZDB-GENE-080204-47] |
| ENSDARG00000078093 | zgc:172065 | zgc:172065_[Source:ZFIN;Acc:ZDB-GENE-080214-2] |
| ENSDARG00000079227 | plekhs1 | pleckstrin_homology_domain_containing,_family_S_member_1_[Source:ZFIN;Acc:ZDB-GENE-080204-50] |
| ENSDARG00000091906 | rbp7a | retinol_binding_protein_7a,_cellular_[Source:ZFIN;Acc:ZDB-GENE-071004-2] |
| ENSDARG00000092719 | AL954655.2 | |
| ENSDARG00000092778 | si:ch73-338o16.4 | si:ch73-338o16.4_[Source:ZFIN;Acc:ZDB-GENE-131119-14] |
| ENSDARG00000093082 | LO018605.1 | |
| ENSDARG00000093936 | si:dkeyp-1h4.6 | si:dkeyp-1h4.6_[Source:ZFIN;Acc:ZDB-GENE-060503-841] |
| ENSDARG00000094104 | AL929237.1 | si:ch211-213i16.3_[Source:NCBI_gene;Acc:100536429] |
| ENSDARG00000095245 | si:ch211-157j23.2 | si:ch211-157j23.2_[Source:ZFIN;Acc:ZDB-GENE-030131-5686] |
| ENSDARG00000095409 | si:ch211-226h7.8 | si:ch211-226h7.8_[Source:ZFIN;Acc:ZDB-GENE-130531-7] |
| ENSDARG00000097080 | si:ch73-181m17.1 | si:ch73-181m17.1_[Source:ZFIN;Acc:ZDB-GENE-131122-49] |
| ENSDARG00000097137 | CR753876.1 | |
| ENSDARG00000097157 | si:ch211-207n23.2 | si:ch211-207n23.2_[Source:ZFIN;Acc:ZDB-GENE-131121-310] |
| ENSDARG00000097539 | si:ch211-39f2.3 | si:ch211-39f2.3_[Source:ZFIN;Acc:ZDB-GENE-131126-52] |
| ENSDARG00000100106 | CR385054.1 | |
| ENSDARG00000102758 | FO704661.1 | gamma-glutamyl_hydrolase_[Source:NCBI_gene;Acc:553228] |
| ENSDARG00000103199 | si:dkey-247k7.2 | si:dkey-247k7.2_[Source:ZFIN;Acc:ZDB-GENE-031118-45] |
| ENSDARG00000103634 | CU914622.2 | si:ch73-329n5.6_[Source:NCBI_gene;Acc:101883339] |
| ENSDARG00000104399 | tppp | tubulin_polymerization_promoting_protein_[Source:ZFIN;Acc:ZDB-GENE-101115-2] |
| ENSDARG00000104919 | si:ch211-153b23.3 | si:ch211-153b23.3_[Source:ZFIN;Acc:ZDB-GENE-141216-408] |
| ENSDARG00000109626 | si:ch211-226h7.3 | si:ch211-226h7.3_[Source:ZFIN;Acc:ZDB-GENE-130531-9] |

**Table I.1 continued**

| Gene ID | Gene name | Gene_description |
|---|---|---|
| ENSDARG00000109648 | si:ch211-147m6.1 | si:ch211-147m6.1_[Source:ZFIN;Acc:ZDB-GENE-131120-57] |
| ENSDARG00000113315 | zgc:153932 | zgc:153932_[Source:ZFIN;Acc:ZDB-GENE-070209-223] |
| ENSDARG00000117266 | FO904966.1 | |
| ENSDARG00000117407 | AL954191.1 | uncharacterized_LOC101885516_[Source:NCBI_gene;Acc:101885516] |
| ENSDARG00000001953 | pfkfb3 | 6-phosphofructo-2-kinase/fructose-2,6-biphosphatase_3_[Source:ZFIN;Acc:ZDB-GENE-040426-2724] |
| ENSDARG00000002259 | ca15c | carbonic_anhydrase_XV_c_[Source:ZFIN;Acc:ZDB-GENE-061013-737] |
| ENSDARG00000003203 | rhcga | Rh_family,_C_glycoprotein_a_[Source:ZFIN;Acc:ZDB-GENE-070424-81] |
| ENSDARG00000003820 | nr1d2a | nuclear_receptor_subfamily_1,_group_D,_member_2a_[Source:ZFIN;Acc:ZDB-GENE-040504-1] |
| ENSDARG00000004187 | zgc:122979 | zgc:122979_[Source:ZFIN;Acc:ZDB-GENE-051127-45] |
| ENSDARG00000005481 | nfkbiaa | nuclear_factor_of_kappa_light_polypeptide_gene_enhancer_in_B-cells_inhibitor,_alpha_a_[Source:ZFIN;Acc:ZDB-GENE-040426-2227] |
| ENSDARG00000005565 | entpd8 | ectonucleoside_triphosphate_diphosphohydrolase_8_[Source:ZFIN;Acc:ZDB-GENE-040724-142] |
| ENSDARG00000006526 | fn1b | fibronectin_1b_[Source:ZFIN;Acc:ZDB-GENE-030131-6545] |
| ENSDARG00000007693 | nfkbiab | nuclear_factor_of_kappa_light_polypeptide_gene_enhancer_in_B-cells_inhibitor,_alpha_b_[Source:ZFIN;Acc:ZDB-GENE-030131-1819] |
| ENSDARG00000010572 | slc25a25a | solute_carrier_family_25_(mitochondrial_carrier;_phosphate_carrier),_member_25a_[Source:ZFIN;Acc:ZDB-GENE-040426-2396] |
| ENSDARG00000012903 | slc34a2a | solute_carrier_family_34_(type_II_sodium/phosphate_cotransporter),_member_2a_[Source:ZFIN;Acc:ZDB-GENE-000524-1] |
| ENSDARG00000013522 | pck1 | phosphoenolpyruvate_carboxykinase_1_(soluble)_[Source:ZFIN;Acc:ZDB-GENE-030909-11] |
| ENSDARG00000013721 | g6pca.2 | glucose-6-phosphatase_a,_catalytic_subunit,_tandem_duplicate_2_[Source:ZFIN;Acc:ZDB-GENE-050309-17] |
| ENSDARG00000013871 | slc5a1 | solute_carrier_family_5_(sodium/glucose_cotransporter),_member_1_[Source:ZFIN;Acc:ZDB-GENE-040426-1524] |
| ENSDARG00000016391 | calcoco1b | calcium_binding_and_coiled-coil_domain_1b_[Source:ZFIN;Acc:ZDB-GENE-031118-126] |
| ENSDARG00000018621 | slc6a19a.1 | solute_carrier_family_6_(neutral_amino_acid_transporter),_member_19a,_tandem_duplicate_1_[Source:ZFIN;Acc:ZDB-GENE-070620-2] |
| ENSDARG00000020239 | lpin1 | lipin_1_[Source:ZFIN;Acc:ZDB-GENE-080722-2] |
| ENSDARG00000020298 | btg2 | B-cell_translocation_gene_2_[Source:ZFIN;Acc:ZDB-GENE-000210-15] |
| ENSDARG00000020364 | fbp1b | fructose-1,6-bisphosphatase_1b_[Source:ZFIN;Acc:ZDB-GENE-021206-11] |
| ENSDARG00000020876 | pdk2a | pyruvate_dehydrogenase_kinase,_isozyme_2a_[Source:ZFIN;Acc:ZDB-GENE-120910-1] |

**Table I.1 continued**

| Gene ID | Gene name | Gene_description |
|---|---|---|
| ENSDARG00000021372 | tob1b | transducer_of_ERBB2,_1b_[Source:ZFIN;Acc:ZDB-GENE-040426-2151] |
| ENSDARG00000023151 | ucp1 | uncoupling_protein_1_[Source:ZFIN;Acc:ZDB-GENE-010503-1] |
| ENSDARG00000023176 | tdo2b | tryptophan_2,3-dioxygenase_b_[Source:ZFIN;Acc:ZDB-GENE-030131-6014] |
| ENSDARG00000025428 | socs3a | suppressor_of_cytokine_signaling_3a_[Source:ZFIN;Acc:ZDB-GENE-030131-7349] |
| ENSDARG00000027249 | btg1 | B-cell_translocation_gene_1,_anti-proliferative_[Source:ZFIN;Acc:ZDB-GENE-010726-1] |
| ENSDARG00000027744 | gadd45ba | growth_arrest_and_DNA-damage-inducible,_beta_a_[Source:ZFIN;Acc:ZDB-GENE-040426-1971] |
| ENSDARG00000028396 | fkbp5 | FK506_binding_protein_5_[Source:ZFIN;Acc:ZDB-GENE-030616-630] |
| ENSDARG00000031683 | fosab | v-fos_FBJ_murine_osteosarcoma_viral_oncogene_homolog_Ab_[Source:ZFIN;Acc:ZDB-GENE-031222-4] |
| ENSDARG00000032619 | tob1a | transducer_of_ERBB2,_1a_[Source:ZFIN;Acc:ZDB-GENE-031030-4] |
| ENSDARG00000033160 | nr1d1 | nuclear_receptor_subfamily_1,_group_d,_member_1_[Source:ZFIN;Acc:ZDB-GENE-050105-1] |
| ENSDARG00000035719 | arl5c | ADP-ribosylation_factor-like_5C_[Source:ZFIN;Acc:ZDB-GENE-040426-1866] |
| ENSDARG00000036107 | txnipa | thioredoxin_interacting_protein_a_[Source:ZFIN;Acc:ZDB-GENE-030804-10] |
| ENSDARG00000036833 | upp2 | uridine_phosphorylase_2_[Source:ZFIN;Acc:ZDB-GENE-040426-830] |
| ENSDARG00000037012 | slc3a2b | solute_carrier_family_3_(amino_acid_transporter_heavy_chain),_member_2b_[Source:ZFIN;Acc:ZDB-GENE-040122-2] |
| ENSDARG00000037421 | egr1 | early_growth_response_1_[Source:ZFIN;Acc:ZDB-GENE-980526-320] |
| ENSDARG00000037618 | ddit4 | DNA-damage-inducible_transcript_4_[Source:ZFIN;Acc:ZDB-GENE-031002-35] |
| ENSDARG00000038095 | socs1a | suppressor_of_cytokine_signaling_1a_[Source:ZFIN;Acc:ZDB-GENE-040801-205] |
| ENSDARG00000038199 | cdab | cytidine_deaminase_b_[Source:ZFIN;Acc:ZDB-GENE-040426-1911] |
| ENSDARG00000039393 | si:ch211-240l19.5 | si:ch211-240l19.5_[Source:ZFIN;Acc:ZDB-GENE-041210-327] |
| ENSDARG00000041540 | sult1st2 | sulfotransferase_family_1,_cytosolic_sulfotransferase_2_[Source:ZFIN;Acc:ZDB-GENE-030804-27] |
| ENSDARG00000041797 | cx28.9 | connexin_28.9_[Source:ZFIN;Acc:ZDB-GENE-041114-200] |
| ENSDARG00000042953 | cyp2n13 | cytochrome_P450,_family_2,_subfamily_N,_polypeptide_13_[Source:ZFIN;Acc:ZDB-GENE-041001-158] |
| ENSDARG00000044528 | slc15a1b | solute_carrier_family_15_(oligopeptide_transporter),_member_1b_[Source:ZFIN;Acc:ZDB-GENE-030131-4661] |
| ENSDARG00000055276 | rel | v-rel_avian_reticuloendotheliosis_viral_oncogene_homolog_[Source:ZFIN;Acc:ZDB-GENE-040718-255] |
| ENSDARG00000055752 | npas4a | neuronal_PAS_domain_protein_4a_[Source:ZFIN;Acc:ZDB-GENE-060616-396] |

**Table I.1 continued**

| Gene ID | Gene name | Gene_description |
|---|---|---|
| ENSDARG00000057671 | epas1b | endothelial_PAS_domain_protein_1b_[Source:ZFIN;Acc:ZDB-GENE-060607-11] |
| ENSDARG00000075666 | tsc22d3 | TSC22_domain_family,_member_3_[Source:ZFIN;Acc:ZDB-GENE-040426-1433] |
| ENSDARG00000077473 | mych | myelocytomatosis_oncogene_homolog_[Source:ZFIN;Acc:ZDB-GENE-030219-51] |
| ENSDARG00000077799 | egr4 | early_growth_response_4_[Source:ZFIN;Acc:ZDB-GENE-080204-90] |
| ENSDARG00000086881 | ier2b | immediate_early_response_2b_[Source:ZFIN;Acc:ZDB-GENE-030131-8244] |
| ENSDARG00000087178 | scpp9 | secretory_calcium-binding_phosphoprotein_9_[Source:ZFIN;Acc:ZDB-GENE-090424-3] |
| ENSDARG00000087303 | cebpd | CCAAT_enhancer_binding_protein_delta_[Source:ZFIN;Acc:ZDB-GENE-020111-4] |
| ENSDARG00000087911 | psme4a | proteasome_activator_subunit_4a_[Source:ZFIN;Acc:ZDB-GENE-091204-452] |
| ENSDARG00000090416 | scpp1 | secretory_calcium-binding_phosphoprotein_1_[Source:ZFIN;Acc:ZDB-GENE-090424-1] |
| ENSDARG00000092553 | slc25a5 | solute_carrier_family_25_(mitochondrial_carrier;_adenine_nucleotide_translocator),_member_5_[Source:ZFIN;Acc:ZDB-GENE-020419-9] |
| ENSDARG00000094696 | si:dkey-201c13.2 | si:dkey-201c13.2_[Source:ZFIN;Acc:ZDB-GENE-060526-243] |
| ENSDARG00000094719 | CR318588.3 | uncharacterized_LOC101884954_[Source:NCBI_gene;Acc:101884954] |
| ENSDARG00000096445 | si:ch211-214p16.3 | si:ch211-214p16.3_[Source:ZFIN;Acc:ZDB-GENE-120709-93] |
| ENSDARG00000097205 | ulk2 | unc-51_like_autophagy_activating_kinase_2_[Source:ZFIN;Acc:ZDB-GENE-090218-30] |
| ENSDARG00000098761 | rgs2 | regulator_of_G_protein_signaling_2_[Source:ZFIN;Acc:ZDB-GENE-040718-410] |
| ENSDARG00000098995 | cyp2k6 | cytochrome_P450,_family_2,_subfamily_K,_polypeptide_6_[Source:ZFIN;Acc:ZDB-GENE-040426-1571] |
| ENSDARG00000099195 | ier2a | immediate_early_response_2a_[Source:ZFIN;Acc:ZDB-GENE-030131-9126] |
| ENSDARG00000099819 | sb:cb1058 | sb:cb1058_[Source:ZFIN;Acc:ZDB-GENE-040108-9] |
| ENSDARG00000100265 | rhcgb | Rh_family,_C_glycoprotein_b_[Source:ZFIN;Acc:ZDB-GENE-040426-2595] |
| ENSDARG00000100515 | dusp1 | dual_specificity_phosphatase_1_[Source:ZFIN;Acc:ZDB-GENE-040426-2018] |
| ENSDARG00000100792 | zgc:154142 | zgc:154142_[Source:ZFIN;Acc:ZDB-GENE-070615-2] |
| ENSDARG00000102020 | pnpla3 | patatin-like_phospholipase_domain_containing_3_[Source:ZFIN;Acc:ZDB-GENE-040718-27] |
| ENSDARG00000102364 | si:dkey-202l22.6 | si:dkey-202l22.6_[Source:ZFIN;Acc:ZDB-GENE-131121-181] |

**Table I.1 continued**

| Gene ID | Gene name | Gene_description |
|---|---|---|
| ENSDARG00000104172 | diabloa | diablo,_IAP-binding_mitochondrial_protein_a_[Source:ZFIN;Acc:ZDB-GENE-040426-1303] |
| ENSDARG00000104177 | cpne3 | copine_III_[Source:ZFIN;Acc:ZDB-GENE-040426-763] |
| ENSDARG00000104773 | junbb | JunB_proto-oncogene,_AP-1_transcription_factor_subunit_b_[Source:ZFIN;Acc:ZDB-GENE-040426-2666] |
| ENSDARG00000004954 | grna | granulin_a_[Source:ZFIN;Acc:ZDB-GENE-030131-8434] |
| ENSDARG00000016939 | itgb2 | integrin,_beta_2_[Source:ZFIN;Acc:ZDB-GENE-110411-4] |
| ENSDARG00000023188 | lcp1 | lymphocyte_cytosolic_protein_1_(L-plastin)_[Source:ZFIN;Acc:ZDB-GENE-991213-5] |
| ENSDARG00000038424 | si:dkey-8k3.2 | si:dkey-8k3.2_[Source:ZFIN;Acc:ZDB-GENE-100922-98] |
| ENSDARG00000051912 | zgc:152945 | zgc:152945_[Source:ZFIN;Acc:ZDB-GENE-060929-800] |
| ENSDARG00000054968 | cd40 | CD40_molecule,_TNF_receptor_superfamily_member_5_[Source:ZFIN;Acc:ZDB-GENE-090313-95] |
| ENSDARG00000056615 | cybb | cytochrome_b-245,_beta_polypeptide_(chronic_granulomatous_disease)_[Source:ZFIN;Acc:ZDB-GENE-040426-1380] |
| ENSDARG00000058731 | slc2a6 | solute_carrier_family_2_(facilitated_glucose_transporter),_member_6_[Source:ZFIN;Acc:ZDB-GENE-081104-301] |
| ENSDARG00000071216 | si:ch211-133n4.9 | si:ch211-133n4.9_[Source:ZFIN;Acc:ZDB-GENE-070424-126] |
| ENSDARG00000071437 | ptprc | protein_tyrosine_phosphatase,_receptor_type,_C_[Source:ZFIN;Acc:ZDB-GENE-050208-585] |
| ENSDARG00000088689 | si:ch211-201o1.1 | si:ch211-201o1.1_[Source:ZFIN;Acc:ZDB-GENE-120709-60] |
| ENSDARG00000090352 | CR855311.1 | uncharacterized_LOC101883708_[Source:NCBI_gene;Acc:101883708] |
| ENSDARG00000090730 | cfbl | complement_factor_b,_like_[Source:ZFIN;Acc:ZDB-GENE-030131-2319] |
| ENSDARG00000090890 | cmklr1 | chemokine-like_receptor_1_[Source:ZFIN;Acc:ZDB-GENE-060526-126] |
| ENSDARG00000105829 | CR788316.4 | neoverrucotoxin_subunit_beta-like_[Source:NCBI_gene;Acc:100004951] |

## APPENDIX J: Motif occurrence in genes upregulated by chronic cortisol

**Table J.1. Motif occurrence in genes upregulated in chronic cortisol**

| GC Responsive Gene (Gans, et al., 2020) | Has E-Box | Has KLF motif | Has GRE |
|---|---|---|---|
| arl5c | arl5c | | arl5c |
| btg1 | btg1 | | btg1 |
| btg2 | btg2 | btg2 | |
| c4b | c4b | c4b | |
| ca15c | ca15c | ca15c | |
| calcoco1b | calcoco1b | calcoco1b | |
| cbx7a | cbx7a | cbx7a | |
| cd40 | cd40 | cd40 | |
| cdab | cdab | cdab | |
| cebpd | cebpd | cebpd | cebpd |
| cfbl | | cfbl | |
| chac1 | chac1 | chac1 | chac1 |
| cmklr1 | cmklr1 | cmklr1 | |
| cpne3 | cpne3 | cpne3 | |
| cx28.9 | cx28.9 | | |
| cybb | cybb | | |
| cyp2k6 | cyp2k6 | cyp2k6 | |
| cyp2n13 | cyp2n13 | cyp2n13 | cyp2n13 |
| ddit4 | | ddit4 | |
| diabloa | diabloa | diabloa | diabloa |
| dusp1 | dusp1 | dusp1 | dusp1 |
| egr1 | egr1 | egr1 | |
| egr4 | egr4 | egr4 | |
| entpd8 | entpd8 | entpd8 | entpd8 |
| epas1b | epas1b | epas1b | |
| fbp1b | fbp1b | fbp1b | |
| fbxo32 | fbxo32 | fbxo32 | fbxo32 |
| fkbp5 | fkbp5 | fkbp5 | fkbp5 |
| fn1b | | fn1b | |
| fosab | fosab | fosab | fosab |
| g6pca.2 | g6pca.2 | | g6pca.2 |
| gadd45ba | gadd45ba | gadd45ba | |
| gbp1 | gbp1 | gbp1 | |
| grna | grna | | |
| ier2a | ier2a | ier2a | |

**Table J.1 continued**

| GC Responsive Gene (Gans, et al., 2020) | Has E-Box | Has KLF motif | Has GRE |
|---|---|---|---|
| ier2b | ier2b | ier2b | ier2b |
| irf1b | irf1b | irf1b | irf1b |
| irg1l | irg1l | | irg1l |
| junba | junba | junba | |
| junbb | junbb | junbb | |
| klf9 | klf9 | klf9 | klf9 |
| lcp1 | lcp1 | lcp1 | |
| LOC553228 | LOC553228 | LOC553228 | |
| lpin1 | lpin1 | lpin1 | lpin1 |
| lygl1 | lygl1 | | lygl1 |
| mmp9 | | mmp9 | |
| mpeg1.2 | mpeg1.2 | mpeg1.2 | mpeg1.2 |
| mych | mych | mych | mych |
| nfkbiaa | nfkbiaa | nfkbiaa | nfkbiab |
| nfkbiab | nfkbiab | nfkbiab | |
| noxo1a | noxo1a | noxo1a | noxo1a |
| npas4a | npas4a | npas4a | npas4a |
| nr1d1 | nr1d1 | nr1d1 | nr1d1 |
| nr1d2a | nr1d2a | nr1d2a | nr1d2a |
| oxgr1a.1 | oxgr1a.1 | oxgr1a.1 | |
| pck1 | pck1 | pck1 | |
| pdk2b | pdk2b | pdk2b | |
| pfkfb3 | pfkfb3 | pfkfb3 | |
| plekhs1 | plekhs1 | plekhs1 | plekhs1 |
| pnpla3 | pnpla3 | pnpla3 | |
| rbp7a | rbp7a | rbp7a | |
| rel | rel | rel | rel |
| rgs2 | rgs2 | rgs2 | rhcga |
| rhcga | rhcga | rhcga | |
| scpp1 | scpp1 | scpp1 | scpp1 |
| scpp9 | scpp9 | scpp9 | scpp9 |
| si:ch211-240l19.5 | si:ch211-240l19.5 | si:ch211-240l19.5 | si:ch211-240l19.5 |
| slc14a2 | slc14a2 | slc14a2 | |
| slc15a1b | slc15a1b | slc15a1b | |
| slc25a25a | slc25a25a | slc25a25a | slc25a25a |
| slc25a5 | slc25a5 | slc25a5 | slc25a5 |

**Table J.1 continued**

| GC Responsive Gene (Gans, et al., 2020) | Has E-Box | Has KLF motif | Has GRE |
|---|---|---|---|
| slc34a2a | slc34a2a | slc34a2a | |
| slc3a2b | slc3a2b | slc3a2b | slc3a2b |
| slc5a1 | slc5a1 | slc5a1 | |
| slc6a19a.1 | slc6a19a.1 | slc6a19a.1 | |
| socs1a | socs1a | socs1a | socs1a |
| socs3a | socs3a | socs3a | |
| stat4 | stat4 | stat4 | |
| sult1st2 | sult1st2 | sult1st2 | sult1st2 |
| sult5a1 | sult5a1 | | |
| tdo2b | tdo2b | tdo2b | |
| tob1a | tob1a | tob1a | tob1a |
| tob1b | tob1b | tob1b | |
| tsc22d3 | tsc22d3 | tsc22d3 | tsc22d3 |
| txnipa | txnipa | txnipa | txnipa |
| ucp1 | ucp1 | ucp1 | |
| ucp3 | ucp3 | ucp3 | |
| upp2 | upp2 | upp2 | upp2 |
| zgc:100868 | zgc:100868 | zgc:100868 | |
| zgc:113625 | zgc:113625 | zgc:113625 | zgc:113625 |
| zgc:122979 | zgc:122979 | zgc:122979 | zgc:122979 |
| zgc:153932 | zgc:153932 | zgc:153932 | zgc:153932 |
| zgc:154142 | zgc:154142 | zgc:154142 | zgc:154142 |
| zgc:172065 | zgc:172065 | zgc:172065 | |
| zgc:172131 | zgc:172131 | zgc:172131 | |
| zgc:173915 | zgc:173915 | zgc:173915 | |

**GC responsive genes not found by HOMER**

| | | | |
|---|---|---|---|
| adgrf8 | tppp | FO904966.1 | si:ch211-226h7.6 |
| cyldb | ulk2 | LO018605.1 | si:ch211-226h7.8 |
| cyp2k6 | urgcp | sb:cb1058 | si:ch211-39f2.3 |
| ier2a | AL929237.1 | si:ch211-133n4.9 | si:ch73-181m17.1 |
| ier2b | AL954191.1 | si:ch211-147m6.1 | si:ch73-338o16.4 |
| itgb2 | AL954655.1 | si:ch211-153b23.3 | si:ch73-63e15.2 |
| itpkcb | AL954655.2 | si:ch211-157j23.2 | si:dkey-201c13.2 |
| klhl38b | CR318588.3 | si:ch211-182p11.1 | si:dkey-201i2.4 |
| MFAP4_(1_of_many) | CR385054.1 | si:ch211-194m7.3 | si:dkey-202l22.6 |
| pdk2a | CR753876.1 | si:ch211-201o1.1 | si:dkey-239b22.1 |
| psme4a | CR788316.4 | si:ch211-207n23.2 | si:dkey-247k7.2 |
| ptprc | CR855311.1 | si:ch211-214p16.3 | si:dkey-8k3.2 |
| rbp7a | CR926130.2 | si:ch211-219a15.4 | si:dkeyp-1h4.6 |
| slc2a6 | CU914622.2 | si:ch211-226h7.3 | zgc:152945 |
| slc6a19a.1 | FO704661.1 | si:ch211-226h7.5 | |

## APPENDIX K: HIF1 and AMPK targets for PCA

(curated by Jia, et al., 2019[254] and adapted for *Danio*)

**Table K.1. List of HIF1 and AMPK targets**

| **Hif1 Targets** | | **AMPK Targets** | |
|---|---|---|---|
| **gene_id** | **gene_name** | **gene_id** | **gene_name** |
| ENSDARG00000015263 | adma | ENSDARG00000088357 | acadl |
| ENSDARG00000069027 | admb | ENSDARG00000038900 | acadm |
| ENSDARG00000038207 | aldh4a1 | ENSDARG00000014727 | acox1 |
| ENSDARG00000011665 | aldoaa | ENSDARG00000038865 | acox3 |
| ENSDARG00000034470 | aldoab | ENSDARG00000003854 | acsl1b |
| ENSDARG00000057661 | aldoca | ENSDARG00000030514 | acsl1a |
| ENSDARG00000019702 | aldocb | ENSDARG00000032079 | acsl3a |
| ENSDARG00000040380 | arhgef1a | ENSDARG00000014674 | acsl3b |
| ENSDARG00000055837 | arhgef1b | ENSDARG00000004078 | acsl4a |
| ENSDARG00000055945 | asph | ENSDARG00000010752 | acsl4b |
| ENSDARG00000004060 | bhlhe40 | ENSDARG00000075931 | acsl5 |
| ENSDARG00000099961 | bnip3 | ENSDARG00000035859 | angptl4 |
| ENSDARG00000060089 | btaf1 | ENSDARG00000102004 | apoea |
| ENSDARG00000102300 | ca9 | ENSDARG00000040295 | apoeb |
| ENSDARG00000051923 | ccnb1 | ENSDARG00000111939 | atf4a |
| ENSDARG00000030905 | cited2 | ENSDARG00000038141 | atf4b |
| ENSDARG00000010312 | cp | ENSDARG00000068096 | atf5a |
| ENSDARG00000037618 | ddit4 | ENSDARG00000077785 | atf5b |
| ENSDARG00000036912 | edn1 | ENSDARG00000020623 | baxa |
| ENSDARG00000038996 | egln1a | ENSDARG00000089129 | baxa |
| ENSDARG00000004632 | egln1b | ENSDARG00000030881 | baxb |
| ENSDARG00000105156 | egln1b | ENSDARG00000079144 | bcl2l11 |
| ENSDARG00000032553 | egln3 | ENSDARG00000020298 | btg2 |
| ENSDARG00000022456 | eno1a | ENSDARG00000104702 | cat |
| ENSDARG00000013750 | eno1b | ENSDARG00000101637 | ccnd1 |
| ENSDARG00000060494 | eprs1 | ENSDARG00000051748 | ccnd2a |
| ENSDARG00000024431 | ets1 | ENSDARG00000070408 | ccnd2b |
| ENSDARG00000019815 | fn1a | ENSDARG00000010434 | clu |
| ENSDARG00000006526 | fn1b | ENSDARG00000059770 | cpt1aa |
| ENSDARG00000008503 | glcci1a | ENSDARG00000062054 | cpt1ab |
| ENSDARG00000032157 | grk6 | ENSDARG00000058285 | cpt1b |
| ENSDARG00000016038 | hacd3 | ENSDARG00000038618 | cpt2 |
| ENSDARG00000003570 | hsp90b1 | ENSDARG00000023217 | crema |

**Table K.1 continued**

| Hif1 Targets | | AMPK Targets | |
|---|---|---|---|
| **gene_id** | **gene_name** | **gene_id** | **gene_name** |
| ENSDARG00000031100 | ivns1abpa | ENSDARG00000102899 | cremb |
| ENSDARG00000013946 | ivns1abpb | ENSDARG00000069186 | cyp27a1.2 |
| ENSDARG00000060808 | mecom | ENSDARG00000055159 | cyp27a1.4 |
| ENSDARG00000070903 | met | ENSDARG00000069018 | cyp7a1 |
| ENSDARG00000032039 | mxd1 | ENSDARG00000074431 | ddb1 |
| ENSDARG00000034801 | mylka | ENSDARG00000103503 | dgat1a |
| ENSDARG00000004753 | mylkb | ENSDARG00000054914 | dgat1b |
| ENSDARG00000030598 | nampta | ENSDARG00000030756 | dnmt1 |
| ENSDARG00000027183 | namptb | ENSDARG00000037421 | egr1 |
| ENSDARG00000032849 | ndrg1a | ENSDARG00000070029 | ehhadh |
| ENSDARG00000010420 | ndrg1b | ENSDARG00000069017 | elnb |
| ENSDARG00000026925 | nos2a | ENSDARG00000019532 | fads2 |
| ENSDARG00000031976 | nos2b | ENSDARG00000040135 | fosaa |
| ENSDARG00000033537 | p4ha1a | ENSDARG00000031683 | fosab |
| ENSDARG00000071082 | p4ha1b | ENSDARG00000055751 | fosb |
| ENSDARG00000010085 | p4ha2 | ENSDARG00000015355 | fosl1a |
| ENSDARG00000075209 | p4htm | ENSDARG00000003411 | foxa2 |
| ENSDARG00000109371 | pdgfaa | ENSDARG00000031616 | g6pca.1 |
| ENSDARG00000110069 | pdgfaa | ENSDARG00000013721 | g6pca.2 |
| ENSDARG00000060504 | pfkla | ENSDARG00000020371 | g6pc3 |
| ENSDARG00000099755 | pfklb | ENSDARG00000071065 | g6pd |
| ENSDARG00000005423 | pgam1a | ENSDARG00000043581 | gadd45aa |
| ENSDARG00000014068 | pgam1b | ENSDARG00000104571 | gadd45ab |
| ENSDARG00000054191 | pgk1 | ENSDARG00000027744 | gadd45ba |
| ENSDARG00000059746 | plod1a | ENSDARG00000013576 | gadd45bb |
| ENSDARG00000056783 | raraa | ENSDARG00000019417 | gadd45ga |
| ENSDARG00000034893 | rarab | ENSDARG00000016725 | gadd45gb.1 |
| ENSDARG00000003398 | rbpja | ENSDARG00000062864 | gk5 |
| ENSDARG00000052091 | rbpjb | ENSDARG00000021494 | hnf4a |
| ENSDARG00000077906 | rnf165a | ENSDARG00000056160 | hspd1 |
| ENSDARG00000078817 | rnf165b | ENSDARG00000040764 | id1 |
| ENSDARG00000006279 | rragd | ENSDARG00000054823 | id3 |
| ENSDARG00000098968 | RSBN1 | ENSDARG00000074378 | junba |
| ENSDARG00000056795 | serpine1 | ENSDARG00000104773 | junbb |
| ENSDARG00000013961 | slc31a1 | ENSDARG00000067850 | jund |
| ENSDARG00000054423 | slc7a6 | ENSDARG00000062106 | klf5b |
| ENSDARG00000015536 | sox6 | ENSDARG00000018757 | klf5l |

**Table K.1 continued**

| Hif1 Targets | | AMPK Targets | |
|---|---|---|---|
| **gene_id** | **gene_name** | **gene_id** | **gene_name** |
| ENSDARG00000037397 | ssrp1a | ENSDARG00000087697 | lpl |
| ENSDARG00000016994 | ssrp1b | ENSDARG00000015890 | mafa |
| ENSDARG00000056680 | stc2a | ENSDARG00000044155 | mafaa |
| ENSDARG00000102206 | stc2b | ENSDARG00000077364 | mapk9 |
| ENSDARG00000077372 | tfr1b | ENSDARG00000032326 | mecr |
| ENSDARG00000019367 | tgfb3 | ENSDARG00000042816 | mmp9 |
| ENSDARG00000008191 | tmeff1a | ENSDARG00000017929 | ncoa2 |
| ENSDARG00000056740 | tmeff1b | ENSDARG00000098439 | nr1h3 |
| ENSDARG00000070743 | tmem45a | ENSDARG00000000796 | nr4a1 |
| ENSDARG00000056239 | tmem45b | ENSDARG00000017007 | nr4a2a |
| ENSDARG00000103542 | vegfaa | ENSDARG00000044532 | nr4a2b |
| ENSDARG00000034700 | vegfab | ENSDARG00000001777 | nup155 |
| | | ENSDARG00000003235 | nup88 |
| | | ENSDARG00000074955 | nup98 |
| | | ENSDARG00000007982 | onecut1 |
| | | ENSDARG00000090387 | onecut2 |
| | | ENSDARG00000013522 | pck1 |
| | | ENSDARG00000020956 | pck2 |
| | | ENSDARG00000054848 | pdk4 |
| | | ENSDARG00000002779 | pdx1 |
| | | ENSDARG00000010246 | prmt1 |
| | | ENSDARG00000019791 | prmt3 |
| | | ENSDARG00000002591 | ruvbl1 |
| | | ENSDARG00000033662 | scd |
| | | ENSDARG00000030265 | scdb |
| | | ENSDARG00000042644 | sod2 |
| | | ENSDARG00000103435 | sorbs1 |
| | | ENSDARG00000088347 | sp1 |
| | | ENSDARG00000019392 | stat5a |
| | | ENSDARG00000032619 | tob1a |
| | | ENSDARG00000021372 | tob1b |
| | | ENSDARG00000036107 | txnipa |
| | | ENSDARG00000070000 | txnipb |

## APPENDIX L: Expression dynamics of *klf9* and *fkbp5* on day 4 post-fertilization

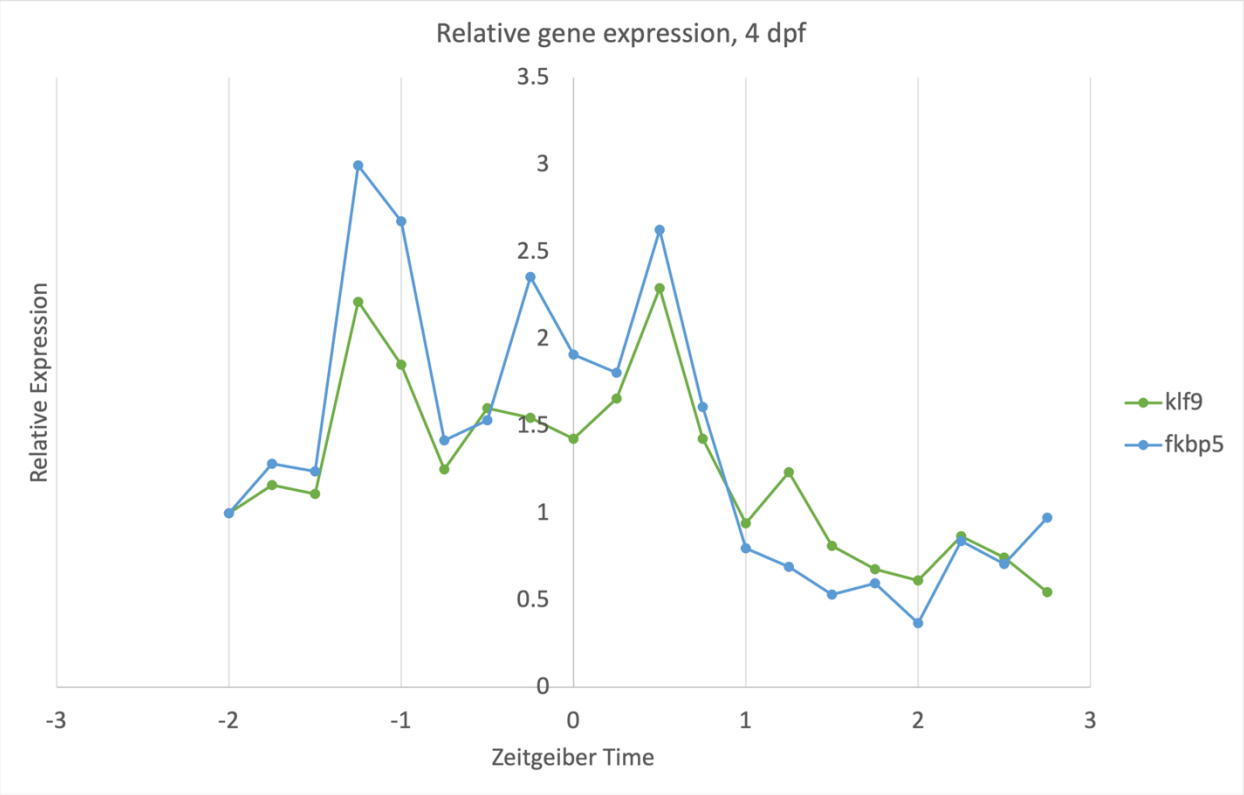


**Figure L.1. Dynamic expression of *klf9* and *fkbp5* on day 4 post-fertilization**. Relative expression of *klf9* and *fkbp5* on day 4 post-fertilization measured by qPCR shows evidence of ultradian and diurnal dynamics, and synchrony between the two genes. Data shown are from a single experiment using pooled larvae (n=3 per sample). Expression of each gene is presented relative to expression of that gene at the first time point.

## APPENDIX M: Sequences of CRISPR-induced *klf9* mutations

### Figure M.1. Heterozygous sequences from F1 mutants


### Table M.1. Mutant allele sequences extracted from chromatographs

| Sample | Nucleotide Sequence | Notes |
|---|---|---|
| WT (not shown) | …AGCGGCATCAGCGCCAAGCGAATAGTGGACAGTGATGCGGAGAATCGGGA… | |
| “42” | …AGCGGCATCAGCGCCAAGCGAATAGTGGACA- - GATGCGGAGAATCGGGA… | 2bp deletion |
| “21” | …AGCGGCATCAGCGCCAAGCGAATAGTGGACAGTG- - - CGGAGAATCGGGA… | 3bp deletion |
| “91” | …AGCGGCATCAGCGCCAAGCGAATAGTGGACAGTGA - - - - - GAATCGGGA… | 6bp deletion |

**Figure M.2. Homozygous F3 sequences**

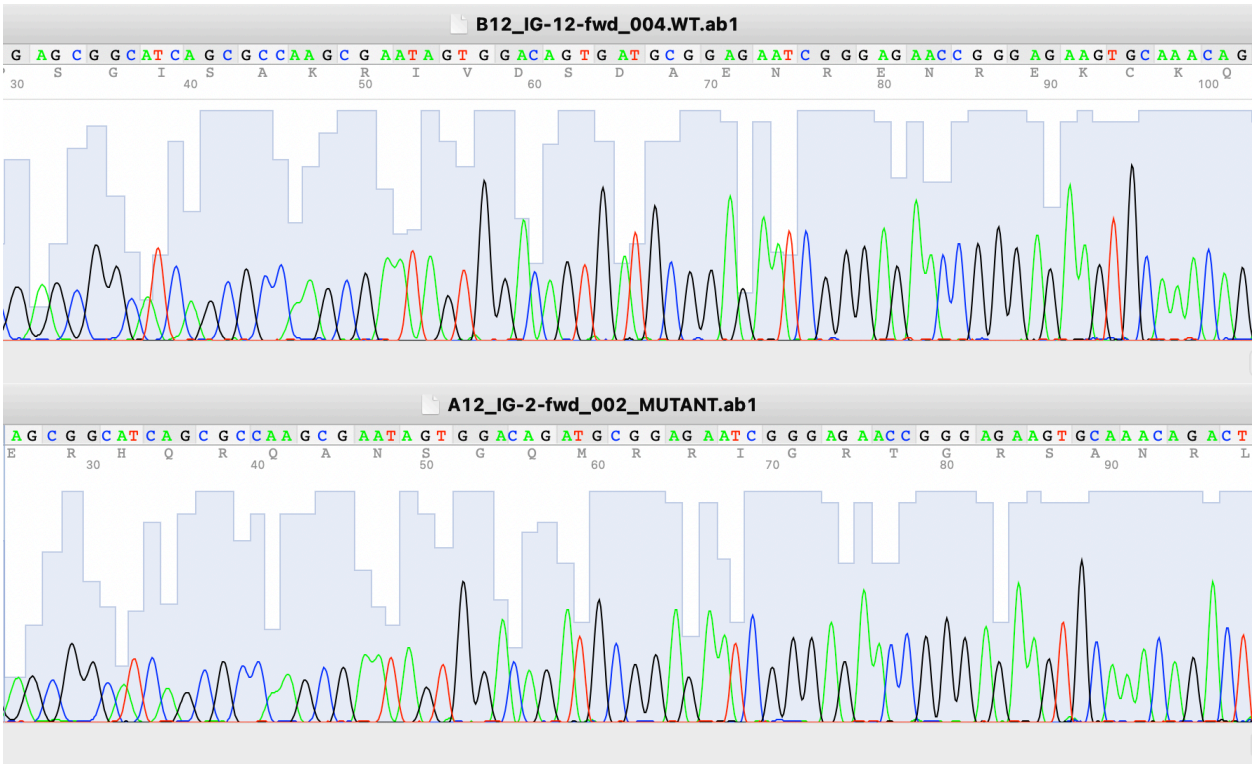

## BIOGRAPHY OF THE AUTHOR

Ian Gans was born in Portland, Maine on November 17, 1982. He was raised in South Portland, Maine and graduated from South Portland High School in 2001. He wasn't accepted to any colleges he initially applied to but attended the University of Southern Maine thanks to his high school guidance counselor who saved him from falling through the cracks. He worked full-time in a deli and studied biology until a terrible chemistry professor inspired him to try something else. He transferred to Arizona State University where he graduated cum laude with a B.A. in journalism in 2006. Ian never worked in journalism, unless you count his blog (which you obviously don't even know exists). A series of temp jobs turned into a cushy full-time seat on a cubicle farm. He played guitar in a bar band at night. The global economy collapsed. He went back to the University of Southern Maine, rediscovered his love for biology and graduated cum laude with a B.S. in human biology in 2015 (despite failing yoga class). With guidance from his unofficial college advisor, Ian applied and was admitted to the University of Maine's Graduate School of Biomedical Science and Engineering. While in the program Ian married his high school sweetheart and they had two beautiful daughters, Iris and Margot. While Ian was doing his dissertation research at the MDI Biological Laboratory, his family and he hunkered down in a crooked farmhouse in Ellsworth, Maine. There they weathered the 45th U.S. "presidency" and COVID19 pandemic, and Ian could often be found moving wheelbarrows full of rocks across the yard in his free time. Following his dissertation, Ian and family moved back to Portland and he accepted a Post-Doctoral Fellowship at the Maine Medical Center Research Institute. Ian is a candidate for the Doctor of Philosophy degree in Biomedical Science from the University of Maine in December 2021.